MULTIPHYSICS MODELING OF GASEOUS CONTAMINANT TRANSPORT IN DEEP OPEN PIT MINES UNDER ARCTIC AIR INVERSIONS
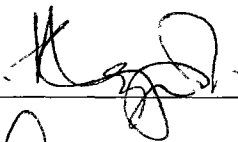
By

Abhishek Choudhury

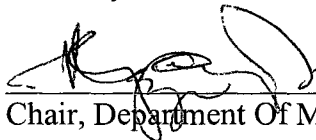RECOMMENDED: _____

_____
Debasmita Misra

_____
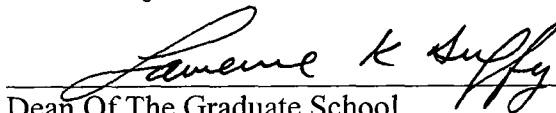
_____
Sukumar Bandopadhyay
Advisory Committee Chair

_____
Chair, Department Of Mining & Geological Engineering

APPROVED: _____
Dean, College Of Engineering And Mines

_____
Dean Of The Graduate School

_____
Date   Apr 12, 2011

MULTIPHYSICS MODELING OF GASEOUS CONTAMINANT TRANSPORT IN

DEEP OPEN PIT MINES UNDER ARCTIC AIR INVERSIONS

A

Dissertation

Presented to the Faculty

of the University of Alaska Fairbanks

in Partial Fulfillment of the Requirements

for the Degree of

DOCTOR OF PHILOSOPHY

By

Abhishek Choudhury M.S.

Fairbanks, Alaska

May 2011

UMI Number: 3463946

UMI®

Dissertation Publishing

ProQuest®

ABSTRACT

Entrapment of pollutants in a deep open pit operating in a cold climate could occur due to atmospheric inversion. The process of air inversion is complex and requires thorough understanding in order to design a mine ventilation plan to remove trapped pollutants in open-pit mines operating in the arctic/sub-arctic regions.

The objective of this dissertation is to develop a model using Computational Fluid Dynamics (CFD) tools for analysis of gaseous pollutant transport in deep, open pit mines under air inversion in arctic or subarctic regions. An Eulerian 3-D model was used for the development and validation of the CFD model of pollutant transport in an idealized open pit mine. No prior assumptions, turbulent or laminar, were considered for the nature of the flow.

The 2-D model results indicated that air velocity, air temperature, diffusivity coefficient and slope angle were important controlling parameters in the inversion process. The flow regime was laminar at the origin, but as the flow progressed toward the center of the pit it changed to quasi-laminar and generated local eddies towards the pit bottom. The total energy of the quasi-laminar flow as well as the small local eddies was not enough to lift the inversion cap. However, a combination of quasi-turbulent flow and the local eddy transport resulted in removal of some of the pollutant mass from the pit bottom, either due to turbulent mixing, or due to advection. Presence of backflow may appear to be a logical mode of flow in deep open-pit mines in arctic regions.

Next, the 3D model was validated using data from a selected open-pit mine. Influent air velocity, diffusivity coefficient, larger pit geometry were found to influence the retention and transport of pollutant out of the pit. The most important conclusion that was drawn from this research is that natural ventilation alone cannot remove the pollutants from an open pit or lift the inversion cap.

Table of Contents

List of Figures

List of Tables

Acknowledgements

CHAPTER I: Introduction

1.1. Background

The northern regions of the earth are underlain by a continuous layer of perennially frozen ground. There are vast mineral resources in the these regions (the arctic and the subarctic). Mining is important in several parts of the arctic or sub-arctic regions. Nowhere are the conditions for mining operations more adverse than in the arctic, where long, cold and severe winters are common. Each season of the year presents its own special set of challenges. One of the problems in a deep open pit operating in a cold climate is atmospheric inversion, that is, when some act of nature (there are several possibilities) causes the temperature of the air over the mine to increase with altitude, with cold, heavy air being trapped in the pit. In itself, this is not hazardous, but the diesel-engine earth-moving equipment used in the mine quickly render the air within the pit severely contaminated, since the air inversion does not provide an outlet for these pollutants.

With advancement of open pit mining technology, the depth to which minerals can be profitably mined has increased, resulting in the pits being dug to deeper depths. Such deep pits in extreme climatic conditions, coupled with the trapping of pollutants due to air inversion, have presented a considerable challenge for the mining community in the area of open pit ventilation. Mine operators in cold regions, however, are very familiar with the problem. Several arctic or sub-arctic mines have reported the occurrence of air inversions, including, Fort Knox gold mine and Red Dog mine in Alaska, Ekati mine in Canada, Aitek open pit mine in Sweden, and Mirni diamond open pit mine in Udachini, Russia. Even Bingham Canyon mine in Utah has reported local air inversion from time to time.

Avoidance of air inversion has been recognized as an important contributing factor to healthy and safe working or living conditions. Extreme cases of unsafe respirable atmospheres have been associated with air inversion in urban areas such as Mumbai,

India; Los Angeles, California; Mexico City ; Sao Paulo, Brazil; Santiago, Chile; and Tehran, Iran, but even also in smaller cities like Oslo, Norway; Salt Lake City, Utah and Boise, Idaho, which are closely surrounded by hills and mountains that together with the inversion effect bottle-caps the air in the city. During a severe inversion, trapped air pollutants form a brownish haze that can cause respiratory problems. The Great Smog, one of the most serious examples of such an inversion, occurred in London in 1952 and was blamed for thousands of deaths.

Peng and Lu (2005) noted that natural ventilation was the preferred means to deal with pollutants in open pit mines. The wind flow pattern in open pit mines is generally of a recirculatory type. The recirculatory region occupies most space in the open pit, and conditions for natural ventilation are bad. Increase of wind speed is useful for the dilution and dispersion of air pollutants in open pit mines. Even in ideal natural convection conditions, there may be an accumulation of pollutants at the bottom of the pit, thus necessitating additional artificial remedial measures. Air inversion can be expected to exacerbate this naturally occurring phenomenon.

Air inversion, particularly in the arctic or sub arctic regions, is initiated by lack of energy that the layers of air at the bottom may receive. This energy is received primarily in the form of long-wave radiation from the ground. The ground receives its energy, in turn, from the sun in the form of short-wave radiation. During winter, in the arctic regions, solar energy incident on the ground is drastically low, thus minimizing the amount of energy reradiated to the layer of air immediately superincumbent to the ground. This immobile layer of air traps pollutants close to the ground, gives rise to air quality that fails mandated regulatory standards. This may also create associated problems such as "ice fogs", which affect visibility. Inversion characteristics are also heavily dependant on density of the fluid. The confluence of these factors frequently leads to air inversion in arctic and sub-arctic regions. In an inversion, vertical motion in the atmosphere is suppressed. Hence vertical heat transport by eddies is suppressed; this reduces (downwards) heat transport, leading to further cooling of the surface,

which may lead to an effective decoupling of the atmosphere from the surface under extreme conditions.
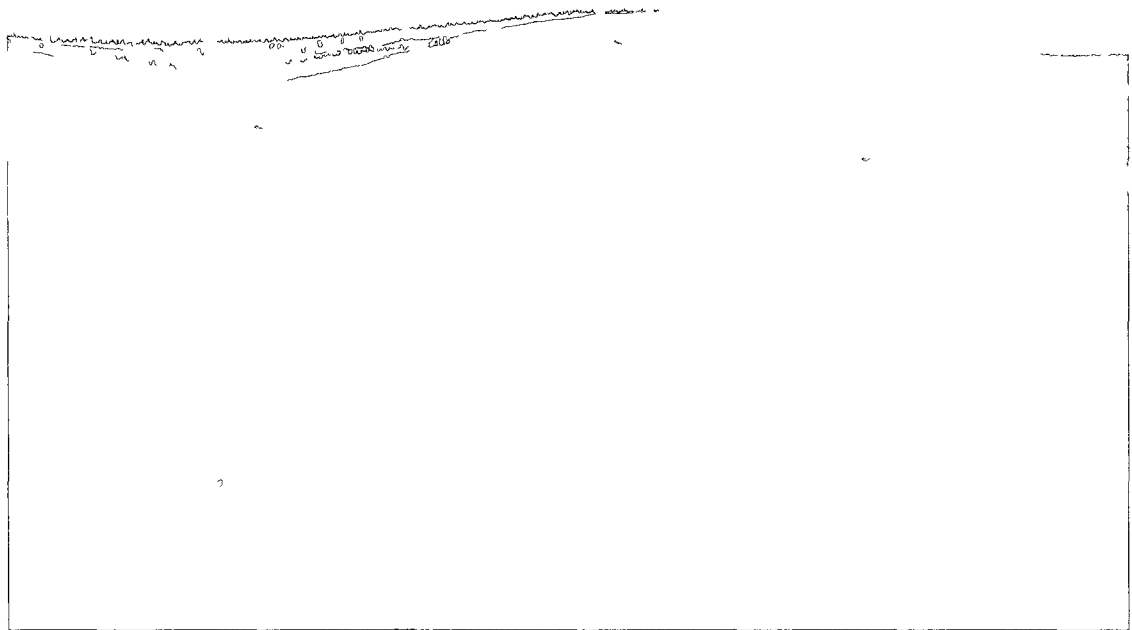
Figure 1.1: An example of air inversion in an Arctic open-pit (Parr, 2004)
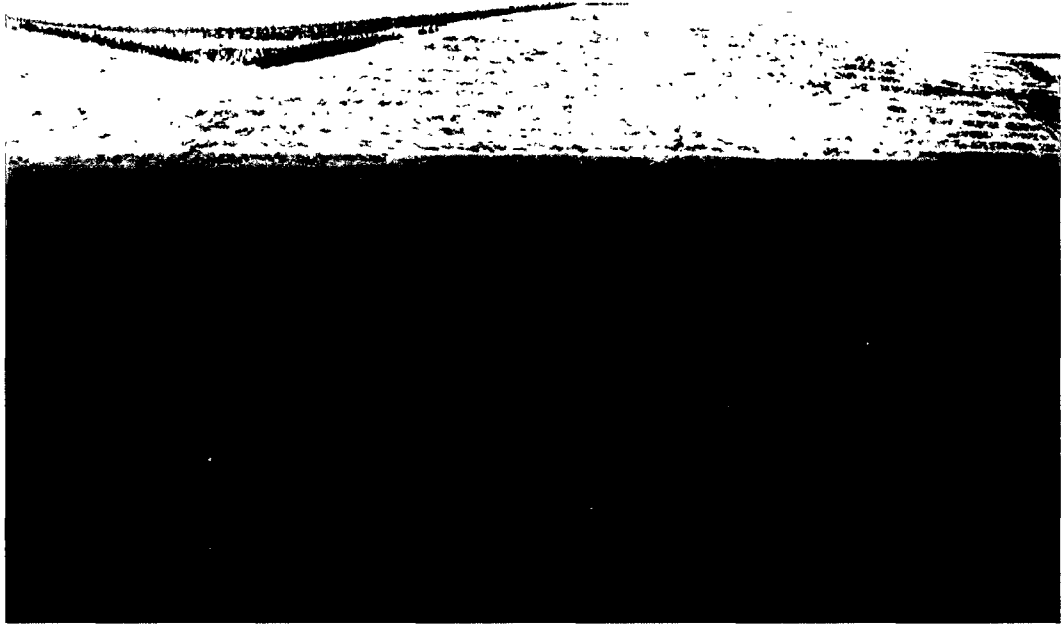
Figure 1.2: Another example of air inversion in an Arctic open-pit (Parr, 2004)

As observed from figures 1.1 & 1.2, air inversion results in poor air quality in open pit mines. If the air quality in mines does not meet the established health standards, in addition to the health hazards to the miners, the mine may be penalized or even shut down, resulting in financial losses. Thus a detailed examination of the cause-effect relationship leading to the predictive model for air inversion is necessary. EPA (Winges,1990), for example, has studied air inversion and atmospheric pollution issues. Unfortunately, the application of such studies and models to the open pit mine ventilation or the specific situations in arctic or sub-arctic mine is limited. The air pollution problem due to air inversion, while quite pronounced in Alaskan mines, is also evident in many other open pit mines around the world and needs special attention.

1.2. Problem Statement

It is important to appreciate that the problem at hand is primarily an aerodynamic problem, where the air flow in an open pit causes advection of pollutants. However, as will be explained in this section, there are several unique features of air flow in and around open pit mines that require detailed and careful consideration for understanding and solving the aerodynamic problem.

The pollutants in open pit mines are primarily of two types, particulate and gaseous. The advective transfer and dispersal of these pollutants, or lack thereof, under extremely cold conditions, makes air unhealthy in deep open pit mines. A negligible amount of transport through diffusion is expected. However, the effect of diffusion and/or thermal recirculation is not sufficient to mitigate the problem.

Natural ventilation cycles exist in open pit mines, and have traditionally been the primary mode of dilution and elimination of pollutants in open pits. Natural ventilation comes into an open pit from the windward side and flows in to the pit as a turbulent jet. This jet has two effects on the concentrations of pollutants in the pit. Firstly, it re-circulates and realigns the concentration profile of substances already existing within the pit. Secondly, it may introduce substances into the pit that do not originate there.

In order to model air inversion for subsequent study of pollutant trapping and air flow in arctic open pit mines, the flow of air through an open pit mine must first be examined. The air flow through the mine profile has several aerodynamic zones. Awareness of these zones can help not only model the air and advective contaminants there, but also determine the final concentration profile, and mitigation of pollutants in the pit.

Ventilation design for open pit mines requires the knowledge of the quantity of the pollutants that are liberated into the pit by various dust and gas sources. The most important items in the total balance of pollutants in open pit mines are the stationary point sources (Drilling rigs, excavators, loading machines) and moving sources (such as the trucks). The spreading of admixtures from these sources in an open pit mine is

directly related to the aerodynamics of the airflows in the open pit space. Evaluation of the atmospheric conditions in an open pit mine requires determination of the concentration of injurious mixtures. Therefore, it is necessary to predict the intensity of continuous point sources of dust and gases and determine the regularities of the dissipation of admixtures from sources located at different aerodynamic zones in the pit.

Aerodynamically, the air current prior to its separation from the upper edge of the pit wall is a boundary layer, which is known in meteorology as the near-ground layer. Concepts of direct flow ventilation systems have been cited in open pit mine ventilation literature (Skobunov, 1962; Belousov, 1985; 1990). This ventilation system is distinguished by flow around the leeward wall of the pit without separation. The flow of air masses and the diffusion of the admixture are determined by the aerodynamic parameters that become established before the flow around the open pit space, as well as by the parameters, which are characteristics of the purely direct-flow ventilation system. Under actual condition one would expect the airflow in the near-ground layer to stabilize prior to the separation of the flow from the top edge of the pit.

Over the past two decades, numerous meteorological and tracer experiments have been conducted to investigate the dispersive characteristics of valley atmospheres (Allwine, et al., 1997). These have led to the identification of key physical processes governing dispersion in valleys, and a more complete understanding of these physical processes is emerging from ongoing research efforts (S. Bandopadhyay, personal communication, February 22, 2011). The important physical processes that influence the distribution of pollutants include up-and down valley wind speeds, up and down slope winds, turbulent diffusion, convective boundary layer growth, temperature inversion descent, nocturnal temperature inversion breakup, tributary flows, cross-valley circulations, and interaction with above ridge top winds. These studies and the

findings therefore are relevant to the study of the mine ventilation conditions in an open pit mine.

The temperature inversion characteristics at sunrise and heating rate of the pit atmosphere determines the evolution of the convective boundary layer (CBL) and inversion top descent during the morning transition period. The morning transition period is when the nocturnal down-pit flow is reversed to an up-pit flow. This is the period when the nocturnal temperature inversion descends into the pit and is destroyed by the growth of the convective boundary layer. The location of the top of the CBL and the top of the temperature inversion define layers with different atmospheric stabilities.

The heat flux that destroys a temperature inversion is distributed quite differently in an open pit than over homogeneous terrain. Over homogeneous terrain, the sensible heat flux destroys the inversion by driving the upward growth from the ground of a convective boundary layer, which warms the inversion air mass from below until the temperature deficit is overcome and inversion is destroyed. In an open pit mine, the upward heat flux also develops a CBL over the pit surfaces, but in contrast, the heated pit slopes cause warmed air parcels to flow up-slope. These up-slope flows remove mass from the base of the temperature inversion and, mass continuity result in a general subsiding motion over the open pit center (Allwine, et al., 1997). The CBL growth—inversion descent are a function of sensible heat flux, atmospheric pressure, density of air, solar flux, pit potential temperature lapse rate at sunrise, and the warm-air advection rate above the pit. While all the discussions above are related to gaseous pollutants in open pit mines, particulates such as dust in open pit mines are also of significant practical interest.

The estimation of concentrations of fugitive dust or gas for an open pit-mining situation has traditionally been done using United States Environmental Protection Agency (EPA) models such as the Industrial Source Complex model (TRC Environmental, 1985). Since the dust –producing operations at an open pit mines may

occur at depths up to several hundred meters below grade, only a fraction of fugitive dust generated inside the pit escapes to the surface, where it may then be transported to mine boundaries. This tendency for particulate matter (PM) to remain inside the pit has been called "pit retention". The magnitude of pit retention is expressed as "escape fraction", defined as the mass fraction of emissions that escapes from the mine pit to the surface. The two mechanisms occurring simultaneously that contribute to the pit retention phenomenon are: the decoupling of the wind field in the pit from the wind field at the surface, and the disposition and settling of particulates on the mine pit surface and along the pit walls. A dispersion model ignoring the influence of pit retention will over predict the downwind concentrations (Tandon and Bhaskar, 1998). The presence of a mine pit disturbs the airflow above and inside the pit, so that the plume of gas and dust may not have the Gaussian distribution imposed by many dispersion models (Reed, 2005). Furthermore, as most Gaussian plume dispersion models used for regulatory purposes have been developed to model downwind dispersion of dust from sources across a flat or undulating terrain, these models cannot account for the influence that the complex flow regime experiences in open pit mines.

There are three primary techniques identified in the literature (TRC Environmental, 1985, Tandon and Bhaskar, 1998) that have been historically used to study problems related to airflow and pit retention of particulate matter such as dust for open-pit mines: field experiments, wind tunnel modeling, and mathematical modeling. Each of these techniques has advantages and limitations. The level of uncertainty involved with these techniques is a function of assumptions utilized, number of independent parameters considered, generalization and extrapolation of results.

Full-scale experiments are expensive and time consuming, especially in complex terrain. Extensive measurements and analyses are required for wind, temperature, and concentration distribution to gain a sufficient understanding of the governing physical processes. Generalization from field data is difficult because of the peculiarities of specific sites and meteorological conditions. Controlled variation of independent

variables is generally not possible, and complicating factors are abundant. However, it is understood that field experiments can provide the "real-world" data to test the models. Although field studies in the vicinity of surface mines have undoubtedly been influenced by pit retention, very few studies have specifically addressed pit retention. There are studies reported in the literature in which the investigators detected discrepancies between the measured and the modeled concentrations at surface mines, and attributed the discrepancies to pit retention (TRC Environmental Inc, 1985). In a field study conducted at four mines in the Western United States, smoke generators at the bottom of the pits were used to release discrete 10-s puffs of diesel fuel smoke. An escape velocity, essentially the net upward velocity within each pit, was computed from the observed retention time of the tracers and the depth of each pit. This upward velocity, when computed to the downward settling and deposition velocity for different size particles, was the basis for the calculation of an escape fraction (TRC Environmental Inc., 1985).

Wind tunnel modeling comes under the general category of physical modeling or fluid modeling, and is an analog modeling technique for fluid-dynamic process. In fluid modeling, a scale model of terrain, plant, buildings, and obstructions are used. Certain non-dimensional parameters must be duplicated in the wind tunnel model and the actual full-scale situation. A wind tunnel study was performed at the EPA's Fluid Modeling Facility (TRC Environmental Inc., 1985) to investigate dispersion from surface coalmines in support of the dispersion modeling activities. The study involved measurement of the steady state tracer gas concentration fields downwind of model mines of various shapes, size, and orientations with low momentum, point-source releases of a neutrally buoyant gas from various locations in the model pits. The mean flow in a mine model was observed as a large vortex, with the flow at the top of the mine in the direction of flow aloft and the flow along the mine floor moving upwind (against the direction of mean flow aloft).

Mathematical model encompass such concepts as empirical box and statistical model, semi-empirical Gaussian plume and trajectory models, and numerical multi-box, grid and particle models. Mathematical models are used to represent the actual physical process governing atmospheric flow dynamics and pollution transport. Advection by wind components, turbulent diffusions, chemical reactions, wet and dry deposition of pollutants, and other atmospheric processes can all be included in a numerical model. The governing equations for the flow problems in mine ventilation are characterized by partial differential equations. The model to be developed has to be very robust. Robustness is an important property. Almost all derivatives of equations to model physical processes make an assumption that certain effects are not important to understand the physical process being studied.

Thus, the problem could be specifically defined as follows: in this dissertation, a three dimensional model of a selected mine will be provided and will be validated with data for concentration of specific pollutants at different locations in the mine. It is also possible to hypothesize that several factors, for example, the influent velocity, the temperature, the diffusivity coefficient, the overall slope of the mine, as well as the overall mine geometry affect distribution of gaseous pollutants in the open pit.

Any solution approach would require a good understanding of the complex interaction of the aerodynamic movement of air, air inversion process, meteorology pollutant sources, and fan applications.

1.3. Scope of Work

In order to understand and analyze air inversion, the complex process by which air inversion and entrapment of pollutants take place must be investigated thoroughly in order to design a mine ventilation plan for open-pit mines in the arctic/sub-arctic regions. Since pollution in a mine is anthropogenic and often is emitted from in-place equipment sources, any proposed solution must include consideration for these factors in addition to the air inversion problem. It is also noted that the selected mine also experiences frequent air inversions, due to its location in a valley, surrounded by

moderate hills. This configuration of the open pit blocks solar radiation from reaching the pit floor. The benches and overall pit slope also generally impede natural ventilation in the open pit.

In order to understand the complex interplay among the many variables affecting air inversion in open pit mine, the following steps are taken: (a) review literature and select available mathematical modeling approach to study the air inversion problem in active open pit mines; (b) collect data from an operating open pit mine and validate the model; (c) investigate air inversion process in mines; (d) identify and categorize the factors influencing air inversion and air pollution; (e) develop a two-dimensional model in COMSOL® to investigate the importance of various parameters in the model; (f) develop a three-dimensional model in COMSOL® and validate it with data collected from the selected sub-arctic mines while the pit is assumed to be under air inversion, and (g) Assuming the pit under inversion, investigate the sensitivity of the governing parameters.

Different dispersion models of Eulerian and Langrangian type can be used with CFD simulation of ventilation flow problems in open pit mines. For development and validation of the CFD model for transport of pollutants in an idealized open pit mine, an Eulerian 3-D model of pollutant transport has been used.

The approach taken in this research for ventilating an open pit is conceptually unique, because, most of the components that have major influence on the nature of pit ventilation and the distribution of gaseous pollutants in the pit have been included in the model. Also, no assumptions have been made regarding the nature of the flow.

The use of Computational Fluid Dynamics (CFD) tools for development of models and analysis of gaseous pollutant transport in deep, open pit mines in arctic or sub-arctic region under air inversion is also presented in the dissertation.

1.4. Thesis Organization

As noted before, literature on open pit mine ventilation, particularly with respect to air inversion, is non-existent in literature that have been presented in English language. Researchers in Kola Mining Institute, Murmansk region of Russia, and Yakutsk Mining Institute of the North, Soviet Academy of Sciences (V. Yakovlev, personal communication, December 17, 2009; M. Melnikov, personal communication, October 21, 2009; V. Izaxon, personal communication, June 24, 2009), have done extensive research in open pit mine ventilation. Published research literatures, available in Russian language, from these research institutes were collected, translated, reviewed, and presented in Chapter II.

The meteorological inputs that impact the contaminant concentration are the wind speed and direction as a function of time, the nocturnal temperature inversion characteristics at sunrise, the heating rate of the pit atmosphere after sunrise, and the turbulent eddy diffusivities as function of atmospheric stability. The wind speed and direction data are used to determine the advection effects. The meteorological data collected is also presented in Chapter II

Advanced technology has made computer faster and more powerful, which allows computational fluid dynamics (CFD) procedures to be applied to many air flow problems. CFD modeling has been widely used in atmospheric pollution studies in urban areas. However, none of these models or studies has addressed ventilation design for deep, open pit mines in general and especially in arctic or sub-arctic condition. The problem is complex and any solution approach would require a good understanding of the interaction of the aerodynamic movement of air, air inversion process, meteorology, pollutant sources, and application of air movers in open pit mines. The mathematical modeling involved here is to solve the coupled conservation equations of mass, momentum, and energy with appropriate initial and boundary equations.

A 2-D model has been developed to determine the flow parameters, to study the influence of relief, thermal inhomogeneity of the atmosphere and the surface, influence of the radiation effects upon the open pit microclimate. Furthermore, the distribution of pollutants was analyzed using the 2D model. The model and its results are presented in Chapter III.

An open pit mine is a closed structure on all sides. It is geometrically different from a valley. This complex topography can lead to re-circulation in the pit. Activities in a pit contribute to pollutants, thus resulting in poor air quality. A 3-D model has been developed (using COMSOL®) to represent the airflow patterns in an idealized model of an open pit mine. The generalized Navier-Stokes equation is used to represent the flow regime in the model space. The Convection-Conduction characteristic equation is used to model the thermal interaction, and the Convection-Diffusion characteristic equation is used to represent the transport of pollutants in the open-pit. No assumption is made regarding the characteristic of the flow in the pit (i.e., turbulent, quasi-turbulent or laminar). For development and validation of the CFD models for transport of pollution in open pit mines, an Eulerian 3-D model is used in the dissertation.

This model is then validated using data collected from a selected open pit mine under air inversion. The development and validation of these models are presented in Chapters IV and V.

Using the developed 3D models, the effects of several governing parameters such as influent air velocity, temperature, slope angle of the pit, diffusivity coefficient and pit geometry are studied and the results are presented in Chapter VI.

The conclusions from this research, and recommendations for future work, are presented in Chapter VII.

CHAPTER II: Literature Review and the Data for the Two-dimensional and Three-dimensional Models of airflow in Open-pit Mines

2.1. Introduction

In the previous chapter, a brief discussion was presented to introduce and define the problem the solution of which is being attempted in this dissertation. Section 2.2 presents a review of the literature collected from various sources. Section 2.3 contains representative samples of the data collected for the model.

2.2. Literature Review for Temperature Inversion

Literature available on open-pit ventilation is sparse. Most of the work was done in the former Soviet Union (U.S.S.R.). The literature cited in this section focus on the phenomenon of temperature inversion in the atmosphere, the movement and quality of air in open pit mines as related to air inversions, as well as possible remediation measures that have been attempted already.

2.2.1. Air Inversion

Air inversion is a specific instance of fluid inversion, which can take place in any fluid contained in or confined by a topographic trough. The word inversion, in this case, refers to the inversion of the normal vertical temperature profile seen in any large mass of fluid, e.g., air or water, in natural containment. For water, such natural containment may be ponds or lakes, which are topographic traps within which water would naturally accumulate due to gravity. For air, natural containment takes the form of low-lying valleys between mountain ranges, lateral containment between pressure/temperature gradients, or even artificially created troughs like open-pit mines. Air inversion is significantly more discernible (than water inversion in lakes) in terms of its extent in area and severity, its effects and consequences. Thus, further elucidation of the concept of temperature inversion will be undertaken with the specific phenomenon of air inversion only.

The lower atmosphere of the earth displays a definite temperature profile with increase in altitude. Jacob (1999) gives an example of such a natural temperature profile, as reproduced in Figure 2.1.
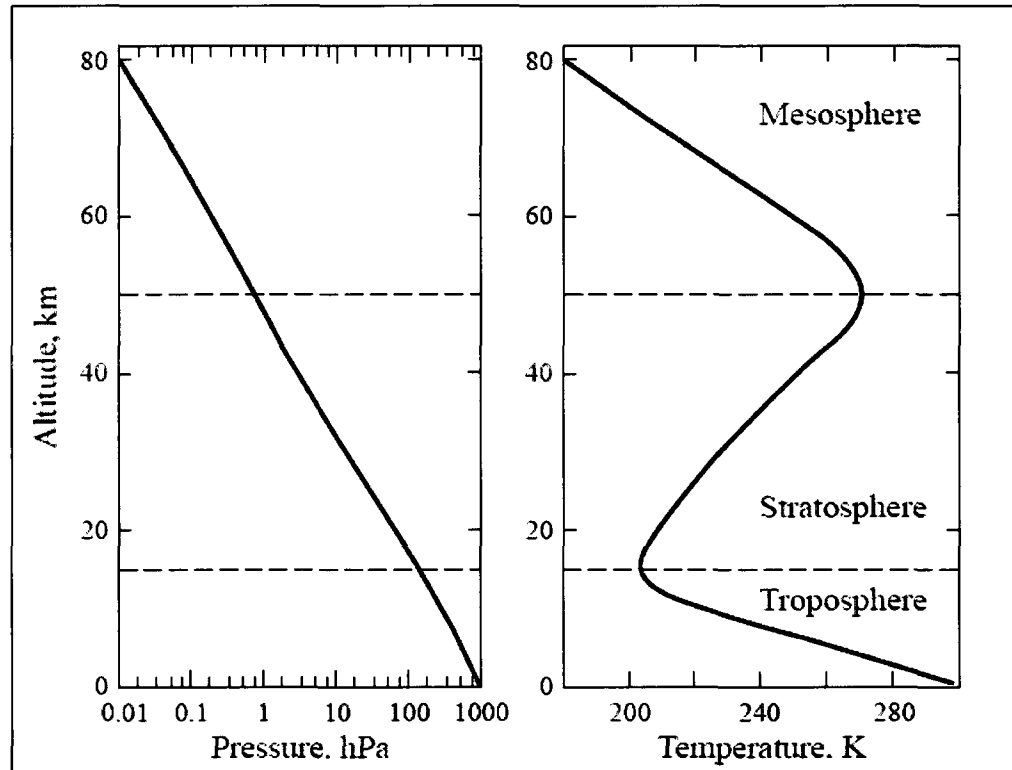
Figure 2.1: Mean Pressure and Temperature vs. Altitude at 30° N in March (Jacob, 1999).

In figure 2.1, the three principal layers that the Earth's atmosphere has been divided into are: Troposphere, Stratosphere and Mesosphere. Troposphere extends from the surface of the earth to 8-18 km, depending on the season and the latitude. The upper limit of the troposphere is called the tropopause. The stratosphere extends from the tropopause to the stratopause, for about 50 km. The mesosphere, the next layer above the stratosphere, extends from the stratopause up to a height of 80 km (Jacob, 1999).

Figure 2.1 also shows that within the troposphere, temperature decreases with increase in altitude. Beyond the tropopause, however, the temperature increases in the stratosphere as altitude is gained, due to absorption of solar radiation by the ozone layer (Jacob, 1999). In the mesosphere, the temperature gradient again reverts to the negative. Thus, Figure 2.1 shows the normal temperature profile that exists in the atmosphere, without the presence of anomalies such as an inversion.

Most human activity is confined to the envelope of the troposphere. The pollutants generated by activities such as mining are confined largely to the troposphere, due to the dearth of energy possessed by both gaseous and particulate pollutants to progress to higher altitudes (greater than 20 km), as well as due to the fact that the tropopause serves to limit the transfer of pollutants to higher altitudes (Jacob, 1999). Jacob also noted that the primary effect of surface based inversion was seen only in the troposphere. Thus, it would be worthwhile to examine the characteristics of inversion in the troposphere.

As stated in the previous paragraph, the temperature gradient in the troposphere is negative under normal circumstances. Normalcy with respect to this gradient is maintained by the presence of sufficient solar radiation during the day to heat the earth's surface. Heat from the sun, incident on the ground, and then re-radiated from the ground into the atmosphere, causes the layer of air immediately superincumbent to the ground to heat up. This causes a rise in the temperature in that layer. The re-radiated energy received from the ground by the air profile reduces as the height increases, thus resulting in a reduction in temperature with height. This gives rise to the temperature profile in the troposphere, as shown in Figure 2.1.

Temperature inversion occurs when this natural cycle is interrupted due to lack of re-radiated heat from the ground. Since the primary source of the heat that the ground re-radiates is solar energy, the relative position of the sun and thus the characteristics of the solar radiation (e.g. the angle and the total quantum of the incident radiation) is the principal cause for surface based inversions. It may be noted that the most common

change in the quantity of solar radiation reaching the ground occurs due to the motion of the earth around its axis. During daytime, the surface of the earth exposed to the sun is heated. After sunset, however, the ground cools down rapidly, interrupting the re-radiation of heat. This renders the layer of air closest to the ground cooler than the layers above, thus reversing the normal temperature profile described in Figure 2.1. During this time, a cap of temperature inverted air settles on the land, trapping the layer of cold air next to the ground. Since this layer cannot convect upwards or readily mix with the layers above it, all the pollution generated in the area is trapped within this layer, thus decreasing the quality of breathable air. Jacob (1999) noted that air inversion may contribute substantially to the pollution problems experienced by an urban settlement, more so if that settlement happens to be located in a topographic trough like a valley. While this diurnal phenomenon is ubiquitous and detrimental to air quality, it is not a cause for urgent concern, because the period of its existence is comparatively small, the situation being alleviated next morning as the sun rises. In arctic and sub-arctic areas, however, the problem takes on different characteristics.

In the case of the high latitudes, i.e., the arctic and sub-arctic regions, solar radiation has to travel through a significantly larger thickness of the atmosphere before reaching the ground, and is incident on the ground at a larger angle. Both factors contribute to the paucity of its strength and effectiveness in supplying the primary heat to the ground. Also, in such regions, the length of time for which daylight is available in winter is less, and this contributes to a less effective heating of the ground. Cold winters in the high latitudes depress the temperature of the air and the ground to a considerable degree, exacerbating the problem. These factors, working in unison, create conditions that generate inverted layers of air not only during the night, but also during the day, with durations of several days at a stretch.

The city of Fairbanks, Alaska, located at 64.34°N, 147.87°W, is located in the high latitudes, and is situated in a valley. As such, the city experiences extremely cold climate, and inversion is common here during winter. Holty (1973) noted one such

instance at the Fairbanks international airport. The data was collected on December 17, 1969 at 2:00 PM, and is presented in Figure 2.2.
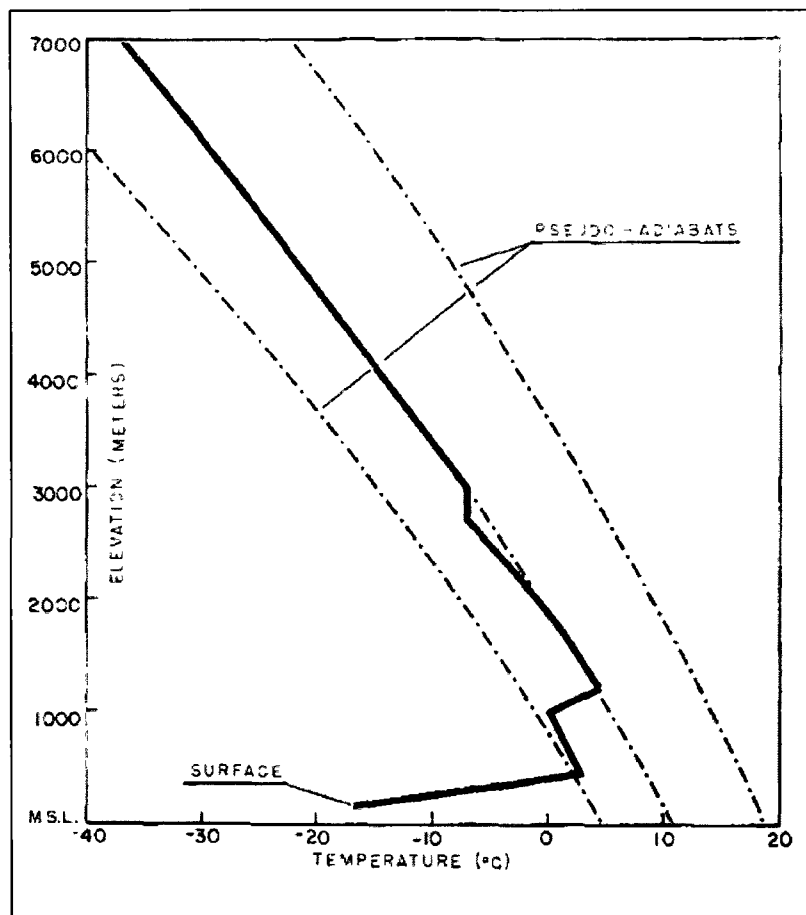
Figure 2.2: Temperature vs. Elevation at the Fairbanks International Airport on December 17, 1969 at 2:00 PM (Holty, 1973)

In Figure 2.2, it can be clearly seen that inversion took place entirely within the troposphere. Inversion started at the surface, presumably due to aforementioned reasons and the inversion cap extended upward for a little more than 1000 m. Moreover, this inverted column existed during the daytime, thus emphasizing the point that inversions in the arctic and sub-arctic regions are not limited to the diurnal movements of the earth around the sun. Holty also noted that during winter in Fairbanks, particularly under inverted caps of air, the CO and particulate

concentrations in the breathable layers of air have been found to exceed the (then) EPA standard by as much as five times. He also noted that lead aerosols have a much longer residence time in such cold air than is normally observed. It can be concluded that in arctic and sub-arctic areas, inverted air columns contribute significantly to the quality of air and pollution characteristics.

Hartmann and Wendler (2005) used the National Climatic Data Center Radiosonde Database, which has been recording radiosonde data from Fairbanks, twice daily starting in 1957, to analyze the trends in surface based inversion in Fairbanks from December 1957 to February 2004. They classified the data into 'surface inversion' and 'no surface inversion' cases; the 'no surface inversion' cases being those in which incident solar radiation lifts the surface inversion, but an elevated inversion may still be observed. They reported no appreciable trends in the overall frequency inversions for the entire winter. However, and month-wise breakdown of the data showed that, over the 47 years of data collected, the months of December and January had experienced a slight decrease in the frequency of inversion, while the month of February had experienced a slight increase. Hartmann and Wendler (2005) also determined the mean depth of the inversion as well as its mean temperature gradient of surface based inversion. Their findings are presented in Figures 2.3 and 2.4.
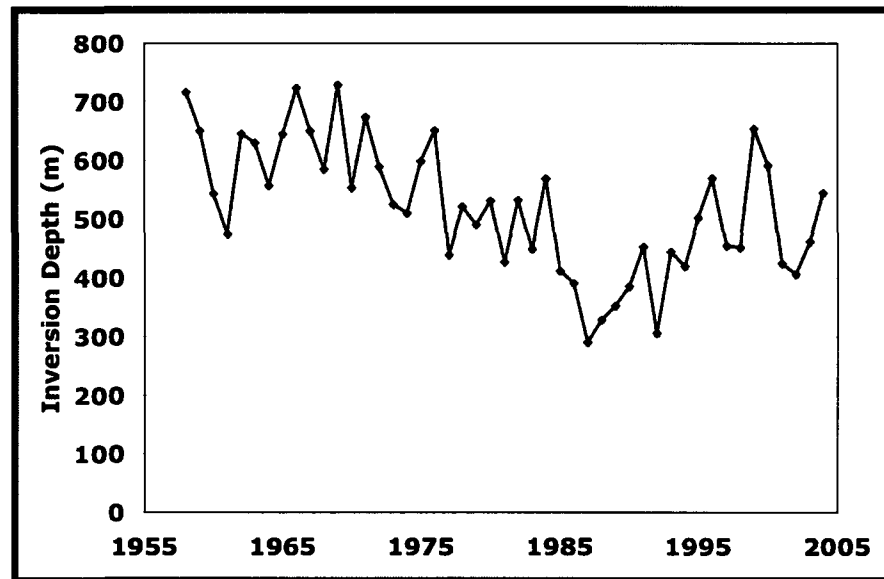
Figure 2.3: Time Series of Mean Surface-Based Inversion Depth over winter

(Hartmann and Wendler, 2005)
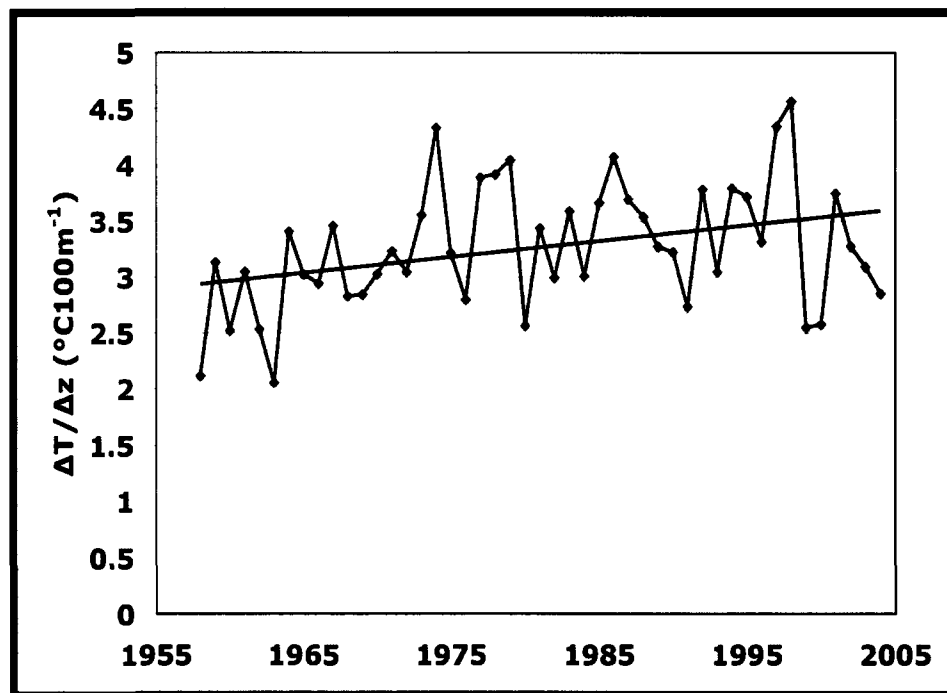
Figure 2.4: Time Series of Mean Temperature Gradient of the Surface-Based

Inversion (Hartmann and Wendler, 2005)

Hartmann and Wendler (2005) observed a decrease in the mean inversion depth of 212 m, as shown in Figure 2.4, They also observed an increase of 0.7° C/ 100 m in the mean temperature gradient of the inversion along its altitude. The trends identified by Hartmann and Wendler possibly suggest that since the depth of inversion is decreasing and the temperature gradient along that depth from the surface upwards is increasing, the difference in temperature between the surface and the top of the inversion layer may remain constant. This signifies that the strength of the inversion (larger the temperature gradient across the inverted layer, the stronger the inversion) may in future remain constant. At the same time however, the decrease in the depth of inversion signifies that the same strength of inversion occurs over a smaller altitude from the surface. The miscibility between the inverted layer of air and the layer overlying it depends on the strength of the inversion, more specifically, the difference in temperature between the top and the bottom of the inverted layer. Thus, a thin inverted layer could now possibly trap the same amount of the pollutants, without any increase in the miscibility characteristics. This occurrence would make the quality of breathable air at ground level progressively worse, contributing to the already acute pollution problem. Hartmann and Wendler also noted that the most common direction from which wind flows in the Fairbanks area during inverted conditions is the North-East quadrant.

Reichardt and Reidy (1980) studied the concentration of Polycyclic Aromatic Hydrocarbons (PAH) in Fairbanks over the winter of 1976-1977. They reported high values of PAH during the month of December 1976 to February 1977, and also found an increase in PAH concentrations with an increase in the strength of inversions. They characterized a strong inversion as one in which the temperature gradient is more than or equal to 7° C for the first 100 m altitude and a weak inversion as one in which the temperature gradient is less than 1° C for the first 100 m altitude, all readings being taken at 2:00 AM. It was found that during strong inversions, the measured PAH concentrations ranged from 15.8 – 154.7 ng/m^3, with a mean of 86.2 ng/m^3. During

weak inversion events, PAH concentration ranged from 8.9 ng/m^3 – 48.3 ng/m^3, with a mean of 25.0 ng/m^3. Thus, it can be clearly stated that trapping of pollutants within the inverted layer is more pronounced with strong inverted conditions.

More specific information on the effect of solar radiation in the initiation of atmospheric inversions and the resulting accumulation of pollutant concentrations was given by Bowling (Bowling, 1986). She listed all possibilities by which solar radiation can affect pollutant accumulation in the high latitudes. She observed that the total daily solar radiation incident on the ground might heat up the ground and destabilize the lower atmosphere. This effect would promote mixing within and between the layers of air superincumbent to the ground, and also lift the inversion cap due to the re-establishment of convection, thus aiding in the dispersion of the pollutants. The timing of the sunrise and the sunset as related to the diurnal variation in pollutant generation (e.g., morning and evening commuter traffic) may also play a part in pollutant accumulation. She noted that during peak winter in Fairbanks, the nighttime inversion remained strong during the morning peak traffic hour, was attenuated around noon, and was re-established before the evening commuter traffic began. Such characteristic of inversion had led to extremely high concentrations of CO (15 ppm or more) being recorded in Fairbanks. She also pointed out that the rate of change of incident solar radiation after sunrise and before sunset and the intensity and the wavelength distribution of the radiation around noon were also major contributing factors to pollutant dispersal or accumulation. She particularly noted the propensity of some pollutant molecules to dissociate photo-chemically in the presence of sunlight, thus transforming into less harmful substances.

It was also noted by Bowling that in many high-latitude areas, the presence of surface winds prevented the formation of strong inversion, although weaker inversion did still persist. However, Fairbanks is situated at a valley bottom, which imposes restrictions on wind movements. Also, wind movement in Fairbanks during winter is known to be weak, and fickle over both space and time. As a result, large eddies are not uncommon

over the Fairbanks valley. Such eddies, while aiding in dispersion, may be confined vertically by atmospheric stratification, and simply move the pollutants around within the same layer of air rather than mixing them vertically.

Dimitriev and Shadrin (1973) noted that apart from dust and individual species of gases (such as CO, CO_2, NOx and SOx), the chemical mix present in open-pit mines might react in the presence of an appropriate amount of solar radiation to form what is known as photochemical smog. The photochemical smog includes photochemical aerosol and toxic photo-oxidants like aldehydes, ketones, organic and nitrogen peroxides, ozone etcetera. Aerosols are known to cause respiratory and ocular problems. They also noted that the presence of strong solar radiation may assist chemical transformation of some species of contaminant molecules present in the open-pit. Such transformations may increase or decrease the noxious potency of the resultant molecules with respect to the original. The reactions are, however, strongly dependent on the concentrations of the reactant molecules. Photochemical smog is a markedly visible aberration from acceptable breathable air quality.

2.2.2. Air flow in open-pit mines

Natural air flow in open pit mines have been studied extensively in the former Soviet Union. Several researchers have thrown light on the mechanism of wind flow, along with a study of the factors that influenced such flow.

Belousov (1995) noted that because the air above the pit cooled slower than the air above the ground at the same altitude, there was a resultant horizontal flow of air toward the pit. He also noted that the air above the pit in such cases would rise due to the standard adiabatic process to a maximum height of :

$$H = \frac{\Delta t_h}{\gamma_a - \gamma} \qquad (2.1)$$

Where:

H is the maximum height air above the pit top can rise (m).

Δt_h is the horizontal temperature difference (degrees).

γ_a is the adiabatic vertical temperature gradient (degrees/m).

γ is the actual vertical temperature gradient (degrees/m).

This rise in the air could result in the removal and mixing of pollutants from the pit, provided the pollutants generated at the pit bottom reach the top layers of the air in the pit. In very cold climates, the movement of pollutants from the bottom to the top of the pit is severely restricted due to lack of energy in the bottom layers and possible inversion caps that may be in place. Belousov noted that it has been observed that the surface flow at the very top of the pit was coupled with flow from the surface adjacent to the mine, but could at the same time be decoupled from the mass of air at the bottom of the pit. Such decoupling and lack of energy in the bottom layers of the air in the pit will actively hinder removal of pollutants from the bottom of the pit, which is where most of the pollutants are generated. This necessitates an artificial ventilation scheme to introduce fresh air into the pit and remove pollutants from the lower reaches of the mine.

Belousov (1985) noted that the ventilation of open pit mines was affected by the fetch and the geometric attributes of the pit. The model scale chosen in their study was 1:1000. The study also used "air walls", which the author defined as a system of vanes or wings on the windward side of the model pit that are used to direct the natural flow of wind toward the pit-bottom. The author found that the removal of pollutants from the bottom of the mine was aided by the placement of such air walls. The removal of pollutants was also aided by the removal of ordinary waste dumps from the leeward-side of the mine, because such dumps increased the effective depth of the pit, decreasing the reach of either the turbulent or the laminar flow zones into the mine. The author has also reported a close agreement with observed results of velocity profiles in mines. However, the incident air velocity on the model that was used to solve this complex problem was much more in magnitude that could be reasonably supported. The model scale being 1:1000, the air velocity used for solving the problem

was roughly the same as the observed velocities in actual mines. It would be more reasonable to scale down the velocities used to numbers more representative of the scale in which the model was placed. Also, the author predefined the expansion angle of the air jet entering the mine (primarily on the basis of the wings placed on the windward side of the flow) to $\alpha = 15°$ (Belousov, 1989). This is schematically shown in Figure 2.5.
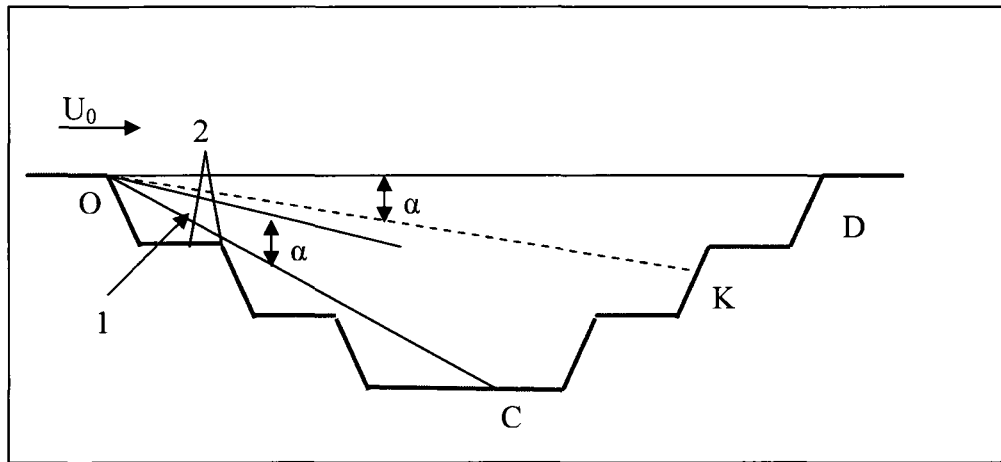
Figure 2.5: The angle of expansion of an air jet in an open-pit mine (modified from Belousov, 1989)

In figure 2.5,

α is the opening angle of the free plane (expansion of the jet), set at 15°.

1 indicates the position of the shield (wing).

2 indicates the position of the mast on to which the shield is attached.

U_0 is the incident velocity of wind across the pit in m/s.

Belousov (1989) regarded the presence of the vanes as an aid to the natural circulation occurring in mines. The author stated that in the absence of the vanes or shields, the air entering the pit with a velocity U_0, would directly ventilate the volume of the pit marked OKDO on the cross section in Figure 2.5. The section OCKO is ventilated by

recirculation. With the presence of the vanes, however, the lower boundary OK is moved downward, and converges with OC, thus ventilating almost the entire pit.

There are several problems with this approach. As described before, there is hardly any crosswind registered when capping inversions are in place, or in extremely cold weather, even without a capping inversion. This counters the possibility that such natural winds may be marshaled to aid in removal of pollutants. Setting of the angle α at 15° may also be erroneous, because the angle is influenced by several factors like the influent air velocity and direction, pit geometry, etcetera and may not be a constant for every open pit.

Peng and Lu (1995) constructed a 1:1000 scale model of a surface mine located in South China. Their study was focused on the movement and circulation of wind in deep open pit mines. An important part of their work comprised of conducting experiments to verify the results published by Belousov and others apropos of the angle α being set at 15°. They considered several variations of the angle α between 6° to 32°. They observe that the angle was not only influenced by the topography surrounding the mine, but also bore a linear relationship with the pit depth. They reported the relation to be:

$$\alpha = -1.234 + 0.0172H \qquad \text{(equation 2.2)}$$

Where,

α is the angle of expansion of the jet in degrees.

H is the height or depth of the pit in m.

They concluded that most of the pit would, under natural ventilation conditions, be ventilated by recirculation. In order to augment natural ventilation and recirculation, they used natural ventilation guides in the form of trumpet shaped air wall or vanes to simulate the venturi-effect. They reported that the recirculation area in the deeper

regions of the pit disappeared with the introduction of the vanes. This, however, had the same drawback described previously: with the absence of a crosswind, there was no possibility of natural circulation aiding in removal of pollution.

When the concept of the angle α is examined thoroughly, two significant problems can be noted. Firstly, the reach of the vane or wing system to influence the angle expansion may have been overestimated. All of the models described in the literature thus far cited have made use of scaled-down models. The problem with this approach lies in the nature of the interaction between the wind and the model environment. Turbulent or laminar air flow, when injected into a model space, would be influenced by the dimensions of that space. In a scaled-down model, the airflow would be shaped by a much smaller space in all three dimensions, thus restricting its movement and creating more turbulence, but on a smaller scale. This situation could be said to mirror actual occurrence in mines, but for two significant problems.

Many of the models used natural or near natural wind velocities as an input. This created a huge disparity in scales between the velocity and the volume on which it would work. Thus, the eddies and the recirculation zones that were formed in the models were grossly over-scaled. This meant that if an eddy was observed in the model, ascertain its location, approximate dimensions and area of influence, and then is scaled up according to the model scale, the resultant eddy would be one that would be very large and would never form under natural conditions, thus misrepresenting reality.

Additionally, when a scaled down model is used, there is very little or no control over the timescale on which processes take place in the model. For example, if a small source of gaseous pollutant is placed at a location in the model, the gas emitted from it will diffuse according to the diffusivity coefficient, which can be expressed dimensionally as $[L^2/T]$. This indicates that the gas, whether or not carried by convection, will travel at roughly the same rate in a model that it would in the natural

environment, with minor adjustments for temperature, pressure and concentration gradient.

The second significant problem with the application of the angle α lies in the nature of the resistance that inflowing air faces once it enters the pit. A detailed examination of the concept of α in the literature, along with the diagrammatic representations of the same, supports the assumption that the inflowing air would have a momentum sufficiently large to displace the existing air in the pit without much resultant compression on the inflowing air. The inflowing air would thus be able to flow wherever its momentum directs without any interference. This appears not to be the case in reality. The air toward the pit bottom is cooler, therefore denser, and contains pollutants in both gaseous and particulate form, resulting in that air having a high inertia. If the inflowing air does not have a sufficient velocity or mass, it would be quite possible that the inflow would be compressed and, on meeting a more massive and denser body of air, the path of its momentum will deflect. Such deflection, coupled with turbulent mixing, will induce the formation of recirculation or eddies in the upper reaches of the pit (where the inflow air comes in contact with the in situ air). These turbulences will destroy the linear motion of the inflow air assumed in the formulation of the angle α, mixing the sharply delineated boundary layers, and invalidating the angle as an indicator of ventilation.

Merony and Grainger (1992) studied the accumulation of gaseous and particulate contaminants in large basins and mining pits. To this end, they constructed a 1:600 scale model of a typical open-pit coal mine. Their focus was to study the dispersion pattern occurring in the presence of clearly defined and stable stratified zones in the atmosphere above the mine. Their modeling solution involved placing the scaled model of the mine on the roof of the Monash Environmental Wind Tunnel. They also placed vertically and horizontally spaced heating elements upwind from the mine, thus surmising that the flow of the wind, propelled by the fan in the wind tunnel, will pass over the heating elements in the model. This will heat the flow of air differentially and

will give rise to the stratification they aimed to study. The scaling of the flow was achieved by considering the Froude number for the scaled down mine and adjusting the gravitational component of the Froude number for temperature due to heating. They then proceeded to study the behavior and movement of contaminants in the pit by placing visible contaminant sources in the pit.

This approach can generate a multitude of problems. The approach to stratification taken by Merony and Grainger, i.e., preheating the air before it reaches the mine pit, presumably generates the stratified layers by addition of heat, while the air at the pit bottom, unaffected by the heat remains cooler. The heated air is then swept past the model pit by momentum imparted by the fan in the wind tunnel, which, with limited mingling with the air at the pit bottom, preserves the stratification. The momentum, otherwise expressed as the velocity head of the fan would have to be unrealistically high for the scaled down model (even with the Froude number adjustment), to achieve this. Thus the stratification enforced upon the model may in reality behave very differently, and the boundary layers between the dynamic and static layers of the wind-flow may not be what have been predicted by the model. Additionally, the scenario modeled here is rather unrealistic, and it can be safely posited that under very specific and rare circumstances would a flow of such warm wind with sufficient lateral velocity impinge upon the stable atmosphere of a mine pit during the night. The Froude number adjustment would, in this case, be difficult to make. The Froude number depends on the hydraulic length of the system, which in this case would amount to the length of the mine in the flow direction. As posited by the investigators, the full length of the mine profile is not in use by the flowing air as it does not affect the lower reaches of the pit. This fact, coupled with the observation that the boundary layer between the static and the dynamic layer of air is spatially variable, would indicate that the effective length for the Froude number would be significantly variable, and thus would be very difficult to evaluate.

Moreover, the placing of the scaled down model of the mine on the roof of the wind tunnel may cause additional problems. After heating, the flowing air is pushed on to the mine pit. Warm air, as is generally known, tends to rise. When on top of the pit, even with the momentum impetus, the air will tend to rise. In the present case, this rise will take it into the pit, rather than out of it. This will destabilize the very inverted layer that was the goal of the experimental setup. Contaminant transport would also be affected by this phenomenon. In the contaminant distribution contours shown in the investigation, it can be clearly noted that contaminant from sources placed on the down wind slope of the mine display a tendency to expand into the mine. This would only happen if the prevalent convection current is forcing the flow of the contaminant toward the bottom of the pit, which in this case is the place which the warmest air, escaping the imparted momentum would accumulate.

Fomin (1996) conducted a thorough investigation of the nature of convective flow in deep open-pit mines. The mathematical model generated during his investigation took into account various factors that affected the flow of air and contaminants in a mine in the absence of a forced convective system. A forced convective system could also include inflow of air into the mine by atmospheric convective processes. Thus the investigator assumed that there was no air flow in the vicinity of the mine and only convection from the heated walls of the pit imparted energy and therefore velocity to the wind. In the model, the contaminants (O_2, N_2, CO_2 and H_2O) are also injected into the pit uniformly from the sides and the bottom of the pit. This injection also carries heat into the model, as exhaust gases are hot. Fomin defines the Grashof number (for heat) as follows:-

$$G_{rq} = \frac{g\beta q h^4}{\lambda \upsilon^2}$$

(equation 2.3)

where,

g – acceleration due to gravity (m/s^2)

β – Volumetric expansion coefficient (1/°K)

q – heat flow due to exhaust gas (Joules)

h – depth of the pit (m)

λ – coefficient of thermal conductivity of air (W/mK)

v – kinematic viscosity coefficient of air (stokes)

He also defines the Grashof number for mass balance as follows:-

$$G_{rR} = \frac{\frac{gR_ih^4}{\rho D\upsilon^2}}{}$$
(equation 2.4)

where,

g – acceleration due to gravity (m/s^2)

R$_i$ – Rate of mass injection of a particular gas (i varies from 1 – 4 for the four

contaminants (kg/s)

h – depth of the pit (m)

ρ – density of the composite gas (assumed to be constant) (kg/m$^{3)}$

D – Diffusivity constant of the contaminant gas in air (m^2/s)

v – kinematic viscosity coefficient of air (stokes)

The Grashof number is a measure of the ratio of the buoyant forces to the viscous forces in a natural convection situation. In this case, however, the investigator has fixed the depth (h) of the model to 500 m or 600 m. This means that the buoyant force experienced by any quantum of air will always be the same as if it were at the bottom of the pit. The buoyant force will decrease as the air moves up in altitude (considering an adiabatic system). Therefore, the ratio of the buoyant force in the Grashof number

is exaggerated, and will result in dramatic upward convective velocities. This is probably the reason why the model results show a vertical chimney effect at the center of the model. The boundary conditions and the initial conditions used by Fomin are standard and often used. He considers the pit walls to be impermeable to mass or momentum and the pit top and sides to be open boundaries. This gives the freedom to establish (convection permitting) a quasi-laminar flow state in the model and simplifies the flow patterns vastly. He observed that the air seemed to roll down the sides of the hot walls of the pit before being taken upwards at the center of the pit by upward convective flows. He explained that while it could naturally be expected for the hot injected gas to rise immediately, after a certain time period, the convected heat is conveyed beyond the horizon of the mine and a stable convection current is established. This creates the vertical convective column that draws all air from the vicinity along the contour. He uses several temperature gradients upward from the floor of the mine, so that the temperature on the vertical axis increases with height, which effectively establishes an inversion cap on the system. This, along with a fixed pit-bottom temperature, ensure that the convective column is established and stable. The force of convection upwards, however, is not only controlled by the heat injection, but also by the momentum balance of the buoyant air, which is exaggerated.

Aloyan et al. (1982) proposed a scheme to solve the flow of air into a mining pit. The scheme of equations solved take into account not only the mass and momentum balance equations that would be solved in the normal course of such a solution, but also takes into account external planetary parameters like the Coriolis force. The effects of temperature and the stratification of the air above the pit due to it, the effects of pressure and contours of the pit are also taken into account. They also take into account the external sources of heat into the system, whether artificial or natural, e.g., solar radiation. Pollutant sources are placed in the model to account for the generation or inflow of pollutants in the model. The system of equations is then solved using a technique called the use of "fictitious" regions in the model space. In this technique,

the irregular topography of the actual mine can be approximated as a set of rectangular parallelepipeds. The mass and momentum equations can then be re-specified for the new boundaries that are generated. The regions of the mine that are compliments to the parallelepiped are then simply continuations of the same boundary and domain conditions as the approximated rectangle. This system brings forth a generalized model that can theoretically be applied to any mine topography and thus is very adaptable. The numerical experiments that the investigators conducted threw light on the correlation between the ventilable depth of an open-pit with respect to the average magnitude and directions of surface wind flow, the behavior of contaminants under different thermal conditions, and an estimate of the time it would take to ventilate the pit after a major pollutant dispersion event occurred, for example, a blast. Very little data is presented from the experimental results. The results that were presented indicated that the escape of pollutants from the pit was directly proportional to the velocity of the influent air. But, at high influent velocities, the lower regions of the pit will be affected by turbulence, and the contaminants would be subject to remixing with the local air, thus altering their concentrations and possibly chemistry. This turbulent zone mixing should be clearly visible in contaminant contours. The data presented, however, showed no sign of turbulent mixing, even with high velocities of 16 m/s, and contours drawn indicated laminar, stratified flow.

The same lack of turbulent mixing was observed in the work of Baklanov (1984). A scheme very similar to Aloyan et al. (1982) has been used in this work. Aloyan et al.'s model was further complicated by the addition of any given number of contaminant components. Each of these contaminants could be modeled with respect to their specific characteristics. The boundary conditions employed stated that the contaminant started with a background value within the pit, after which the injection of pollutants inside the pit and the convection resulting from the mass and momentum balance equation for the flow changed the concentration values in the model space. The top of the pit was capped with a concentration gradient equal to zero, which implied that any

contaminant mass reaching the top boundary would encounter no further concentration gradient and would not be taken any farther. This boundary condition was specified by:-

$$\frac{\partial \vec{c}}{\partial z} = 0 \quad , \text{at } z = H$$

(equation 2.5)

where,

c – concentration vector field (mols/m^3)

H – the height of the model from the pit-bottom to the top boundary (m)

The concentration values at the Cartesian X and Y extremities of the model were set to the original background concentration. The application of the concentration gradient limit on any boundary of the model may give rise to a problem. If the concentration gradient is zero, it implies that the mass will not have any impetus to travel beyond that boundary due to lack of a favorable concentration gradient, unless it is convected. Such convection would be the only way to take mass out of the system. Since, in these models, such atmospheric boundaries are normally considered to be no-slip walls from the flow mechanics point of view, chances of such forced convection are minimal. This means that for lack of movement, the mass coming into contact with the boundary may accumulate at the boundary, and, if a high enough boundary concentration is achieved, will try to diffuse back into the model space, even against the flow gradient.

The next section describes several solution approaches that have been tried to model the flow of air in open pits under inversion and solve the problem of pollutant accumulation in the open pit.

2.2.3. Ventilation Approaches

There have been several approaches used to ventilate open pit mines in the Soviet Union. Baklanov and Rigina (1993) have presented their research on the application of cascade ventilation to the dilution of contaminants in large, open pit mines. A number of different open pit ventilation configurations were simulated using numerical models. The majority of the models were executed under conditions of atmospheric inversion with no wind. In their study, pits ranging from 420-750 m in depth were modeled. Ventilation configurations ranging from 2-7 units were simulated during the study. The only cascade ventilation system that was effectively able to remove contaminants from the pit was a system of seven units applied to a pit of 450 m in depth. The power consumption for this scenario was 3.4×105 kW. The authors of the study concluded that cascade ventilation was not an effective means of ventilating open pits. No specific details were given as to the construction of the numerical models used in their study or the assumptions made in applying the cascading ventilation systems to the models.

Belousov (1990) discussed how improved ventilation in open pit mines could be achieved by the installation of "aerodynamic foils" (i.e., wings) on the windward side of open pits. The author conducted 210 wind tunnel tests with a 1:1000 scale model of an open pit coupled with an aerodynamic foil. Mathematical relationships were developed from the wind tunnel tests that related the required geometrical parameters of the wing to wind speed and the dimensions of the open pit. The author suggested that additional benefits could be realized by combining aerodynamic foils with combinations of fans and pipes located in the pit. The author claimed that "when wings are installed with optimal parameters, virtually the entire pit is ventilated by direct flow." The effectiveness of this technique requires, of course, that a constant wind of suitable velocity is flowing over the open pit.

Belousov (1995) has also discussed yet another approach to ventilate an open pit mine, and examined the ventilation of open pits due to thermodynamic processes (i.e.,

temperature differences.) This form of air exchange is referred to as "breeze circulation." In open pit mines, breeze circulation tends to develop naturally in warm months when there is a temperature gradient between the center and the edges of the pit. In cold months, this temperature gradient trends towards zero, and breeze circulation typically is not present.

The author has developed mathematical relationships for the development of stable breeze circulation based upon thermodynamic first principles. Relationships have been developed for both circular and elongated pits. The magnitude of breeze circulation was greater in elongated pits for the same initial conditions than it was for circular pits. The relationships developed by the author showed that stable breeze circulation could develop when a temperature gradient of 5-10°C was present. The efficiency of this circulation could be improved by "turbulizing" the flow via the installation of air vanes above the pit.

2.2.4. Summary of the Literature Review

- From the literature reviewed, it can be clearly seen that the air inversion phenomenon is very complex. Most of the papers reviewed here discuss only a few aspects of the natural phenomena that contribute to air inversion in general. Literature available on open-pit ventilation is sparse, most of the work having been done in the former Soviet Union. Most of these results are not publicly available.

- The interrelations among the parameters in the ventilation of an open pit under inversion are very complex. A comprehensive study of these parameters and their interrelationships would encompass many fields such as meteorology, pit geometry, solar radiation, exhaust gas potential of the working equipment, air temperature profile in the mine and close atmospheric monitoring in the mine pit. Mathematical models of air flow, boundary layer phenomena, exhaust air quality and the transport of the gaseous pollutants from the equipment exhaust,

among others, are integral components of planning the ventilation of an open pit mine.

- All the models discussed above have assumed the characteristic of flow to be turbulent and often used the hydrostatic approximation, without consideration of compressibility. This supposes that the model space has a-priori knowledge of the flow. The air flow in an open pit mine is a complex phenomenon, and may have laminar, quasi-laminar and turbulent flows coexisting within the same space.

2.3. Data for Model

As described in the previous section, several factors such as the boundary layer and the temperature affect the inversion cap in arctic open pit mines. This chapter presents the data that have been collected for the model. In cases, only representative data is presented, while the rest are presented in the Appendix. The data and information presented here have been directly utilized in the development of the two-dimensional and the three dimensional models. Other information presented here pertains to the physics of the flow that describes the behavior of air under different physical conditions, and these equations are programmed into the model.

In order to successfully develop the model of an open pit ventilation problem, the model must have relevant and realistic boundary and initial conditions. The model space must also be modeled to emulate the behavior of the actual geometry. The initial and boundary conditions required for the model can be both atmospheric, topographic and those pertaining to mining operations (pertaining to the engines of operating equipment). Thus, the first and the third categories of data provide the initial and the boundary conditions necessary to develop and execute the model. The second category of information presented here, that of the physical equations describing the behavior of air under different conditions, simulates the behavior of air in the actual mine under consideration.

The meteorological inputs needed to determine the contaminant concentration are the wind speed and direction as a function of time at one height, the nocturnal temperature inversion characteristics at sunrise, the heating rate of the pit atmosphere after sunrise, and the turbulent eddy diffusivities as function of atmospheric stability. The wind speed and direction observations at one height will be used to determine the advection term.

Among others, the following information has been collected during the CFD model building phases:

1. Mean diurnal wind velocity (mean values for each month);
2. Number of calm days, their distribution both daily and monthly, the mean and maximum duration of clam weather;
3. Number of foggy days according to the months and their duration (Mean and Maximum);
4. Mean monthly humidity of the atmospheric air (for the warm period of the year);
5. Duration of the period with freezing soil temperature (below 0 deg. C);
6. Mean monthly air temperature with absolute maxima and minima.
7. Sources of air pollution, volume and rate of contaminants for each point source.
8. Air inversion frequencies and durations.
9. Air Quality values during air inversions, and required standards that need to be met.
10. Waste heat and engine exhaust data from the working equipment in the mine.

These data, collected in close cooperation with the management of the selected mine, are presented below.

2.3.1. Data for the Atmospheric conditions around the Mine

Most of the data presented in this section was collected from the NOAA weather station codenamed "CLRA2". Since there is no weather station data from the mine premises, the data from the NOAA station is the only indication of the true values of the atmospheric variables in the area. Moreover, validation of the model was done using the 2004 – 2005 pit geometry of the selected open-pit. Historical data for that period is only available through NOAA. The relative location of the station to the mine is shown in Figure 2.6.
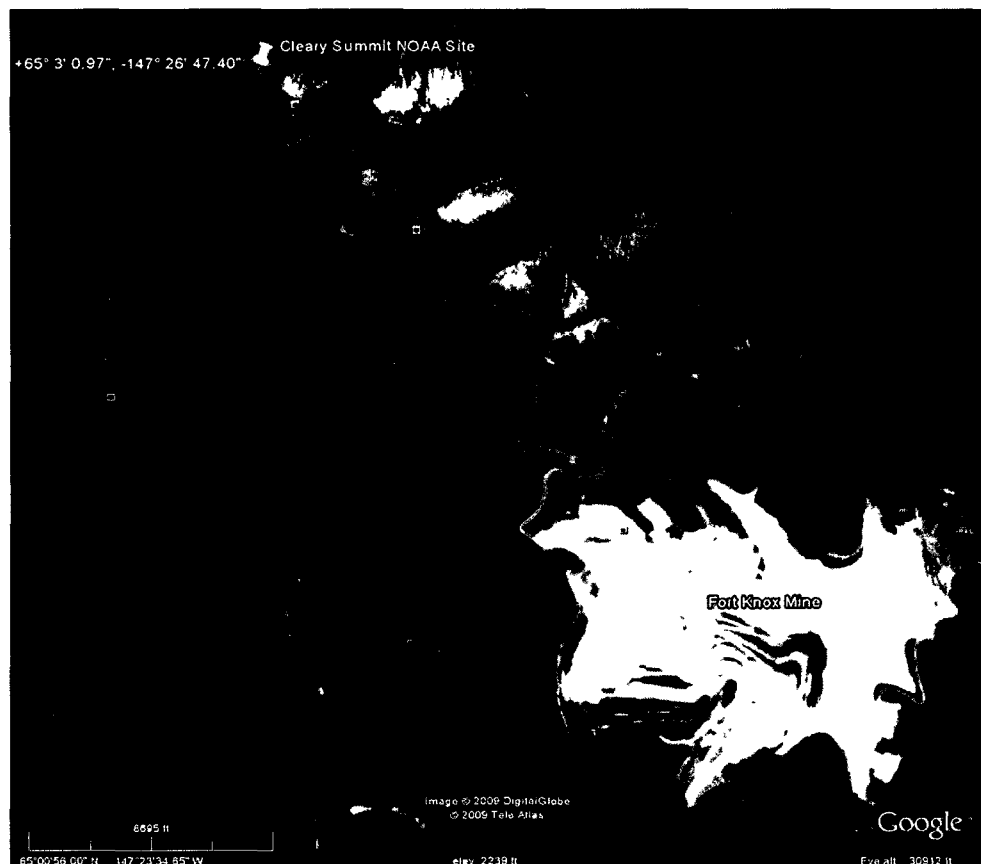
Figure 2.6: Location of the Cleary Summit Weather Site (CLRA2)

The station is identified as the Cleary Summit Weather site on Steese Highway. It is located at Latitude 65.05027 N and Longitude 147.44650 W. While the location of the

site does not provide adequate proximity to the selected open-pit, thus compromising the data for variables like wind direction. It is, however, located at close proximity to the mine to provide a reasonable estimate of the various atmospheric conditions that affect the mine microclimate and thus the dispersion of contaminants within the open-pit.

The atmospheric data were collected for the period of time between November 2004 and February 2005, as the selected open-pit geometry for model validation is based on the 2004-2005 open-pit geometry. Only a representative sample of the data, for November 2004, is presented below.
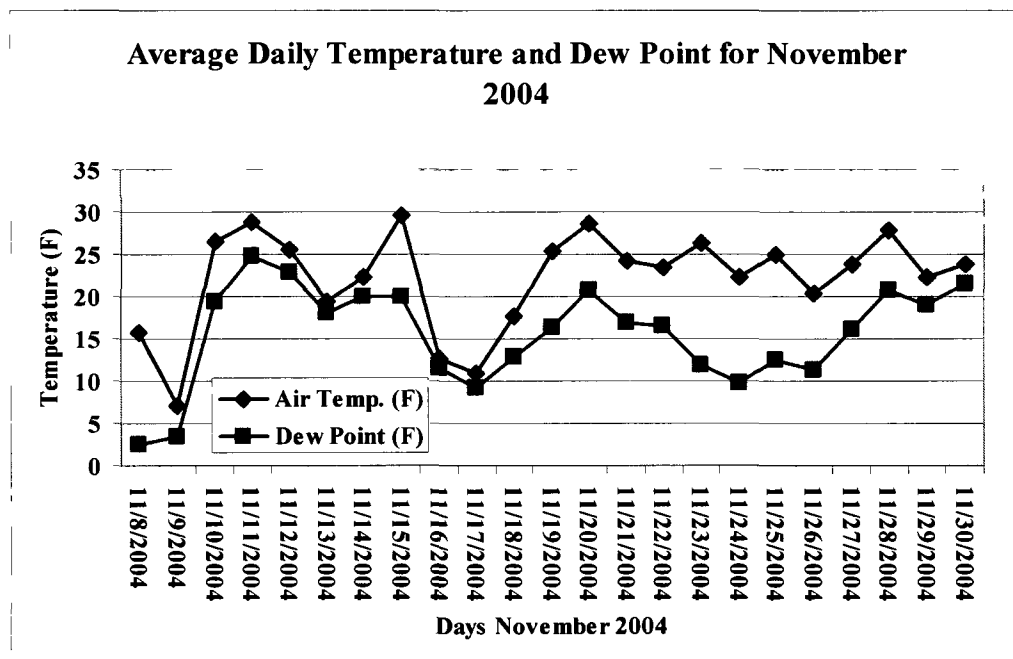
Figure 2.7: Average Daily Temperature and Dew Point for November 2004
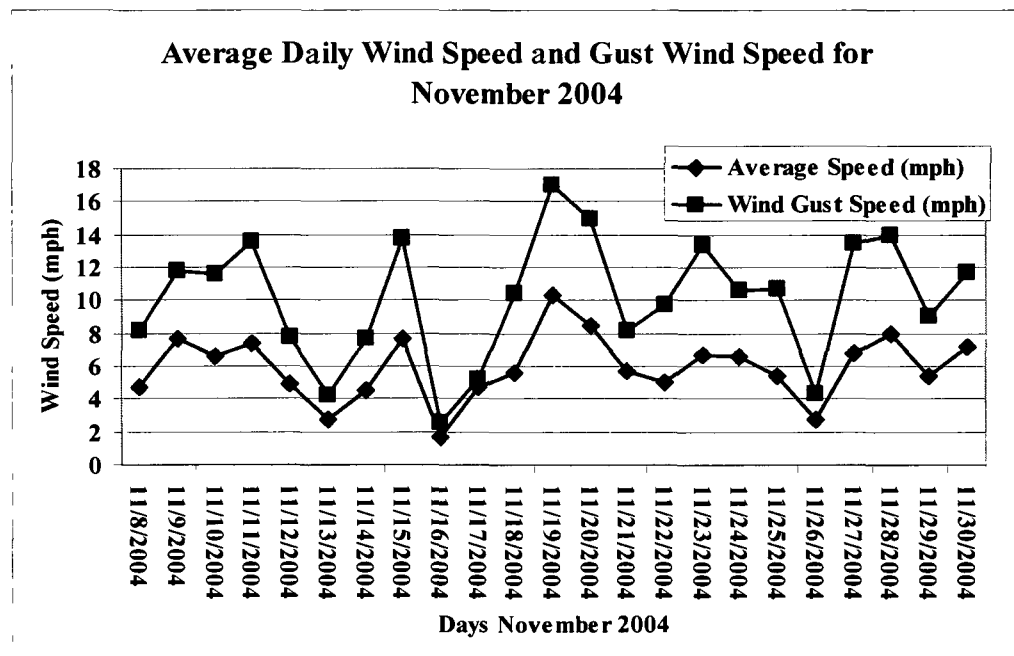
Figure 2.8: Average Daily Wind Speed and Gust Wind Speed for November 2004
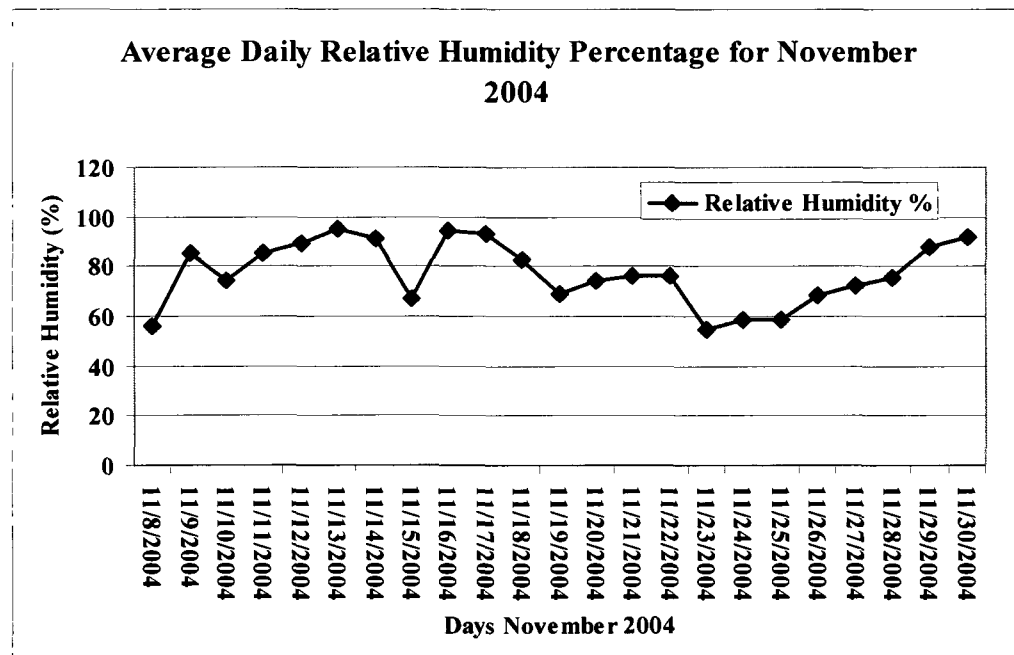
Figure 2.9: Average Daily Relative Humidity Percentage for November 2004

Average Daily Pressure for November 2004
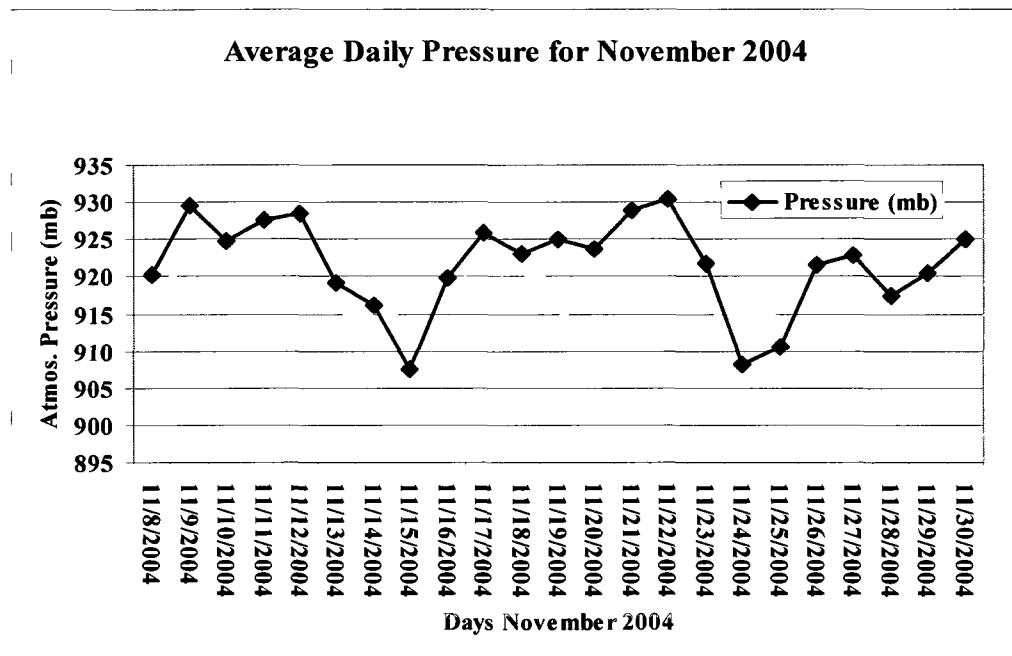
Figure 2.10: Average Daily Pressure for November 2004

Histogram of Wind Direction for November 2004
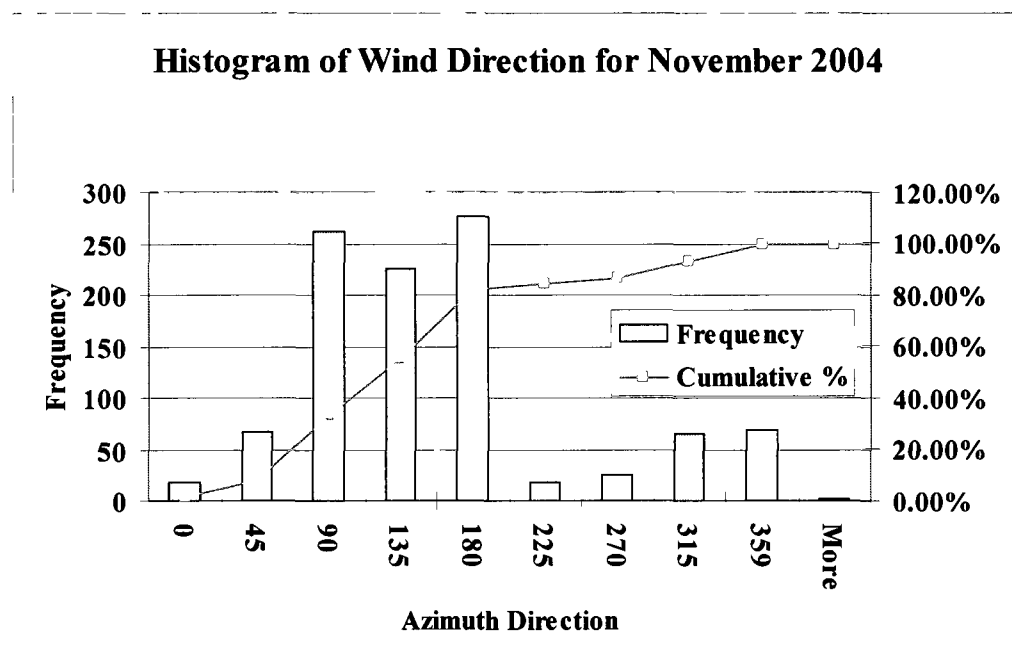
Figure 2.11: Histogram of Wind Direction for November 2004

Histogram of Gust Wind Direction for November 2004
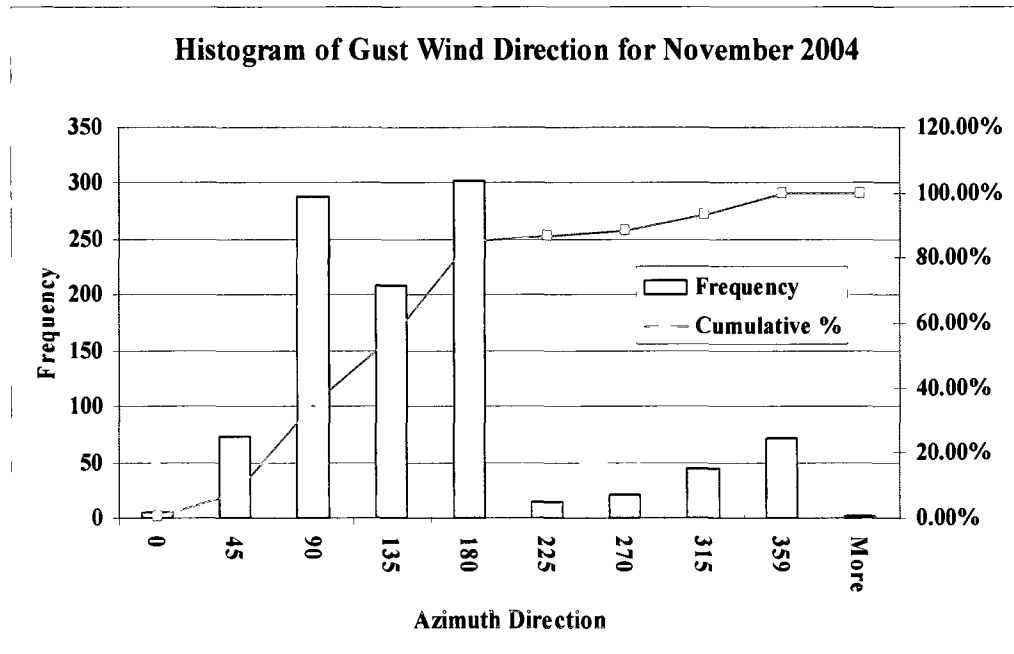
Figure 2.12: Histogram of Gust Wind Direction for November 2004

Another important atmospheric factor that effects the dispersion of contaminants within the mine is the amount of solar radiation that the mine environment receives. The solar radiation is obviously only received during daylight hours. The duration of the daylight hours for November 2004 to February 2005 are presented below (Source: www.timeanddate.com).
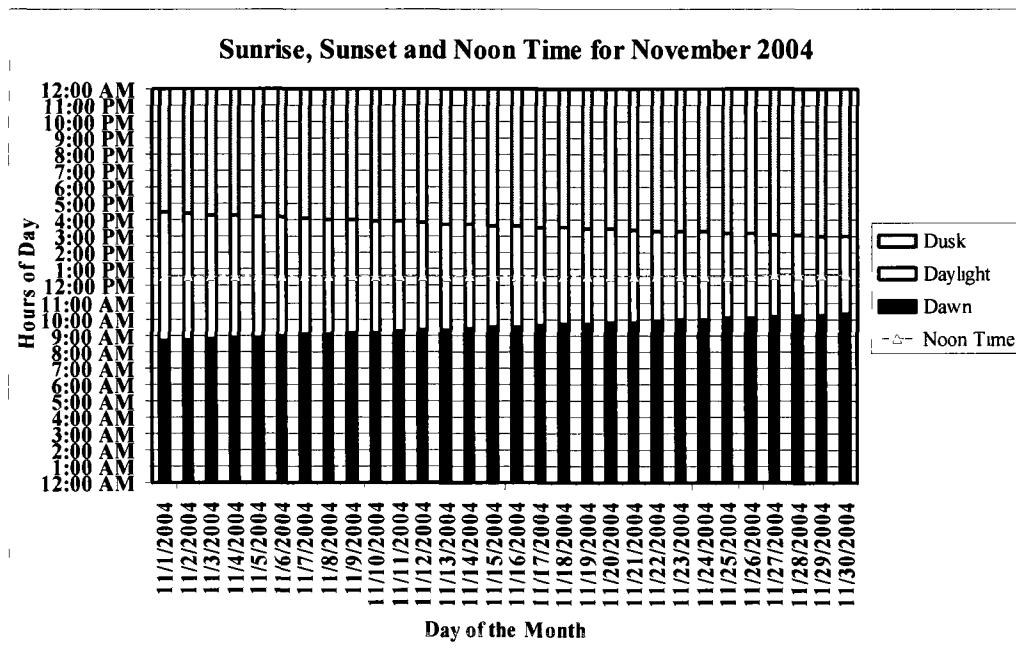
Figure 2.13: Sunrise, Sunset and Noon Time for November 2004
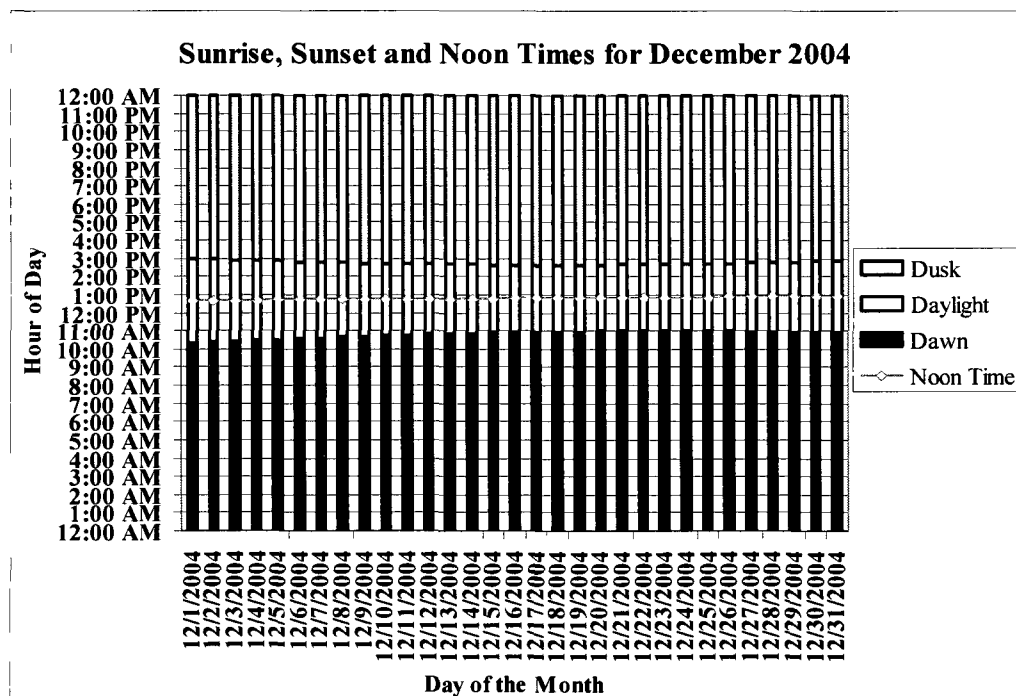
Figure 2.14: Sunrise, Sunset and Noon Time for December 2004

Sunrise, Sunset and Noon Times for January 2005
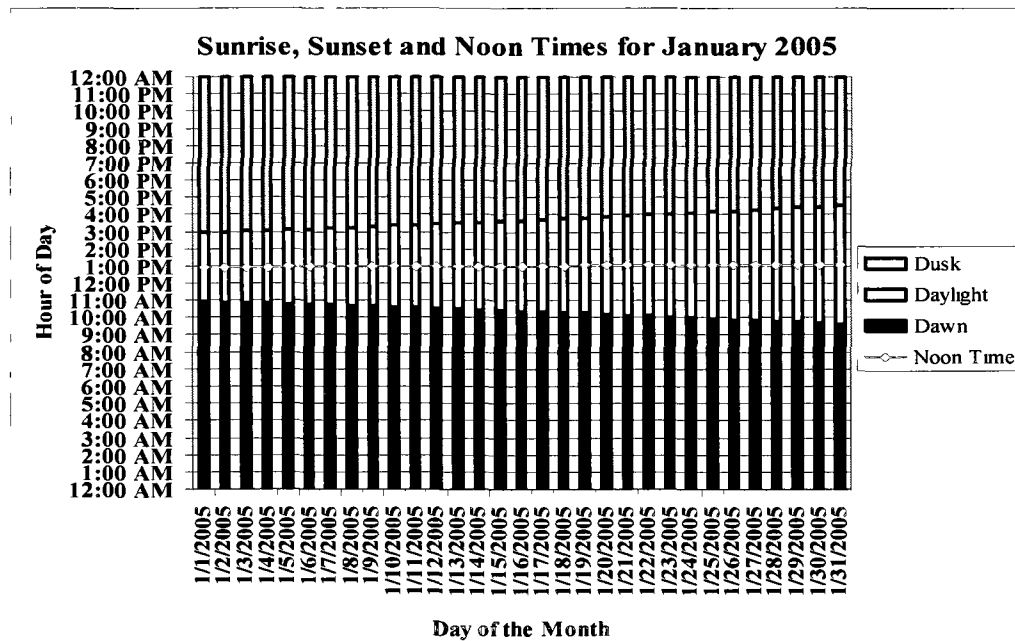
Figure 2.15: Sunrise, Sunset and Noon Time for January 2005

Sunrise, Sunset and Noon Times for February 2005
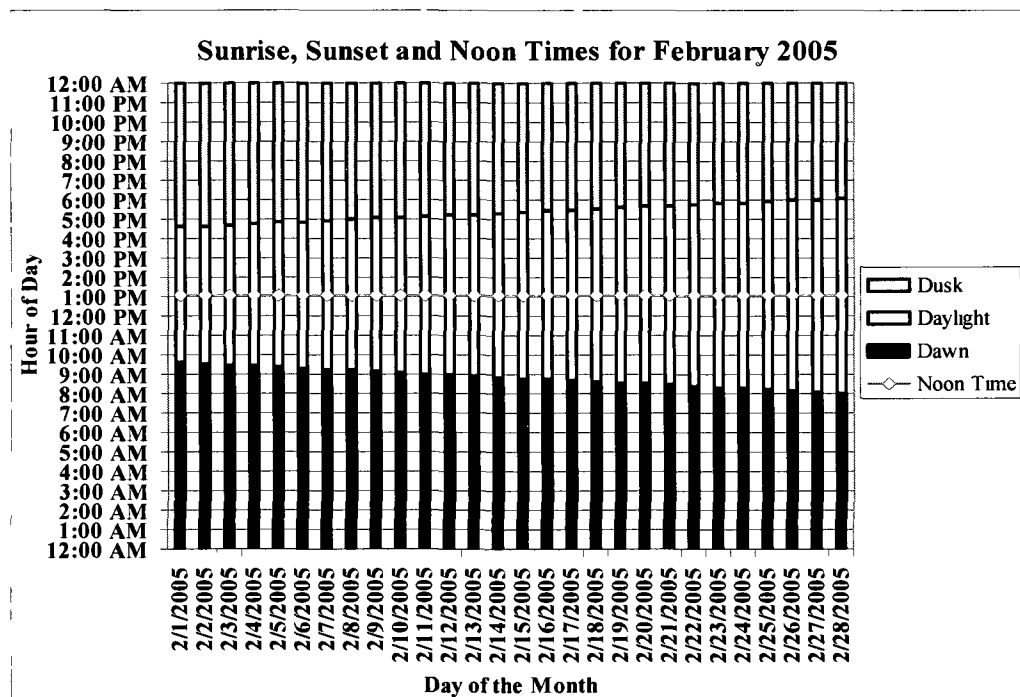
Figure 2.16: Sunrise, Sunset and Noon Time for February 2005

Figures 2.13 to 2.16 present the time for which the sun irradiates the area around the mine. However, the intensity of the solar radiation does not remain the same throughout the day. In order to neutralize these diurnal variations, an average daily value for individual months are taken. If an average daily value of the solar radiation for a single month (e.g. October) is considered, it can be easily seen that only a horizontal surface would receive the full extent of this radiation. Any surface that is not horizontal, would receive only a component of the total radiation. The received component of the radiation will also vary according to the orientation of the surface with respect to azimuth direction. The National Renewable Energy Laboratory has published a comprehensive guide to the amount of received solar radiation for all major population centers in the U.S., including for Fairbanks AK. Table 2.1 presents this data.

Table 2.1a: Average Incident Solar Radiation for Fairbanks AK, Jan - Jun (All Numbers in BTU/Sq. ft./day)

Orientation		Jan	Feb	Mar	Apr	May	Jun
Horiz.	**Global**	38	240	720	1270	1610	1780
	Std. Dev.	4	18	49	94	99	134
	Min.	32	220	570	1030	1430	1490
	Max.	44	290	810	1470	1820	2010
	Diffuse	26	140	360	640	770	900
Clear Day	**Global**	44	260	810	1580	2190	2500
North	**Global**	16	87	230	410	610	750
	Diffuse	16	87	230	390	500	590
Clear Day	**Global**	19	73	180	370	710	1000
East	**Global**	46	230	620	970	1190	1210
	Diffuse	20	120	310	520	620	690
Clear Day	**Global**	86	340	830	1380	1720	1870
South	**Global**	240	740	1280	1380	1290	1230
	Diffuse	60	240	440	600	650	700
Clear Day	**Global**	500	1250	1890	2030	1870	1780
West	**Global**	47	240	620	950	1080	1180
	Diffuse	21	120	310	520	620	700
Clear Day	**Global**	86	340	830	1380	1720	1870

Table 2.1b: Average Incident Solar Radiation for Fairbanks AK, Jul - Dec (All Numbers in BTU/Sq. ft./day)

Orientation		Jul	Aug	Sep	Oct	Nov	Dec	Year
Horiz.	Global	1630	1190	720	300	83	5	800
	Std. Dev.	122	81	76	23	7	2	26
	Min.	1300	1020	570	250	73	3	750
	Max.	1840	1350	920	340	98	6	860
	Diffuse	840	660	400	210	58	3	420
Clear Day	Global	2320	1730	1000	390	79	6	1080
North	Global	650	430	240	120	340	1	300
	Diffuse	540	400	240	120	34	1	260
Clear Day	Global	840	460	220	100	29	0	340
East	Global	1090	810	550	240	84	11	590
	Diffuse	630	480	310	150	45	2	330
Clear Day	Global	1770	1440	960	460	130	25	920
South	Global	1180	1060	940	590	350	94	860
	Diffuse	660	540	390	240	110	5	390
Clear Day	Global	1790	1870	1860	1430	680	240	1430
West	Global	1090	850	560	250	85	11	580
	Diffuse	650	500	310	150	45	2	330
Clear Day	Global	1770	1440	960	460	130	25	920

In Table 2.1, the surface denoted by "Horiz." is a horizontal surface, "Clear Day" denotes readings on a cloudless day, and "North", "East", "South" and "West" denote vertical surfaces facing those directions respectively.

Figures 2.17 to 2.21 present the incident solar radiation for the city of Fairbanks over the period of a year, for surfaces that are either horizontal, or vertical surfaces facing north, south, east and west.
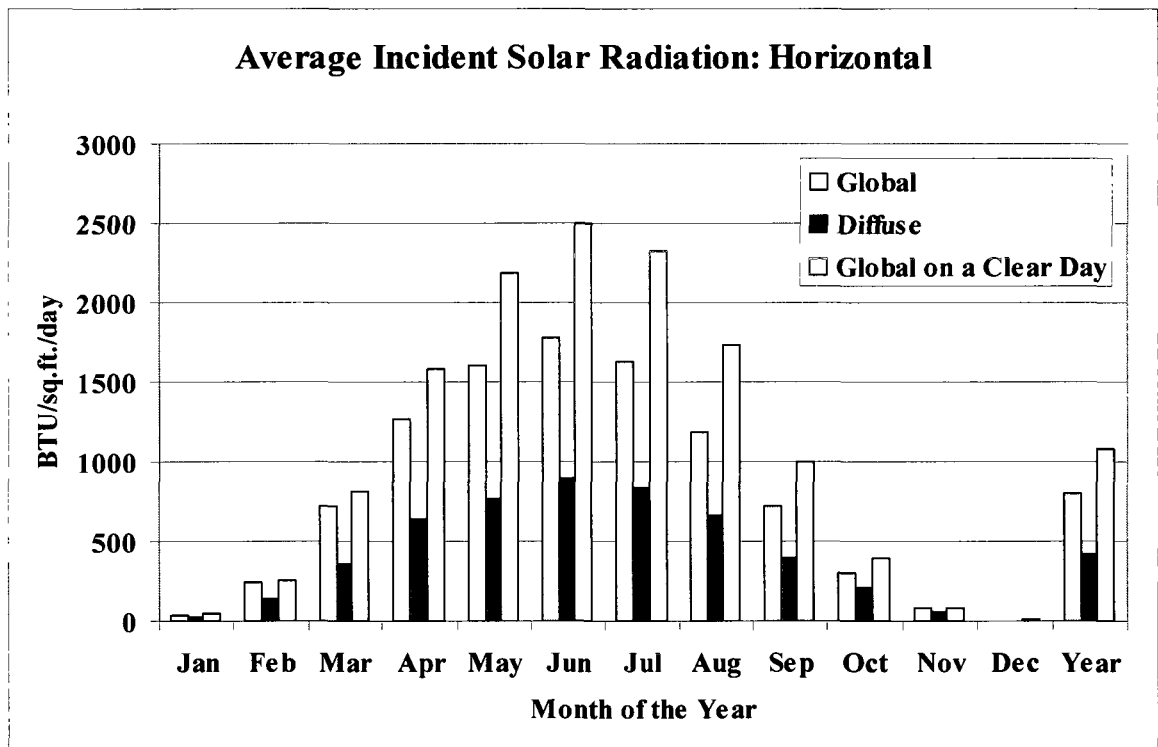
Figure 2.17: Average Incident Solar Radiation for Fairbanks AK for a horizontal surface
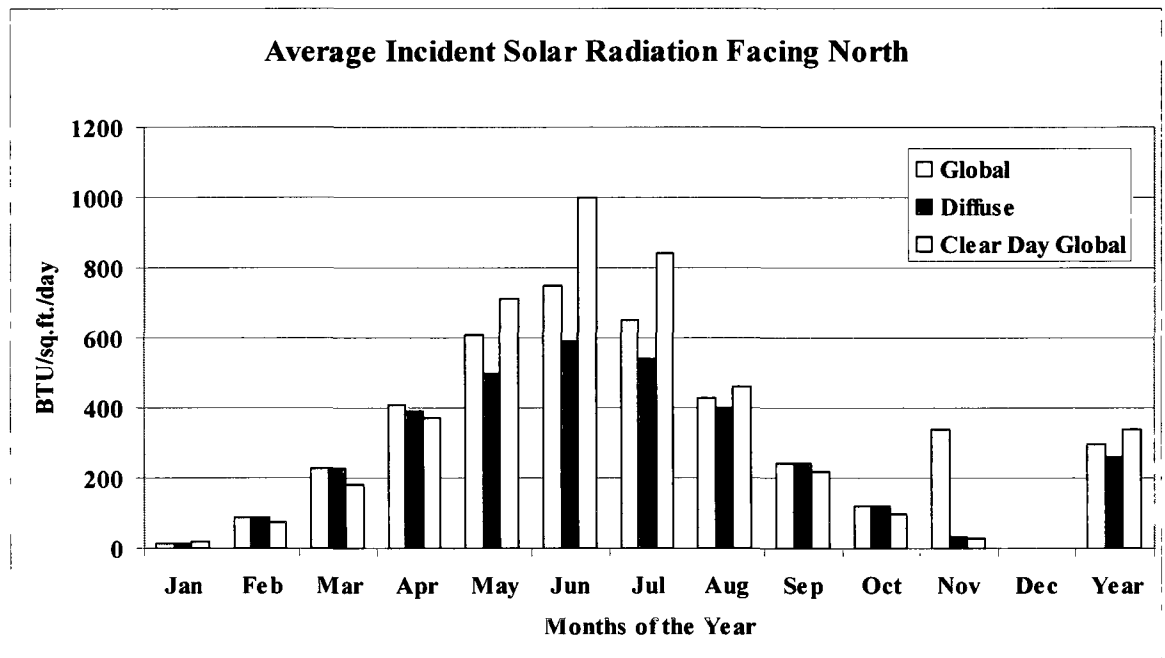
Figure 2.18: Average Incident Solar Radiation for Fairbanks AK for a vertical surface facing North

Average Incident Solar Radiation Facing South
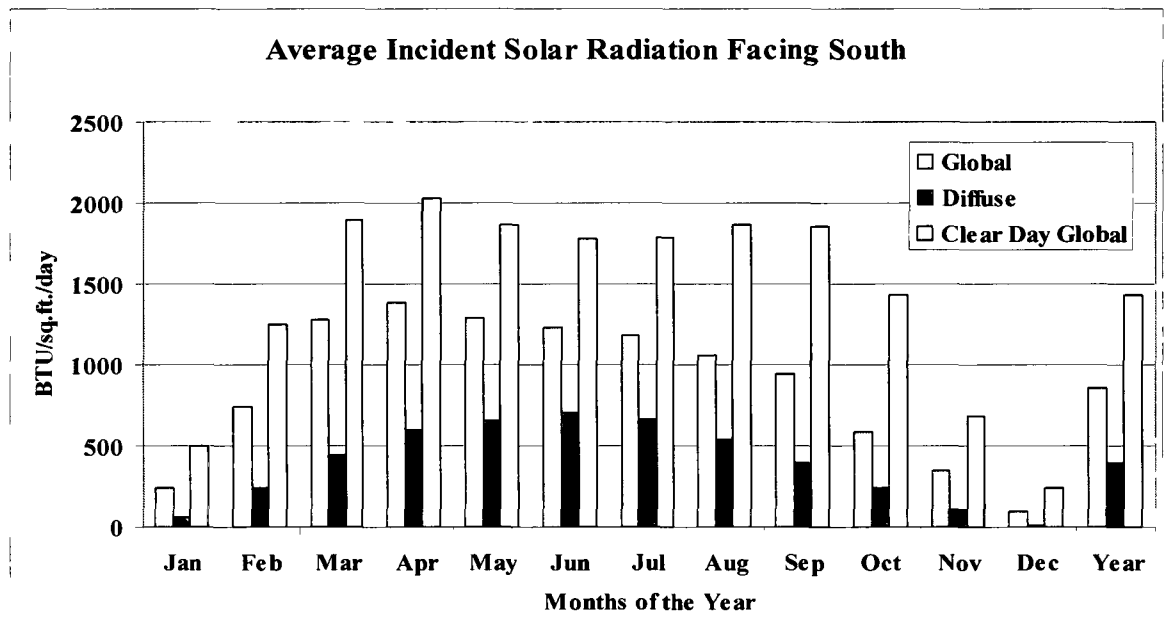
Figure 2.19: Average Incident Solar Radiation for Fairbanks AK for a vertical surface facing South

Average Incident Solar Radiation Facing East
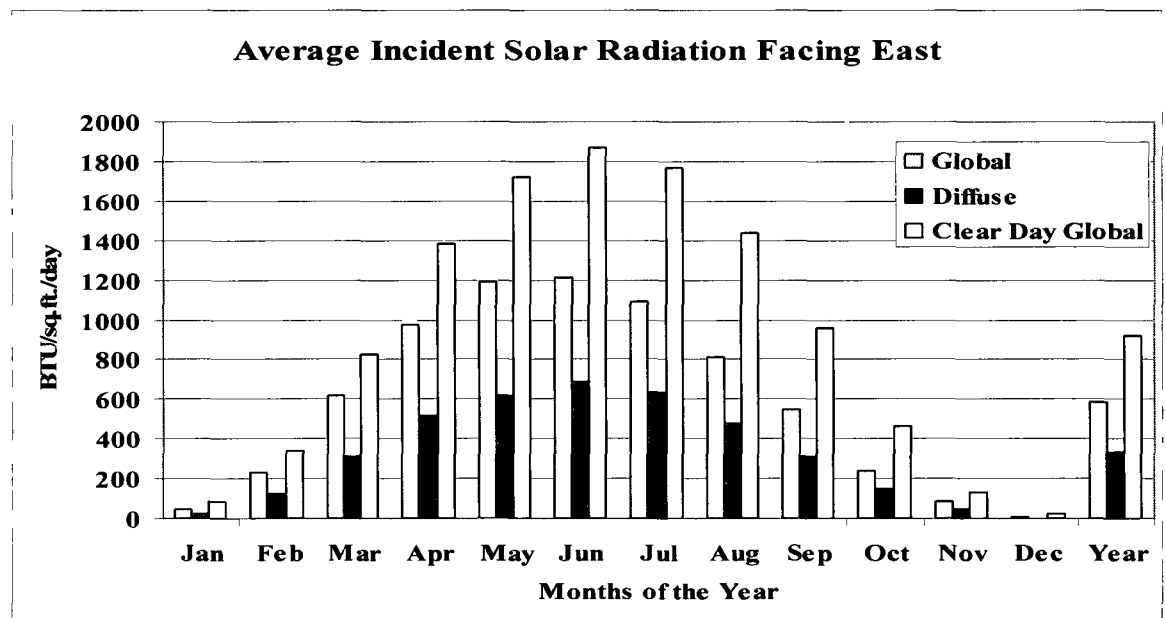
Figure 2.20: Average Incident Solar Radiation for Fairbanks AK for a vertical surface facing East
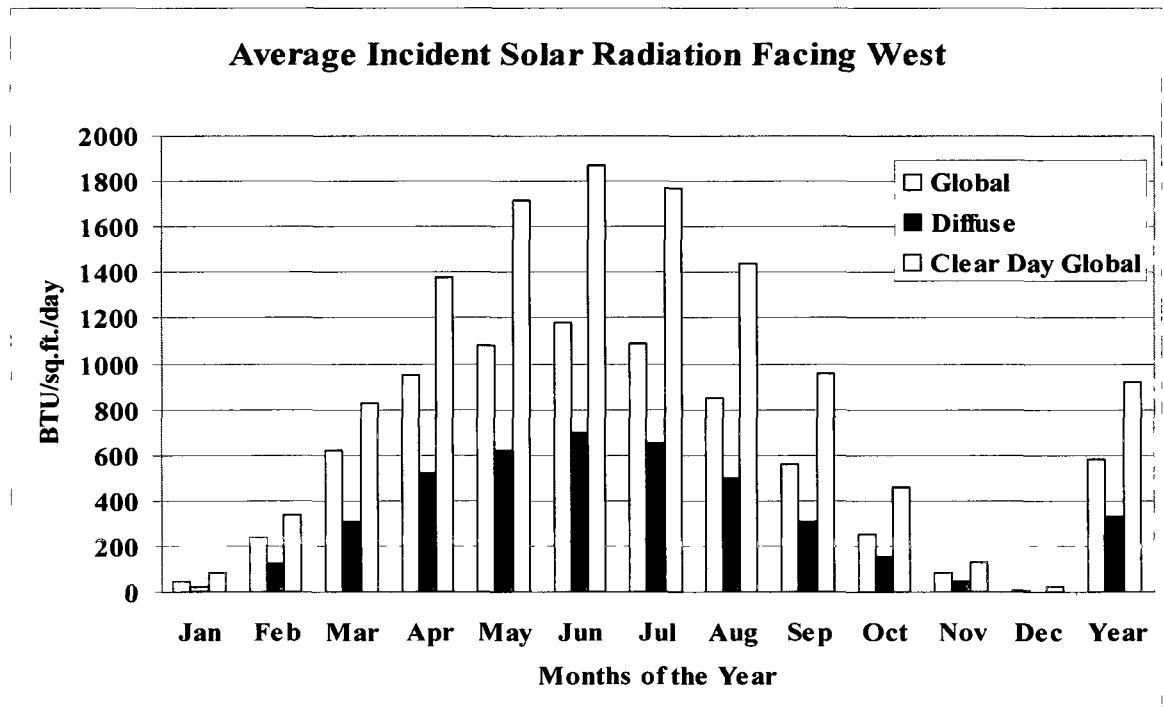
Figure 2.21: Average Incident Solar Radiation for Fairbanks AK for a vertical surface facing West

This concludes the presentation of the data collected for atmospheric conditions in the area where the selected mine is located. In the next section, the details of the numerical model have been presented and discussed.

2.3.2. Properties of Air

The model space used to solve the problem of gaseous contaminant dispersion in open-pit mines undergoes a significant variation of temperature. Certain properties of air, e.g., specific heat and thermal conductivity, vary according to temperature.. The relationships between the properties of air and temperature are presented in this section. This information was collected through personal communication (J. Ierardi, personal communication, August 14, 2009).

Specific Heat of Air vs. Temperature

c_p = 1.9327E-10*T^4 - 7.9999E-07*T^3 + 1.1407E-03*T^2 - 4.4890E-01*T + 1.0575E+03

R^2 = 0.99961
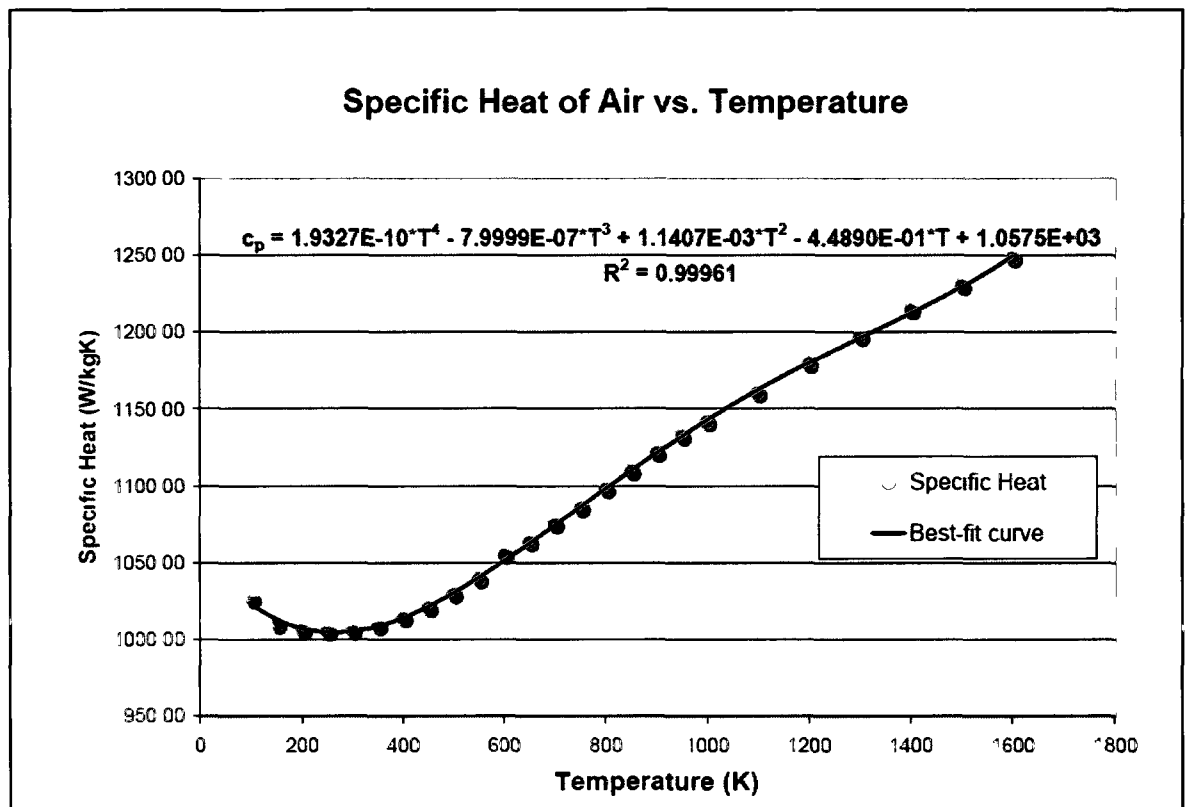
Figure 2.22: Change in Specific Heat of Air with change in Temperature (Ierardi, J.A., 2009)

The equation in figure 2.22 is presented here:

$$C_p = 1.9327 \times 10^{-10} T^4 - 7.9999 \times 10^{-7} T^3 + 1.1407 \times 10^{-3} T^2 - 4.489 \times 10^{-1} T + 1.0575 \times 10^3$$

........(equation 2.6)

Where,

C_p is the specific heat capacity of air (W/kg.K)

T is the absolute temperature of air in Kelvin
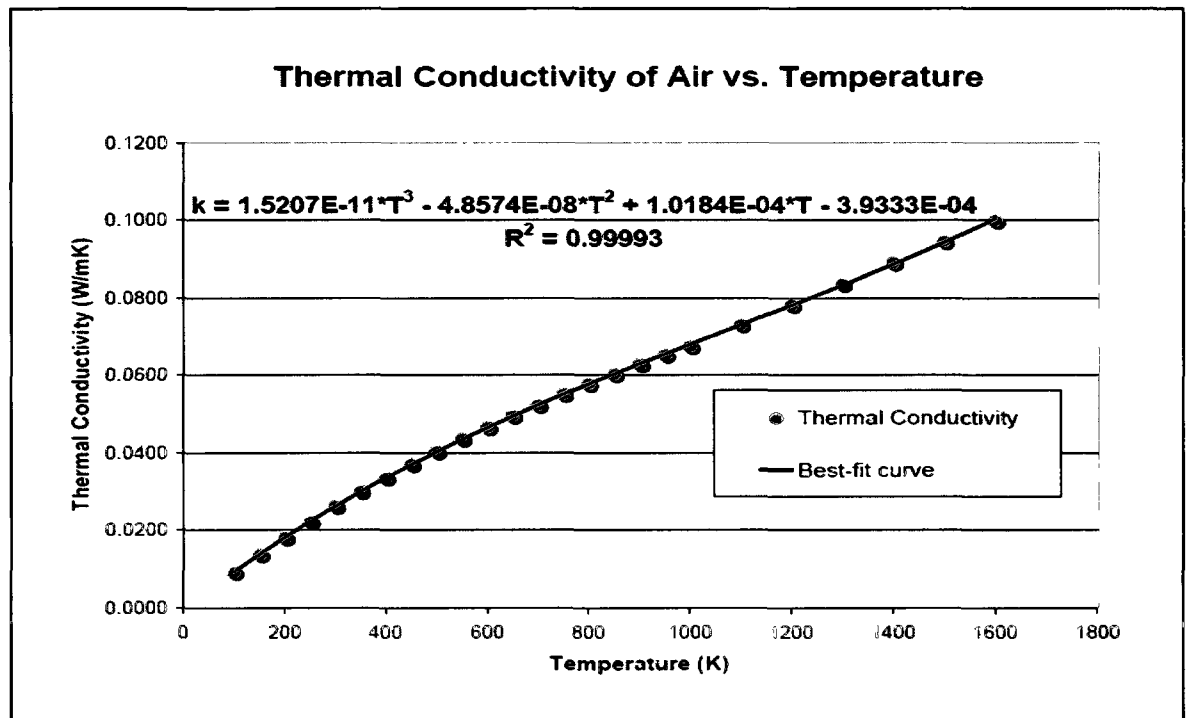
Figure 2.23: Change in Thermal Conductivity of Air with change in Temperature

(Ierardi, J.A., 2009)

The equation in figure 2.18 is presented here:

$$k = 1.5207 \times 10^{-11} T^3 - 4.8574 \times 10^{-8} T^2 + 1.0184 \times 10^{-4} T - 3.9333 \times 10^{-4}$$

(equation 2.7)

Where,

k is the thermal conductivity of air (W/m.K)

T is the absolute temperature of air in Kelvin
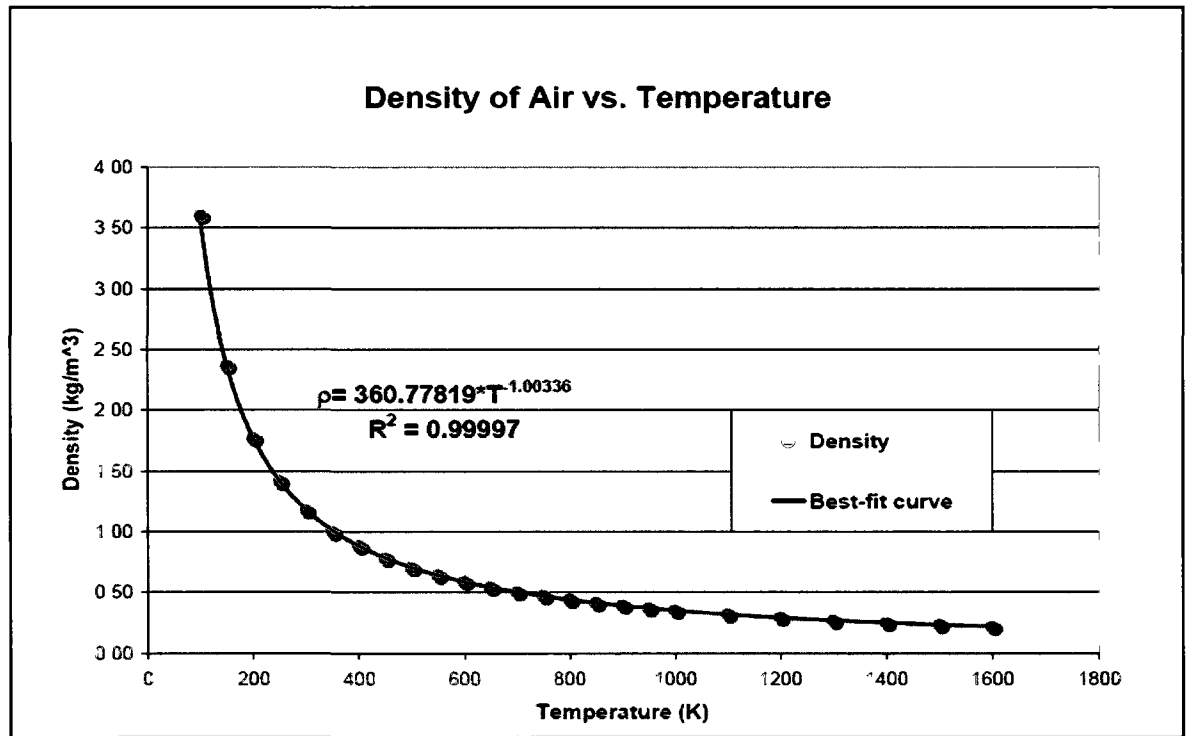
Figure 2.24: Change in the Density of Air with change in Temperature (Ierardi, J.A., 2009)

The equation in figure 2.19 is presented here:

$$\rho = 360.77819T^{-1.00336}$$ (equation 2.8)

Where,

ρ is the density of air (kg/m^3)

T is the absolute temperature of air in Kelvin

The equations 2.6 to 2.8 are programmed directly into the model to allow the critical property values for air in the model space to be directly calculated as a function of the temperature. Obviously, the incompressibility assumption negates the use of equation 2.8. The next section presents the data gathered on operating equipment in the mine.

2.3.3. Equipment Data from the Mine

This section presents the equipment data collected from the mine. Primarily, the number and type of the operating equipment in the mine, their exhaust characteristics, and their fuel consumption were collected. Table 2.2 presents the number and type of equipment (in terms of their operating engines) that are usually in place during production.

Table 2.2: Number and Types of Equipment Engines Operating in the Mine

Type	Number
CAT 3508	4
CAT 3512	10
CAT 3516	9
CAT 3126	2
CAT 3116	1
CAT 3412	1
CUMMINS KTA19	6
CUMMINS KT38	1
CUMMINS M11	7
HITACHI S16R	2
CAT C10	2

The column denoting "Type" in Table 2.2 denotes the type of engines that operate in the mine, and the next column denotes the number of equipment that are powered by a given engine.

Fuel consumption and emissions data for all the engine types presented in Table 2.2 were not available from the respective manufacturers. The following figures present the aforementioned data (as far as available). The values presented are at a peak load.

Fuel Consumption Rate for Different Engines
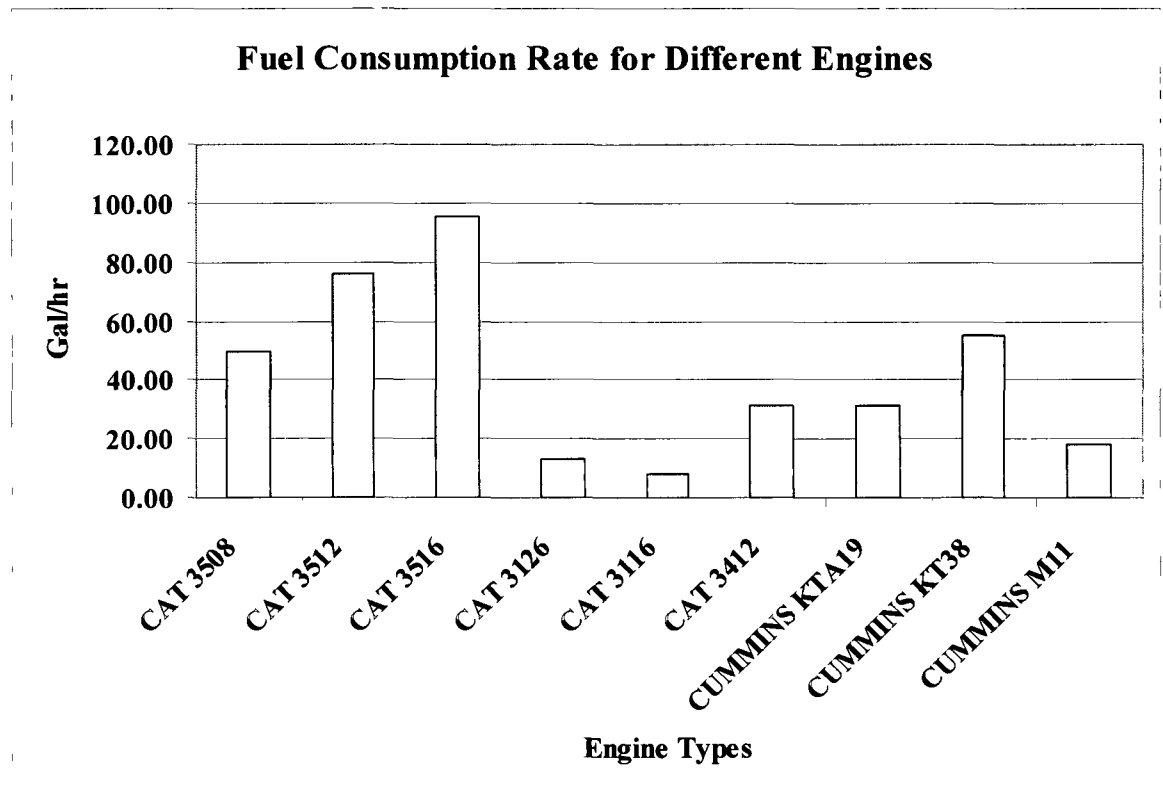
Figure 2.25: Fuel Consumption rates for Operating Engines in the Mine

About 60% of the fuel consumed by these engines does not translate to any useful work for the machine, and the energy generated from this fraction of the fuel is lost as waste heat. This is the waste heat from the engines which add to the thermal input into the mine environment. The figures for the waste heat are presented in figure 2.26.

Waste Heat from Engines
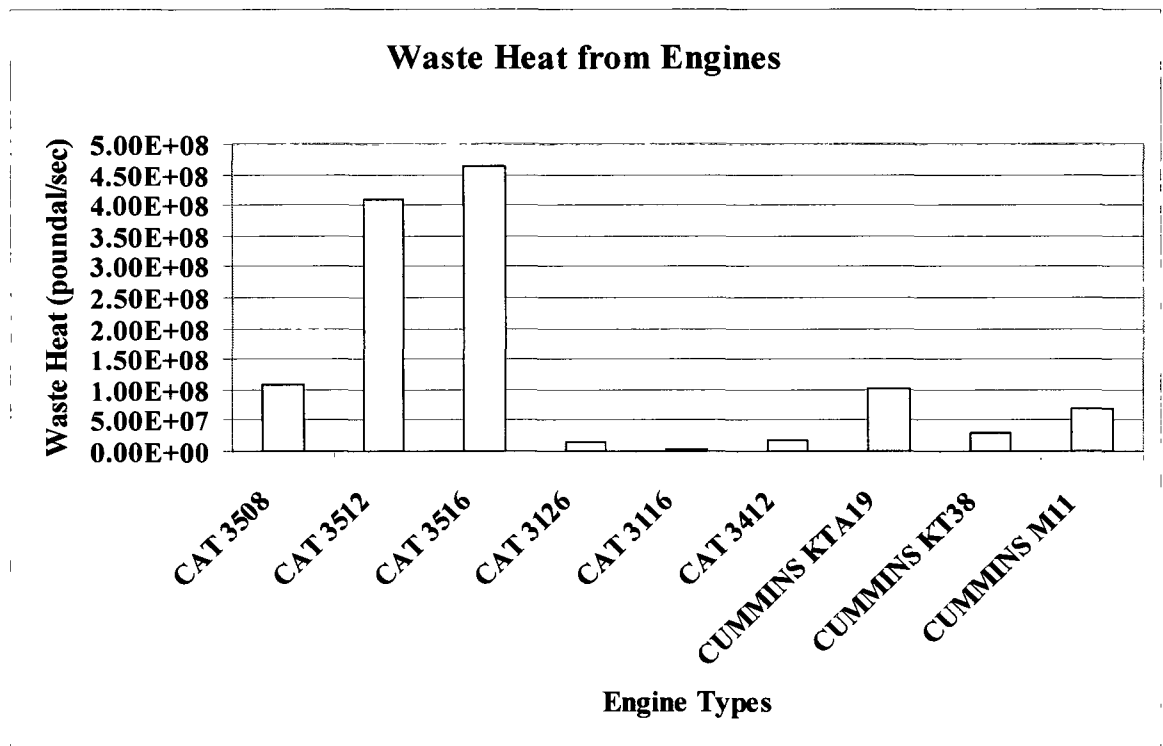
Figure 2.26: Waste Heat from Operating Engines in the Mine

It is extremely difficult to acquire reliable data for the emission characteristics for most industrial engines. Shah et al. (2006) and Huai et al. (2006) provided a comprehensive review of the engine emissions based on engine types. This data, as far as relevant to the engines operating in the mine, are presented in Figure 2.27.
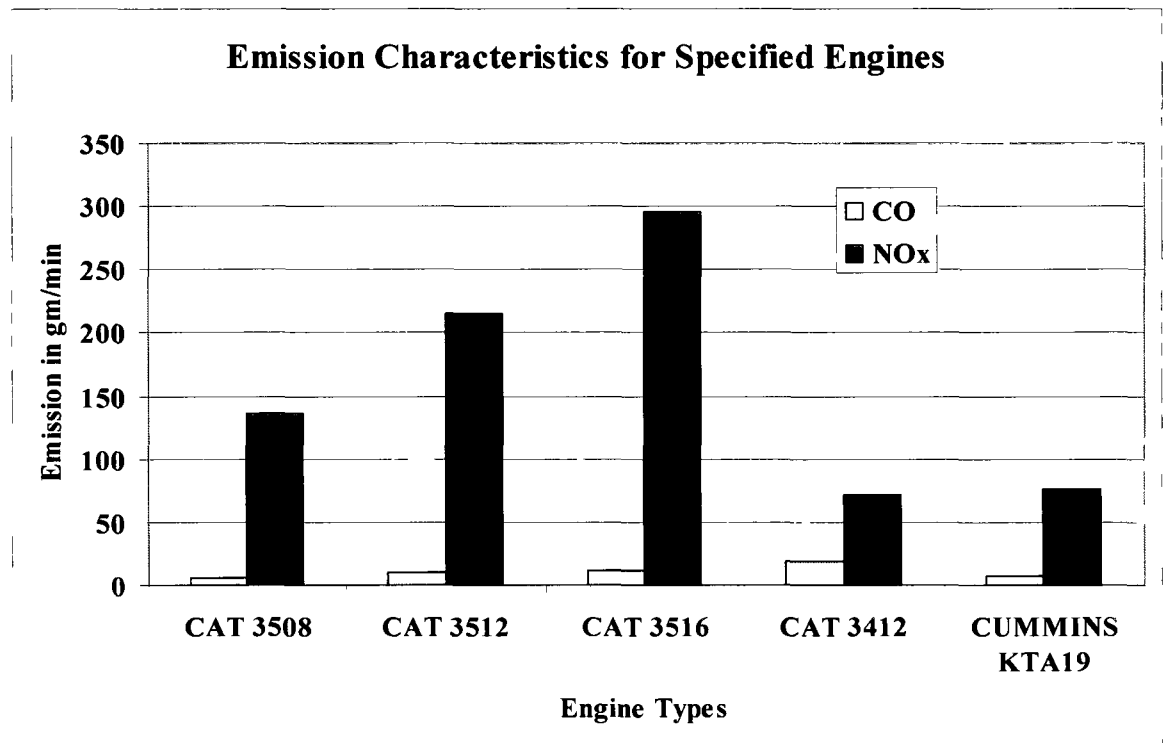
Figure 2.27: Emission Data for Various Engines

The next chapter discusses in detail the development, simulation and results of a two-dimensional model.

CHAPTER III: A Two-dimensional Model for Transport of Gaseous Pollutants in an Arctic Open-Pit Mine

3.1. Introduction

In this chapter, the development of a two-dimensional (2D) model is presented. The two-dimensional model is a longitudinal section of an idealized open pit, such that the selected longitudinal section is aligned with the flow of air in the pit. A large number of Computational Fluid Dynamics (CFD) programs such as Fluent, COMSOL® etcetera are commercially available for solving CFD problems. In this thesis, COMSOL® was used to simulate the air flow in the model pit with the requisite heat and pollutant addition, and the pollutant transportation in the pit under air inversion was simulated.

3.2. Assumptions for the Two-dimensional Model

A two-dimensional model can provide useful preliminary understanding in solving complex aerodynamic and heat transfer problems. A real system is, however, best represented by a three-dimensional (3D) model with a geometry that closely resembles the actual system. Such models, however, are computationally expensive and due to their complexity, the models may encounter convergence problems. In complex flow problems through symmetric geometries, the efficacy of 2D models in particular is an important attribute. 2D models help provide high-fidelity solutions to complex problems while maintaining computational economy. Also, in the case of flow problems over or through symmetric, integrated geometries (e.g. aerofoils), the 2D model provides easy and accurate solutions.

However, there are differences that exist in the inherent characteristics of a 2D and a 3D models. Most of these differences arise out of the fact that the 2D space lacks the third dimension, which modifies the balance of energy and mass. Accordingly, appropriate assumptions are made for the 2D models. These assumptions are useful in rendering a 2D model to closely simulate an actual 3D space. It is, however,

recognized that the flow of energy and mass are altered to such an extent that the results obtained in the process cannot be reasonably assumed to be accurate representations of a 3D model. Some of the assumptions and characterizations made for the particular model presented in this chapter are discussed below.

- A two-dimensional (2D) model has a length and a height, and lacks the third dimension, i.e., width. In most CFD software, including COMSOL®, the width of a 2D model is assumed to be one unit of length.

- The 2D model is aligned with the air flow direction in the selected open pit mine. Due to the lack of a third dimension, a 2D model can only accommodate flow along either its length or height.

- For Open pit mines with complex geometry and topography during a clam day the radiation and thermal budget of a surface can strongly effect dispersion of pollutants in the pit. Many ventilation models for open pit mines do not pay much attention to this. The effect of large incidence angles of the slope/wall in the open pit was also considered. Besides orientation and incidence, the radiation budget also depends on the fluxes of its various components.

- The sources of pollutants in the 2D model are placed along the floor of the mine. This brings the pollutant sources in direct alignment with the air flow direction, which may not be the case in the mine in-situ.

- It is assumed that the air in the 2D model space is incompressible. Mathematically, the assumption is expressed in terms of constant density of the fluid. Air does not vary in density significantly over the range of temperature (about 7 °F) and pressure (negligible) normally encountered in open-pit mines. Air is highly compressible and its density varies with significant changes in temperature and pressure. Data from the selected mine has shown that the difference in temperature between the rim and the pit bottom of the mine, with constant pressure, does not result in any significant difference in density of the air in the mine. Therefore, it seems to be a

reasonable assumption for the model to regard the density of air as constant, and the flow as incompressible.

- The initial atmospheric pressure in the 2D model is taken to be a constant (14.4 psi). This pressure is taken as the constant initial pressure throughout the model space. The pressure of 14.4 psia is recorded at the Fairbanks International Airport, and is considered the mean atmospheric pressure at Fairbanks. While the pressure at the mine could be slightly different from that pressure, no reliable data are available, and the depth of the pit, which ranges between 800 ft and 1500 ft, will not exert any significant effect on the density and pressure of air. However, during the simulation, air flow and heat are introduced in the model space, as a result of which the pressure is modified.

- It is assumed that flow in the model space is characterized by the incompressible Navier-Stokes equations. The air flow is introduced into the model space. Air subsequently gains heat from the mine surface and the equipment present in the mine.

- One of the most important assumptions made is that the model has no *a priori* information about the nature of the flow in the simulation space. Most of the published research (Chapters 1.3.1 & 1.3.2) attempting to solve the open-pit ventilation problem has assumed that the flow in open-pit mines is either quasi-turbulent or entirely turbulent. In quasi turbulent schemes, the laminar flow of the air that occurs at the rim of the open-pit is completely disconnected from the turbulent eddy currents near the pit bottom. Thus the turbulent eddy currents are manifested through the velocity shear interaction with the laminar part of the flow, and there is only minimal mass transfer between the two flow regimes. This assumption violates the conservation of mass and principles of momentum transfer between the influent air and the extant air in the open-pit. Because at low air velocities (which is generally observed during air inversion), the influent air would not have sufficient momentum to displace the mass of the colder, trapped air at the pit bottom.

The flow will thus take the path of least resistance and in the process, transfer its momentum to the extant cold air mass at the pit bottom. The overarching pattern of this flow can be justified as turbulent in nature if the Reynolds Number of the flow is taken as the sole measure of turbulence. Reynolds Number (Re) is given as:

$$Re = \frac{\rho V L}{\eta} = \frac{Q D_H}{v A}$$ (equation 3.1)

Where,

ρ is the density of the fluid (lb/ft^3)

V is the velocity of the fluid (ft/s)

L is the characteristic length of flow (ft)

η is the dynamic viscosity ((poundal/ft^2)-s)

Q is the volumetric flow of the fluid (ft^3/s)

D_H is the hydraulic diameter of the cross-section of the flow (ft)

v is the kinematic viscosity of the fluid (ft^2/s)

A is the cross-sectional area of the flow (ft^2)

The hydraulic diameter D_H is defined as:-

$$D_H = \frac{4A}{P}$$ (equation 3.2)

Where,

A is the cross-sectional area of the flow (ft^2)

P is the wetted perimeter of the cross-section of the flow (ft)

Given the large dimensions of any open pit mine periphery through which air flows into the pit, the Reynolds Number is likely to be very large, thus rendering the flow as turbulent in conventional terms. This may not be the case

in reality; as such flow may be quasi-turbulent or even laminar, depending on the geometry of the flow regime and the velocity of flow. Thus, the assumption that the flow regime in an open pit mine is necessarily turbulent may not hold true, and that assumption has been modified in the present model.

3.3. Representative Diagram of the Two-dimensional Model

A representative diagram of a 2D model is shown below:-
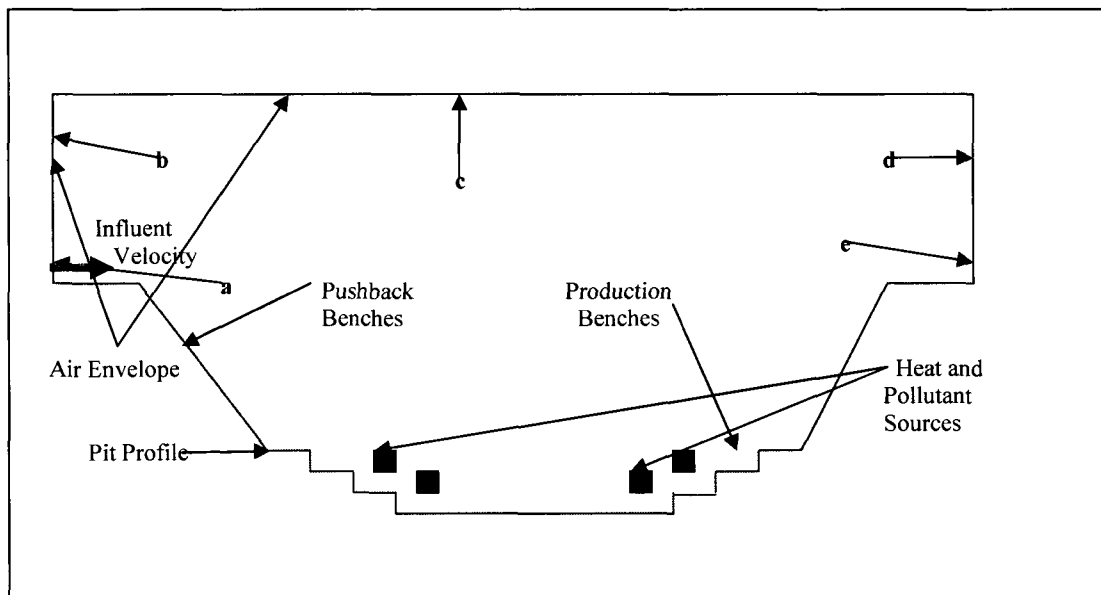
Figure 3.1: A representative diagram of a 2D model (not to scale)

In Figure 3.1 a schema of a 2D model has been presented. As can be seen in figure 3.1, the model represents a longitudinal section of an open mine pit. Various model boundaries (a, b, c, d and e) have been used to designate the air envelope around the mine. It is at these boundaries that the atmospheric extent of the model is considered beyond the physical boundary of the mine.. As shown in the figure, the air envelope does not rise from the very edge of the pit, but encompasses an extent of ground around the pit. This allows simulation of a more realistic flow conditions in the pit environment. The inclined line marked "Pushback Benches" represent the area near the rim of the pit where no production activities are taking place, waste materials from there must, however be removed in order to gain access to the value matrix. Pushback

benches, which are used to remove waste rock, are not represented in the current model, as very few of these benches would have working personnel, and because of the location of the benches, the personnel would be above the inverted layer. The production benches near and at the pit bottom are those where production takes place. Consequently, most equipment and personnel are found at these locations, making the concentration of gaseous pollutants and health hazards due to them maximum in this area. For modeling purposes, the atmosphere of the pit extends from the pit bottom to the top boundary of the air envelope above the pit rim. The flow dynamics, heat and pollutant transport that are being simulated are situated in this model space.

The red arrow to the left of the model space represents the boundary through which air flows at varying velocities. Usually, very low velocities are present, because inverted air conditions in mines do not actuate large air velocities. This air flow is a vectored convective force which disperses the pollutants generated in the pit.

Two sources of heat are considered in the model. The reradiated heat from the mine surfaces forms the most tangible heat source. This heat is transferred to the layer of air immediately above it, and the pollutant-laden air contained in it gains energy. The other sources of heat considered in the model are large quantities of waste heat generated from production and support equipment in the pit.

The only sources of gaseous pollutants in the mine are the exhaust from the equipment. Since only gaseous pollutants are considered in this model, dust particulates generated by the equipment or gases produced as a result of blasting are not considered in this dissertation.

3.4. Construction of the Two-dimensional Model

The 2D model is constructed in the COMSOL® environment. The rendition of the 2D model is shown in Figure 3.2.
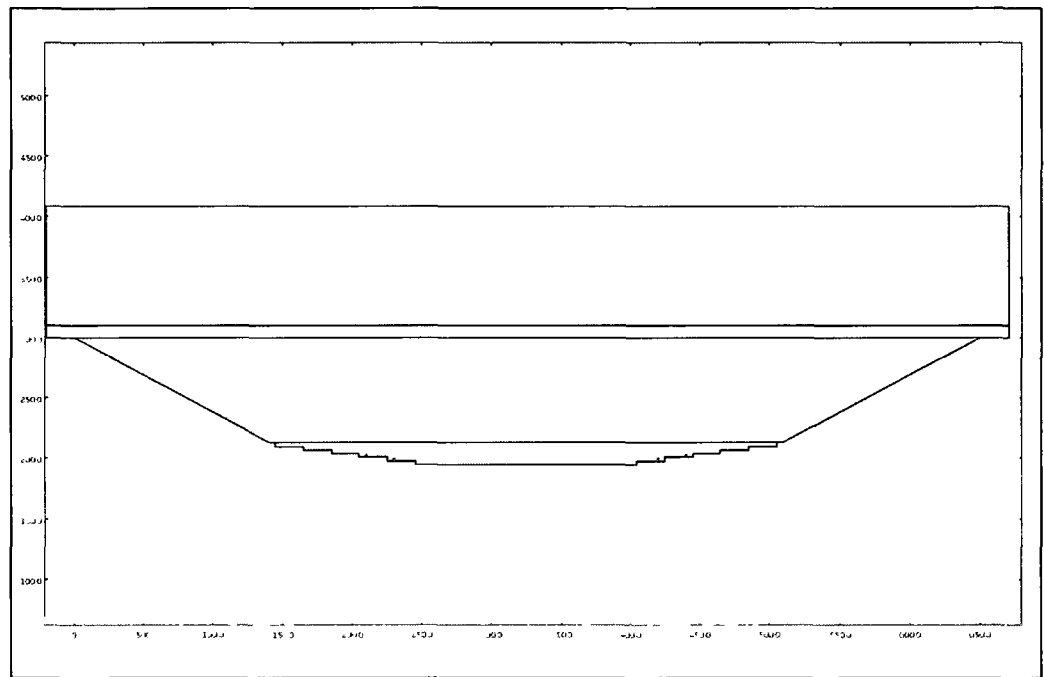
Figure 3.2: 2D Model rendition using COMSOL

The model is a combination of eight rectangles and a trapezoid integrated in sequence to represent an idealized open pit. The hypothetical mine extends 4500 ft in the horizontal direction (x-direction) at pit top and 1500 ft in the x-direction at the pit bottom. The depth of the hypothetical mine is 1050 ft from the pit rim to the pit bottom. The maximum height of the air envelope considered is 2150 ft from the pit bottom. The top of the pit, a trapezoid, represents the pushback part of the open pit. This part of the pit is not important insofar as the pollutant concentration is concerned and is therefore approximated as an inclined straight line. The overall highwall slope of the inclined lines is fixed at 40°. The production benches toward the pit bottom are, however, clearly represented. The bench height in this area is 30 ft, and the bench width is 200 ft. The length of the pit bottom in the x direction is 1600 ft. All the boundaries shown in the diagram have appropriate boundary conditions; viz., the flow of air in the mine, the convection-conduction subroutine (the addition of heat to the model from the reradiated heat from the ground as well as the waste heat from the equipment), and the convection diffusion system (the gaseous pollutants being

introduced into the model from the equipment pieces).The flow system is modeled by the Navier-Stokes system, which feeds into the conduction-convection system. The results for the conduction-convection system are then input into the convection-diffusion phenomenon transporting the pollutants from the sources to various areas in the model space. The following subsections detail the conditions that were imposed on the model based on the Navier-Stokes, Convection-Conduction and the Convection-Diffusion subroutines.

3.4.1. The Navier-Stokes Equations

The Navier-Stokes equations are a set of non-linear partial differential equations that describe the flow of fluids, either liquids or gases, in natural or artificially induced conditions. Natural flows might include atmospheric and oceanic flows, and artificial conditions might be induced by flow in pipes. These equations consider the balance of mass, momentum and energy within an infinitesimal unit volume.

The incompressible Navier-Stokes equations in three dimensions are given as follows:-

$$\rho\left(\frac{\partial u}{\partial t} + u\frac{\partial u}{\partial x} + v\frac{\partial u}{\partial y} + w\frac{\partial u}{\partial z}\right) = -\frac{\partial p}{\partial x} + \eta\left(\frac{\partial^2 u}{\partial x^2} + \frac{\partial^2 u}{\partial y^2} + \frac{\partial^2 u}{\partial z^2}\right) + F_x \qquad \text{(equation 3.3)}$$

$$\rho\left(\frac{\partial v}{\partial t} + u\frac{\partial v}{\partial x} + v\frac{\partial v}{\partial y} + w\frac{\partial v}{\partial z}\right) = -\frac{\partial p}{\partial y} + \eta\left(\frac{\partial^2 v}{\partial x^2} + \frac{\partial^2 v}{\partial y^2} + \frac{\partial^2 v}{\partial z^2}\right) + F_y \qquad \text{(equation 3.4)}$$

$$\rho\left(\frac{\partial w}{\partial t} + u\frac{\partial w}{\partial x} + v\frac{\partial w}{\partial y} + w\frac{\partial w}{\partial z}\right) = -\frac{\partial p}{\partial z} + \eta\left(\frac{\partial^2 w}{\partial x^2} + \frac{\partial^2 w}{\partial y^2} + \frac{\partial^2 w}{\partial z^2}\right) + F_z \qquad \text{(equation 3.5)}$$

$$\frac{\partial u}{\partial x} + \frac{\partial v}{\partial y} + \frac{\partial w}{\partial z} = 0 \qquad \text{(equation 3.6)}$$

In the above equations,

ρ is the density of the fluid (lb/ft^3)

p is the pressure of the fluid (poundal/ft^2)

η is the dynamic viscosity ((poundal/ft^2)-s)

t is the time (s)

x, y and z are the Cartesian coordinates

u, v and w are the velocities in the x, y and z directions, respectively

In equations 3.3 to 3.5, x, y, z and t are the independent variables. η, is the dynamic viscosity. Under certain conditions, η can vary with space and/or time. Dynamic viscosity varies with temperature; but the variation is relatively small over the observed temperature range (about 7 °F). In this model, therefore, it is held constant. Due to the incompressibility assumption, the density, ρ, is also held constant. Consequently, the equation is being solved for the pressure, p, and the three velocity components u, v and w in the x, y and z directions. As all the variables appear in all the equations (3.3 − 3.5), the system of equations has to be solved simultaneously. It may be noted that there are four unknown variables but only three equations. A fourth equation is thus needed for a unique solution, which is provided by equation 3.6 (the mass continuity equation with constant density). Equations 3.3 to 3.5 are also known as the momentum transfer equations, because they describe the flow of the fluid in terms of rate of change of momentum.

The terms F_x, F_y and F_z in the x-, y-, and z-direction are the respective components of the volume forces (e.g., the gravitational force) acting on the unit volume of the fluid respectively. In the present model, however, the gravitational force experienced by a unit volume of the fluid is already accounted for by the terms $\partial p/\partial x$, $\partial p/\partial y$ and $\partial p/\partial z$, i.e., the components of the pressure in the three Cartesian directions. There are no other force fields acting on the unit volume of fluid, and thus, the volume forces are taken as zero.

In the 2D model, only the equations in the x and y directions are used due to the lack of a third dimension

3.4.1.1. Navier-Stokes Boundary Conditions

Boundary types for the Navier-Stokes subroutine are of three kinds, viz., a flow boundary, constant pressure, open boundaries and walls. These boundary conditions are discussed below.
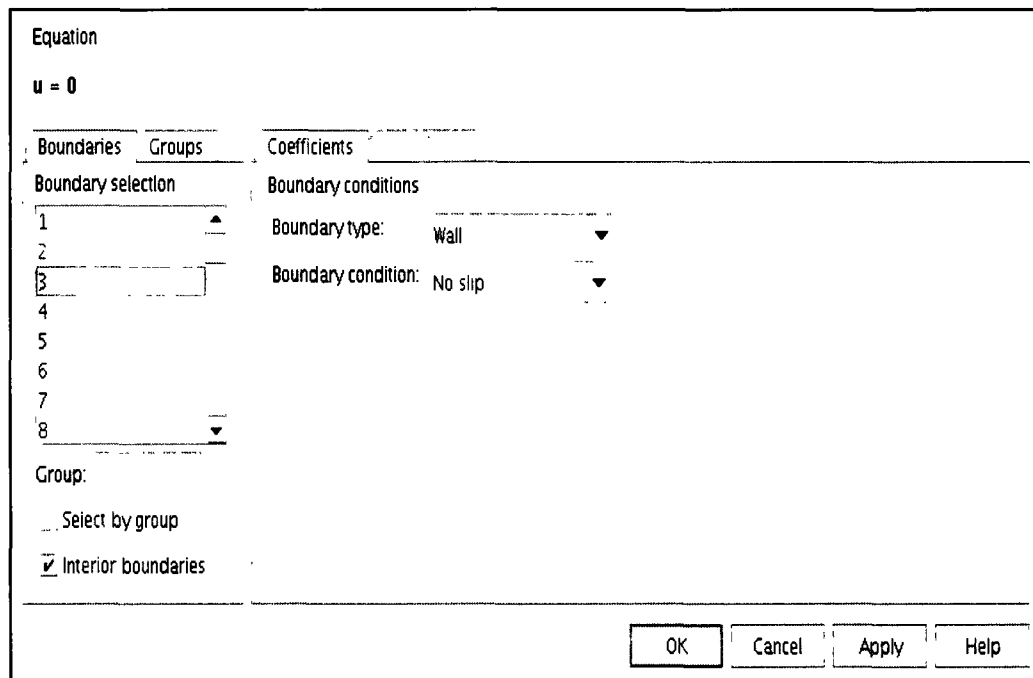
Figure 3.3: Navier-Stokes Boundary Conditions – Wall

Figure 5.3 shows the dialogue box in COMSOL® for assigning the wall boundary condition representing a solid wall. The wall has a no-slip condition attached. The no-slip condition (COMSOL® 3.4 Manual, Modeling, pp. 134) stipulates that when the velocity vectors impinge on the wall, they are rendered zero values,

$$u = 0 \qquad \text{(equation 3.7)}$$

$$v = 0 \qquad \text{(equation 3.8)}$$

This boundary condition is applied to the mine profile, i.e., the boundaries of the mine representing the ground, as well as the boundaries representing the equipment working in the mine. As the wall function renders all the velocity vectors that impinge on it as zero, these boundaries have no mechanical interaction with the element of air hitting it. The air is not reflected or "bounced back", or translated along the boundary in other any way (the no-slip condition), which implies that the momentum of the air is completely absorbed into the wall. The air thus loses all its momentum without losing any mass, and then the air mass is free to move according to the prevalent convection currents or other external forces such as gravity. The no-slip wall condition thus has the advantage of preventing the flow of air without taking the mass out of the system and, thereby assists in re-circulating that mass within the model space. Another major advantage of the no-slip wall condition is that due to the velocities being zero at the wall, local, small-scale turbulence that may occur when air flows over impediments are automatically eliminated. These small-scale turbulences are quite complex, and are often so small that any attempt to model them within an extensive large model space, such as the one being considered, would give rise to convergence problems due to the difference in scaling. Even if these are modeled successfully, the turbulences would not add any significant value to the solution.

An inflow velocity boundary is used to introduce airflow into the model. This is the only boundary, which is explicitly expressed as a set of vectors. The inflow boundary represents the equation $u = u_0$ and $v = v_0$, where u_0 and v_0 are numerical values. These boundary conditions can be classified as Dirichlet conditions. An example of that boundary condition is shown in Figure 3.4.

Figure 3.4: Inflow Velocity Boundary

The location of inflow boundary is shown in Figure 3.5 below.
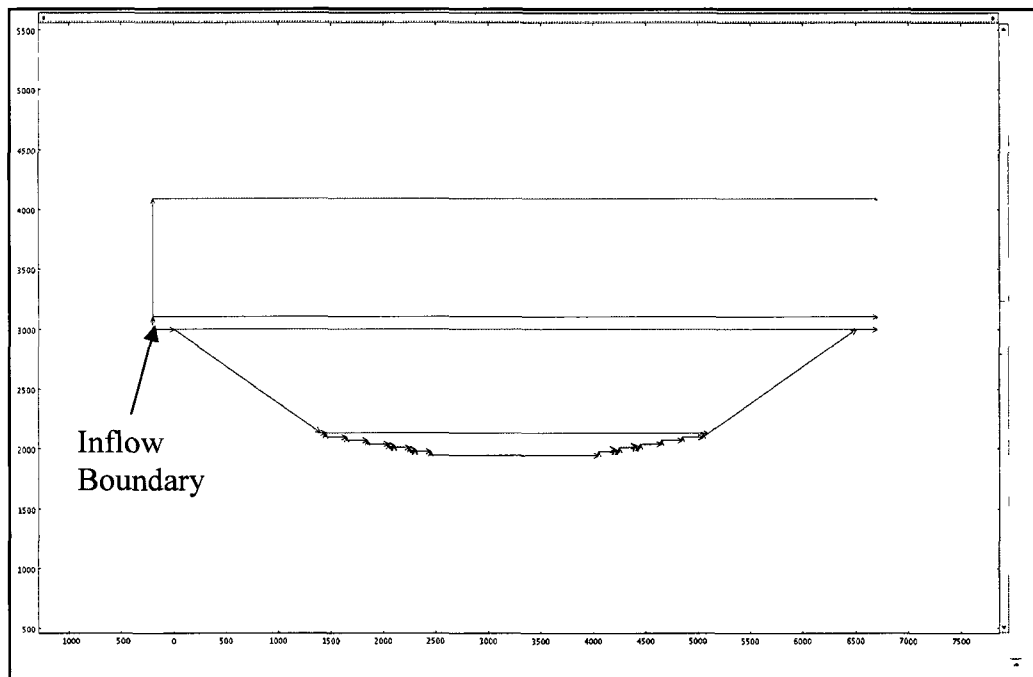
Figure 3.5: Inflow Boundary in Model

The boundary indicated in Figure 3.5 (colored red) is one which connects the model to, or, limits the model from the extended atmosphere which is far beyond the zone of influence of the mine. It is from this atmospheric region that air is presumed to flow into the mine. Other boundaries also exist that perform a similar function. They are showed in Figure 3.6 below.
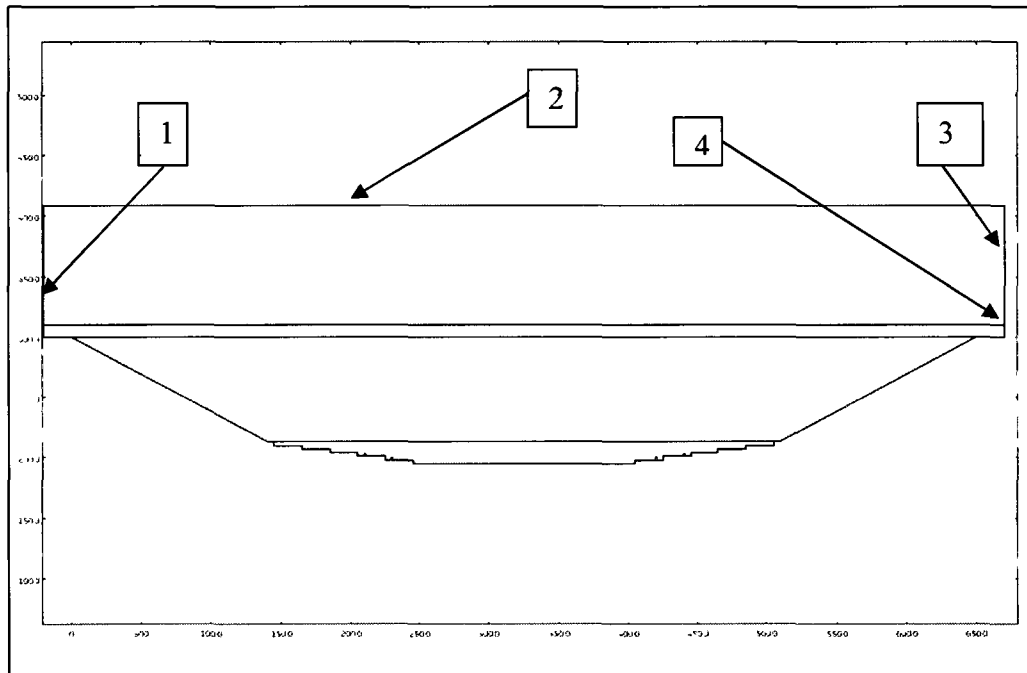
Figure 3.6: Boundaries Communicating with the Outside Atmosphere.

As indicated in figure 3.6 above, the boundaries 1, 2, 3 and 4 define the zonal extent of the model with respect to the extended atmosphere beyond the mine. These boundaries do not necessarily, however, have similar defining conditions. Boundary 1, for example, which is located vertically above the inflow boundary, is represented as a wall. This prevents the air entering the model space through the inlet boundary from short-circuiting out of the model through an immediately available outlet. The same argument can be made for boundary 2 which is also defined as a wall. Apart from preventing influent air from exiting the model space prematurely, the wall condition at boundary 2 is used to define the inversion cap in the model. These two boundaries thus act as limiting boundaries and, at least from the flow perspective, keep the

influent air and the native air in the model space. But, as influent air enters the model over a period of time, mass in the model space increases, and unless there are conditions imposed that allow the air mass to exit the system, mass balance conditions will be violated. Therefore, the mass outflow conditions are assigned to the boundaries 3 and 4, shown in Figure 3.6. These two boundaries are characterized as open boundaries, with a constant normal pressure of $p \approx f_0 = 2073.6$ poundal/ft^2 (also a Dirichlet condition). As example of the COMSOL® dialogue box for this condition is given in Figure 3.7.

Figure 3.7: Dialogue Box for Input of Open Boundary Condition (Different Pressure)

An open boundary is needed when a large amount of air is required to pass through a model space. The direction in which air flows across the boundary is primarily determined by the air pressure, not just globally, but locally as well. If there is a localized flow near the boundary such that a partial vacuum is created close to the boundary, the boundary layer then might generate a mass flow into the model space to

mitigate the mass imbalance. The equation describing the open boundary with a constant normal stress is as follows (COMSOL® 3.4 Manual, Modeling, pp. 138):-

$$\left(-p\begin{vmatrix} 1 & 0 & 0 \\ 0 & 1 & 0 \\ 0 & 0 & 1 \end{vmatrix} + \eta\begin{vmatrix} 2\dfrac{\partial u}{\partial x} & \dfrac{\partial v}{\partial x}+\dfrac{\partial u}{\partial y} & \dfrac{\partial w}{\partial x}+\dfrac{\partial u}{\partial z} \\ \dfrac{\partial u}{\partial y}+\dfrac{\partial v}{\partial x} & 2\dfrac{\partial v}{\partial y} & \dfrac{\partial w}{\partial y}+\dfrac{\partial v}{\partial z} \\ \dfrac{\partial u}{\partial z}+\dfrac{\partial w}{\partial x} & \dfrac{\partial v}{\partial z}+\dfrac{\partial w}{\partial y} & 2\dfrac{\partial w}{\partial z} \end{vmatrix} \right)\vec{n} = -f_0\vec{n}$$ (equation 3.9)

In the above equation,

p is the pressure (poundal/ft^2),

η is the dynamic viscosity ((poundal/ft^2)-s),

$\vec{n}$ is the normal in the direction perpendicular to the open boundary, pointing away from

the domain,

f_0 is the stress set at the boundary (poundal/ft^2), directed into the domain (in the negative $\vec{n}$ direction),

x, y and z are the Cartesian coordinates, and

u, v and w are the velocities in the x, y and z directions respectively.

This equation (3.9) represents the air flowing out of the model through the open boundary. It has to, however, overcome the opposing normal stress at the boundary. This requires the setting of a pressure at the open boundary which is commensurate with the atmospheric pressure in the system. The pressure at the inlet boundary is set slightly higher than that at the open boundary, and this difference in air pressure causes air to flow from one boundary to another.

In equation 3.9, the matrix multiplied with η reduces to

$$\begin{vmatrix} 2\dfrac{\partial u}{\partial x} & 0 & 0 \\[2mm] 0 & 2\dfrac{\partial v}{\partial y} & 0 \\[2mm] 0 & 0 & 2\dfrac{\partial w}{\partial z} \end{vmatrix},$$

Since, $\dfrac{\partial u}{\partial y}, \dfrac{\partial u}{\partial z}, \dfrac{\partial v}{\partial x}, \dfrac{\partial v}{\partial z}, \dfrac{\partial w}{\partial x}$ and $\dfrac{\partial w}{\partial y}$ are all equal to zero.

Therefore, equation 3.9 reduces to

$$p_x = 2\eta \frac{\partial u}{\partial x} + f_{0x} \qquad\qquad \text{(equation 3.10)}$$

$$p_y = 2\eta \frac{\partial v}{\partial y} + f_{0y} \qquad\qquad \text{(equation 3.11)}$$

$$p_z = 2\eta \frac{\partial w}{\partial z} + f_{0z} \qquad\qquad \text{(equation 3.12)}$$

Equation 3.12 for the z-direction is not relevant in a 2D model, and is, thus, disregarded. The open boundaries serving as outlets, shown as boundaries 3 and 4 in

Figure 3.6, are orientated along the y-direction. This necessitates that the applied normal stress f_0 be also oriented perpendicular to the boundaries, i.e., along the x-direction only. Equation 3.11, which is the component of the stress in the y-direction, is thus eliminated also. Therefore the entire normal stress set at the open boundary, f0, is represented only by equation 3.10:

$$p = 2\eta \frac{\partial u}{\partial x} + f_0 \qquad\qquad \text{(equation 3.13)}$$

In equation 3.13, the term $\dfrac{\partial u}{\partial x}$ is the rate of change of the x-component velocity. The initial velocity given at the inflow boundary is significantly small, thus its variation in

the x-direction would also be substantially small. This small number when multiplied with η, which is of the order of 10^{-7}, generates a much smaller number for the term $2\eta \dfrac{\partial u}{\partial x}$, and, thus, for all practical purposes, can be neglected. Equation 3.13 therefore, becomes

$$p \approx f_0 \qquad\qquad \text{(equation 3.14)}$$

The normal stress f_0 in equation 3.14 is thus approximately the same as the pressure, p, in the system, e.g., the initial pressure defined as an initial condition. This initial pressure is $(14.4 \text{ psi} \times 12^2) = 2073.6 \text{ poundal/ft}^2$.

Along with the boundary conditions described in the previous sections, the model must also have relevant sub-domain and initial conditions, which are discussed in the following sections.

3.4.1.2. Navier-Stokes Sub-Domain Conditions

The sub-domain conditions for the Navier-Stokes subroutine have the principal assumption that the Navier-Stokes equations (equations 3.3, 3.4, 3.5 and 3.6) are continuous over the entire domain. The need for validating the equations over the space therefore, does not arise, as the space is constructed such that the continuity of the equations is maintained. Also, as mentioned in section 3.2, the model does not have a priori knowledge of the nature of the flow, i.e., the presence and absence of turbulence.

In case of an air inversion, the presence of large-scale turbulence in the model space would perturb the inverted air column and lift the air inversion, and thus may mitigate the problem to a large extent. The existence of an inverted air column, therefore, indicates the presence of either small-scale local turbulence, or a complete lack thereof. As stated before, the inclusion of small-scale turbulences in the model does

not add any significant value to the model solution even if solved, and thus can be approximated by linear and/or quasi-linear flow without any loss of accuracy.

A possible critique of the approach considered above may be that if there is large-scale turbulence in the system, the assumption of the non-turbulent Navier-Stokes equation over the model space may "smooth over" the turbulence and force the flow to linearize, making it either laminar or quasi-laminar flow. This may lead to errors in the final predicted distribution of pollutants in the model space, since the distribution of the pollutants is highly dependant on the prevalent convective velocities.

Such concern may be resolved by considering the fact that the inflow air into the model space, introduced at the inflow boundary, is effectively a laminar flow. Since the air flow into a mine atmosphere under air inversion is significantly small in magnitude, and the geometry of the outer boundaries of the mine restricts the movement of such flow in a particular direction, it is expedient to consider the inflow boundary to introduce a constant average flow into the model space in an open pit known direction. As in the previous case, the small turbulences occurring at the inflow boundary offer no consequential effects, when compared with the extensively large mass of colder, heavier air, to which the influent air attempts to transfer its momentum. As the influent air flows laminally, the only turbulence that can subsequently be regenerated would be due to the momentum interaction between the dynamic influent air and the relatively static air under the inverted air column. The dimensions of the flow regime are rather large, placing the Reynolds Number (Re) for the flow firmly in the turbulent region. This may give rise to an inclination to classify the flow primarily as turbulent, and construe that if the flow loses enough momentum, it will approach, quasi-turbulence or laminar flow conditions from an initial turbulent flow situation. However, a closer analysis may indicate that the influent velocity is so very small, and the mass of the inverted air column so extensively large, that the influent air will take the path of least resistance, thus preserving the laminarity of flow, and would not result in a turbulent flow regime due to lack of sufficient kinetic

energy. This flow may be classified as quasi-laminar, and inhabits the same contextual space as a quasi-turbulent flow, with the only significant difference being that it approaches this flow characteristic from a laminar flow situation by gaining additional energy, and not from an initial turbulent flow situation by losing energy. By establishing the non-turbulent Navier-Stokes equations as the primary sub-domain condition for the model space, the laminarity of the influent air, as well as its potential to reach a quasi-laminar flow regime, can be resolved.

For solving the Navier-Stokes equations several appropriate parameters values are required. The value of the constant density of air, ρ, is taken to be 0.094 lb/ft^3. Density of air is a function of temperature and was calculated according to the following equation (Ierardi, 2009):

$$\rho = 360.77819 \times T^{-1.00336} \hspace{4cm} \text{(equation 3.15)}$$

where,

ρ is the density of air in kg/m^3

T is the absolute temperature in Kelvin.

In equation 3.15, with temperature T set at 233.16 K (-40 °F) the density was converted from kg/m^3 to lb/ft^3. The equation, which is formulated at standard atmospheric pressure (14.7 psi), neglects the effect of the variation of pressure on air density. In an incompressible flow model, the density of air is held constant regardless of the change in temperature and pressure. Also, while the pressure assigned in the model (14.4 psi) is not the standard atmospheric pressure, it is, however, very close, and thus, the variation in density as a result of this small difference in pressure is negligible.

The dynamic viscosity, η, is set at 3.29 × 10-7 (poundal • s/ft^2) at -40 °F (www.engineeringtoolbox.com). A dialogue box for the parameters mentioned above is shown in the figure 3.8.

```
Equations

p∂u/∂t + pu•∇u = ∇•[-pI + η(∇u + (∇u)ᵀ)] + F

∇•u = 0

Subdomains ` Groups          Physics  Init   Element

Subdomain selection          Fluid properties and sources/sinks

1                      ▲      Library material:        ▼     Load...
2
3                             Quantity  Value/Expression   Unit            Description
4 (default)                      p      0.094              lb/ft³          Density

                                 η      3.29e-7            (poundal/ft²)·s Dynamic viscosity

                                 Fₓ     0                  poundal/ft³     Volume force, x-dir.

                          ▼      Fᵧ     0                  poundal/ft³     Volume force, y-dir.

Group:                    ▼
                                       Artificial Diffusion...
   Select by group

 ✔ Active in this domain


                                           OK      Cancel     Apply      Help
```

Figure 3.8: Dialogue Box for Input of the Navier-Stokes Sub-domain Conditions

As shown in Figure 3.8, apart from the density and the dynamic viscosity, The model input requires a value for "artificial diffusion".

Artificial diffusion refers to certain stabilization techniques in the solution algorithm that are used when the solution for a system of equations becomes unstable due to an inordinate increase in the Peclet Number of a cell in the grid imposed on the model space. The Peclet Number (Pe) for a cell is defined as follows:

$$Pe_{cell} = \frac{|\vec{u}|h}{c} \qquad \qquad \text{(equation 3.16)}$$

where,

$\vec{u}$ is the velocity vector in x-, y- or z-direction in ft/s

h is the dimension of the grid element along the corresponding direction in ft

c is the mass diffusivity in ft²/s

The Peclet Number for a cell can also be expressed as

$$Pe_{cell} = Re_{cell} \times \text{Prandtl Number} \qquad \text{(equation 3.17)}$$

where the Prandtl Number is a dimensionless quantity which is calculated as a ratio of the viscous diffusion rate and the thermal diffusion rate.

Since the Reynolds Number (Re) value in an open-pit mine can be very large because of a low η and a large characteristic length (which may be thought of as the dimension of the grid cell in the relevant direction), Pe_{cell} can also be very high, which can lead to convergence problems due to undesirable oscillations of the solution. One approach to mitigate this problem is to refine the grid size so that the Pe_{cell} is less the one. This, however, is not feasible in large-dimensioned problems such as the one under consideration. Therefore, in such situations, stabilization methods such as artificial diffusion are used in order to stabilize the solution without a significant alternation of the grid. The dialogue box for artificial diffusion is given in figure 3.9.

Figure 3.9: Dialogue Box for Input of Artificial Diffusion

Although a number of choices are available, the method of "Isotropic Diffusion" was selected for the present problem. In this method, an extra term of artificial isotropic diffusion (c_{art}) is added to the Peclet Number (equation 3.16) in the following manner (COMSOL® 3.4 Manual, Modeling, pp. 439):

$$c_{art} = \delta_{id}|\vec{u}|h \qquad \text{(equation 3.18)}$$

where, δ_{id} is a dimensionless tuning parameter.

With the addition of an artificial diffusion parameters, the equation for Pe changes to

$$Pe = \frac{|\vec{u}|h}{c + c_{art}} \qquad \text{(equation 3.19)}$$

If δ_{id} in equation 3.18 is held constant with a default value of 0.5 (Figure 3.9), the value of Pe may approach but never exceed two, thus significantly stabilizing the solution to convergence. The isotropic diffusion parameter (c_{art}) is only used at places in the grid where the Peclet Number is noted to be increasing rapidly. The disadvantage of this method lies in the fact that with the addition of c_{art}, the problem departs from consistency, and what is actually computed is a set of matrices with a slight perturbation error. Thus in a situation where extreme accuracy is desired, this method is often not recommended. In the present model, however, it is observed that the model dimensions are extensive and the values in the initial matrix are sufficiently small, so the errors due to perturbations are insignificant.

3.4.1.3. Navier-Stokes Initial Conditions

Only the initial condition related to pressure plays an important role in the Navier-Stokes subroutine. The initial air pressure throughout the model is set at 14.4 psi, or,

2073.6 poundal/ft^2. This is the average atmospheric pressure recorded at the Fairbanks International airport and, in the absence of better data, it is considered to be very close to the pressure at the hypothetical mine site.

3.4.2. The Convection-Conduction Equations

The Convection-Conduction equations are a set of non-linear partial differential equations that describe the transfer of heat by the convection of a fluid. The heat is initially conveyed to the fluid mass primarily through conduction from an adjacent source, and it is then conveyed throughout the fluid mass through fluid convection. The characteristic equations, representing the physics of the problem, are as follows (COMSOL® 3.4 Manual, Modeling, pp. 175):

$$\rho C_p \left(\frac{\partial T_x}{\partial t} + u \frac{\partial T_x}{\partial x} \right) - k \frac{\partial^2 T_x}{\partial x^2} = Q_x \qquad \text{(equation 3.20)}$$

$$\rho C_p \left(\frac{\partial T_y}{\partial t} + v \frac{\partial T_y}{\partial y} \right) - k \frac{\partial^2 T_y}{\partial y^2} = Q_y \qquad \text{(equation 3.21)}$$

$$\rho C_p \left(\frac{\partial T_z}{\partial t} + w \frac{\partial T_z}{\partial z} \right) - k \frac{\partial^2 T_z}{\partial z^2} = Q_z \qquad \text{(equation 3.22)}$$

With the assumption of an incompressible fluid, the mass continuity equation is given by

$$\frac{\partial u}{\partial x} + \frac{\partial v}{\partial y} + \frac{\partial w}{\partial z} = 0 \qquad \text{(equation 3.23)}$$

In equations 3.20 to 3.23,

ρ is the density of air (lb/ft^3)

T_x, T_y and T_z are the air temperatures in the x-, y- and z-directions (°F)

C_p is the heat capacity of air at constant pressure (poundal·ft/(lb· °F))

k is the isotropic thermal conductivity of air (poundal/(s· °F))

Q_x, Q_y and Q_z are the heat sources releasing heat in the x-, y- and z-directions (poundal/(ft^2·s))

u, v and w are the advective air velocities in the corresponding x-, y- and z-directions.

Equations 3.20 to 3.23 are used to calculate the temperature variations that occur in the model space due to addition of heat from various surface heat sources. These heat sources transmit heat to the supernatant air through a thin conduction layer. Once heated, this thin layer of air rises and the cooler air on top settles, giving rise to a convective current. The convective velocity of the fluid that results in the model space is a sum of the convective velocity due to heat, as well as the velocity due to the transfer of momentum (the Navier-Stokes equations).

The first part of the general convection-conduction equations, $\rho C_p\left(\dfrac{\partial T_s}{\partial t} + \dot{s}\dfrac{\partial T_s}{\partial s}\right)$,

where s is the relevant Cartesian coordinate, represents the rate of change in heat input to the air with respect to time, as well as the convective velocity which transports the heat. The velocity $\dot{s}$ can initially be considered as the result of the momentum, but is updated as the heat is transferred to the system giving rise to the convective velocity.

The term $k\dfrac{\partial^2 T_s}{\partial s^2}$ represents the rate of diffusion of heat from the surface heat sources to the air mass. The term on the right hand side of the equation, Q_s, is the heat source or sink term that adds or removes heat from the model space. This term has a defined magnitude or has a relevant expression at the surfaces or boundaries which add heat to the model. In the sub-domains, however, the values of Q_s are zero, since there are no inherent sources of heat in the sub-domains.

Equations 3.20 to 3.23 are simultaneously solved at each time step in conjunction with the Navier-Stokes equations with appropriate initial and boundary conditions to obtain

the temperature profile in the model space, as well as the modified advective velocity vectors in the three Cartesian coordinates.

3.4.2.1. Convection-Conduction Boundary Conditions

The convection-conduction subroutine defines the transport of heat in and out of the model space. Therefore, all of the boundary conditions are concerned with the transport of heat, and specified either in terms of temperature, or in terms of heat flux. These boundary conditions are discussed below.

The inflow boundary shown in Figure 3.5 and the four boundaries shown in Figure 3.6 are inherently linked with the extensive atmosphere beyond the model space. Since the heat addition to the model is not atmospheric and temperatures in arctic regions are very low during the time inversions are mostly observed, a constant temperature condition (Dirichlet condition) is deemed most appropriate for these boundaries. A constant temperature imposes the following condition on a boundary:

$$T = T_0 \hspace{6cm} \text{(equation 3.24)}$$

where, T_0 is a numerical value best describing the temperature conditions at the boundary. The condition is imposed isotropically. The boundaries containing this constant temperature boundary condition denote the limit beyond which the heat generated in the mine does not have any influence on the atmosphere. A dialogue box describing this condition is shown in figure 3.10.

Figure 3.10: Dialogue Box for Input of Temperature Boundaries from COMSOL

The remaining boundaries (the walls of the mine) for the model are considered to be heat flux boundaries because they are involved in transporting heat into model space. The heat flux condition can be expressed by the following equations:

$$-\vec{n}\cdot\left(-k\frac{\partial T_x}{\partial x}+\rho C_p u T_x\right)=q_{0x} \qquad \text{(equation 3.25)}$$

$$-\vec{n}\cdot\left(-k\frac{\partial T_y}{\partial y}+\rho C_p v T_y\right)=q_{0y} \qquad \text{(equation 3.26)}$$

$$-\vec{n}\cdot\left(-k\frac{\partial T_z}{\partial z}+\rho C_p w T_z\right)=q_{0z} \qquad \text{(equation 3.27)}$$

where,

$\vec{n}$ is the normal in the direction perpendicular to the boundary, pointing away from the domain

ρ is the density of air (lb/ft^3)

T_x, T_y and T_z are the air temperatures in the x-, y- and z-directions (°F)

C_p is the heat capacity of air at constant pressure (poundal·ft/(lb· °F))

k is the isotropic thermal conductivity of air (poundal/(s· °F))

q_{0x}, q_{0y} and q_{0z} are the heat flux across the boundary (poundal/ft·s)

Equation 3.25 to 3.27 can be generally classified as Robin boundary conditions. With equation 3.27 obviated for dimensional restrictions, q_{0x} and q_{0y} are incorporated into the model.

As stated before, the diesel-operated equipment present in the mine, in addition to injecting gaseous pollutants into the environment, also add heat to the mine air due to the waste heat produced by the engines. Data for the fuel consumption, production of waste heat and the engine test data for gaseous pollutants are sparse, and most manufacturing companies hold such data as proprietary in nature. Some data have been collected from publicly available sources, but have not been used in the 2D model. Since the data being referred to here are field data, the 2D model is unable to accommodate them due to lack of appropriate dimensions. Figure 3.11 shows the setting of the thermal boundary conditions for the model geometries that represent the equipment in the mine.
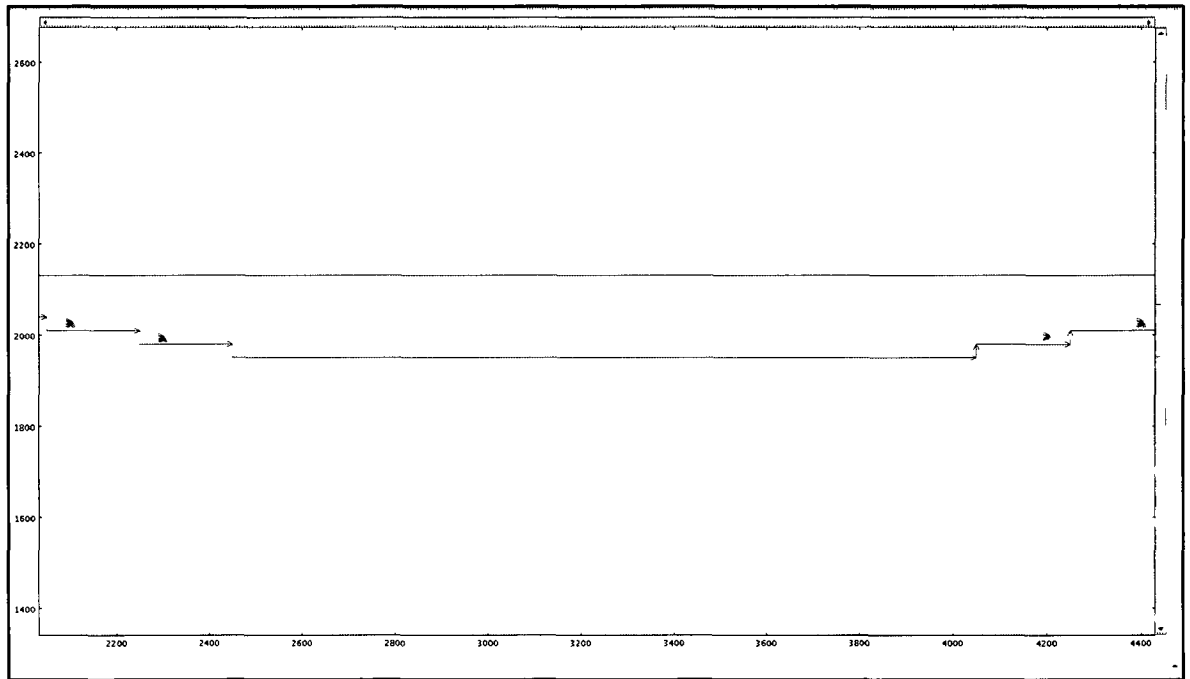
Figure 3.11: Assumed Positioning Equipments in a typical Mine Pit

In Figure 3.11 the geometry marked in red represent the positions of the production equipment. A zoomed view of the position of the equipments is shown in Figure 3.12.
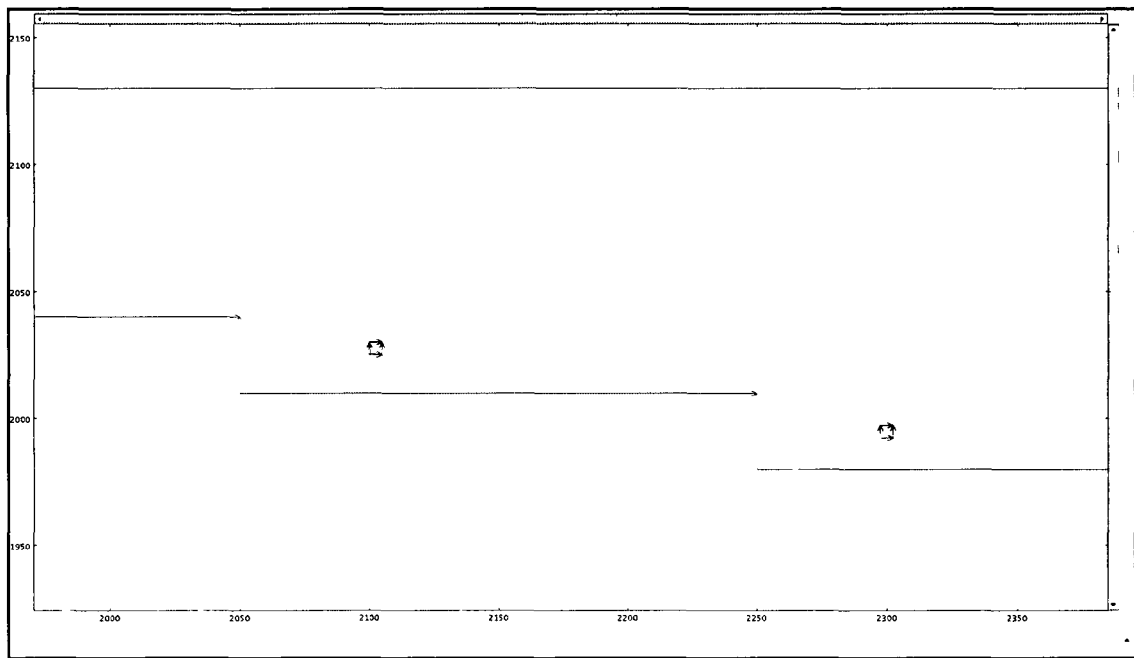
Figure 3.12: Zoomed view of the Position of the Equipments in a typical Mine Pit

The equipments are viewed geometrically as two-dimensional squares with 5 ft sides. The bottom left corners of the boxes are placed at a height of 10 ft from the floor or bench beneath it, and 50 ft from the adjoining wall. Each box has four boundaries, all of which adds both heat and pollutants.

Assuming a constant power rating for a constant workload, the engines of the equipment represented here release heat at a constant rate, thus, imposing a constant heat flux boundary is an appropriate representation of reality here. Equations 3.25 through 3.27 represent the heat flux boundary condition applied in this case. The value of q_0 chosen in this case is not, as mentioned before, from field data, rather it is fixed artificially at a high value of 5000 poundal/ft·s. An example of the relevant dialogue box is given below:

Boundary Settings - Convection and Conduction (cc)

Equation

$-\mathbf{n} \cdot \mathbf{q} = q_0, \quad \mathbf{q} = -k\nabla T + \rho C_p T \mathbf{u}$

Boundaries | Groups | Coefficients

Boundary selection

Boundary conditions

14	Boundary condition	Heat flux
15		
16	Quantity	Value/Expression	Unit	Description
17	q_0	5000	poundal/(ft·s)	Inward heat flux
18	T_0		°F	Temperature
19				
20				
21				

Group

Select by group

☑ Interior boundaries

OK   Cancel   Apply   Help
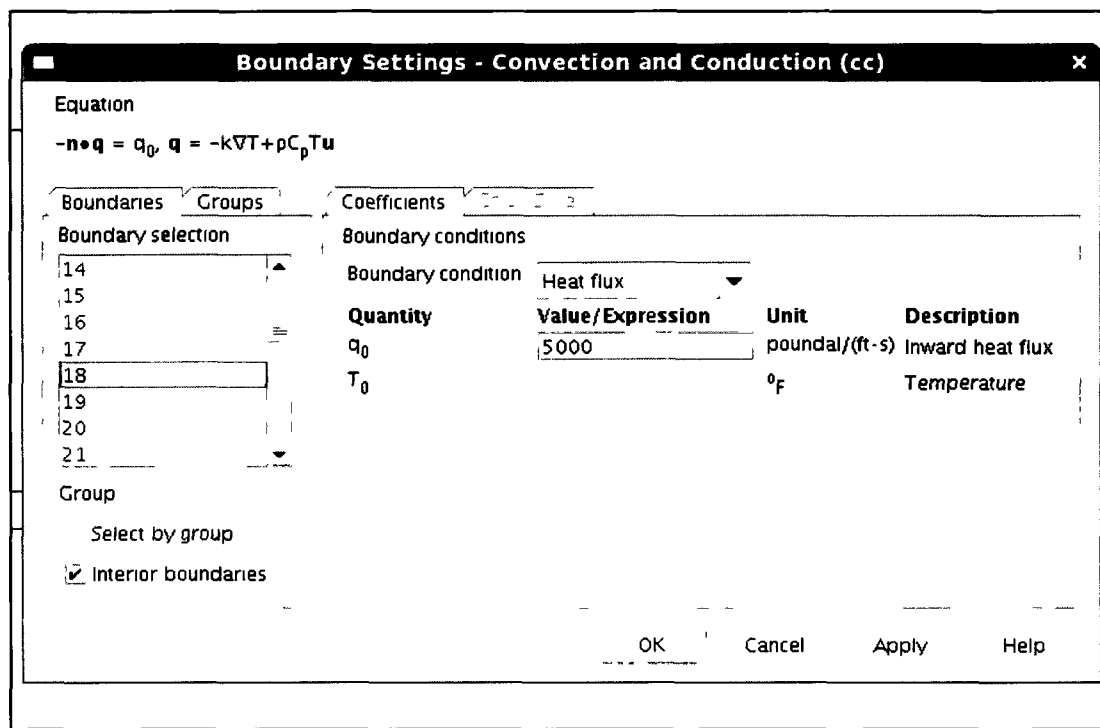
Figure 3.13: Dialogue box to input Equipment Boundary condition from COMSOL

The surface of the pit is irradiated by sunlight during the day. A fraction of this heat is then retransmitted back to the layer of air adjacent to it. Although there is a component of radiation in the transfer of heat between the surface of the pit and the layer of air immediately enveloping it, the primary mode of heat transfer is one of conduction. The air heated up in this manner then rises, and colder air from the upper reaches of the mine atmosphere sinks close to the pit surface, is reheated in turn, and thus a vertical convection current is established. This convection current can be instrumental in lifting the inversion cap and dispersing the trapped gaseous pollutants to an acceptable level. The assumption of incompressible flow condition, however, preclude the possibility of introducing buoyancy as prime cause of the convection current, as buoyancy is inexorably a function of density. Thus in the absence of buoyancy, simulating the process of convection entails the Convection-Conduction (equations 3.20 to 3.23) phenomenon. Updating of the influent air velocity at every time step,

which in turn is influenced by temperature change due to heat addition is deemed to satisfactorily simulate this process.

The heat transmitted to the air from the surface varies according to the nature of the surface and its physical attributes. Of the incident solar radiation, a part is always absorbed, and the remaining amount is emitted to the air. The surface of the pit, although icy during winter, undergoes significant changes from production and transportation activities. Although most of the surface of a pit in the arctic could conceivably be covered with packed ice - which would reflect a large part of the incident radiation - for the purpose of this model, it was deemed appropriate to assume the worst case scenario of the surface consisting of exposed rock and dirt. This assumption results in transmission of very little heat to the air (about 10% of the received radiation) and thus makes the inversion cap much more difficult to lift. On inspection it can be seen that there are primarily three kinds of surfaces in the mine – horizontal, vertical and inclined.

Regardless of orientation, a horizontal surface would receive solar radiation more or less equally throughout the day. The amount of solar radiation received by a vertical surface, however, would depend on the orientation of the surface, i.e., north, south, east or west. At high northern latitudes, solar energy received by a vertical surface oriented north is very small, and consists of only diffused or reflected radiation. A surface oriented east or west receives more direct radiation during the morning and the evening. The maximum radiation received is by a south oriented surface, as it receives direct sunlight all through the daylight hours. The information presented below in a table (Table 3.1) for received radiation is obtained from the National Renewable energy Laboratories (NREL). For this model, solar radiation data from the coldest month of the year, December, is used. A tabulation of the data for the four coldest months of the year for the Fairbanks area is shown below.

Table 3.1: Average Incident Solar Radiation (BTU/ft^2/day) for the Fairbanks Area

Orientation		Jan	Feb	Nov	Dec
Horiz.	Global	38	240	83	5
	Std. Dev.	4	18	7	2
	Min.	32	220	73	3
	Max.	44	290	98	6
	Diffuse	26	140	58	3
Clear Day	Global	44	260	79	6
North	Global	16	87	340	1
	Diffuse	16	87	34	1
Clear Day	Global	19	73	29	0
East	Global	46	230	84	11
	Diffuse	20	120	45	2
Clear Day	Global	86	340	130	25
South	Global	240	740	350	94
	Diffuse	60	240	110	5
Clear Day	Global	500	1250	680	240
West	Global	47	240	85	11
	Diffuse	21	120	45	2
Clear Day	Global	86	340	130	25

An inspection of the table 3.1 above indicates that the least amount of solar radiation is received in the month of December. It is also to be noted that for this model, only the data for global radiation is considered. These values are then converted to a unit suitable to the modeling software, i.e., poundal/ft·s, and 10% of that value (for retransmission into the air) in turn is considered for the model. A tabulation of the final values is shown below.

Table 3.2: Retransmitted Radiation for December (poundal/ft·s) for December

Orientation		BTU/sq.ft./s	Poundal/ft.s
Horiz.	Global	5	0.1449
	Std. Dev.	2	0.0580
	Min.	3	0.0869
	Max.	6	0.1739
	Diffuse	3	0.0869
Clear Day	Global	6	0.1739
North	Global	1	0.0290
	Diffuse	1	0.0290
Clear Day	Global	0	0.0000
East	Global	11	0.3188
	Diffuse	2	0.0580
Clear Day	Global	25	0.7245
South	Global	94	2.7242
	Diffuse	5	0.1449
Clear Day	Global	240	6.9553
West	Global	11	0.3188
	Diffuse	2	0.0580
Clear Day	Global	25	0.7245

In the above table (table 3.2), the column headed "BTU/sq.ft./s" enumerates the incident solar radiation values for a given surface, and the column headed "Poundal/ft·s" shows the values for the retransmitted energy for the corresponding surface.

Another feature of the heat retransmitted by an open-pit surface is that unlike the heat generated by production equipment, it is not constant. Open pit surfaces retransmit heat only when the solar radiation impinges on the surface, and thus, if the runtime of the model is more than the daylight hours, the heat is turned on at a specific time, and

off at another specific instant. This is achieved by a mathematical step function known as the Heaviside function.

A Heaviside function is best explained as an anti-derivative of a Dirac Delta function. A Dirac Delta function can theoretically be used to switch processes on or off in a simulation, but for the fact that its slope tends towards infinity. A Heaviside function solves this problem by taking a step back in space in terms of an anti-derivative, so that the same peak value is achieved starting from an earlier point in space, thus rendering the slope finite. Heaviside functions can be varied with respect to space as well as time. For the retransmitted heat values in Table 3.2, the Heaviside function derived used for the horizontal surfaces is given below:

$$q_0 = -0.14 \times \text{flc1hs}(t\text{-}950,900) + 0.28 \times \text{flc1hs}(t\text{-}36000,2700) - 0.15 \times \text{flc1hs}(t\text{-}50400,5400)$$

(equation 3.28)

where,

q_0 is the heat flux in poundal/ft·s

flc1hs is the function call for a first order Heaviside function

t is the time in s.

For vertical surfaces, similar Heaviside equations can be formulated. In the case of vertical surfaces, however, critical assumptions for surface orientation have to be made first. The pit is assumed to be oriented in a north-south direction . An elucidation of the orientation is given in the figure 3.16 below.
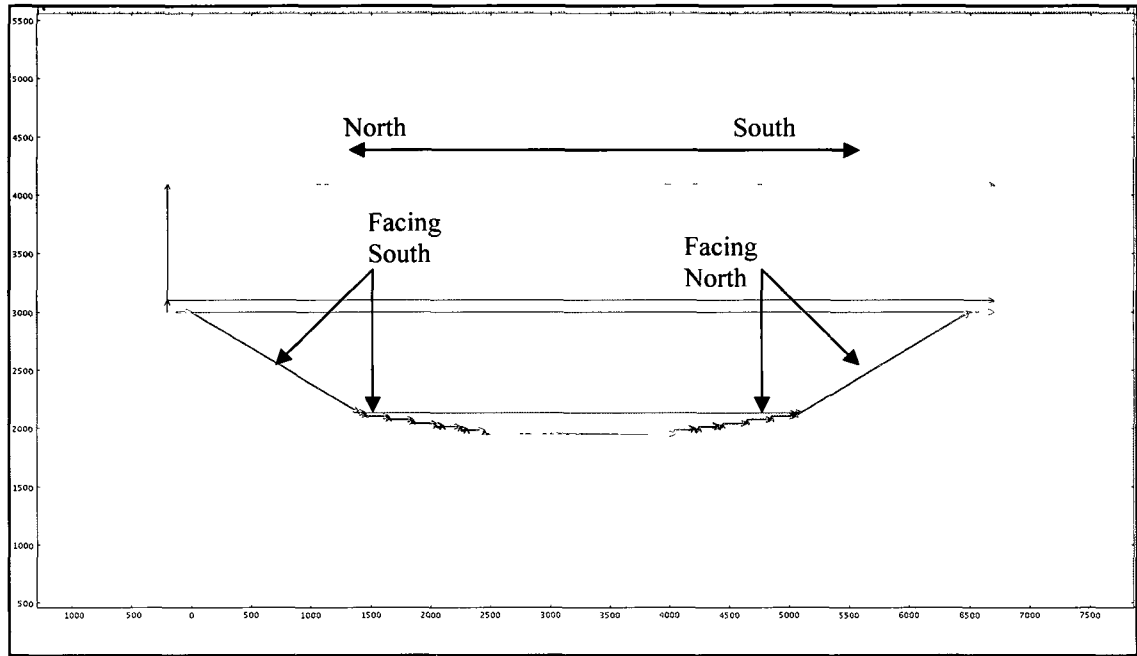
Figure 3.14: Pit Orientation

In figure 3.14, the boundaries colored red represent the open pit profile, and the boundaries facing north and south respectively are indicated.

For vertical boundaries facing south (Figure 3.15), an appropriate Heaviside equation is given below (δ values according to Table 3.2).

q_0 = -2.72×flc1hs(t-950,900)+5.44×flc1hs(t-36000,2700)-2.73×flc1hs(t-50400,5400)

(equation 3.29)
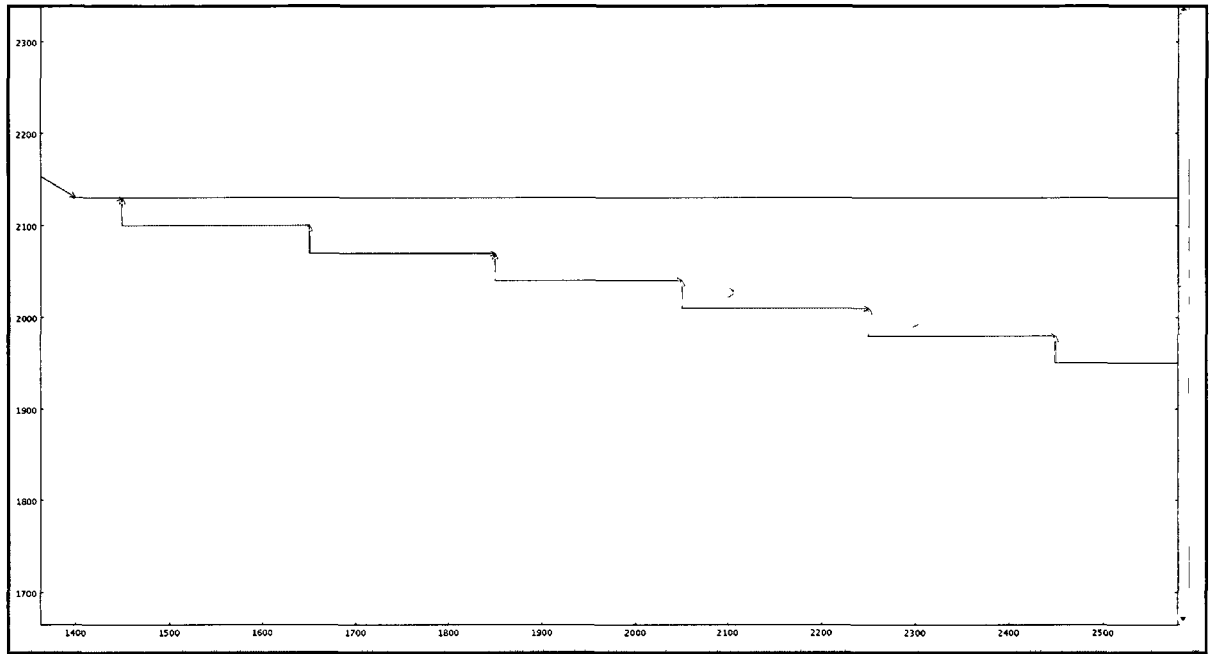
Figure 3.15: Vertical Boundaries Facing South (colored red)

For vertical boundaries facing north (Figure 3.16), a corresponding Heaviside equation is given below (δ values according to Table 3.2).

$$q_0 = -0.03 \times flc1hs(t\text{-}950,900) + 0.06 \times flc1hs(t\text{-}36000,2700) - 0.04 \times flc1hs(t\text{-}50400,5400)$$

(equation 3.30)
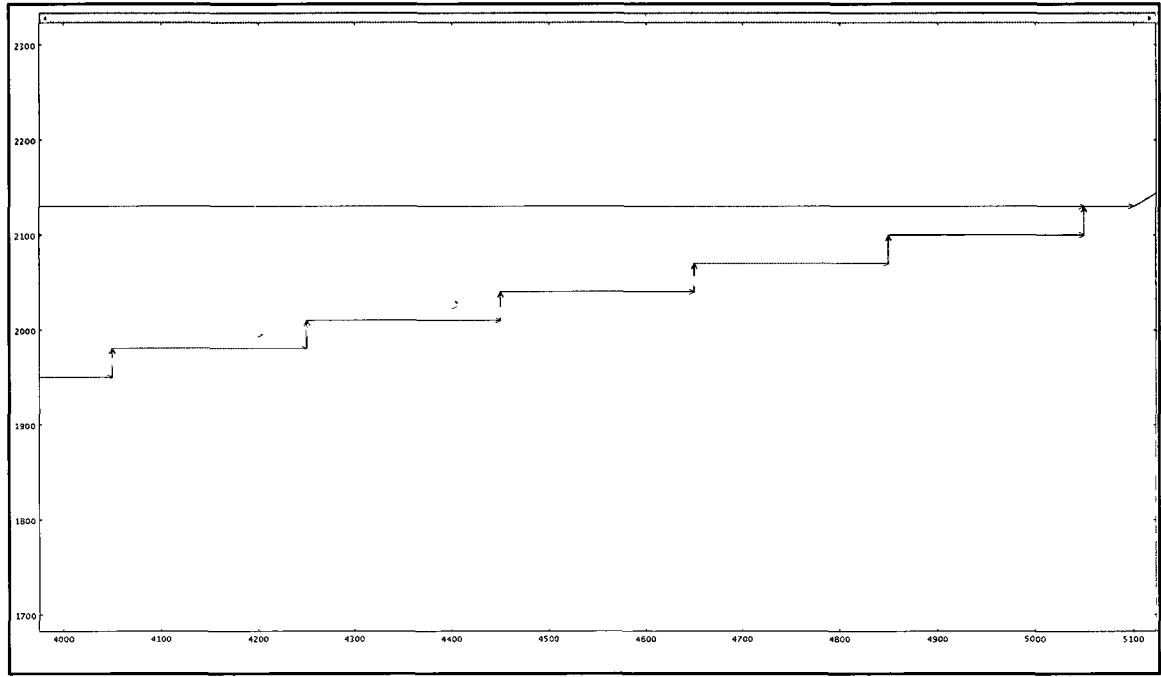
Figure 3.16: Vertical Boundaries Facing North (colored red)

Calculating the incident energy for an inclined surface, to a large extent, is more complicated. Polubelova and Izakson (1996) provide the equation for radiation received by an inclined surface:

$$\overline{Q}_t = r_1 Q_t \cos\alpha + bQ_t \sin\alpha + r_2 Q_t \cos^2\left(\frac{\alpha}{2}\right) + r_3 Q_t \sin^2\left(\frac{\alpha}{2}\right) \qquad \text{(equation 3.31)}$$

where,

$\overline{Q}$ is the average received radiation by an inclined surface in W/m^{2}day

Q_t is the average radiation received by a horizontal surface in W/m^{2}day

r_1, r_2 and r_3 are constants that vary according to the month of the year

b is a constant that varies according to the orientation of the surface

α is the angle of inclination of the inclined surface

The two inclined surfaces for which the incident radiation values required to be calculated using equation 3.31 are showed in figure 3.17.
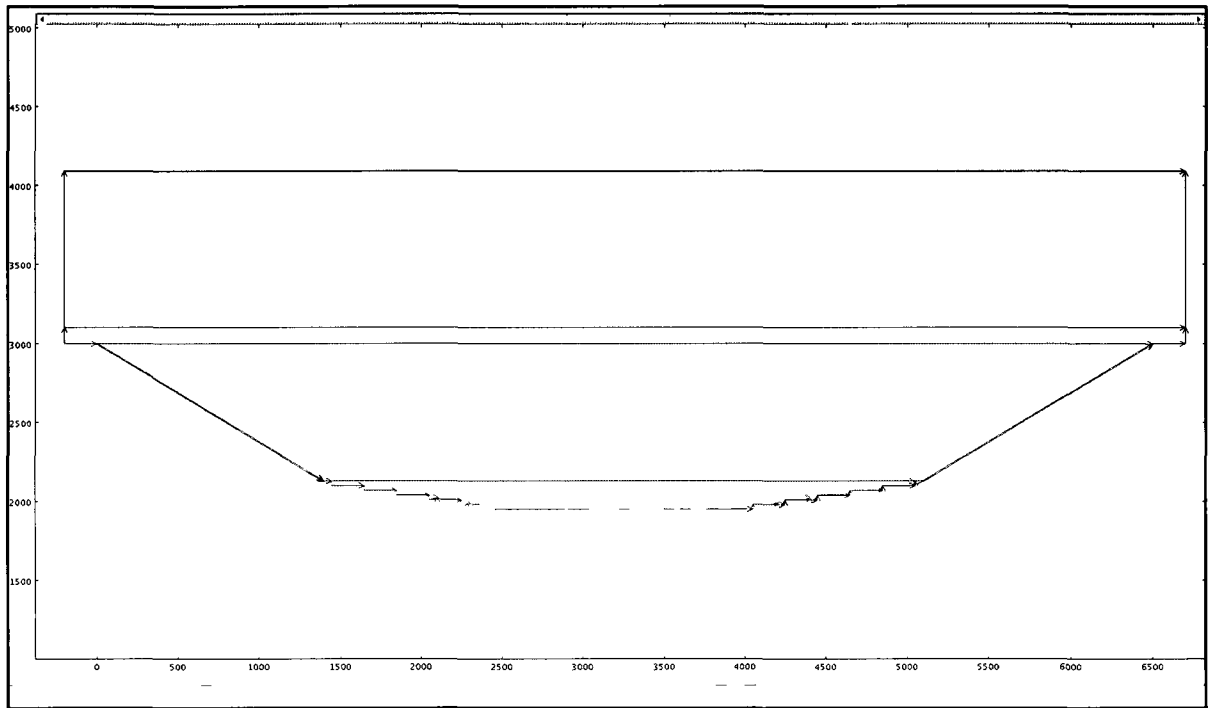
Figure 3.17: Inclined Thermal Boundaries

In figure 3.17, the inclined thermal boundaries are colored red. It can be seen that one of the boundaries face south and the other faces north. Since the value of incident radiation, consequently the retransmitted radiation is very small for inclined surfaces, and the dimension of the surface is large, it was decided that both the inclined boundaries would be approximated using the values for a south-facing surface. This allows the mitigation of the convergence problems that arise due to near-zero values at a large boundary of the model.

According to Table 3.1, the value of Q_i is 5 BTU/sq.ft./s (global). The values for r_1, r_2 and r_3 for the month of December are 0.14, 0.847 and 0.013 respectively (Polubelova and Izakson, 1996). The value for b for a north-facing slope is 0.76, and the observed overall inclination angle was at 40° (based on the slope angle of the selected arctic mine). Using these values and converting from BTU/sq.ft./s to poundal/ft·s, in equation 3.31, $\overline{Q}$ equals 1.949 poundal/ft·s as the total incident radiation on the inclined surface. Only 10% of this heat amount is retransmitted into the atmosphere.

Thus the value of the retransmitted heat is approximated as $q_0 = 0.195$ poundal/ft·s. As this surface also transmits heat as a result of incident solar radiation, the heat emission has to be coincident with daylight hours, thus resulting in the following Heaviside equation for both the inclined boundaries:

$$q_0 = -0.195 \times \text{flc1hs}(t\text{-}950,900) + 0.39 \times \text{flc1hs}(t\text{-}36000,2700) - 0.205 \times \text{flc1hs}(t\text{-}50400,5400)$$

(equation 3.32)

3.4.2.2. Sub-domain Conditions for the Convection-Conduction Equations

As in the case of the Navier –Stokes Equations, the primary sub-domain condition for the Convection-Conduction subroutine is the assumption of validity of the equations over the model space. The model is constructed such that equations 3.20 to 3.23 are valid in the model space. Since there is no in-situ heat source in the sub-domain, heat transmitted by the surface of the open-pit is entirely consumed by the in-situ mine air, thus preserving the principle of conservation of energy.

An inspection of equations 3.20 to 3.23 indicates that three attributes of air properties, viz., ρ, C_p and k are present in the equations. In order for the equations to be solved, values for these parameters, either numerical or in quantifiable expressions, therefore, must be provided.

Air density, ρ, is held constant for the flow system (Navier-Stokes). The same value must necessarily be used here. Therefore, ρ has a value of 0.094 lb/ft^3. A different strategy, however, can be used to define the parameter value of C_p and k, as both these properties are highly temperature dependant.

Since the Convection-Conduction subroutine is solved primarily for temperature, it is possible, therefore, to update the values of C_p and k at every time step when temperature is calculated. This would allow for a more accurate representation of the

actual system, albeit at the cost of making the model computationally expensive. The value of C_p is calculated as a function of temperature:-

$$C_p = 1.9327 \times 10^{-10} T^4 - 7.9999 \times 10^{-7} T^3 + 1.1407 \times 10^{-3} T^2 - 4.489 \times 10^{-1} T + 1.0575 \times 10^3$$

(equation 3.33)

where,

T is the temperature in degree K

C_p is the specific heat of air at constant pressure in J/kg-K

In this case, the value of C_p is held constant at the temperature at which the model is set as an initial condition. The value of C_p changes very little over temperature, and in the interest of convergence and simplicity, the value is calculated at -40 F° using equation 3.33.

Equation 3.33, however, is in S.I. units and need to be converted to F.P.S. units in order to conform to the norm established in this model. The converted equation is as follows:-

$$C_p = 6.009 \left(\begin{array}{l} 1.9327 \times 10^{-10} (0.56T + 255.22)^4 - 7.9999 \times 10^{-7} (0.56T + 255.22)^3 + \\ 1.1407 \times 10^{-3} (0.56T + 255.22)^2 - 4.489 \times 10^{-1} (0.56T + 255.22) + 1.0575 \times 10^3 \end{array} \right)$$

(equation 3.34)

In equation 3.34, T is in °F and C_p is in poundal-foot/lb-°F. The value of C_p is calculated as 6040.7 poundals/lb-°F.

The equation for calculating the isotropic conductivity k is given below.

$$k = 1.5207 \times 10^{-11} T^3 - 4.8574 \times 10^{-8} T^2 + 1.0184 \times 10^{-4} T - 3.9333 \times 10^{-4} \text{ (equation 3.35)}$$

where, *T* is the temperature in degree K.

Equation 3.36 in the F.P.S. system can be written as follows:-

$$k = 4.0136 \left(\begin{array}{l} 1.5207 \times 10^{-11} (0.56T + 255.22)^3 - 4.8574 \times 10^{-8} (0.56T + 255.22)^2 + \\ 1.0184 \times 10^{-4} (0.56T + 255.22) - 3.9333 \times 10^{-4} \end{array} \right)$$

(equation 3.36)

where, T is in °F.

This equation is entered into COMSOL® environment, and is updated every time step when a new temperature is calculated.

Additionally, to keep symmetry with the Navier-Stokes equations, the artificial diffusion parameter is chosen to be isotropic in nature, and its tuning parameter held at 0.5.

3.4.2.3. Initial Conditions for the Convection-Conduction Equations

The important initial condition for the Convection-Conduction subroutine is the temperature condition that imposes an initial temperature on the entire model space. This temperature, however, can be varied between model runs. The model is started from a neutral position, i.e., without an inversion cap. The Inversion cap is then established on the model by transporting heat away from the model space through the pit surfaces. Heat is then added to the model space through the same surfaces at sunrise to model ideal conditions.

3.4.3. The Convection-Diffusion Equations

The Convection-Diffusion equations are a set of non-linear partial differential equations that describe the movement of a gaseous pollutant due to the convection of a

fluid. The characteristics equations governing the convention-diffusion phenomenon are as follows:

$$\frac{\partial c_x}{\partial t} = D\frac{\partial^2 c_x}{\partial x^2} - u\frac{\partial c_x}{\partial x} + Q_x$$

(equation 3.37)

$$\frac{\partial c_y}{\partial t} = D\frac{\partial^2 c_y}{\partial y^2} - v\frac{\partial c_y}{\partial y} + Q_y$$

(equation 3.38)

$$\frac{\partial c_z}{\partial t} = D\frac{\partial^2 c_z}{\partial z^2} - w\frac{\partial c_z}{\partial z} + Q_z$$

(equation 3.39)

$$c_x\frac{\partial u}{\partial x} + c_y\frac{\partial v}{\partial y} + c_z\frac{\partial w}{\partial z} = 0$$

(equation 3.40)

where,

c_x, c_y and c_z are the concentrations in the x-, y- and z-directions in mols/ft^3

D is the isotropic diffusion coefficient in ft^2/s

u, v and w are the advective air velocities in the x-, y- and z-directions in ft/s.

Q_x, Q_y and Q_z are the sources/sinks of mass in the model source in the three Cartesian directions (mols/s)

Equations 3.37 to 3.40 are used to calculate the concentration variations that occur in the model grid after the pollutant is injected into the model space and then transported by the advective currents as well as by molecular diffusion. The pollutant sources could emit noxious gases at a constant rate or can be functionalized with respect to space or time. Once released, the mass is carried by diffusion as well as by the advective current present in the model space. The advective current is a result of the Navier-Stokes velocity updated as a result of the Convection-Conduction phenomenon. The air flow rearranges the concentration profile of the pollutant. This concentration profile, under varying boundary, sub-domain and initial conditions, is the resultant pollutant concentration at various points in the model space.

In equations 3.37 to 3.39, the term $\frac{\partial c_s}{\partial t}$ (where s is the relevant Cartesian coordinate) is the rate of change of pollutants concentration over time. The pollutant, entering the model space, is then transported throughout the space with the help of the diffusion and advection terms $D\frac{\partial^2 c_s}{\partial s^2} - \dot{s}\frac{\partial c_s}{\partial s}$, where the first part, $D\frac{\partial^2 c_s}{\partial s^2}$ transports the mass using solely diffusion, and the second part, $\dot{s}\frac{\partial c_s}{\partial s}$, adds to or modifies that transport action using the advective velocities calculated by the first two subroutines. Equation 3.40 is held true in this case as the flow does not have variable density and is non-conservative in terms of pollutant mass. As usual, equation 3.39 is obviated due to the lack of the z-dimension in the model.

In order to solve this system of equations, a number of appropriate boundary, sub-domain and initial conditions have to be applied, which are discussed in the following sections.

3.4.3.1. Boundary Conditions for the Convection-Diffusion Subroutine

The boundary types for the Convection-Diffusion subroutine are relatively simple. They fall into three categories, viz., a constant concentration boundary, a wall boundary where the mass flow is ceased, and a mass generation boundary.

Figures 3.5 and 3.6 show the boundaries of the model separating it from the space beyond the mine atmosphere. When a mass of pollutant hits these boundaries they are at the threshold of overstepping the boundary. As noted before, the mass is transported to these boundaries via the velocities generated by Navier-Stokes and Convection-Conduction. It has already been established that at some of these boundaries the velocity vectors are neutralized (wall), or they flow in and out of the model space freely (inflow and open boundaries). Given the wide array of flow boundary conditions, the concentration boundary conditions chosen must be such that they maintain the mass balance in the model space. To that end, a constant concentration

boundary (Dirichlet condition) is chosen for all the six boundaries, and a constant value for concentration is held at zero. Mathematically, this boundary condition is represented as follows:

$$c = c_0 \qquad \text{(equation 3.41)}$$

where, c_0 is the constant concentration in moles/ft^3.

This equation can be decomposed into sub-equations for all three Cartesian coordinates. The condition shown in equation 3.41 helps maintain the flow of mass out of the system, because a zero concentration helps maintain a concentration gradient along which mass can always flow.

The pit profile of the model is assigned the insulation/symmetry boundary condition (Robin conditions). The condition of insulation/symmetry can be mathematically described as follows:

$$\vec{n} \cdot \left(-D\frac{\partial c_x}{\partial x} - c_x u \right) = 0 \qquad \text{(equation 3.42)}$$

$$\vec{n} \cdot \left(-D\frac{\partial c_y}{\partial y} - c_y v \right) = 0 \qquad \text{(equation 3.43)}$$

$$\vec{n} \cdot \left(-D\frac{\partial c_z}{\partial z} - c_z w \right) = 0 \qquad \text{(equation 3.44)}$$

Here,

$\vec{n}$ is the normal in the direction perpendicular to the boundary, pointing away from the domain

c_x, c_y and c_z are the concentrations in the x-, y- and z-directions in moles/ft^3

D is the isotropic diffusion coefficient in ft^2/s

u, *v* and *w* are the corresponding advective air velocities in the x-, y- and z-directions in ft/s.

With equation 3.44 disregarded, the condition stipulates that the flow of mass out of the model space at those boundaries is zero, thus enforcing the wall condition.

While the sources are point sources for model purposes, they have definite geometry. Thus the sources participate in the model through the source boundaries. The source boundaries representing the production equipment in the pit, shown in Figures 3.11 and 3.12, are assigned constant flux boundaries (Robin conditions), such that the boundaries emit pollutant mass at a constant rate into the model space. This condition is mathematically represented as follows:

$$-\vec{n} \cdot \left(-D\frac{\partial c_x}{\partial x} - c_x u \right) = \vec{N}_{0x} \qquad \text{(equation 3.45)}$$

$$-\vec{n} \cdot \left(-D\frac{\partial c_y}{\partial y} - c_y v \right) = \vec{N}_{0y} \qquad \text{(equation 3.46)}$$

$$-\vec{n} \cdot \left(-D\frac{\partial c_z}{\partial z} - c_z w \right) = \vec{N}_{0z} \qquad \text{(equation 3.47)}$$

where,

N_{0x}, N_{0y} and N_{0z} are the constant mass fluxes in the three Cartesian coordinates in mol/ft^2·s.

The above three equations describe a condition where pollutant mass is being injected into the model space at a constant rate. As noted before, hypothetical data were used to describe the mass inflow, as the field data could not be adequately used in a 2D model. The value for N_0 in totality, without the vector components, was taken to be a sufficiently small value (0.04 mol/ft^2·s). Since multispecies modeling would add significant complications to the existing model, it was decided to model only one species of gas. The reason for choosing NO was that NO is one of the most toxic gases

present in the open-pit environment. To this end, Nitrous Oxide (NO) was selected as the gas to be modeled. Thus the value indicated here actually represents 0.04 mol/ft^2·s of NO. The appropriate dialogue box is shown below.
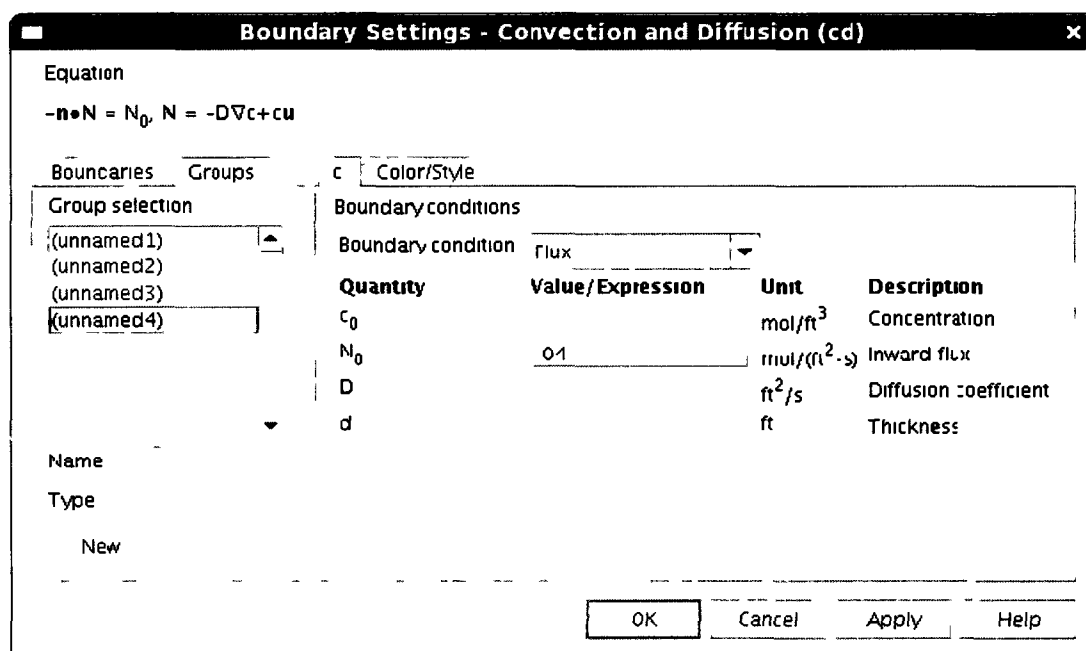
Figure 3.18: Dialogue Box for Input of Pollutant Flux into the Model

3.4.3.2. Sub-domain Conditions for the Convection-Diffusion Subroutine

The most important attribute for the sub-domain condition in the Convection-Diffusion subroutine is the isotropic diffusion coefficient. This parameter depends on several physical properties, the most important of those being the temperature, viscosity and the mass concentration. The diffusion coefficient is a measure of the speed with which a substance with an imbalanced concentration in another medium, if left undisturbed, travels through the medium. Its concentration would eventually reach equilibrium throughout the mass of the medium. Thus, it is a sum of isotropic molecular diffusion and other such forces, as may be applicable, that project the pollutant into the medium (e.g. temperature, pressure, projection velocity etcetera). Thus, the diffusion coefficient can be used to account for a large number of factors

that influence the transport of the substance through the massive medium. This diffusion coefficient is then often termed as the effective diffusion coefficient.

Although some literature describing the process and the rate of molecular diffusion for different gases under varying conditions is available, the study of effective diffusion coefficient for in-mine conditions, has been sparse. In the absence of any reliable value for diffusion coefficient, the value assumed for D in this case is 0.5 ft^2/s. Although this value may be extremely high when compared to strictly molecular diffusion, it was understood that due to the action of other factors such as projection velocity, temperature, etcetera, on the influent gas, a higher value of effective diffusion coefficient may be appropriate. The dialogue box is shown in figure 3.19.

Figure 3.19: Dialogue box for Input of Diffusion Coefficient

In addition, as mentioned in the two previous subroutines, isotropic diffusion with a tuning parameter value of 0.5 is chosen as the predominant mode of artificial diffusion.

3.4.3.3. Initial Conditions for the Convection-Diffusion Subroutine

The important initial condition for the Convection-Diffusion subroutine is the initial pollutant concentration of the substance in the medium. Since the concentration of NO in fresh air is negligible, the initial concentration was assumed to be zero.

3.5. Steps in Preparation for Model Solution

After completion of the development of the model, its geometry and application of all relevant boundary, sub-domain and initial conditions, additional steps are still needed before it can be executed to obtain the desired solutions. These consist of applying an appropriate grid to the model space and choosing an appropriate solution algorithm for the system of equations. These two steps are discussed in the following sections.

3.5.1 Applying a Grid

The equations presented in section 3.4 are partial differential equations that characterize or approximate the governing physical processes. A close form solution for these equations over the continuous space is extremely complex and is difficult to obtain or may not be available. The only feasible alternative is to discretize the model space and solve the equations using numerical techniques such as finite difference or finite element methods. The model space is complex and symmetry cannot be assumed, therefore, both the numerical solution approaches would require the establishment of a grid over the entire model space.

Figure 3.20 illustrates a typical spatial discretization using either finite elements or finite difference.
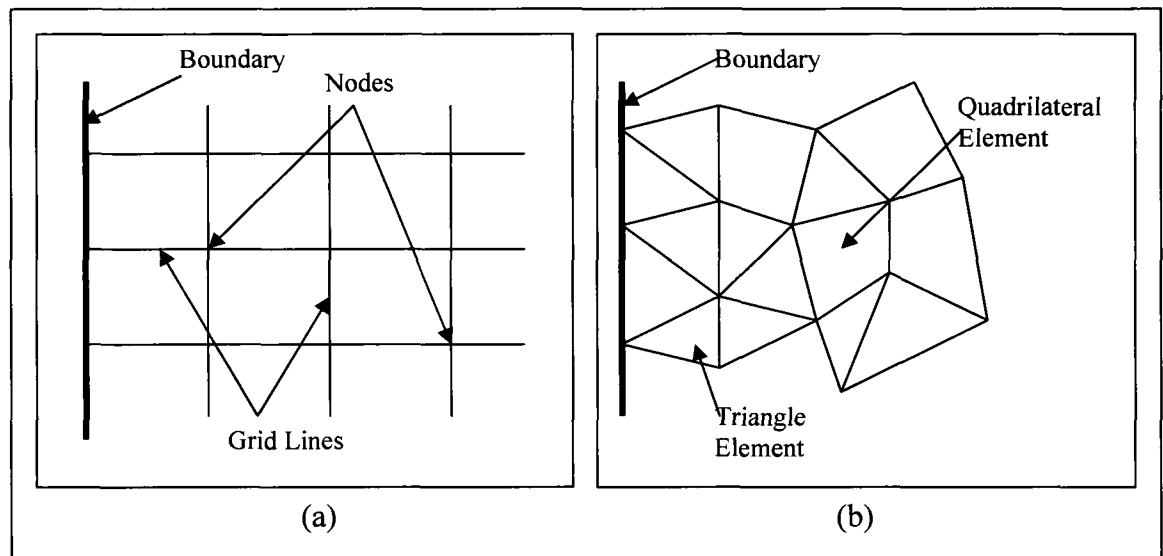
Figure 3.20: Discretization of Model Space – (a) Finite Difference (b) Finite Element

Figure 3.20(b) The solution of the system of equations in a discretized space as such propagates from element to adjacent element with vectored continuity boundaries at the edges. This method is very effective in handling complex geometries.

COMSOL® uses a finite element grid, and offers a choice to the user to plot a grid according to specific needs. For this research, however, it was found by trial and error that the dynamic gridding function inbuilt in COMSOL® produces the most effective grid for the problem being modeled. The grid consists of triangular elements. A depiction of the gridded model follows (figure 3.21).
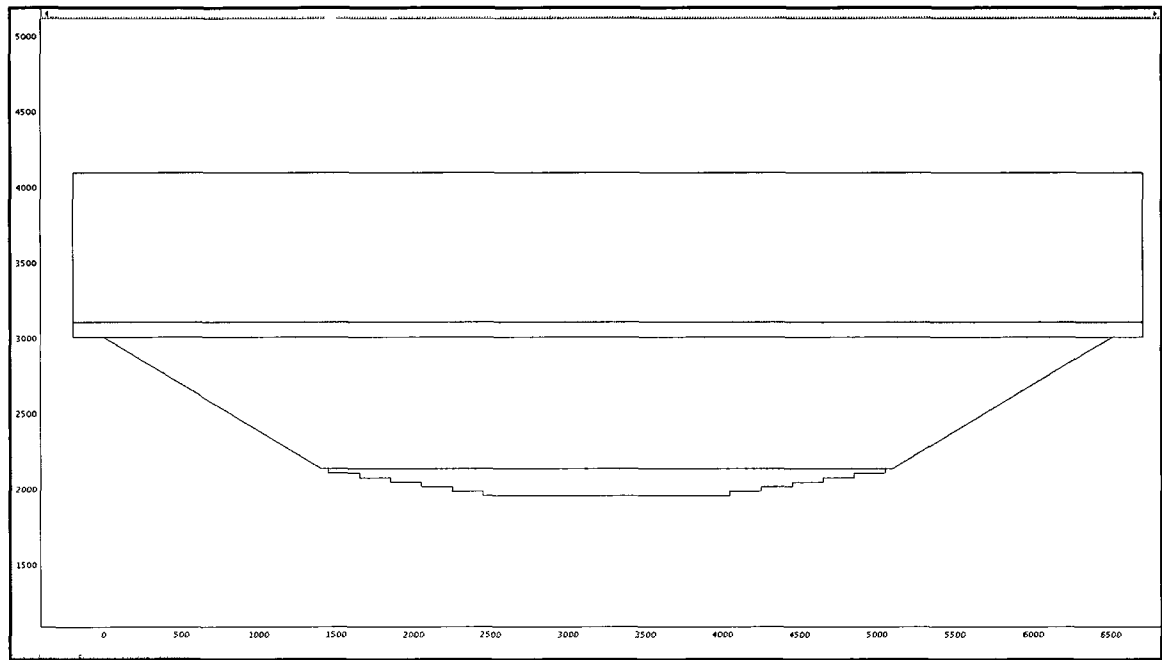
Figure 3.21: The 2D Model Space with Grid Imposed on the Model Space

3.5.2 Choosing Solver Algorithm

A large number of solutions algorithms appropriate for complex flow of problems are available. Since the present problem, when represented as matrices, presents a significant sparsity problem and a large geometry, the algorithm known as the Sparse Object Oriented Linear Equation Solver (SPOOLES) was chosen. SPOOLES was chosen because it is a self-adjusting algorithm that can factorize and solve sparse matrices.

3.6. Model Results and Discussions

This section presents the results obtained from simulation of the developed model. The model was run for a total of 63000 seconds, or, 17.5 hours. Solutions for the system of equations described in section 3.6 are obtained for every element of the model. This spatial solution is a static solution, which is obtained without the benefit of the temporal steps. The process of the static solution is repeated at every predetermined time interval, until the entire model time period is exhausted. This process of

calculating the solution at the end of every definite time interval is called time-stepping and is an integral and important part of the model solution. The convergence of a model is critically dependant on the time-step chosen. Too large a time-step would possibly overstep a solution critical to the convergence of the problem at the end of the model time period; too small a time-step might lock the solution algorithm into a recursive loop, thus rendering a solution impossible. The initial time step chosen for this model is 0.5 seconds and the solution is updated every 2 seconds, which denotes the regular time step. Figure 3.22 shows the time-steps chosen for the model.
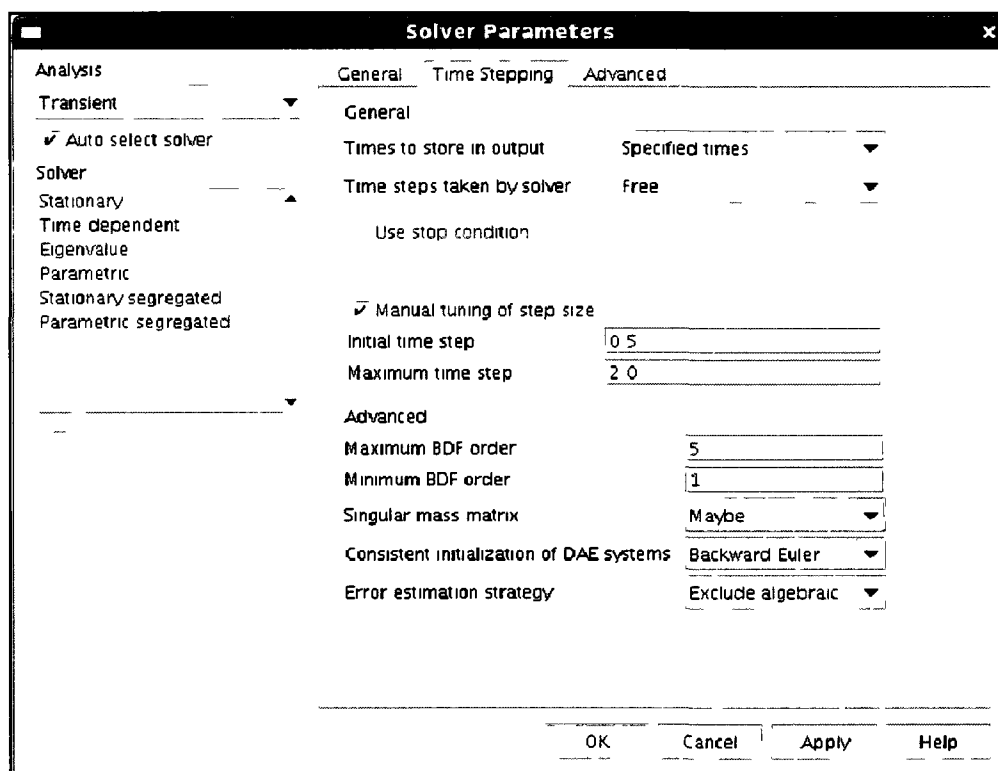
Figure 3.22: Dialogue Box for the Solver – Time-stepping

While the model was solved over the entire time domain (63000 seconds), not all the results calculated at every step are used to plot the concentration trendlines shown later in this section. Since the amount of pollutant introduced into the mine atmosphere and the incident velocity carrying the pollutant via advection are both small, it is deemed appropriate that a measure of the pollutant concentration

distribution is taken every two hours (7200 seconds) in order to study the trends. The dialogue box for the SPOOLES solution algorithm is shown in Figure 3.23.
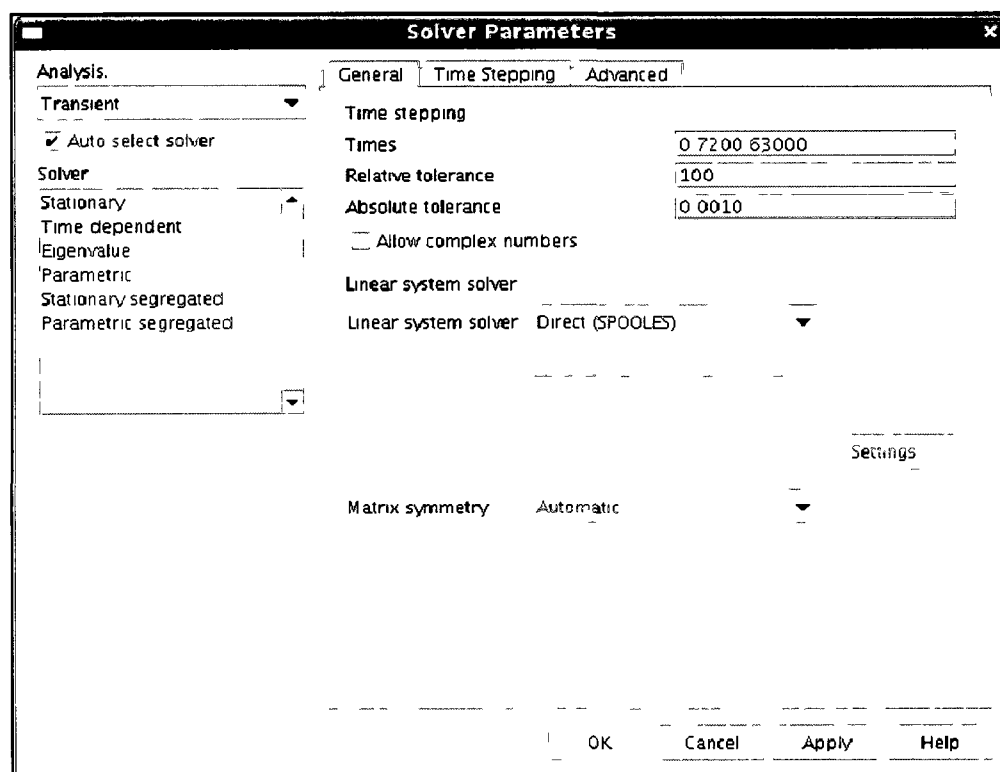
Figure 3.23: Dialogue Box for the Solver

The solutions for the velocities in the two corresponding Cartesian coordinates, the pressure and the concentration are calculated over the entire model space. The contaminant concentration trends were obtained at several pre-specified locations within the model domain as shown in Figs. 3.24 and 3.25. These locations should likely correspond with areas where people tend to work mostly within the mine.
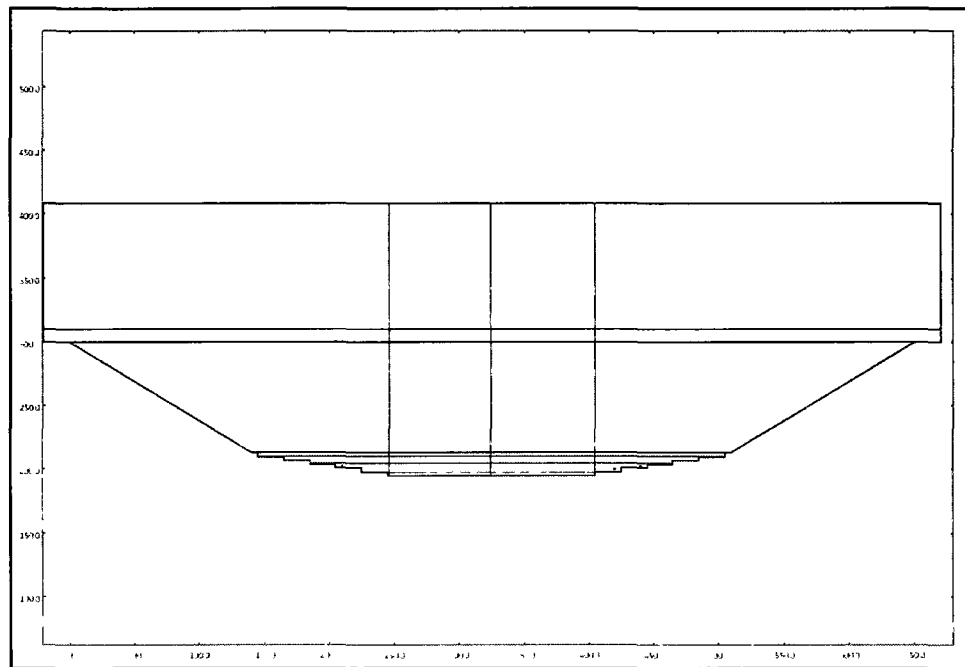
Figure 3.24: Locations of Lines along which Concentration and Temperature Profiles are Plotted
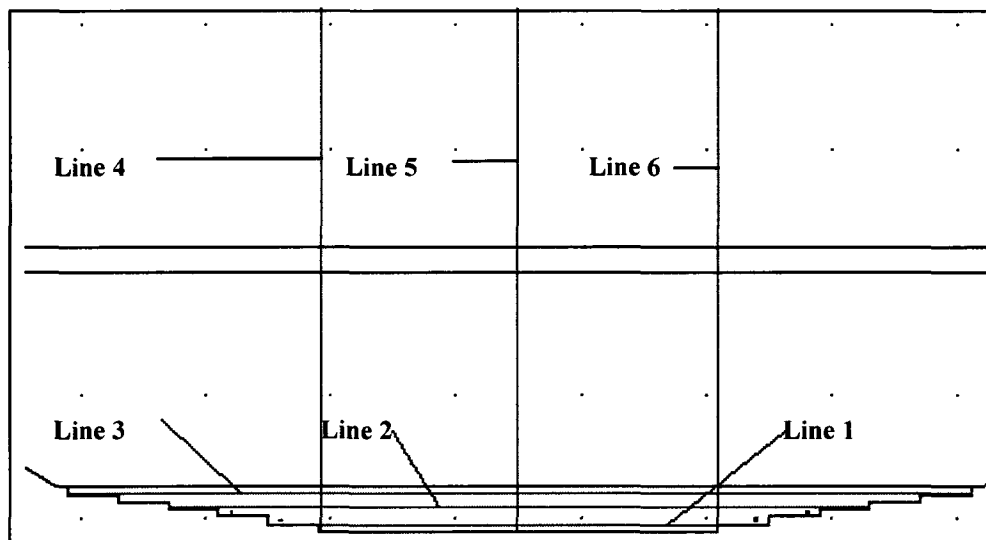
Figure 3.25: Close-up of the Locations of Lines along which Concentration and Temperature Profiles are Plotted.

The blue lines shown in Figure 3.24 and magnified in figure 3.25 are parallel to the floor of the pit (or the longitudinal section of the model). Line 1 is located 6 ft above the floor of the mine. This is because the concentration of the pollutant at the floor of

the mine, while hazardous to health, does not raise any immediate concern, as it is located too low for it to be breathed in by a person, while the atmosphere at the height of 6 ft is likely to be in the breathing zone. Similarly Line 2 and Line 3 are also located 6 ft above the second and the fifth production benches respectively. The red lines shown in the figures are located at either the edge of the pit bottom or the center of the pit, and, are parallel to the vertical axis of the model, extend to the limit of the model space in the y-direction. These lines are chosen because the atmosphere above the center of the pit (pit bottom) is where the strongest inversion exists, the removal of pollutants from this region is generally most difficult.

3.6.1. Dispersion of Pollutants with an Influent Velocity 2 ft/s and an Initial Temperature -40 °F

This section provides the results of the simulation with an influent velocity of 2 ft/s and an ambient temperature of -40 °F. Figure 3.26 shows the velocity vector profile in the model space at the end of the model run time (63000 seconds). Figure 3.27 shows the pollutant concentration profile in the model space. Figures 3.28 to 3.33 are the representations of the temporal variation of the concentration profiles in the model space along each pre-selected location. All times denoted in the figures are in seconds.
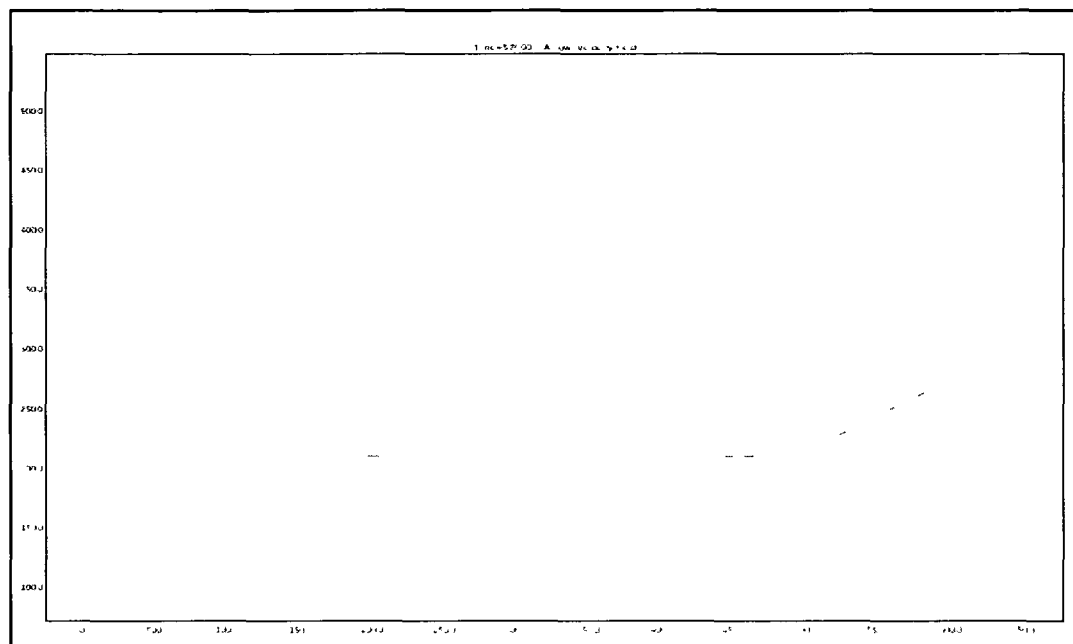
Figure 3.26: Velocity Profile with an Influent Velocity 2 ft/s and an Initial Temp. -40 °F
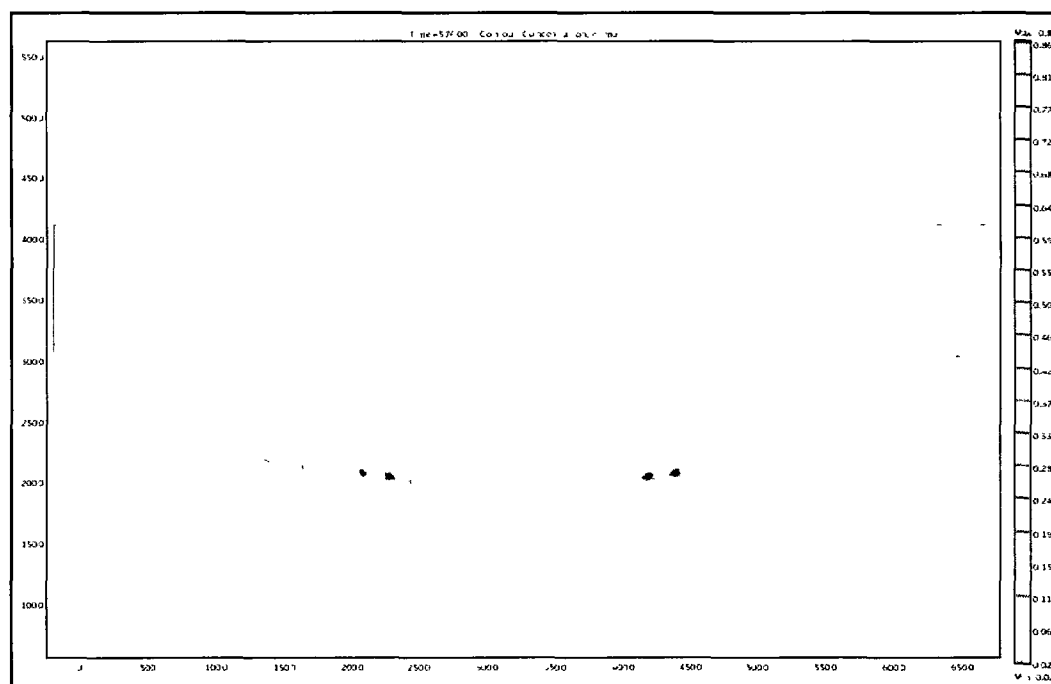
Figure 3.27: Concentration Profile with an Influent Velocity 2 ft/s and an Initial Temp. -40 °F

NO Concentration along Line 1 with a Velocity of 2 ft/s and a T of -40 °F
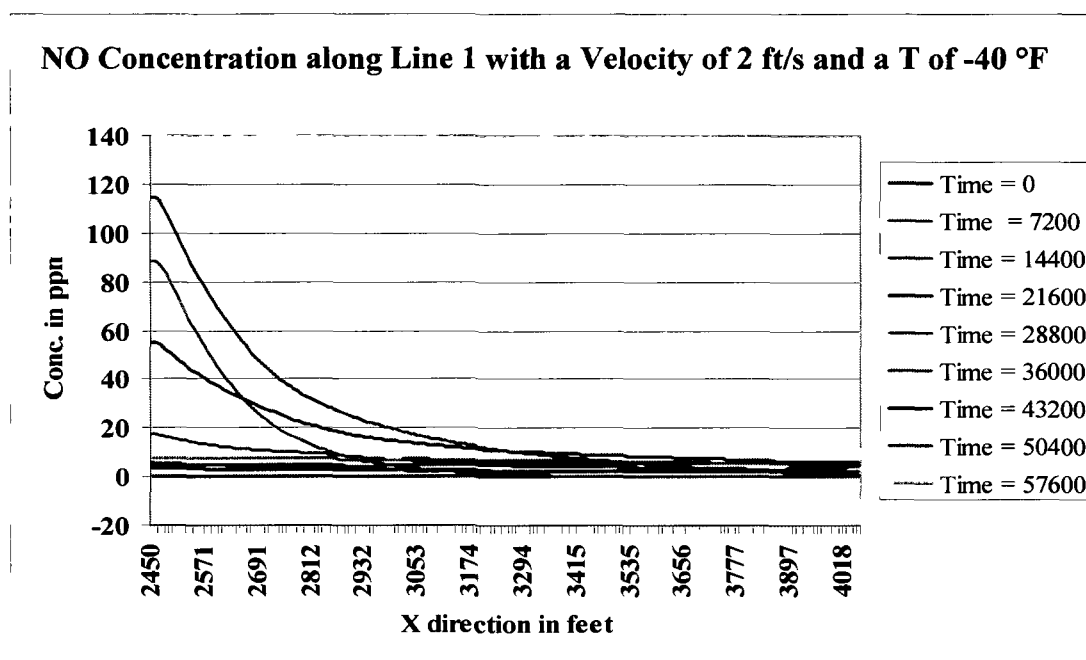
Figure 3.28: Concentration Profile along Line 1 with an Influent Velocity 2 ft/s and an Initial Temp. of -40 °F

NO Concentration along Line 2 with a Velocity of 2 ft/s and a T of -40 °F
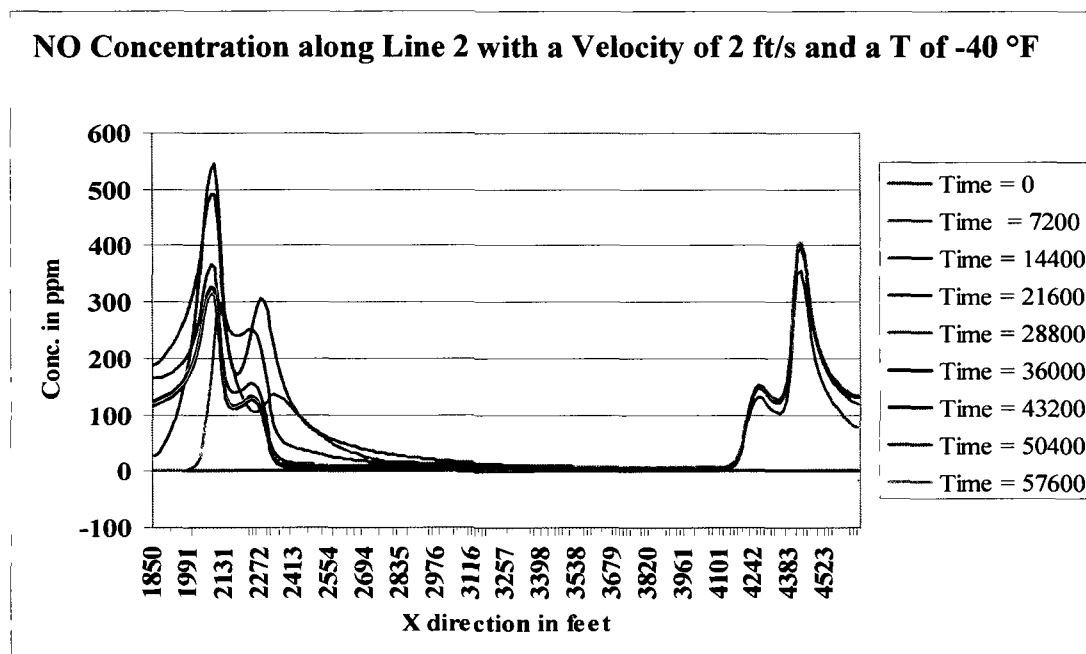
Figure 3.29: Concentration Profile along Line 1 with an Influent Velocity 2 ft/s and an Initial Temp. of -40 °F

NO Concentration along Line 3 with a Velocity of 2 ft/s and a T of -40 °F
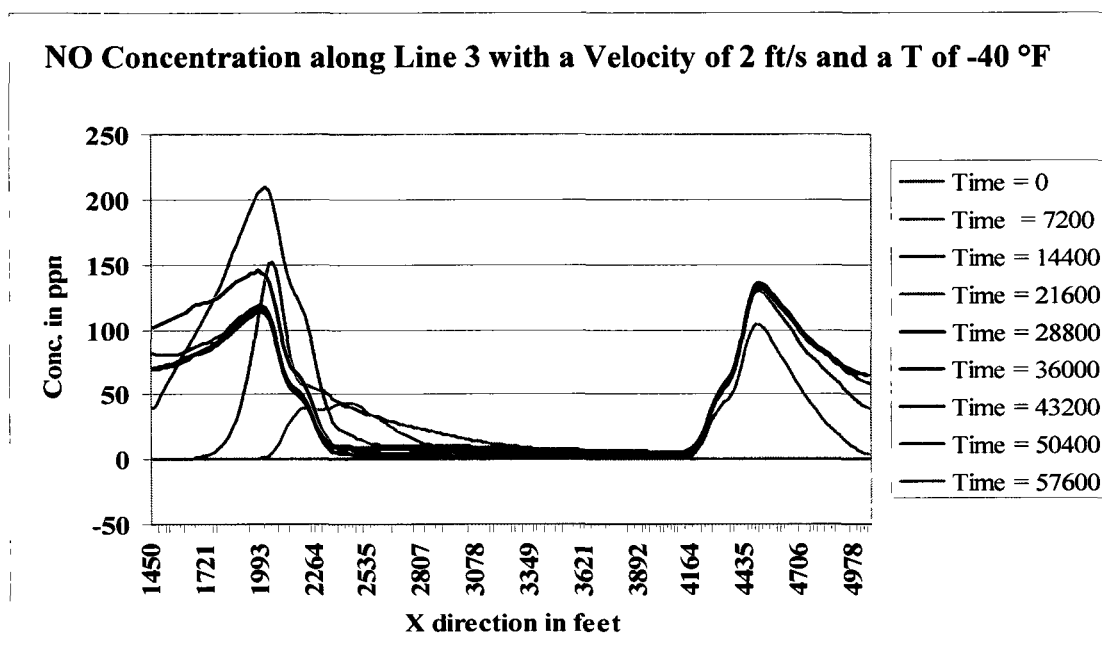
Figure 3.30: Concentration Profile along Line 3 with an Influent Velocity 2 ft/s and an Initial Temp. of -40 °F

NO Concentration along Line 4 with a Velocity of 2 ft/s and a T of -40 °F
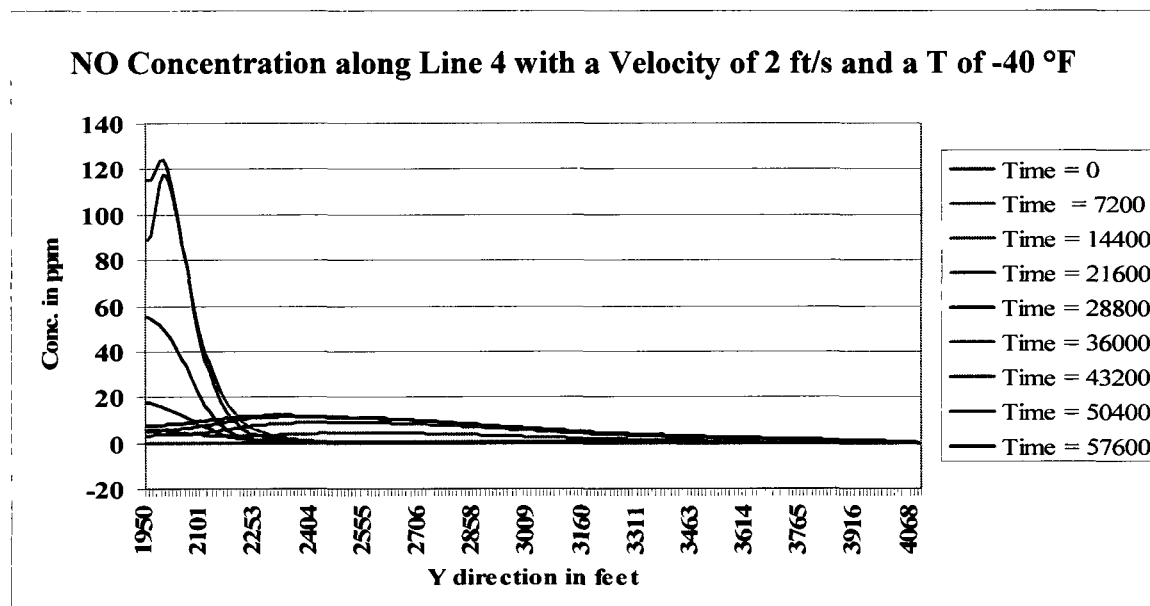
Figure 3.31: Concentration Profile along Line 4 with an Influent Velocity of 2 ft/s and an Initial Temp. of -40 °F

NO Concentration along Line 5 with a Velocity of 2 ft/s and a T of -40 °F
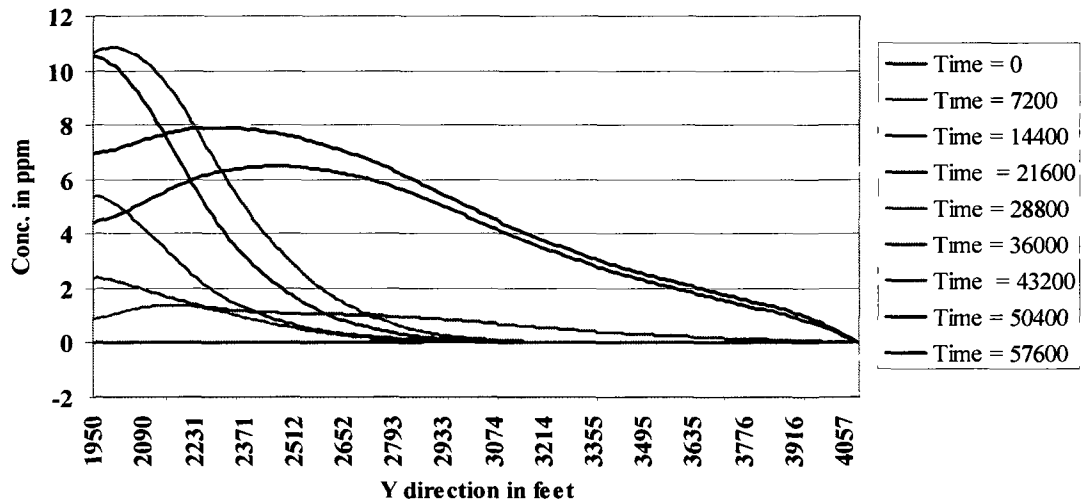
Figure 3.32: Concentration Profile along Line 5 with an Influent Velocity 2 ft/s and an Initial Temp. of -40 °F

NO Concentration along Line 6 with a Velocity of 2 ft/s and a T of -40 °F
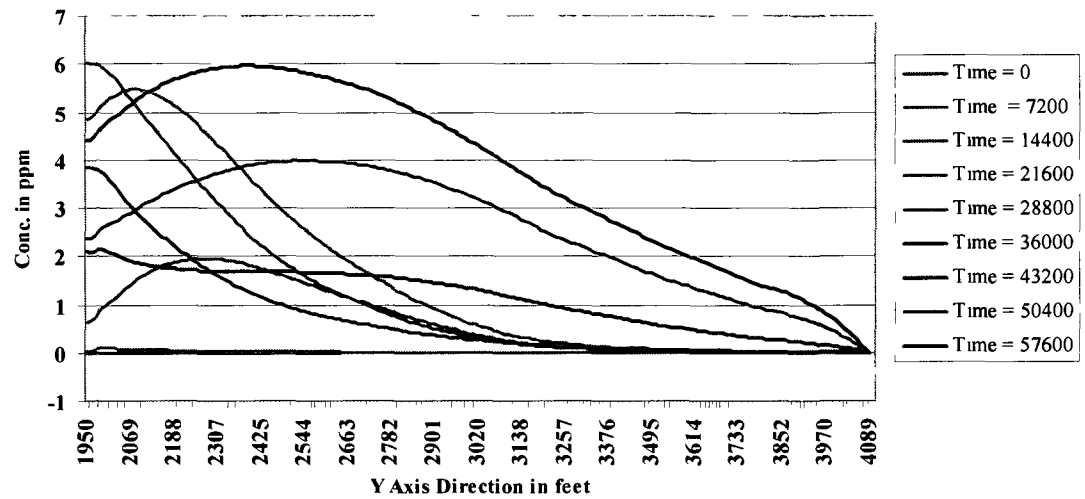
Figure 3.33: Concentration Profile along Line 6 with an Influent Velocity 2 ft/s and an Initial Temp. of -40 °F

In figure 3.26 the velocity of the wind is denoted by the magnitude of the arrow (in this case simply its scaled size), and the arrow points to the direction of flow. The arrows near the left hand side of the pit, close to the inflow boundary, are the largest, which is expected as the influent air has the highest magnitude near the inlet. Though the influent air is projected parallel to the model x-axis (perpendicular to the inflow boundary), its direction changes as it travels in the model space and flows either toward the ceiling of the model or toward the floor of the mine. This is primarily due to the fact that the influent air, initially on entering the model space, collides with the in-situ mass of cold air, and lacks enough kinetic energy to displace it. While some momentum is transferred to the in-situ mass of cold air, the remaining kinetic energy in the influent air forces it to take the path of least resistance, and thus attempts to streamline around the model space. However, once a steady flow is established between the influent and the open boundaries serving as outlets, the patterns of flow established in the model space influences the trajectory of the influent air. A close examination of the vector field shows that while most of the flow, notably the flow in the space above the rim of the pit, simulates a quasi-laminar flow condition, the lower reaches of the pit on the windward side (adjacent to the inflow boundary) shows that the velocity vectors move in a recirculatory fashion along the slope. It can be noted that the influent air travels in a slight curve upwards and then descends into the pit, and eventually a part of the air mass cycles back along the slope upward toward the inflow boundary. This flow forms a steady vortex, albeit of very low velocity eddies.

The presence of the aforementioned vortex is of significant interest. The existence of this flow is counterintuitive, because it shows that in an open-pit mine with low influent velocities, some of the air flowing into the space is likely to cycle back toward the origin of the flow. Most flow problems are visualized as analogous to pipe or channel flows, in which case given restricted space, the flow must follow the pressure gradient and such a backflow in a recirculatory pattern should occur. The presence of the backflow would indicate that the cold air in the open pit cannot in many cases be

displaced easily and due to higher pressure, the influent air is directed back to the origin of flow, which may be at lower pressure. It may also be the result of a partial vacuum created close to the inflow boundary due to the presence of the velocity at the inlet. It is also possible that as the flow enters the pit, it comes across a larger open space in y-dimension and expands suddenly, sapping it of energy and causing it to sink toward the pit bottom, until impetus from higher pressure at the bottom of the mine propels it back.

It is possible to view this flow as turbulent flow. However, close inspection indicates that the flow velocities are very small, and the change in the magnitude and direction of the flow occurs over a large effective flow length, which means that the trajectory of the flow is very small. Thus it can be said to be approaching turbulence from a laminar flow regime, and can be classified as quasi-laminar.

The backflow exerts a powerful influence on the advective transport of pollutants in an open pit, as illustrated in Figure 3.26. It can be clearly seen that the pollutants from the sources located near the inflow boundary, once released into the model space, travel back toward the source, while those released from sources located at the outflow boundary (leeward side of the pit) travel with the general pattern of flow toward that boundary. Although the actual values of the concentration contours may not be realistic due to the lack of the third dimension, the trends in mass transport shown here provide important clues to the actual movement of pollutants in similar situations. Knowledge of this particular pattern of pollutant transport would be useful in planning mitigation measures.

Figure 3.28 illustrates the transport of the pollutant—chosen as nitrous oxide (NO)—across Line 1. The x-axis (longitudinal axis) shown in the graph is in feet, but is not the length of the line, but rather the x-coordinates of the points along the line. Thus the pollutant trend along different points along a line can be seen clearly. Line 1 is located below the pollutant sources and due to the flow pattern described above, encounters very little NO. It can be seen that the line encounters a much higher concentration of

NO towards the inflow boundary. This is an expected pattern, because the backflow described above re-circulates the NO generated from the neighboring sources and some of that pollutant superimposes along Line 1. A notable fact is that the highest concentration on NO is encountered at 14400 seconds (4 hours after the model is started). It can also be seen that the sources located on the leeward side, though generating NO at the same rate has very little influence on concentration along Line 1, as the NO generated here is transported directly to the outflow boundary following the predominant air flow pattern.

Figure 3.29 describes the concentration of NO across Line 2. This line is located just above the pollutant sources (Figure 3.25), consequently registering the two sets of pollutant sources on two sides. The two composite peaks are clearly exhibited here. The two peaks are not single, distinct peaks, but a composite, and superimposed. The reason for this is the presence of two pollutant sources in close proximity on both sides, superimposes and reinforces their effects on the concentration of NO on Line 2. As can be seen, the dual peaks closer to the inflow boundary is not superimposed, while on the leeward side, the flow is more streamlined. This can be attributed to the presence of a steadier flow toward the leeward side, as opposed to a quasi-laminar flow toward windward side of the open pit. It should also be noted that the highest value is reached after the same 4 hours in the time domain.

Figure 3.30 shows a peak profile which is similar to Figure 3.29. It shows the NO concentration profile along Line 3. The twin peaks that are prominent in Figure 3.29 are not as sharp here, partly due to the location from the sources. As previously noted, the peaks on the windward side are more integrated than those on the leeward side, but the highest value is reached at a later time in the time domain (21600 seconds or 6 hours). The lag in reaching the peak value can be attributed to the distance of the line from the sources, as well as to a possibility of the inversion cap being lifted and, as a result, the trapped NO may be dispersing.

Figure 3.31 describes the concentration profile along Line 4. This line extends from the pit bottom of the open-pit to the top boundary of the model space and is parallel to the y-axis. The line is placed at the windward edge of the pit bottom (Figure 3.25) and extends from 1900 ft to 4100 ft in the model space. It can be seen that the highest concentration value is reached after the model is execute for 4 hours in the time domain, and occurs close to, but not at, the bottom of the open-pit. The pollutant sources are placed 30 ft and 60 ft above the pit bottom, and the pollutants emitted are carried away by advection from the pit bottom of the mine, resulting in the position of the peak value being higher than the pit bottom. It can be seen that apart from the peak values, not much pollutant is present along the line. This is due to the vortex created by the backflow, which re-circulates the pollutant in the zone of influence of the vortex. During recirculation, substantial mass of NO is pushed up by advection, but not transported en-masse across the line from the sources, but is moved back toward the source. An examination of this flow pattern indicates that most of the re-circulated pollutant only encounters the section of the line closer to the pit bottom, which concentrates the mass of NO toward the bottom of the line. The NO concentration encountered by the rest of the line (along the y-axis in the model) is transported due to advection, and thus very little pollutant concentration can be found there. The high peak values near the lower segment of the line suppress important trends found in the upper segment of the line and are explained with the help of Figure 3.32 and 3.33.

Figure 3.32 describes the concentration profile along Line 5. This line is similar to Line 4, but located in the mid-section of the pit. The concentration values observed here are much less than in other locations, because very little advection is encountered by the mass of NO along this line. The lower peak value in this figure indicates the trends that are clearly evident in the previous figures. The peak value is reached after 4 hours in the time domain. After six hours in the time domain, a relatively decreasing concentration values, can be observed, which may be attributed to the concentration near the pit bottom, which is very high, and the diffusive process is transporting some

of the pollutants away from the pit bottom. This downward trend in concentration continues for another two hours (8 hours of model run time). The heat from the ground is turned on after approximately nine and a half hours in the time domain and reaches its peak value according to equations 3.28, 3.30, 3.31 and 3.33 after ten and a half hours. The heat aids in the removal of pollutants from the bottom by re-establishing the convective current which was initially lacking due to the inversion, and thus the downward trend of the pollutant concentration is intensified after 12 hours in the time domain. The sudden jump in the peak value after 14 hours, however, is a noticeable deviation from this trend. It is also apparent that the peak value is moved from the pit bottom and travels up along the y-axis. The reason for these two observations is as follows-

The heat from the ground coupled with that from the equipment is built up for a significant period of time within the model and establishes a strong convective current, which can be visualized as a vector field oriented vertically upwards. Such a field was not visible in Figure 3.26 because of its low magnitude. This vector field directs the flow of pollutants upward, and is significantly aided by the positive concentration gradient in the upward direction. Once the pollutants have attained sufficient height, they are transported up by the advective current of the vortex in the windward side of the pit and transported across Line 5, naturally intersecting Line 5 high up from the pit bottom. This effect is not pronounced in the results after 10 hour and 12 hour in the time domain due to the weakness of both the convective current and the concentration gradient. This effect is reversed at the very end of the time domain.

The heat is switched off at 13 hours 15 minutes in the time domain (in order to represent sunset) and reaches initial values after 14 hours 45 minutes. This means that the concentration results plotted after 16 hours of model run have very little influence of heat in pollutant transport. Thus, as convective current subsides, the concentration gradient from the constantly emanating sources remains as the only driving force to propel the pollutants upwards. Though the peak value of the concentration along the

line is higher, the peak is seen to settle back towards the bottom of the open-pit, which suggests the re-establishment of the inversion cap.

The trend described for the temporal variation of the concentration profile along Line 5 is repeated along Line 6 (showed in Figure 3.33) with minor differences. The peak concentration values in all cases in this figure are lower, because the location of the line is upwind from the two closest pollutant sources. Also, existence of a more or less laminar flow regime from the source boundary to the outlet makes the advective transport all but impossible. The location of the line is far away to be influenced by diffusion driven concentration only from the two sources which are much closer to the inflow. Thus, the peak concentration values are reached later in time domain than that was observed along Line 5.

Velocities were also varied to 3 ft/s and 5 ft/s, and similar trands were observed. The following section summarizes the 2D model results.

3.7. Summary

- In the 2D model, no assumption has been made regarding the nature of the flow in the model space.

- The model geometry is hypothetical, but was developed to simulate a possible real mine profile

- It can be noted that a significant backflow takes place from the interior of the model space toward the inflow boundary (windward side). This unique flow characteristic influences the distribution of pollutants in the model space.

- Local turbulences may be occurring in the model space, but may be overwhelmed by the influent air flow. Large eddies occur near the top of the model space (near the uppermost boundary), and may be an important cause of the observed backflow.

- It can be observed that influent velocity has a significant effect on the concentration distribution or transport of pollutants in the pit. Higher velocities transport more pollutants out of the open pit.

- Though the variation of temperature does not indicate any significant effect on the pollutants, the lack of variation may be explained by the fact that the heat supplied here may not be enough to lift the inversion cap. The constant air density assumed for the model space may also neutralize temperature effects.

- Due to the lack of a third dimension, a 2D model is not a representative model, and a 3D model must be constructed to simulate closer results to reality.

- The 2D model is primarily used as an indicator of the importance of the parameters in the model. The 2D model results show that velocity is a very important parameter that influences the pollutant concentration in the pit. It may be surmised as well that the diffusivity coefficient and the model geometry may also be important parameters in determining the pollutant concentration profiles in the pit.

- The flow regime is laminar at the origin, but as the flow progresses toward the center of the pit, the influent air, in its attempt to displace the in-situ colder, heavier air, may take the path of least resistance and lose its laminar character. This does not, however, mean that the flow automatically becomes turbulent. The flow becomes quasi-laminar, and generates local eddies toward the pit bottom. The total energy of the quasi-laminar flow as well as the small local eddies is not enough to lift the inversion cap that settled on the mine profile, but both the quasi-turbulent flow and the local eddies do remove some pollutant mass from the pit bottom, either due to turbulent mixing, or due to advection.

CHAPTER IV: The Development of a Three-dimensional Model for Transport of Pollutants in an Idealized Open-Pit Mine in the Arctic

4.1. Introduction

In Chapter III, a two-dimensional (2D) model for the flow of air in an idealized, deep, open-pit mine in the arctic and the characteristics of pollutant distribution was discussed. One of the goals for the 2D model development and analysis was to characterize the parameters and values of the governing parameters. In the model results, various trends were observed with respect to both the recirculatory patterns and the distribution of the pollutants. Though the 2D model shows significant features of the patterns of re-circulatory air flow and pollutant transport, it fails to provide a realistic assessment because of the lack of the third dimension. This shortcoming would be mitigated by a geometrical three-dimensional (3D) model, which, in addition to providing a third dimension to the model space, would also resemble the actual mine geometry, thus capturing the geometry-initiated inflections of both the velocity and the pollutant fields. This chapter describes the development of a generalized 3D model. This model conforms to an idealized geometry of an open pit mine. The model space is constructed in the COMSOL® environment. COMSOL is a finite element multi-physics software through which most physical fluid dynamic processes can be modeled. The software consists of subroutines, representing various physical air flow phenomenon, that can be linked together in specific sequences to model complex physical processes. For this research, COMSOL® 3.4 was chosen as the appropriate modeling tool.

4.2. Assumptions for the Three-dimensional Model

For the development and validation of the CFD model for transport of pollutants in an idealized open pit mine, an Eulerian 3-D model of pollutant transport was used.

A 3D model is generally used to simulate non-symmetric flow within complex and non-repetitive geometries. A non-symmetric flow is one in which the salient characteristics of the flow vary along all three Cartesian axes of the flow regime, and

thus cannot be accounted for by a 2D model. In such cases, 3D models are used to model the entire flow regime, and if the geometry of the model is close to that of the actual flow regime, accurate results may be expected. These are complex models and generally cannot be solved analytically except for very simple boundary conditions. In fact, no analytical solution exists for the three-dimensional Navier-Stokes equations. While a 3D model is a close representative of reality, still, certain assumptions have to be made. These assumptions pertain to the model space as well as to conditions imposed on the model and are,

- The sources of heat and pollutants can be placed anywhere within the model space with respect to the inflow of air. The air flow in the mine can be oriented in any Cartesian coordinate direction with respect to the mine geometry.

- The pollutants and the heat are released into the model space based on the duty-cycle of the operating equipment and the daylight hours.

- The equipment in the mine do not move within or outside the model space.

In many mines in the far north, whether open-pit or underground, extreme cold during the winter months makes it difficult to restart internal combustion engines once they are shut off. Consequently, most equipment that are exposed to the elements are never shut down but are left running all throughout the winter months. Thus during that period, the equipment emit a minimum amount of gaseous pollutants and waste heat regardless of their material output.

The occurrence of an inversion cap in an arctic mine during production hours often necessitates that all personnel be evacuated from the pit as the pit air often violates MSHA standards for breathable air. The equipment, if possible and convenient, are driven out of the mine pit at the time of evacuation, but often can be left in situ to avoid the loss of time in repositioning of the same when production is reinitiated. This may give rise to a situation where non-

productive equipment in an open pit generate pollutants and heat, thus contributing to the fouling of air quality in the pit. Thus, in simulating a 3D problem, it was thought expedient to consider this scenario (worst case), which, if successfully mitigated, can ensure that less intense problems can easily be solved.

Another important point to be noted in this regard is that the movement of equipment in the mine pit, particularly that of haul trucks, is a fairly complicated scheduling problem, and usually requires a simulation setup of its own. The selected software COMSOL® simulates physico-chemical processes, is not equipped to set up and simulate a scheduling problem of this magnitude. As the two models are entirely distinct from each other, it would be extremely difficult to integrate them mathematically and solve within the same grid structure. Since the primary focus of the present research is to simulate the physical processes in the open pit pertaining to the generation and transport of pollutants, it is thought expedient to dispense with the scheduling problem.

- Pollutant sources in the 3D model release a preset amount of a specific gaseous product. In reality, the exhaust pipes of working equipment in a mine emit a mixture of gases. The simulation of the transport of such a mixture in COMSOL® requires data for each component of the gaseous mixture (e.g. partial pressures, temperatures, etcetera.). Also, simulating a mixture of gases in COMSOL® would require the setting up and running, parallel to the pollutant transport simulation, a speciation simulation, which COMSOL 3.4® is not very well equipped to handle.

- In the 3D model, air is assumed to be incompressible, and the atmospheric air pressure is considered constant, (14.4 psia).

- No prior assumption is made on the nature of air flow in the open pit. The physics of the flow regime is set forth from a point of neutrality, and it defines the nature of the flow regime.

4.3. Generalized Geometry of the Three-dimensional Model
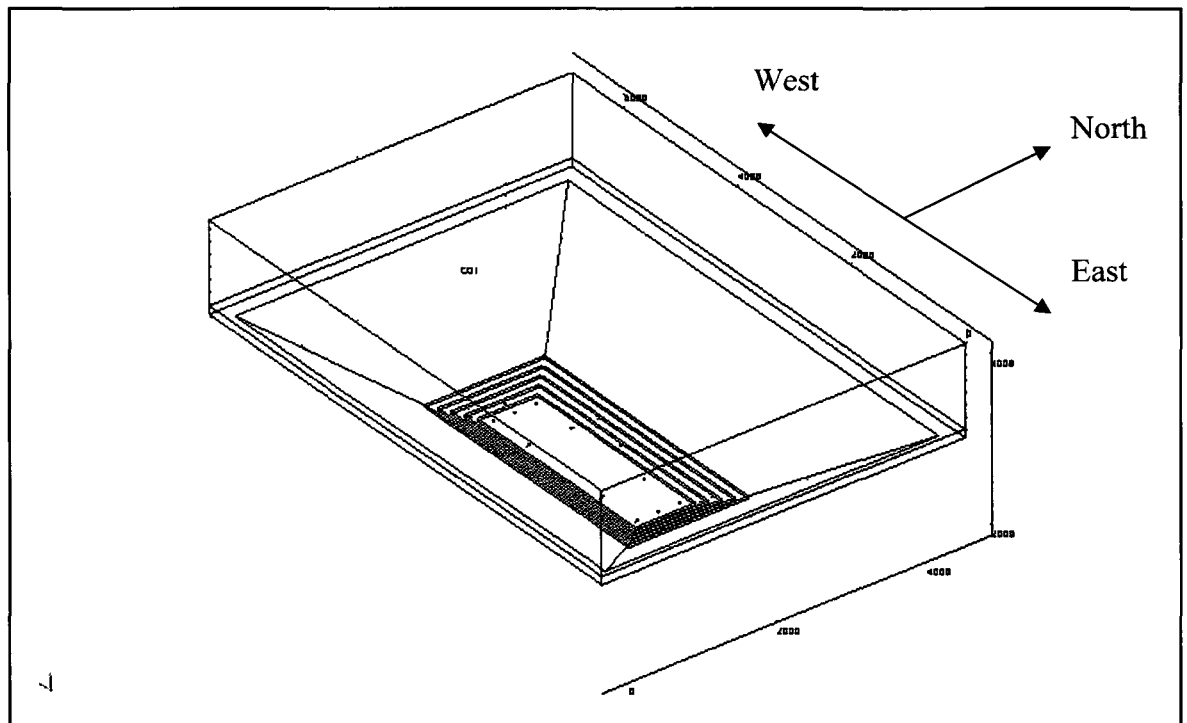
Figure 4.1: A schema of a Three-dimensional Model Domain.

A generalized representation of a 3D model is shown in figure 4.1. As seen, the geometry resembles the general trough shape of an open pit. The floor of the open-pit is 620 ft in the X-direction and 2575 ft in the Y-direction. Four benches, each of 100 ft width and 30 ft height, are located above the pit bottom. Above that, the ground rises in an open trapezoidal trough to the rim of the pit. The average slope of the trapezoidal trough is 40°. The mine is approximately 4500 ft in the X-direction and 6500 ft in the Y-direction at the rim. The depth of the mine from the floor to the rim is 1050 ft. The

envelope of air above the rim of the open pit has a cross-section of 4600 ft in the X-direction and 6600 ft in the Y-direction. The height of the model space from the floor in the Z-direction is 4100 ft. Orientation of the model shown in figure 4.1, has the longer dimension in the east-west direction.

Sixteen sources of heat and gaseous pollutant are located in the pit. Figure 4.2 illustrates the location of the pollutant sources.
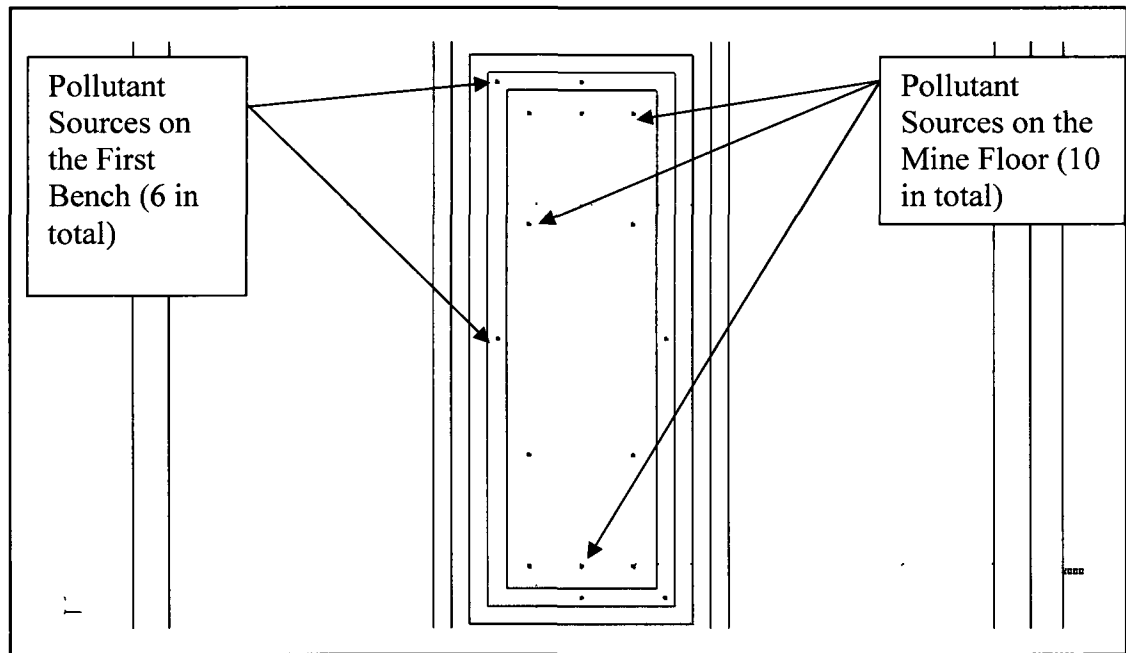
Figure 4.2: Locations of Pollutant Sources in a Hypothetical Open-pit Mine Pit (Plan View)

As shown in figure 4.2, ten of the pollutant/heat sources are placed on the floor of the mine. These sources are located along the edges of the pit bottom and all around it in a symmetrical fashion. Similarly, the remaining six more sources are placed on the first bench from the floor. In a working mine, the equipment are not positioned symmetrically along the edges of the pit or the benches, but are grouped together near the production areas. Since the model is a hypothetical one, the pollutant sources are dispersed throughout so that the effect of the flow pattern on the advective transfer of the pollutant concentration can be adequately examined.

The 3D model has the same physical properties as those of the 2D model. The addition of the extra dimension necessitates that all conditions and equations applied must also take into account the Z-direction Cartesian coordinate. As in the 2D model, the 3D model has three subroutines, the Navier-Stokes, Convection-Conduction and Convection-Diffusion. For these three subroutines as discussed in Chapter III before, boundary, sub-domain and initial conditions must be defined. The equations applied to the model to enforce these conditions are generated and applied in the same manner as in the 2D model. The conditions have been discussed in detail in the previous chapter, and therefore, and are only enumerated briefly in this chapter. In the following sections, boundary conditions are discussed first, followed by subdomain and initial conditions.

4.4. Boundary Conditions for the Three-dimensional Model

Since model results can be strongly dependent on the boundary conditions in any CFD model, the physical conditions imposed on the various boundaries that delineate the 3D model space are presented in this section. The boundaries, in this case, are surfaces rather than edges or lines as in the case of a 2D model. The surfaces of solid faces have been placed in the model space and integrated to create the 3D model. The physical conditions imposed on these surface boundaries belong to three main categories: (1) Navier-Stokes boundary conditions, (2) Convection-Conduction boundary conditions and (3) Convection-Diffusion boundary conditions. A brief description of the boundary conditions follows.

4.4.1. Navier-Stokes Boundary Conditions

The 3D model is required to contain an inflow boundary that would generate mass at that boundary and move toward the interior of the model space with a predetermined velocity. This boundary in the 3D model is shown in figure 4.3.
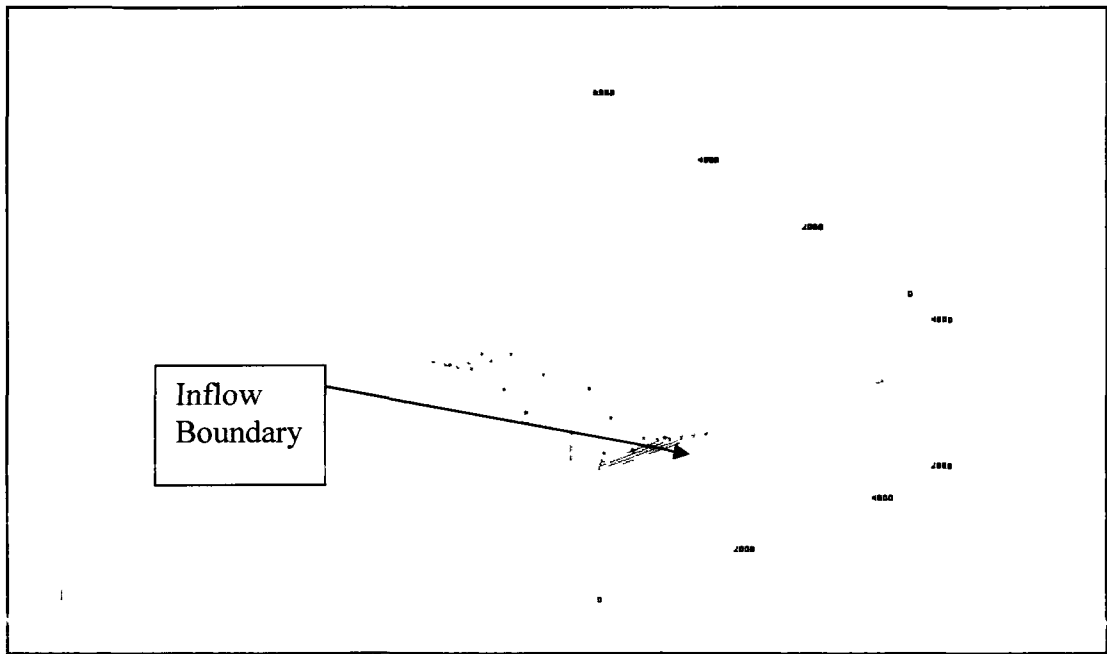
Figure 4.3: Inflow Boundary for 3D Model

The inflow boundary shown in figure 4.3 is oriented along the north-south direction, and is located at the eastern edge of the model. Thus it moves the mass of air in a westerly direction, into the model space. The boundary condition can be generally classified as a Dirichlet condition and mathematically expressed as the following:-

$$u = u_0 \qquad\qquad \text{(equation 4.1)}$$

$$v = v_0 \qquad\qquad \text{(equation 4.2)}$$

$$w = w_0 \qquad\qquad \text{(equation 4.3)}$$

In the above equations, u, v and w are the velocities in the x-, y- and z-directions respectively, and u_0, v_0 and w_0 are the numerical values for the velocities along the axes. The three velocity vector components can be added up to generate a resultant velocity in 3D space, thus velocity along any direction into the pit can be simulated.

The ceiling of the model geometry in the Z-direction is an important boundary condition as it not only marks the limit of the model space, but also is influences the mass and energy balance of the system. Furthermore, it limits the height of the

inversion cap, whether it is generated in the model or defined as an initial condition. For this model, the ceiling is represented as a no-slip wall, or a Dirichlet boundary condition, and expressed mathematically as:

$u = 0$ (equation 4.4)

$v = 0$ (equation 4.5)

$w = 0$ (equation 4.6)

Thus all velocities impinging on the ceiling are set to zero velocity. The no-slip boundary is shown in figure 4.4.
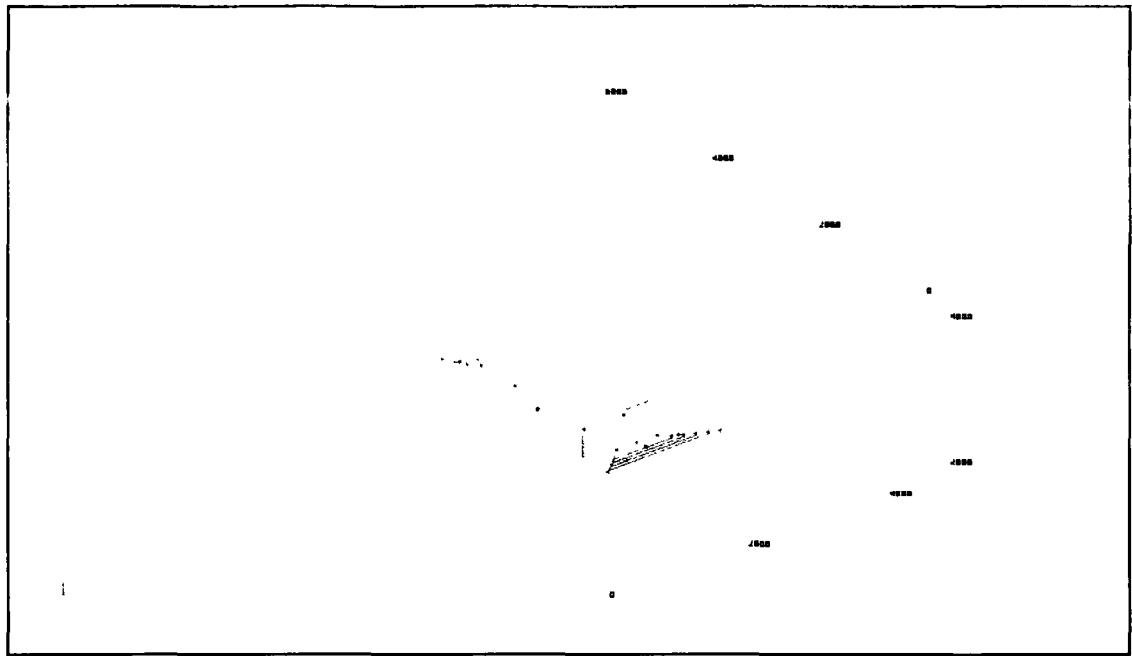
Figure 4.4: Cap Height for the 3D Model – No-slip Wall Boundary (Colored Pink)

Since mass of air is introduced into the model space by the inflow boundary, conservation of mass dictates that a set of boundaries must be established to facilitate the outflow of mass from the model space. This is done by the boundaries shown in Figure 4.5. These boundaries are characterized as open boundaries and are represented by the following equation:

$$p \approx f_0 \qquad\qquad (\text{equation } 4.7)$$

The magnitude of the stress f_0 in equation 4.7 is thus approximately the same as the pressure, p, in the system, e.g., the initial pressure given in the model as an initial condition. This initial pressure is 14.4 psi times 12^2,or, 2073.6 poundal/ft^2. Figure 6.5 shows the open boundaries (colored pink) in the 3D model.
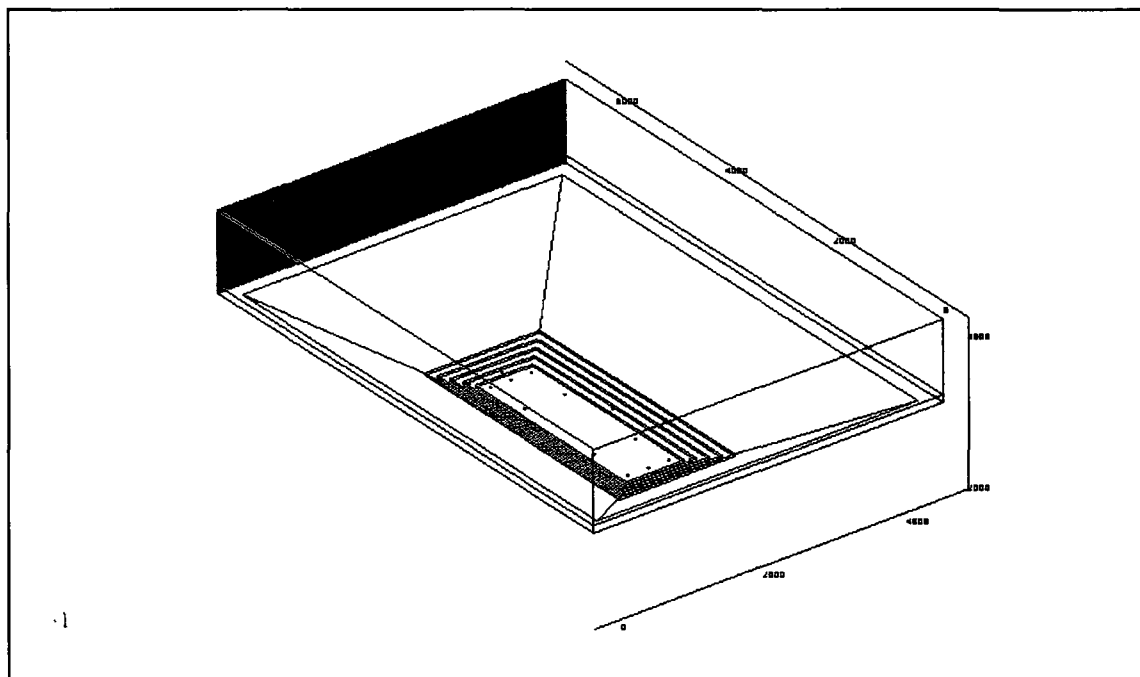
Figure 4.5: Outflow Boundary for 3D Model – Open Boundary (Colored Pink)

All other boundaries of the model, both atmospheric and topographical (the actual mine profile or geometry), are considered to be wall boundaries.

4.4.2. Convection-Conduction Boundary Conditions

The Convection-Conduction boundary types are generally classified into three categories, viz., atmospheric boundary conditions, topographical boundary conditions and equipment boundary conditions. The atmospheric boundaries are those which limit the extent of the air superincumbent to the pit. Topographical boundaries are those that represent the pit geometry and the equipment boundaries are those that

represent the equipment in the mine. As stated before, the equipment boundaries represent the faces of the cubes placed in the mine pit to simulate the effect of the mass and the heat released into the pit environment. Since only the mass and energy released from the equipment are of interest and the equipment do not move, it is considered unnecessary to simulate the size and shape of the equipment. The blocks are 15 ft × 15 ft × 15 ft in dimension and all the six surfaces are used to supply heat to the model.

The equipment boundaries are conditioned as constant heat flux boundaries. These boundaries generate heat throughout the model runtime. A large constant value is given as heat flux from equipment. From available data, based on fuel consumption and release of waste heat, it is calculated as approximately 21932 poundal/ft·s. This heat is released into the mine atmosphere from all 6 surfaces of every cube representing equipment in the mine.

The remaining boundaries are applied according to section 3.4.5.2

4.4.3. Convection-Diffusion Boundary Conditions

These boundary conditions were applied in accordance with the discussion in section 3.4.3.1.

4.5. Sub-domain Conditions for the Three-Dimensional Model

In this section, the sub-domain conditions for the three dimensional model are presented.

4.5.1. Navier-Stokes Sub-Domain Conditions

One of the principle assumption made in this sub-domain that the Navier-Stokes equations described in section 4.3 (equations 4.1, 4.2, 4.3 and 4.4) is continuous and represent the flow regime. The model does not assume a priori knowledge of the nature of the flow (laminar, quasi-laminar or turbulent).

The 2D model simulation indicated that the presence of large-scale turbulence eddies in the space would perturb the inverted air mass in the mine due to temperature difference, and thus may mitigate the problem partially. The existence of the inverted air mass, therefore, indicates the presence of either small-scale local turbulence, or a complete lack thereof. The small-scale turbulences do not add any significant energy to lift the air inversion and therefore, has been approximated as a linear and/or quasi-linear flow without any loss of generality.

If, however, there is large-scale turbulence present in the system, the non-turbulent Navier-Stokes equation over the model space would fail to account for the turbulence, and force the flow to linearize, thus making it laminar or quasi-laminar. This assumption of non-turbulent Navier-Stokes flow condition may lead to incorrect pollutant concentration values in the model space, since such dispersion is heavily dependant on the prevalent convective velocities.

The concern cited above may be resolved by considering the fact that the inflow air into the model space, introduced at the inflow boundary, is effectively a laminar flow. Since the air flow into a mine atmosphere under an inverted air mass is very small in magnitude, and the geometry of the outer boundaries of an open pit restricts the movement of such flow. It is, therefore, expedient to introduce a constant average flow through the inflow boundaries into the model space in a specific direction. The small, local turbulences that may be present at the inflow offer no consequential information, particularly when compared with the extremely large mass of colder, heavier air, to which the influent air attempts to transfer its momentum. As the influent air, which has laminar characteristics moves into the mine, the only turbulence that can subsequently occur would be as a result of momentum interaction between the dynamic influent air and the relatively static inverted air mass.

4.5.2. Convection-Conduction Sub-Domain Conditions

These sub-domain conditions were applied in accordance with the discussion in section 3.4.2.2.

4.5.3. Convection-Diffusion Sub-Domain Conditions

These sub-domain conditions were applied in accordance with the discussion in section 3.4.3.2.

4.6. Initial Conditions for the Three-Dimensional Model

Initial conditions were applied to the model according to the discussion in section 3.4.3.

4.6.1. Initial Conditions for Navier-Stokes Subroutine

These initial conditions were applied to the model according to the section 3.4.1.3.

4.6.2. Initial Conditions for Convection-Conduction Subroutine

The important initial condition for the convection-conduction subroutine is that the inversion cap is already established at the beginning of the model. This initial condition differs from the initial condition for the 2D model. The inversion cap is initially established in the 3D model to reduce the model run time, which would dramatically increase if the 3D model was started from a neutral position.

4.6.3. Initial Conditions for Convection-Diffusion Subroutine

After the model construction is complete, it was then executed or "run" to obtain solutions for pollutant transport in the model domain. There are two more steps that are undertaken before model is ready for execution. They are – (1) the application of a grid, and, (2) the choice of a solution algorithm. In the following, these two steps are discussed briefly:

The grid imposed on the model discretize the model space into a large number of interconnected elements or subparts for which the sub-domain or boundary conditions are solved individually, taking the final values of one of the grid elements as the initial condition of the next. Since the model is solved within a finite element scheme, the

model is divided into solid elements in order to actuate the above. A dynamic gridding algorithm, available in COMSOL®, is chosen as the method to grid the space.

There are several solution algorithms available in COMSOL® to solve systems of linear and non-liner equations. Since the problem at hand produces a very large sparse matrix, the degrees of freedom of the system is, therefore, very large and beyond the capability of most algorithms specifically designed to solve sparse problems. Thus, it was thought expedient to try to invert the matrix directly, and to this end, the algorithm known as PARDISO (the Parallel Direct Solver) is chosen. PARDISO is a parallelized solver which can take advantage of parallel computer architecture, if available. The algorithm solves systems of equations by directly inverting the "A" matrix in an Ax = b form.

4.7. Summary

In summary it can be said that the generalized 3D model is constructed according to realistic boundary and sub-domain conditions. Although it does not represent any particular mine, the processes occurring within the mine geometry with respect to the air flow have been described adequately by this model. In this model, no assumption has been made about the flow regime (i.e., turbulent, non-turbulent or laminar). This is an important step in modeling the 3D problem, because a generalized model provides valuable information for tuning the model for specific cases. Validation was not attempted with this model as it does not pertain to a specified mine. A validation model is a specific case of the generalized model. The validation model constructed on the basis of the selected mine near Fairbanks, AK is described in the next chapter.

CHAPTER V: Validation of the Three-dimensional Model

5.1. Introduction

The model presented in the previous chapter is a geometrical representation of a hypothetical open pit mine. While this model is mathematically relevant and provides results of pollutant concentration trends. It cannot be used to predict the pollutant concentration in an actual mine or ventilation planning for an open pit mine. The mathematical model must be validated with actual data and geometry. The purpose of this chapter is to use actual data from a sub-arctic mine, develop a relevant model and validate the model. The selected mine, on the basis of which the validation exercise is developed, is an open pit gold mine near Fairbanks, Alaska. It is located in the North Star Borough. The pit geometry from the winter of 2004 – 2005 was used to validate the model.

In order to validate the model of the flow phenomenon, it is necessary to construct another model similar to the hypothetical mine model. The new model is different in one crucial aspect, viz., that it simulates the geometry of the selected open-pit mine. The model predicted gaseous pollutant concentrations are compared with field data obtained from the mine, and if the values are found to be reasonably close, the model can be said to be validated. As with all previous models, COMSOL® has been used to develop and execute these models.

5.2. Assumptions for the Validation Model

The validation model is a variation of the generalized 3D model described in the previous chapter. As such, the assumptions for the generalized 3D model are equally valid for the validation purposes. The point of departure for the validation model is the size and shape of the mine profile, as well as the number and positions of the production equipment in the pit.

5.3 Development of the Validation Model

In this section, the geometric and physical properties of the validation model are discussed in detail. The geometry of the validation model is very similar to the generalized model, however, with slight variations, is discussed below.
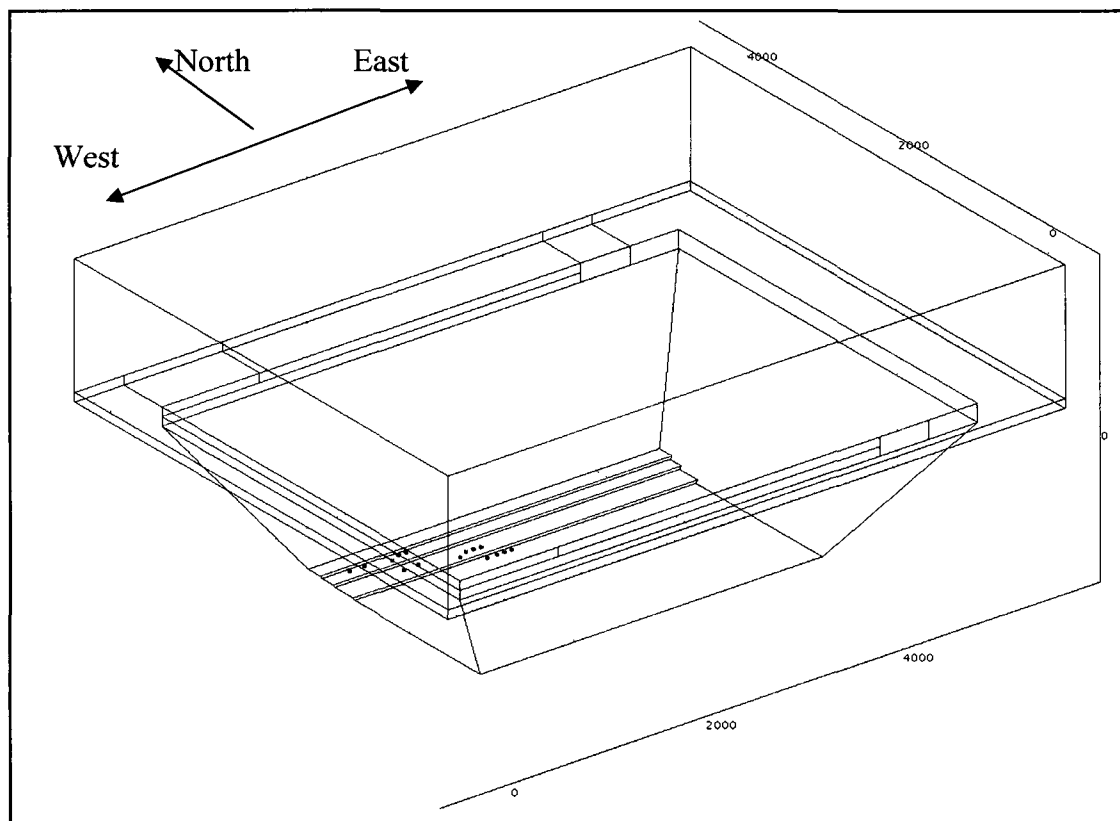

Figure 5.1: 3D Validation Model of the Arctic Mine

Figure 5.1 shows the validation model along with its orientation. The eastern boundary of the model at the rim of the open pit is also considered the inflow boundary for the model, as showed in Figure 5.2. The orientation of the open pit is east-west along its longer axis.
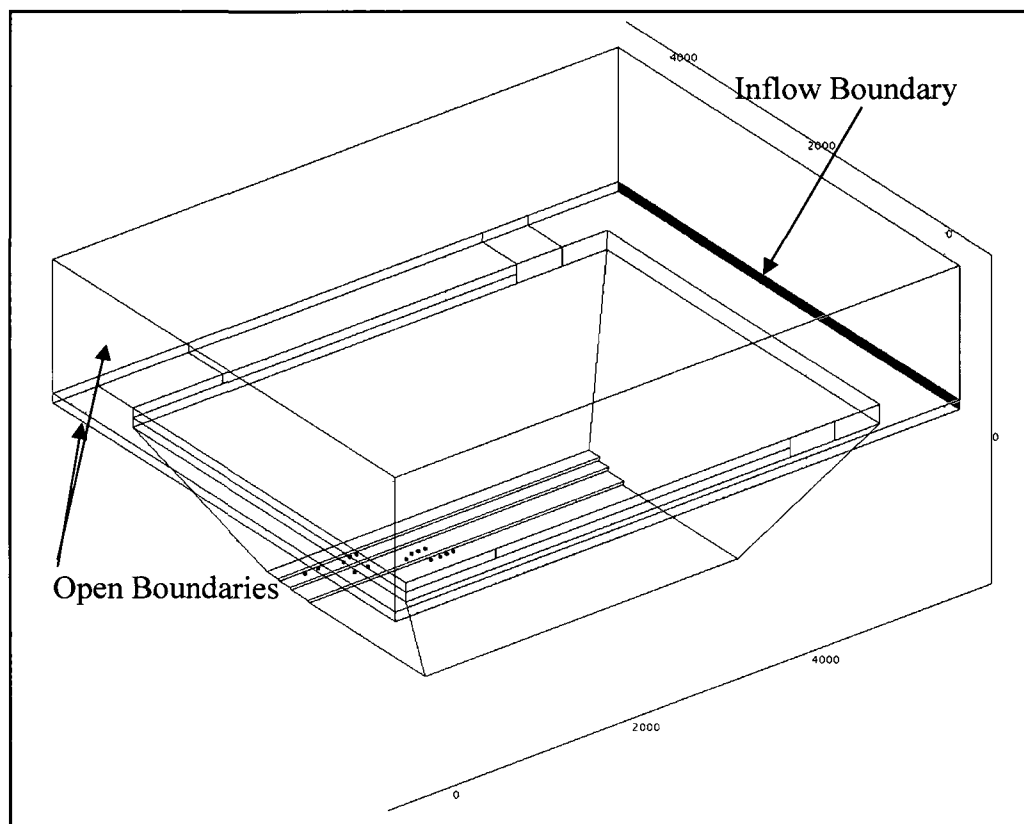
Figure 5.2: Inflow and Open Boundaries for Validation Model

Data collected from the selected mine indicates that the wind flowing into the mine space is directed inwards from a north-easterly direction. As explained before, the presence of an inversion cap reduces the wind flow in a region. Thus, the inflow boundary projects a very low velocity (approximately 3 ft/s) inward into the mine from a north-easterly direction. The two atmospheric boundaries at the western extreme of the model pit are designated as the outflow boundaries at a constant pressure of 2073.6 poundal/ft^2. In addition to those two outflow boundaries, there are two other locations where mass may exit the model space. Those two locations are considered open boundaries and are shown in Figures 5.3 and 5.4.
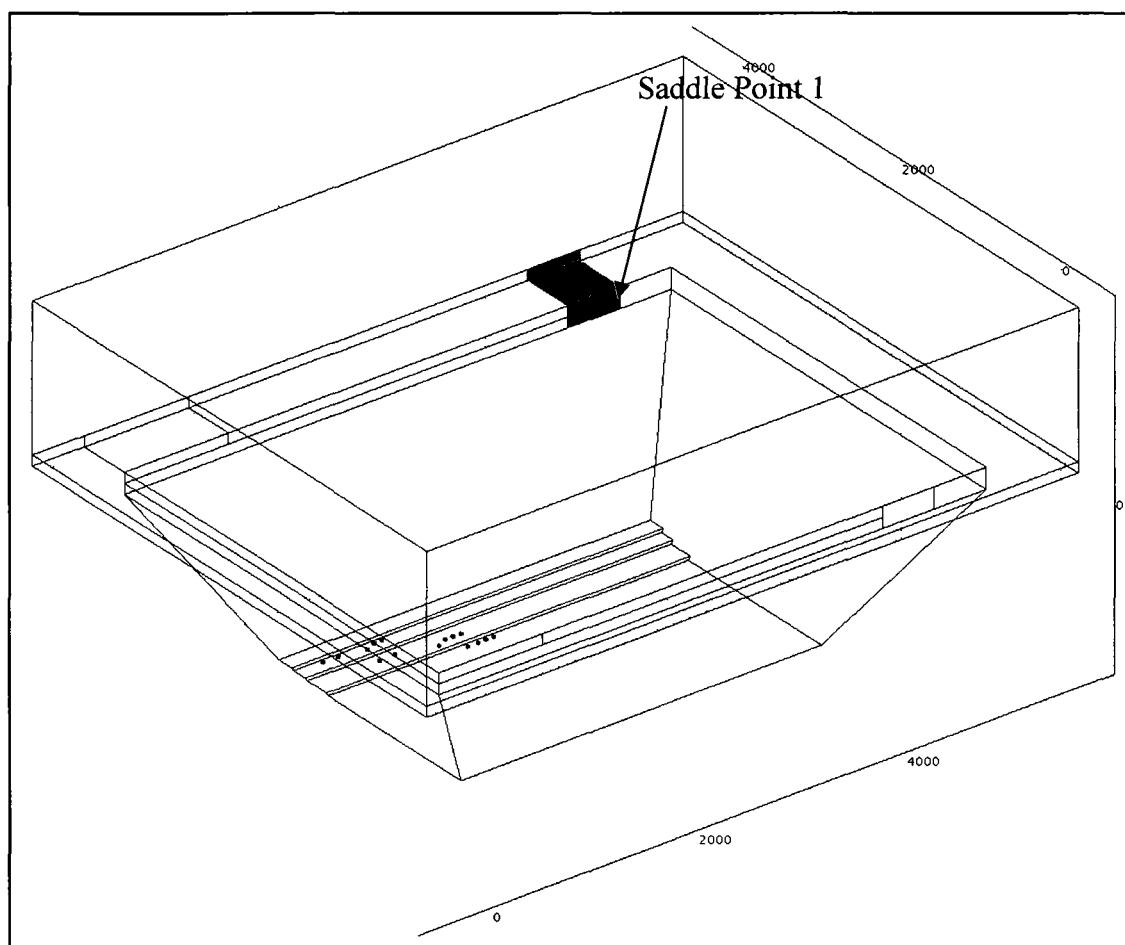
Figure 5.3: Open Boundary for Validation Model-Saddle Point 1

Figure 5.3 shows additional open boundaries in the model space, which is designated in the figure as Saddle Point 1. This boundary represents an actual saddle point on the rim of the selected open pit mine, which lowers the containment boundary for the air inside the pit. Due to lack of relevant data, the dimensions of the saddle point are hypothetical. Length of the saddle point is 500 ft, and its depth is 200 ft. The boundary is characterized as an open boundary with a constant atmospheric pressure of 2073.6 poundal/ft^2. It is also placed at the same temperature as the air at the rim of the pit. The concentration condition at this boundary is designated as a constant concentration (0.0 moles/ft^3), same as the other atmospheric boundaries. Similarly, a second saddle point on the rim of the pit is also located as shown in Figure 5.4.

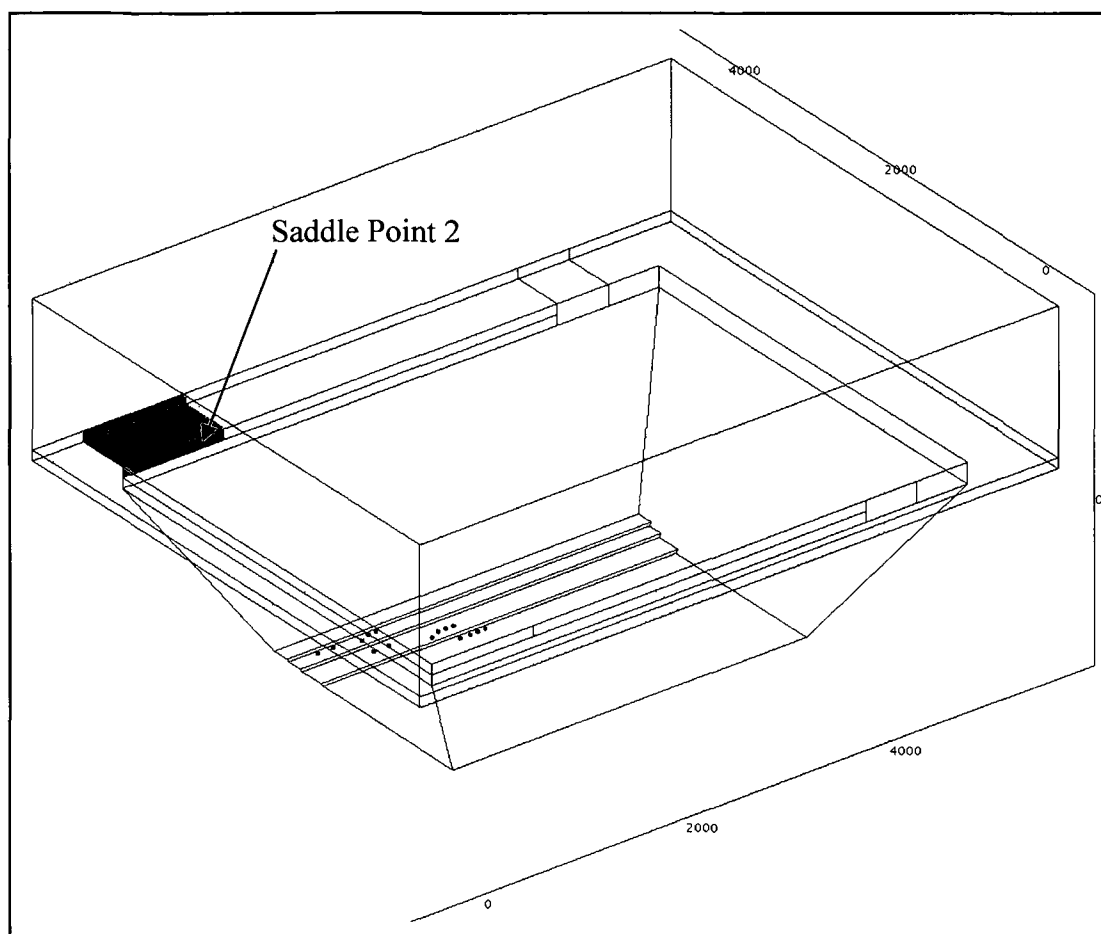Figure 5.4: Open Boundary for Validation Model-Saddle Point 2

This boundary is 1000 ft in length and 100 ft in depth. The boundary conditions imposed on this boundary are similar to those imposed on Saddle Point 1.

The dimensions of the validation model, as stated before, are different from the hypothetical mine model. The dimensions at the rim of the pit for the validation model are given in Figure 5.5.
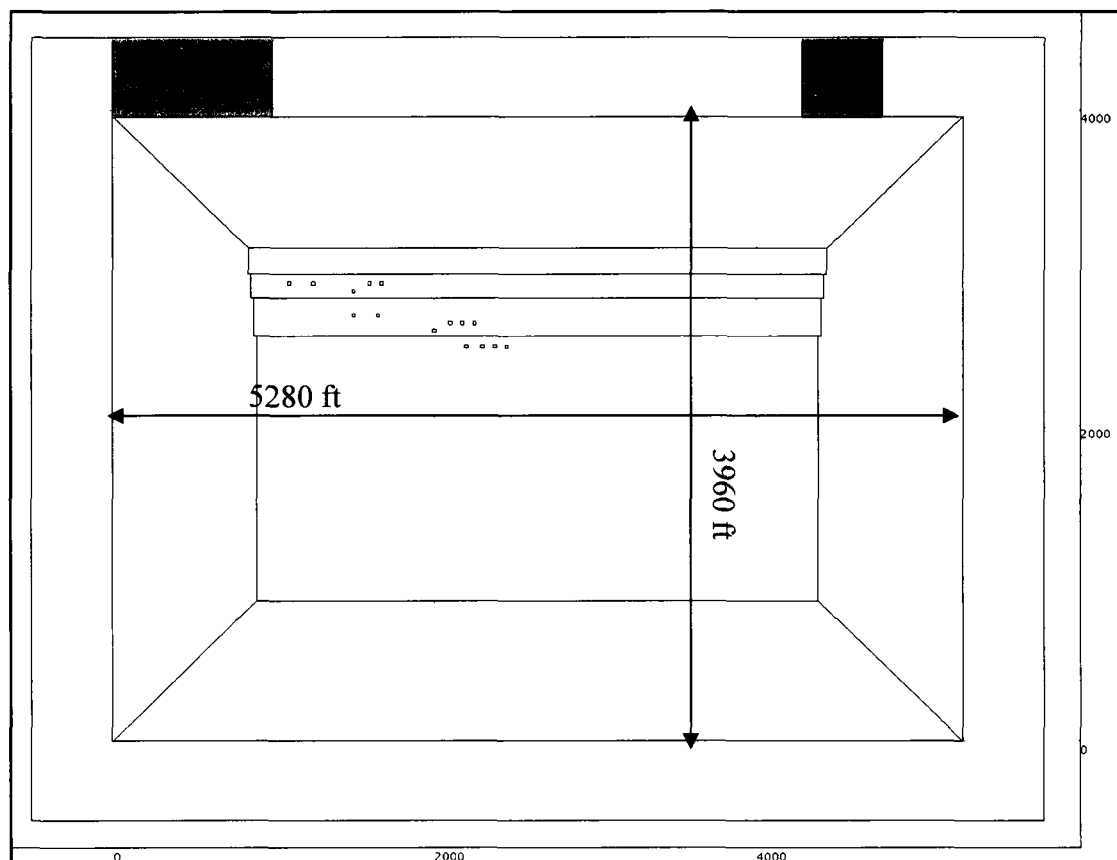
Figure 5.5: Pit Top Dimensions for the Validation Model

The overall slope of the walls is 40°. Three production benches above the floor of the mine are considered in the model, with a constant bench height of 30 ft. A total of 15 production equipment (i.e., pollutant and heat sources), are placed on the open pit floor and the first two production benches. The height of the open pit mine and that of the air envelope superincumbent to the pit are showed in Figure 5.6.

Figure 5.6: Heights of Mine Pit and Air Envelope for the Validation Model

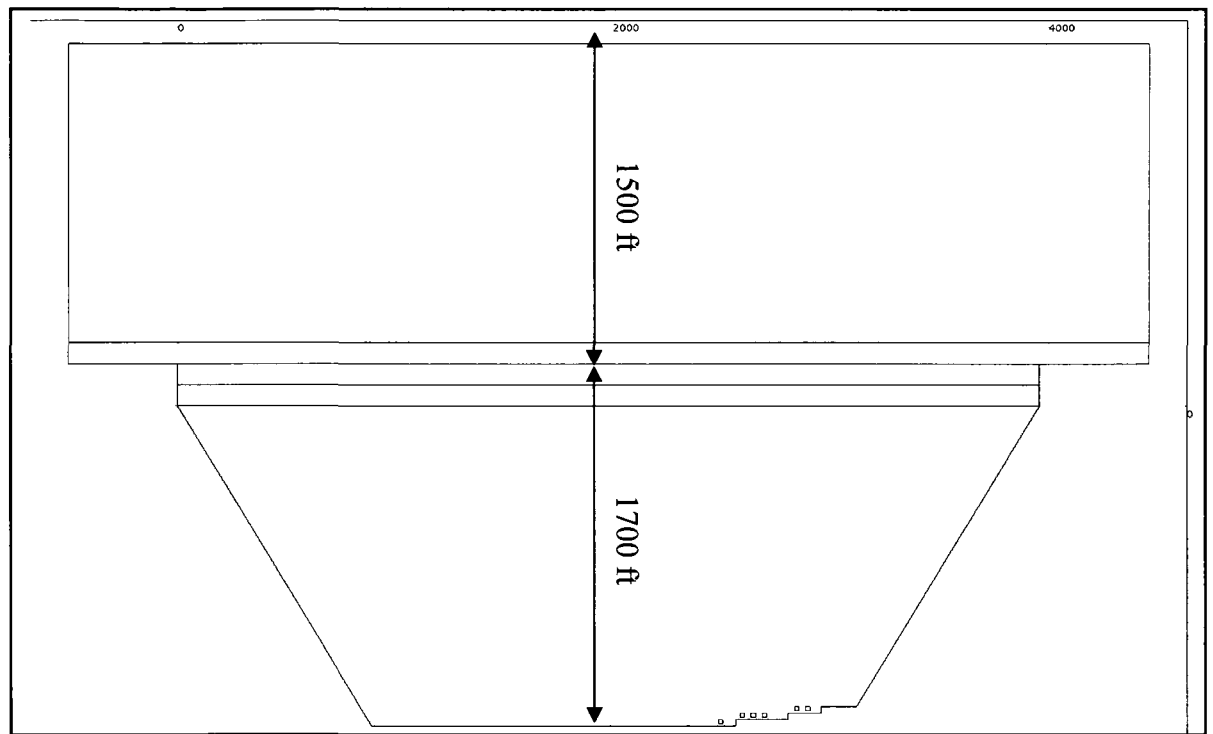The pollutant and heat sources placed in the open pit are characterized as shovels, haul trucks, drills and ANFO trucks. The equipment have been placed at the working face of the mine, and are located on benches in the sequence and order in which they would be located during an active production event. The pollutant sources are geometrically represented as block cubes of 20' × 20' × 20' dimension. Waste heat released from the equipment is transferred to the model space through all the six surfaces of each cube, while the gaseous pollutant is added to the model environment only through the top surfaces.
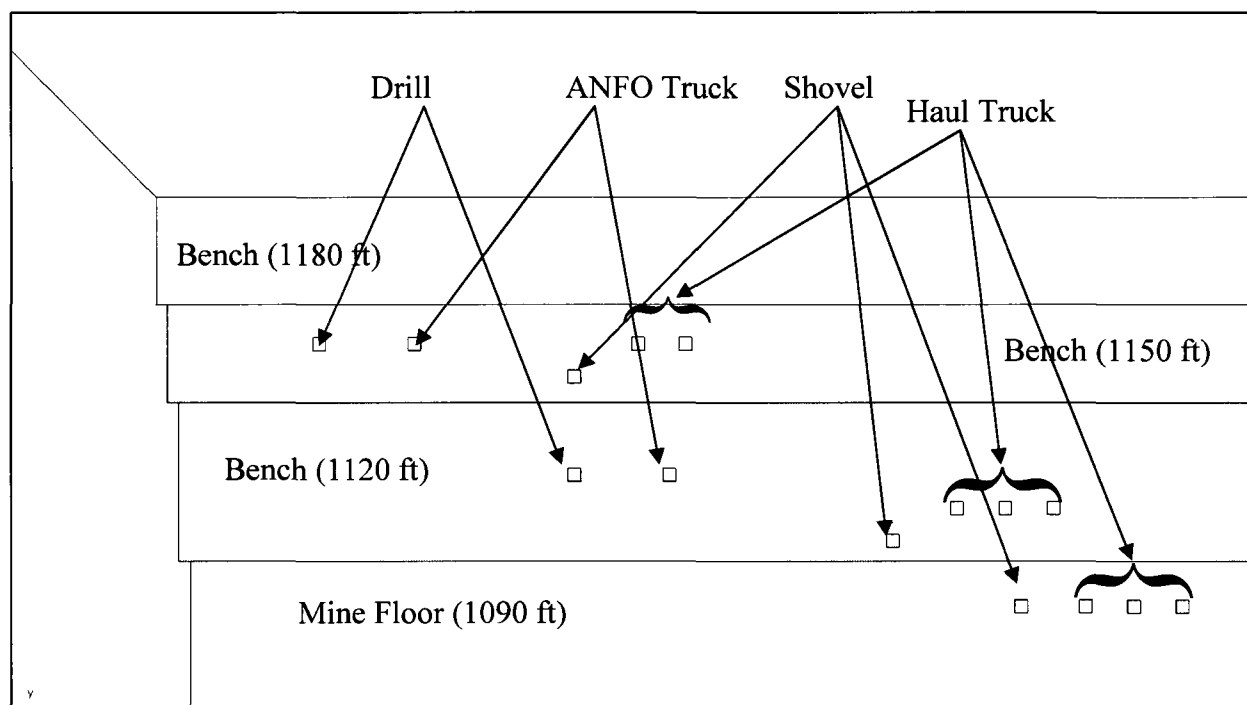
Figure 5.7: Position and Characterization of Production Equipment (Heat and Pollution Sources) in the Validation Model

The amount of heat added from the equipment sources are presented in detail in Table 5.1.

Table 5.1: Heat Addition to the Model space from Equipment Sources

	Block No	Type	X	Y	Z	Engine	Waste heat	W.H./area
1	BLK10	Shovel	2200	2500	-1480	CAT 3516	51466070.25	21444.20
2	BLK11	Truck	2300	2500	-1480	CAT 3512	40882755.18	17034.48
3	BLK12	Truck	2375	2500	-1480	CAT 3512	40882755.18	17034.48
4	BLK13	Truck	2450	2500	-1480	CAT 3512	40882755.18	17034.48
5	BLK14	Drill	1500	2700	-1450	CUKTA19	17030004.46	7095.84
6	BLK15	Shovel	2000	2600	-1450	CAT 3516	51466070.25	21444.20
7	BLK16	Truck	2100	2650	-1450	CAT 3512	40882755.18	17034.48
8	BLK17	Truck	2175	2650	-1450	CAT 3512	40882755.18	17034.48
9	BLK18	Truck	2250	2650	-1450	CAT 3512	40882755.18	17034.48
10	BLK19	Drill	1100	2900	-1420	CUKTA19	17030004.46	7095.84
11	BLK20	Shovel	1500	2850	-1420	CAT 3516	51466070.25	21444.20
12	BLK21	Truck	1600	2900	-1420	CAT 3512	40882755.18	17034.48
13	BLK22	Truck	1675	2900	-1420	CAT 3512	40882755.18	17034.48
14	BLK23	ANFO	1650	2900	-1450	CUM11	9686150.8	4035.90
15	BLK24	ANFO	1250	2900	-1420	CUM11	9686150.8	4035.90

In the above table 5.1, the figures for waste heat are in poundals/s, and those for waste heat/unit area are in poundals/ft^2-s. The location coordinates given in the table are not indicative of actual positions of the equipment in the pit, but the exact location of the equipment in the model space. As the heat sources act as pollutant sources as well, Table 5.2 describes the data used to add gaseous pollutants to the model space from the sources.

Table 5.2: Gaseous Pollutant Addition to the Model space from Equipment Sources

	Block No	Type	X	Y	Z	Engine	CO	CO/unit area	NOx	NOx/unit area
1	BLK10	Shovel	2200	2500	-1480	CAT 3516	0.007259312	1.81483E-05	0.164389648	0.000410974
2	BLK11	Truck	2300	2500	-1480	CAT 3512	0.006009758	1.50244E-05	0.119404643	0.000298512
3	BLK12	Truck	2375	2500	-1480	CAT 3512	0.006009758	1.50244E-05	0.119404643	0.000298512
4	BLK13	Truck	2450	2500	-1480	CAT 3512	0.006009758	1.50244E-05	0.119404643	0.000298512
5	BLK14	Drill	1500	2700	-1450	CUKTA19	0.004058074	1.01452E-05	0.041930468	0.000104826
6	BLK15	Shovel	2000	2600	-1450	CAT 3516	0.007259312	1.81483E-05	0.164389648	0.000410974
7	BLK16	Truck	2100	2650	-1450	CAT 3512	0.006009758	1.50244E-05	0.119404643	0.000298512
8	BLK17	Truck	2175	2650	-1450	CAT 3512	0.006009758	1.50244E-05	0.119404643	0.000298512
9	BLK18	Truck	2250	2650	-1450	CAT 3512	0.006009758	1.50244E-05	0.119404643	0.000298512
10	BLK19	Drill	1100	2900	-1420	CUKTA19	0.004058074	1.01452E-05	0.041930468	0.000104826
11	BLK20	Shovel	1500	2850	-1420	CAT 3516	0.007259312	1.81483E-05	0.164389648	0.000410974
12	BLK21	Truck	1600	2900	-1420	CAT 3512	0.006009758	1.50244E-05	0.119404643	0.000298512
13	BLK22	Truck	1675	2900	-1420	CAT 3512	0.006009758	1.50244E-05	0.119404643	0.000298512
14	BLK23	ANFO	1650	2900	-1450	CUM11	0.004058074	1.01452E-05	0.041930468	0.000104826
15	BLK24	ANFO	1250	2900	-1420	CUM11	0.004058074	1.01452E-05	0.041930468	0.000104826

In table 5.2, the numbers in the columns headed "CO" and "NOx" are in mol/s, and those in the columns headed "CO/unit area" and "NOx/unit area" are in mol/ft^2-s.

For Open pit mines with complex geometry and topography, during a clam day, the radiation and thermal budget of a surface can strongly affect dispersion of pollutants in the pit. Many ventilation models for open pit mines do not pay much attention to this. The effect of large incidence angles of the slope/wall on pollutant concentration in the open pit was accounted for. Besides orientation and incidence, the radiation budget also depends on the fluxes of its various components.

In both the 2D and the 3D model, all the surfaces of the open pit were considered to be a source of reradiated heat. However, data collected from the selected mine, as showed in Figure 5.8, indicates that all the surfaces of the open pit are not exposed to direct impingement of sunlight. These surfaces, therefore, cannot reradiate heat into the model, thus negating their participation in the thermal exchange. Therefore, for validation of the model, re-radiation from the ground is restricted to the surfaces of the ground outside the rim of the pit, and only those surfaces are used to represent the heat balance from radiation. The heaviside functions are adjusted to reflect the sunrise and sunset times for the various conditions used in this validation of the model.
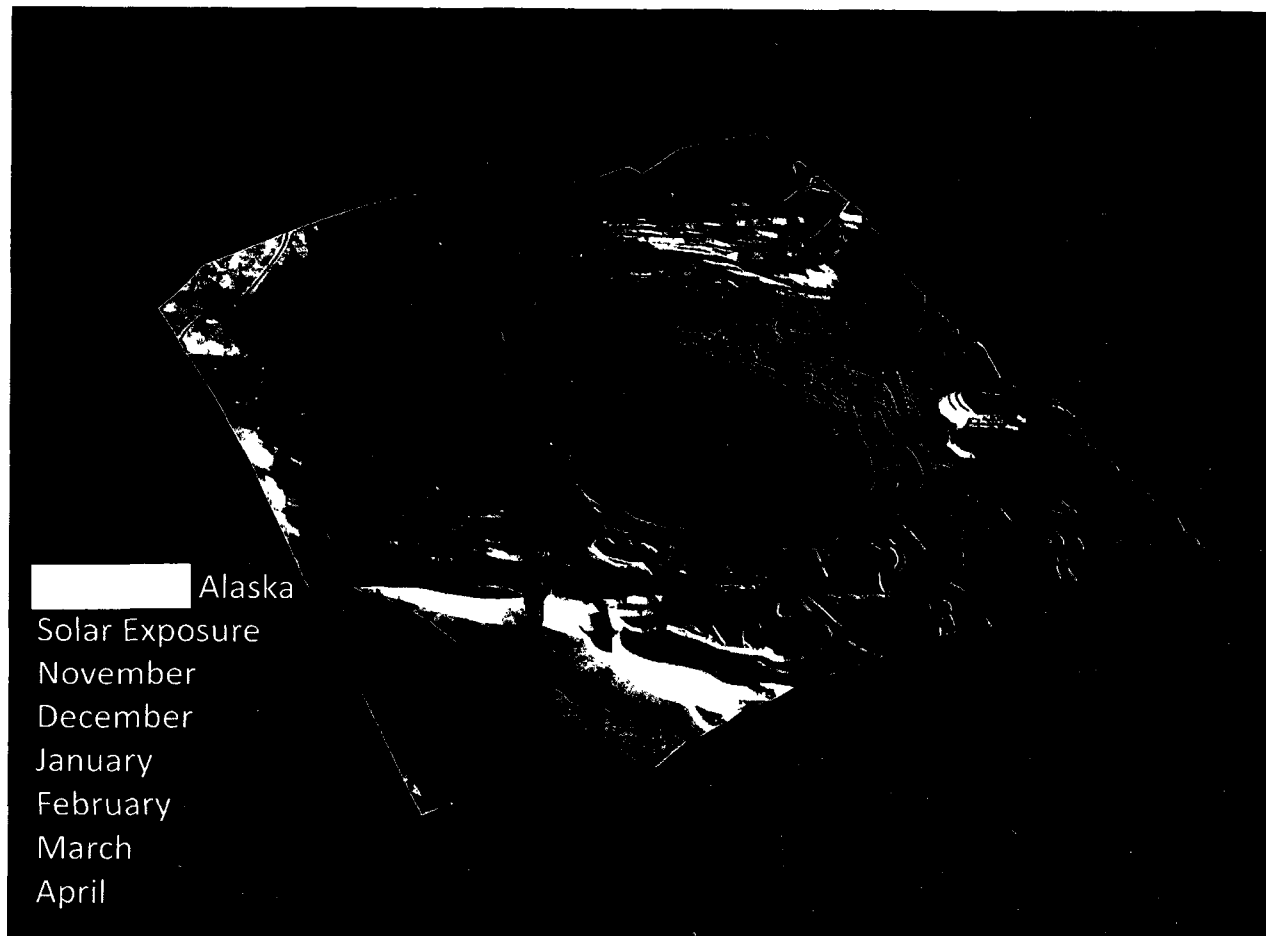
Figure 5.8: Solar Exposure for the Chosen Mine in Winter (November – April)

5.4 Validation Data

The model validation is attempted on three separate days and on three separate locations for which data from the selected open-pit mine are available. The three dates are as follows:

- December 13, 2004
- January 3, 2005
- February 24, 2005

The model is validated with respect to both NO and NO$_2$ dispersion on all the three previously mentioned dates. It may be noted that the open pit was under inversion at those times.

5.4.1 Validation of the Model with Data from December 13, 2004 at Bench 1150

The model validation for December 13, 2004 was done with data collected from the selected open pit mine and other external sources. Table 5.3 below presents the pit bottom and pit top temperatures on that day, as well as the concentrations of O$_2$, CO, NO and NO$_2$ at bench 1150 at different hours of the day.

Table 5.3: Data from the Chosen Arctic Mine for December 13, 2004

		Pit Temp.(F)			1150 Bench (ppm)			
		Time	Top	Bottom	O$_2$	CO	NO	NO$_2$
12/13/2004	1	1:30	15.2	0.4	21.2	0	0	2.1
	2	6:14	14.2	1.6	21.3	4	2	3.2
	3	7:15	15.1	5.5	21.3	5	2	3.6
	4	9:00	14.3	1.5	20.9	4	3	4.6
	5	10:00	16	2	20.9	4	4	4.8
	6	10:58	18	4	20.7	5	3	5
	7	12:00	18	2.4	20.7	4	0	4.9
	8	13:15	18.1	2.1	20.8	4	2	5
	9	14:45	19	4.2	21.2	6	2	4.9
	10	16:00	24	5	21.0	5	2	4.8
	11	20:00			21.1	5	0	5.2
	12	20:35			21.1	3	0	5.3
	13	21:37			21.2	4	0	5.1
	14	22:50			21.2	4	0	4.5

In the table above, the time at which the model is started is shown in Row 1, and the relevant data at the time, viz., the temperature data at the pit top and the pit bottom as well as the concentrations of the various gases in the pit. The model is initialized with

this data, and then is conditioned according to the daylight hours of that day. The total daylight hour for the day is calculated on the basis of the sunrise and sunset times for the day. After the model is executed for a sufficient length of time, the model generated results are compared with the observed data (in Row 9) in Table 5.3. If a close agreement is established between the predicted and observed data, the model is considered to be validated. The sunrise and sunset times for December 13, 2004 are given below:

Sunrise: 10:52 AM

Sunset: 2:40 PM

Length of Day: 3 hr 48 min 34 sec

The initial concentration of the chosen gas in the model is distributed along the vertical axis of the mine, i.e., the maximum concentration according to Table 5.3 is at the bottom of the pit, which uniformly reduces to zero at the top of the pit. If the concentration at the bottom of the pit is observed to be zero at the start of the model, then there is a uniform zero concentration all along the vertical axis of the model.

The model was executed for 14 hours and 30 minutes and the model predicted values for both NO and NO_2 are compared with the observed values. These model predicted results are shown below in figures 5.9 through 5.12.
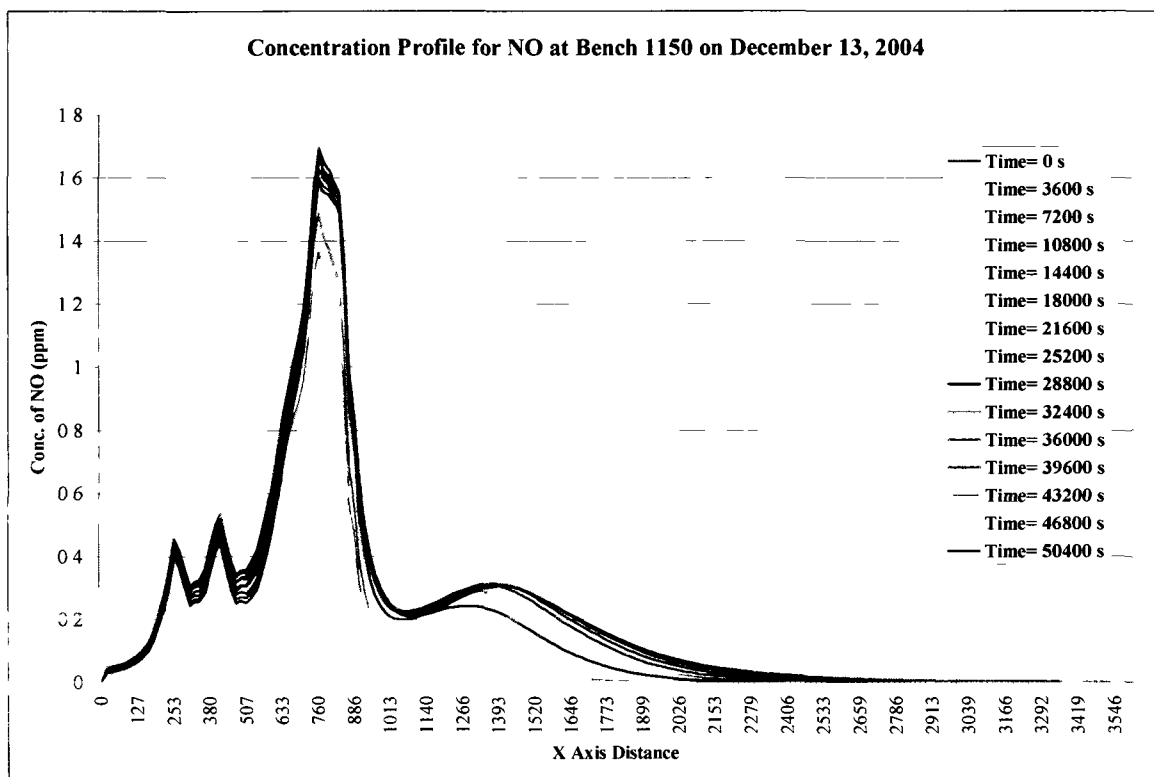
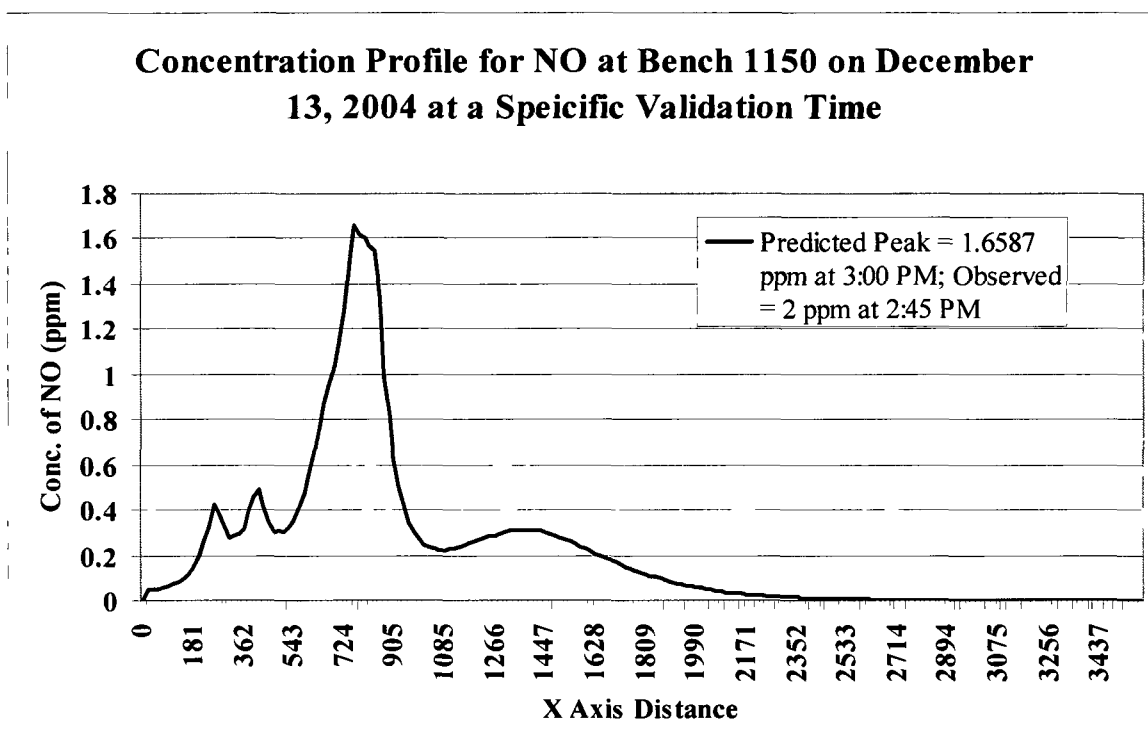Figure 5.9: NO Concentration Profiles Over Time for Bench 1150 (12/13/2004)

Figure 5.10: NO Concentration Profile at Validation Time for Bench 1150
(12/13/2004)

Figure 5.10 shows a very close agreement between the observed value for NO at bench 1150 (2 ppm) and the model predicted peak value for NO (1.6587). Thus, it may be conclude that the model is valid for predicting pollutant concentrations in the open pit. A similar validation exercise was undertaken for NO_2, the results for the validation exercise are presented below in figures 5.11 and 5.12.
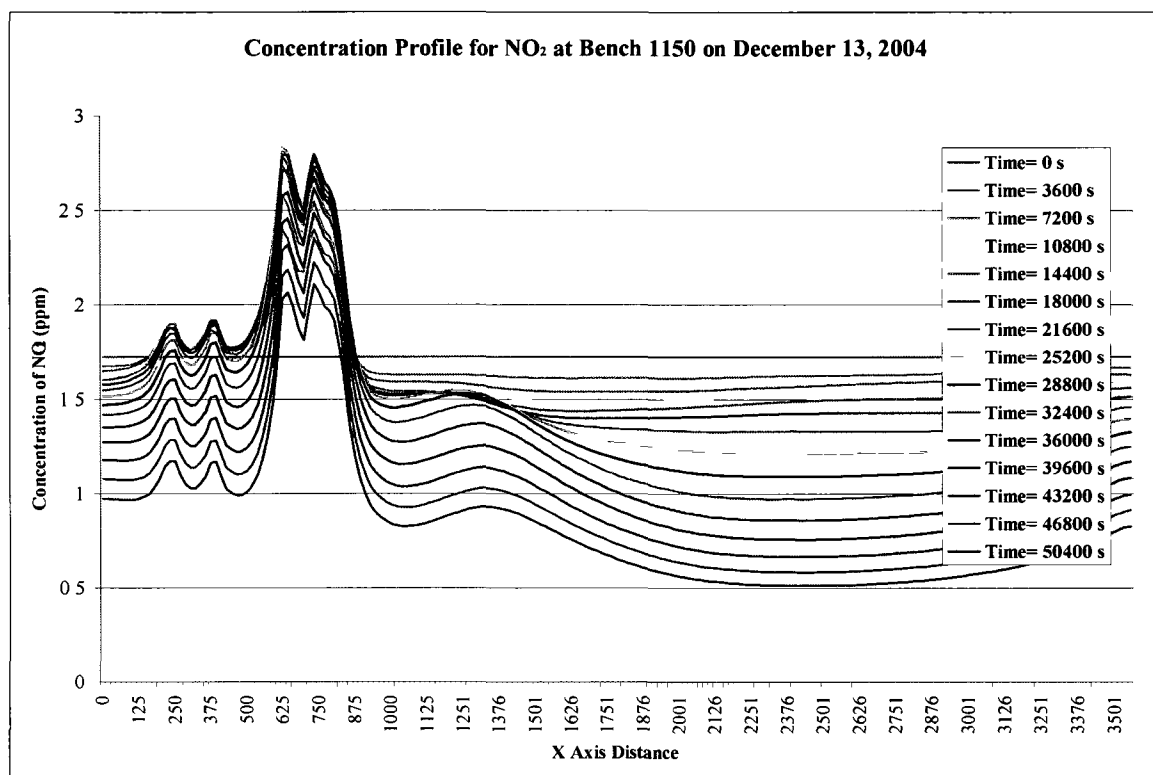
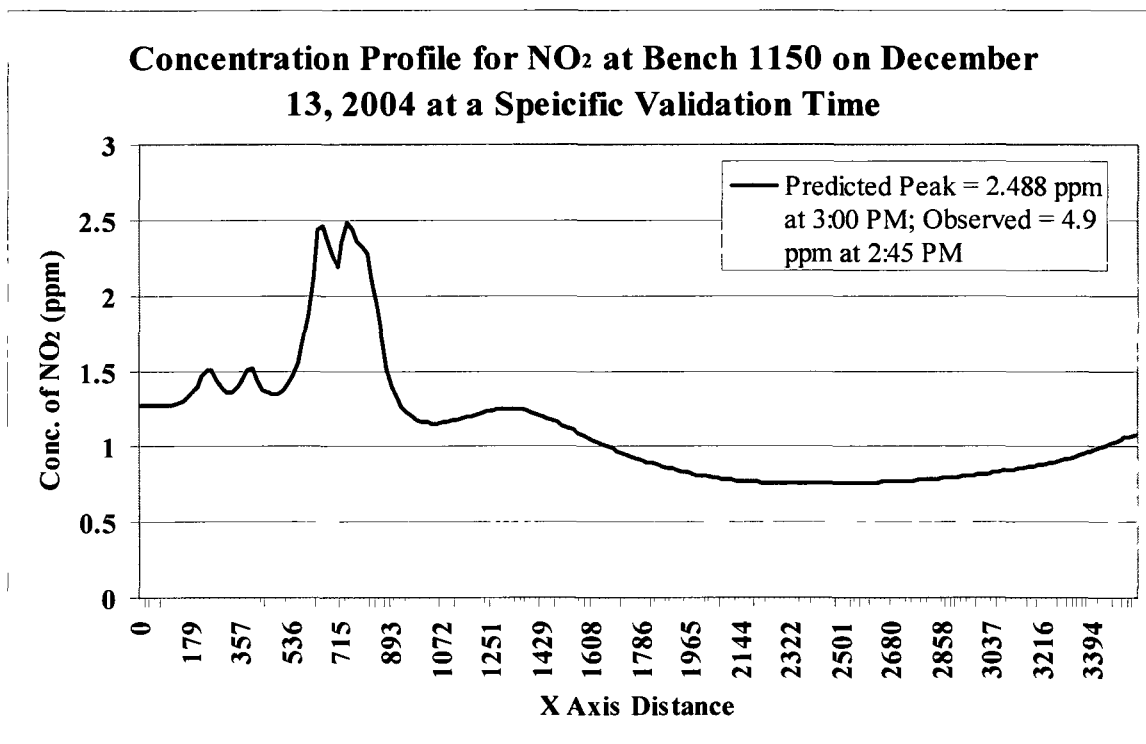Figure 5.11: NO₂ Concentration Profiles Over Time for Bench 1150 (12/13/2004)

Concentration Profile for NO₂ at Bench 1150 on December 13, 2004 at a Speicific Validation Time

Predicted Peak = 2.488 ppm at 3:00 PM; Observed = 4.9 ppm at 2:45 PM

Conc. of NO₂ (ppm)

X Axis Distance

Figure 5.12: NO$_2$ Concentration Profile at Validation Time for Bench 1150 (12/13/2004)

Figures 5.11 and 5.12 show a detailed distribution of the concentration profiles for NO$_2$ over a period of time on bench 1150. Figure 5.12 shows the model predicted concentration profile of NO$_2$ (2.488 ppm) at the selected location. While the values agree closely, it is observed that there is more error in the prediction of NO$_2$ than of NO. This may be because of external sources of NO$_2$ that have not been taken into account in the model space, such as the addition of residual nitrogen oxides due to blasting.

5.4.2 Validation on the January 3, 2005 at Bench 1120

Table 5.4 below presents the pit bottom and pit top temperatures on January 3 2005, as well as the concentrations of O_2, CO, NO and NO_2 at bench 1120 at different hours of the day.

Table 5.4: Data from the Selected Mine for January 3, 2005

		Pit Temp			**1120 Bench (ppm)**			
		Time	**Top**	**Bottom**	**O_2**	**CO**	**NO**	**NO_2**
1/3/2005	**1**	232			20.9	18	3	1.9
	2	800	35	24	20.7	8	4	2.1
	3	1000	35	25	20.9	10	4	2.1
	4	1216	38	33	20.7	4	2	1.6
	5	1600	40	31	20.9	2	0	0

The sunrise and sunset times for January 3, 2005 are given below:

Sunrise: 10:51 AM

Sunset: 3:01 PM

Length of Day: 4 hr 9 min 41 sec

The model was executed for 13 hours and validated for both NO and NO_2. The results are given below in figures 5.13 through 5.16.
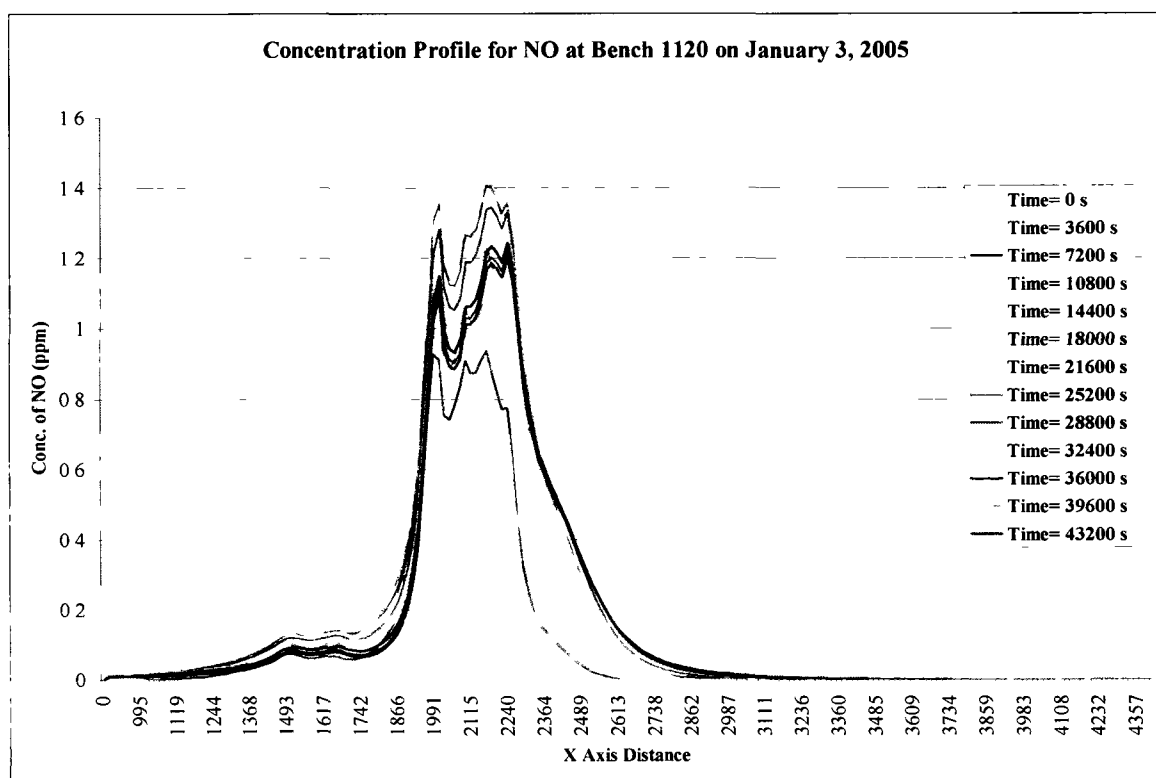
Figure 5.13: NO Concentration Profiles Over Time for Bench 1120 (1/3/2005)

Concentration Profile for NO at Bench 1120 on January 3, 2005 at Speicific Validation Times
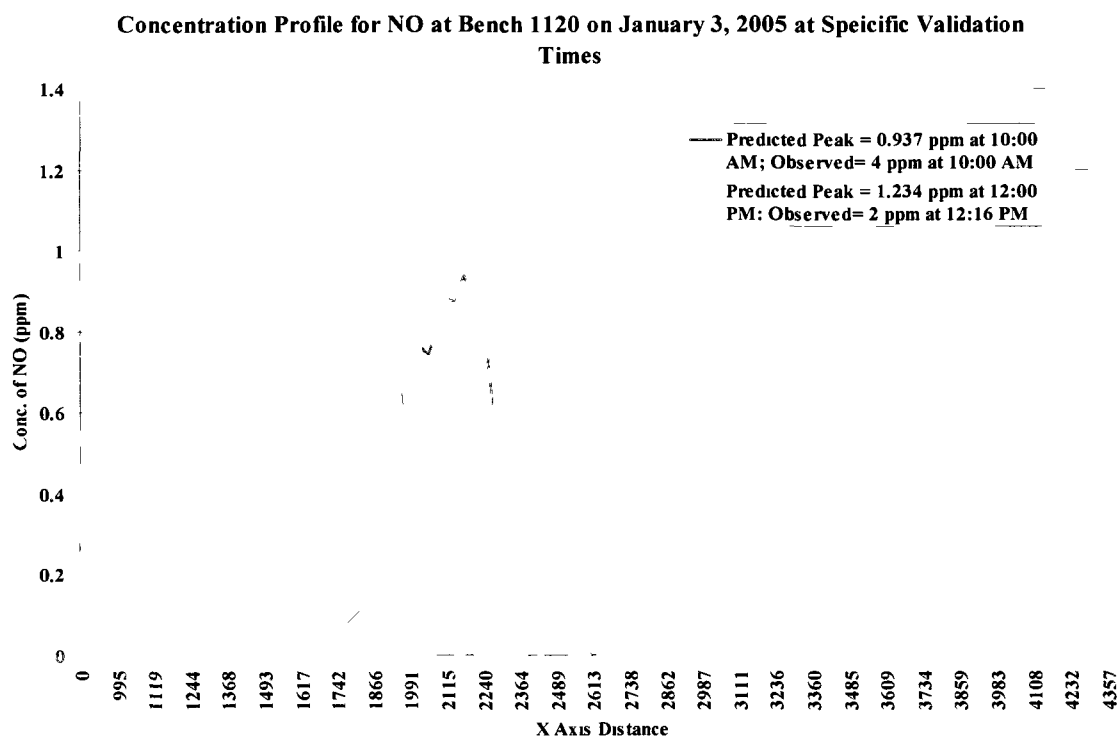

Figure 5.14: NO Concentration Profile at Validation Time for Bench 1120 (1/3/2005)

Figures 5.13 and 5.14 show the temporal distribution of NO at bench 1120 on January 3, 2005. It can be seen that while the predicted concentration value (0.937 ppm) at 10:00 AM is significantly less than the observed (1.234 ppm) one. The same at 12:00 PM is, however, much closer to the model predicted value. The difference can be explained by the presence of residual concentrations of pollutants in the mine, as well as initial bias present in the model. The system is reasonably validated for NO, on January 3, 2005. The results for the validation research for NO_2 are given below in figures 5.15 and 5.16.
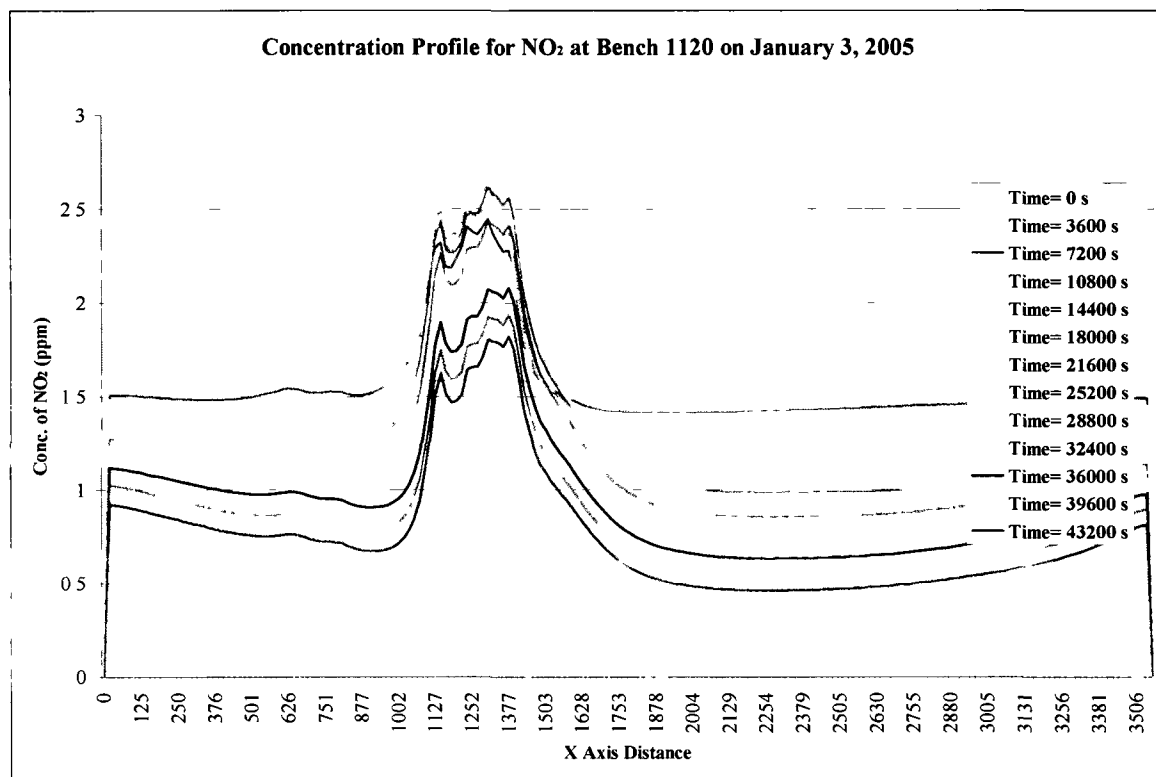
Figure 5.15: NO$_2$ Concentration Profiles Over Time for Bench 1120 (1/3/2005)

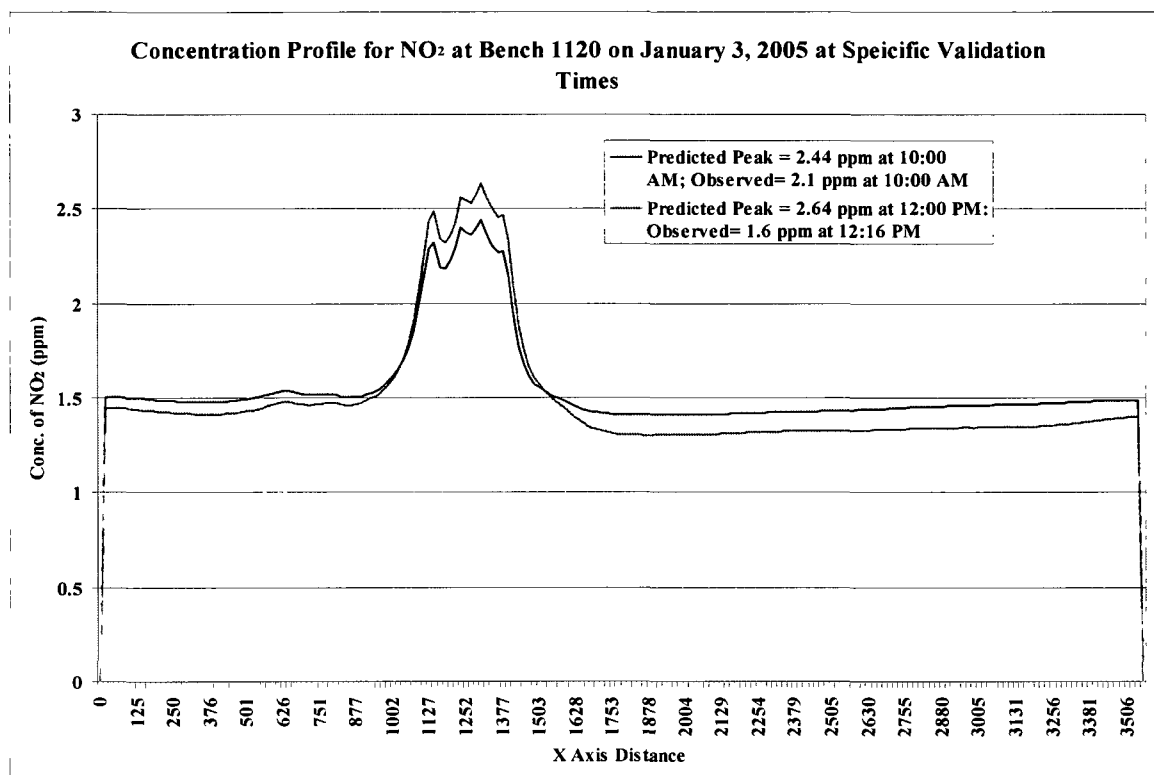**Concentration Profile for NO₂ at Bench 1120 on January 3, 2005 at Speicific Validation Times**

Figure 5.16: NO₂ Concentration Profile at Validation Time for Bench 1120 (1/3/2005)

As seen in Figure 5.16, NO₂ in this case behaves differently from what is observed in Figure 5.14. The predicted value at 10:00 AM is seen to be very close to the observed value at 10:00 AM, but the predicted value at 12:00 noon is seen to be significantly over-predicting the observed value. This difference is possibly a result of extraneous sources of NO₂, as well as initial bias in the model.

5.4.3 Validation of the Model with Data from February 24, 2005 at Bench 1090

Table 5.5 below presents the pit bottom and pit top temperatures on that day, as well as the concentrations of O₂, CO, NO and NO₂ at bench 1090 at different hours of the day.

Table 5.5: Data from the Chosen Arctic Mine for February 24, 2005

		Pit Temp			1090 Bench (ppm)			
		Time	Top	Bottom	O_2	CO	NO	NO_2
2/24/2005	1	7:52	18	14	20.7	0	0	2.0
	2	8:10			20.9	0	3	2.2
	3	12:35			20.9	0	3	3.1
	4	15:00	36	27	20.5	2	2	3.2
	5	16:45			20.6	15	6	4.5
	6	18:04			21.9	15	5	4.1
	7	20:20			20.9	6	4	3.5
	8	23:09			20.9	4	0	3.0

The sunrise and sunset times for February 24, 2005 are given below:

Sunrise: 8:17 AM

Sunset: 5:53 PM

Length of Day: 9 hr 36 min 00 sec

The model was executed for 13 hours and validated for both NO and NO_2. The results are given below in figures 5.17 through 5.20.
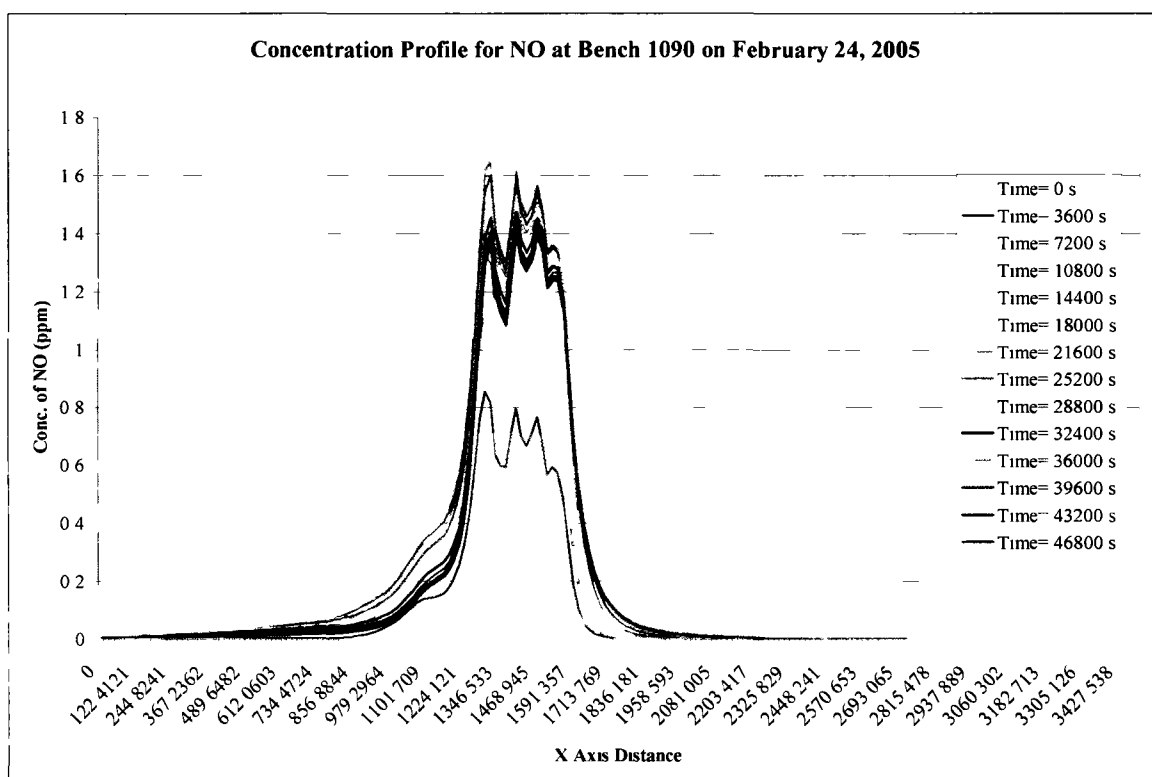
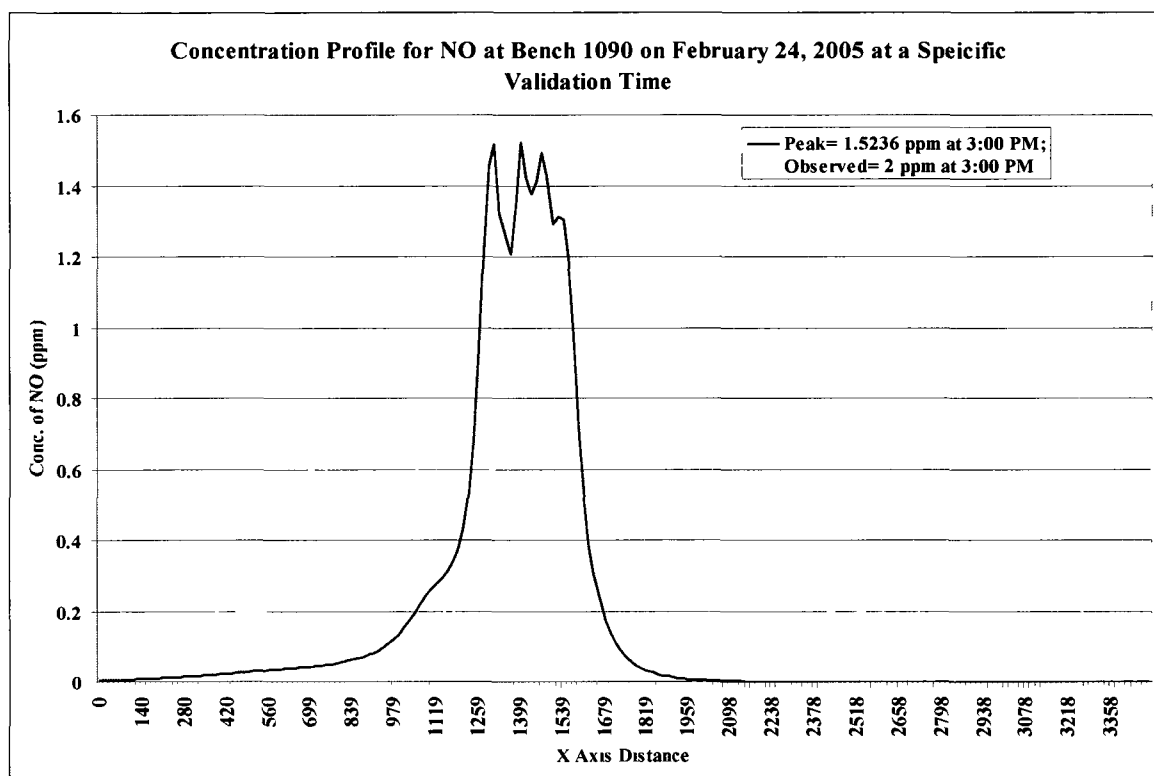Figure 5.17: NO Concentration Profiles Over Time for Bench 1090 (2/24/2005)

Figure 5.18: NO Concentration Profiles at Validation Time for Bench 1090
(2/24/2005)

Figure 5.18 shows a very close agreement between the observed value for NO (2 ppm) at bench 1090 and the peak predicted value (1.5236 ppm). Thus it can be concluded that the model is valid for predicting the concentration of NO on bench 1090 on February 24, 2005.

A similar validation exercise is undertaken for NO_2, the results for which are presented below in figures 5.19 and 5.20.
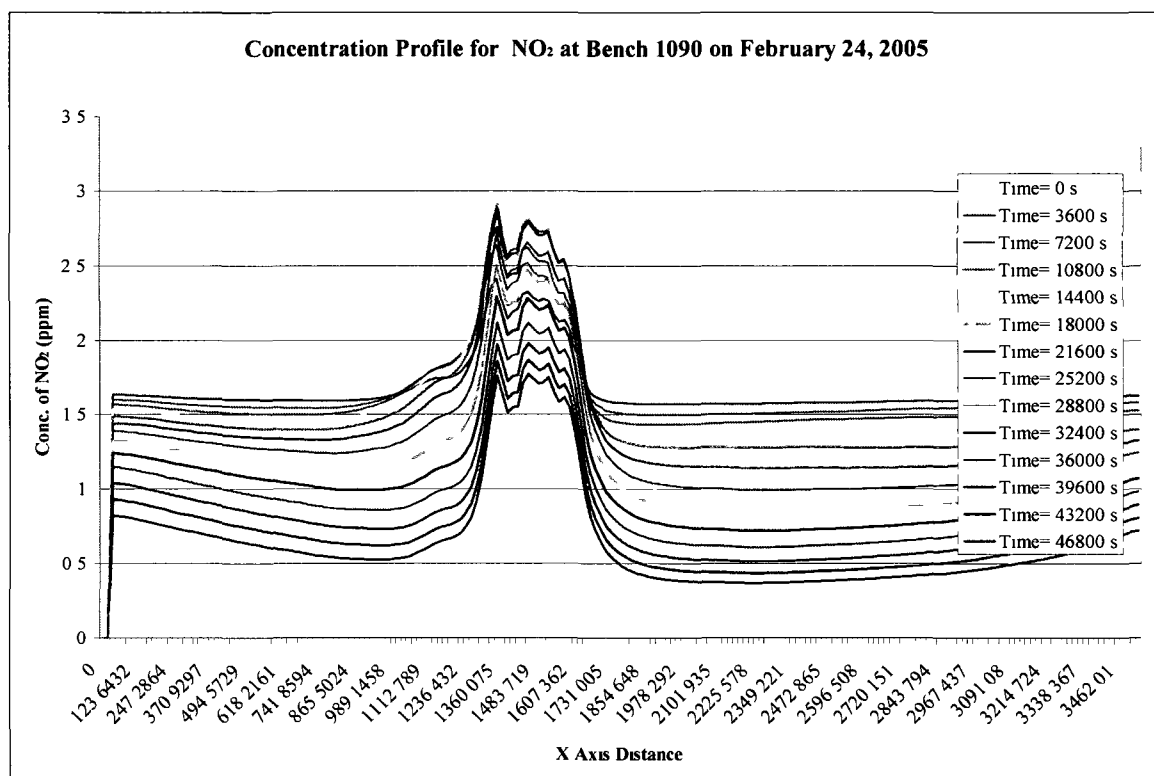
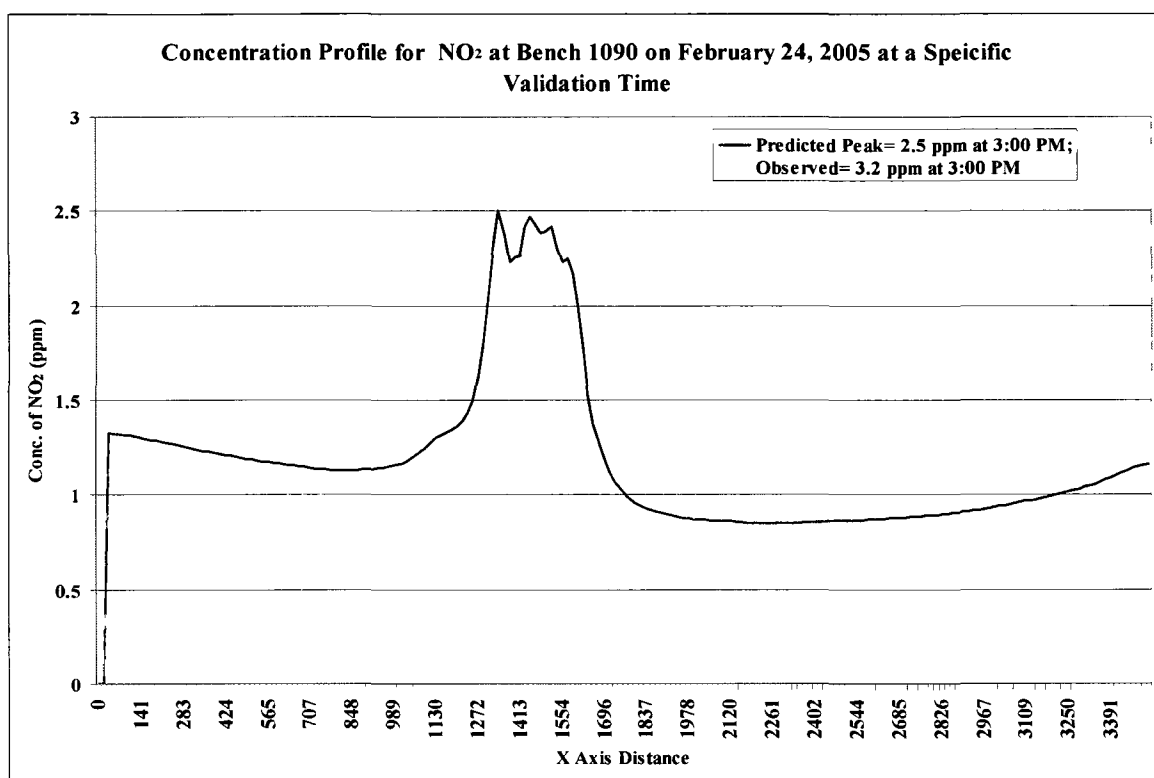Figure 5.19: NO$_2$ Concentration Profiles over Time for Bench 1090 (2/24/2005)

Concentration Profile for NO₂ at Bench 1090 on February 24, 2005 at a Speicific Validation Time

Figure 5.20: NO₂ Concentration Profile at Validation Time for Bench 1090 (2/24/2005)

Figure 5.20 shows a very close agreement between the observed value for NO₂ (3.2 ppm) at bench 1090 and the peak predicted value (2.5 ppm). Thus we can conclude that the model is valid for the concentration of NO₂ on bench 1090 on February 24, 2005.

5.5. Turbulence

Turbulent mixing is one of the most important phenomena in the model space. An important indicator of turbulence is the Reynolds number (Re). The model chosen for investigating the characteristics of the Re is that for December 13, 2004. The Re was plotted along several axes in model space. These plots are shown in figures 5.21 to 5.25.
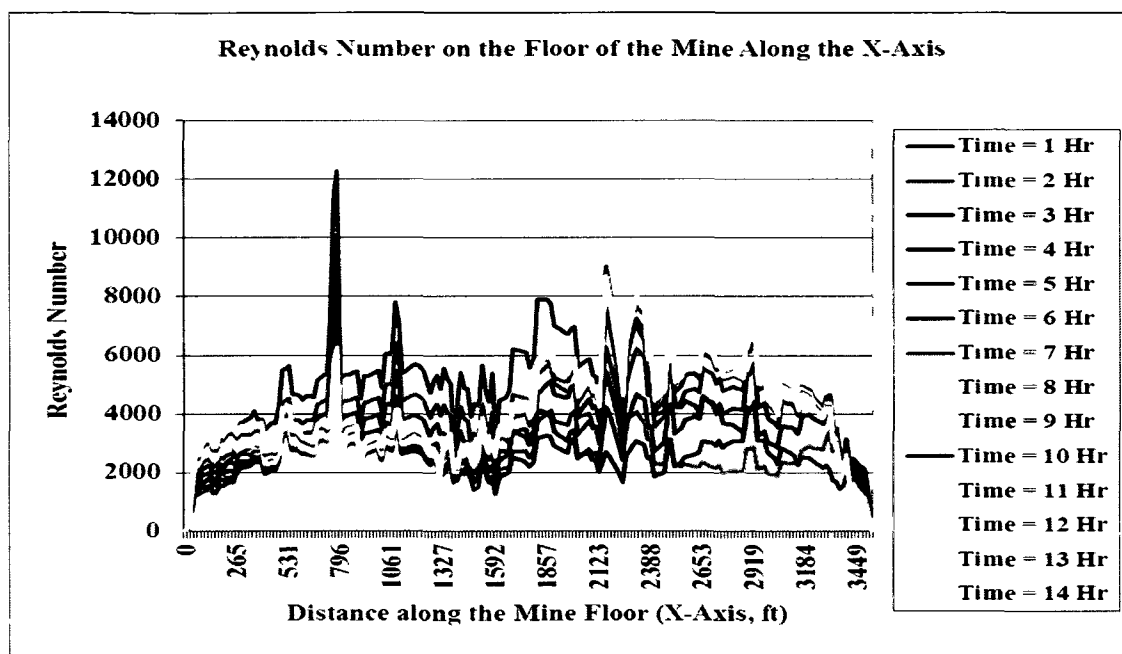
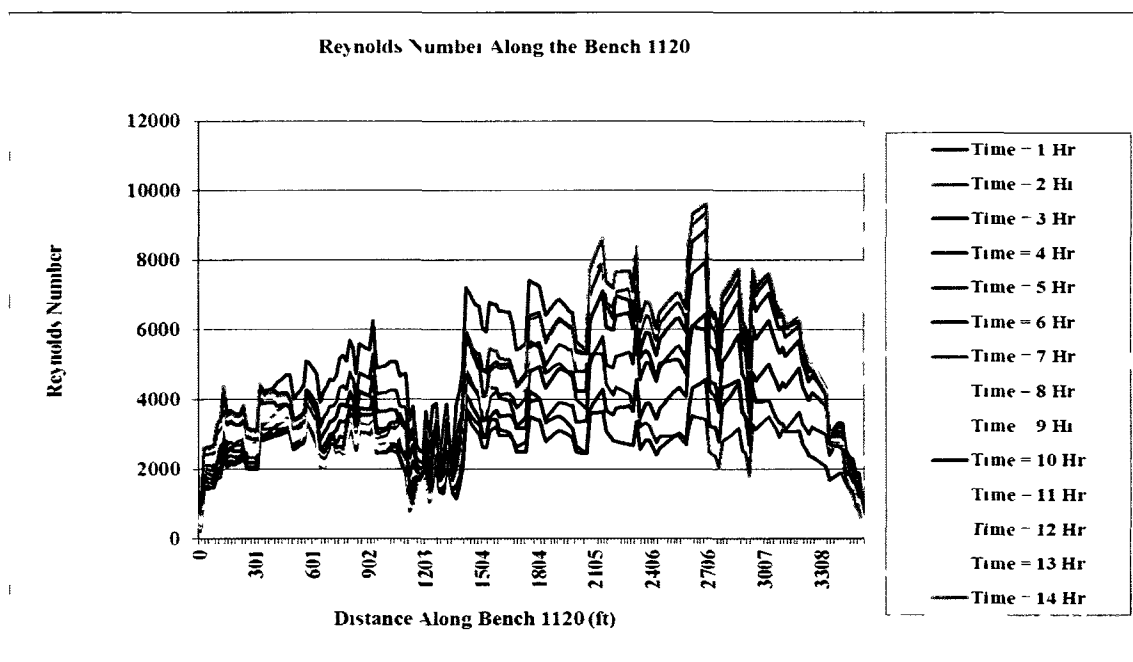Figure 5.21: Re at the Mine Floor on December 13, 2004

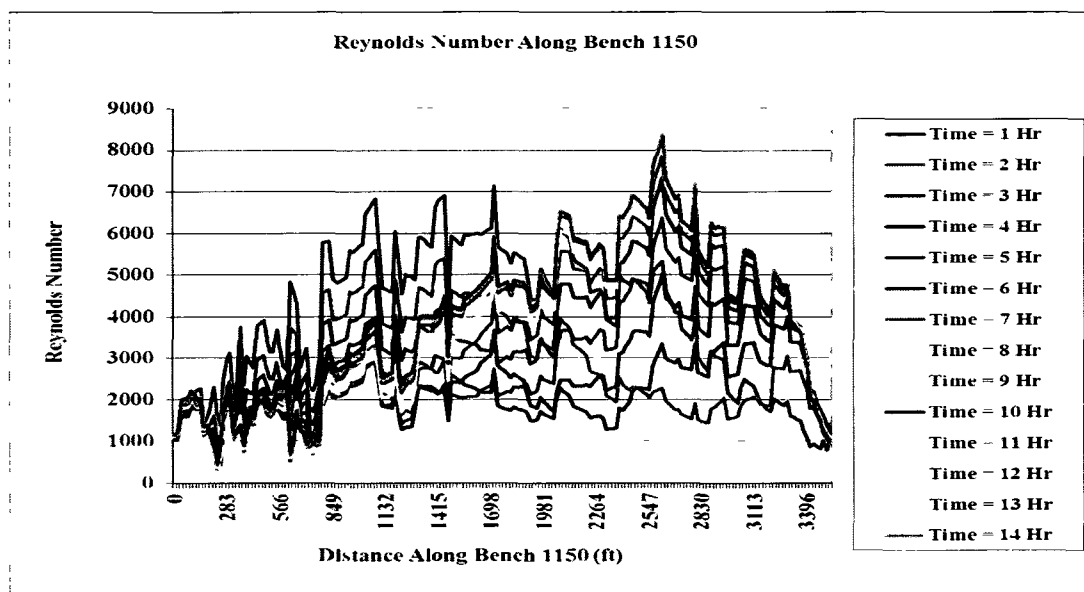Figure 5.22: Re along Bench 1120 on December 13, 2004

Reynolds Number Along Bench 1150

Figure 5.23: Re along Bench 1150 on December 13, 2004

Reynolds Number Along a Vertical Axis on the Leeward Side of the Mine

Figure 5.24: Re along a Vertical Axis on the Leeward Side on December 13, 2004

168

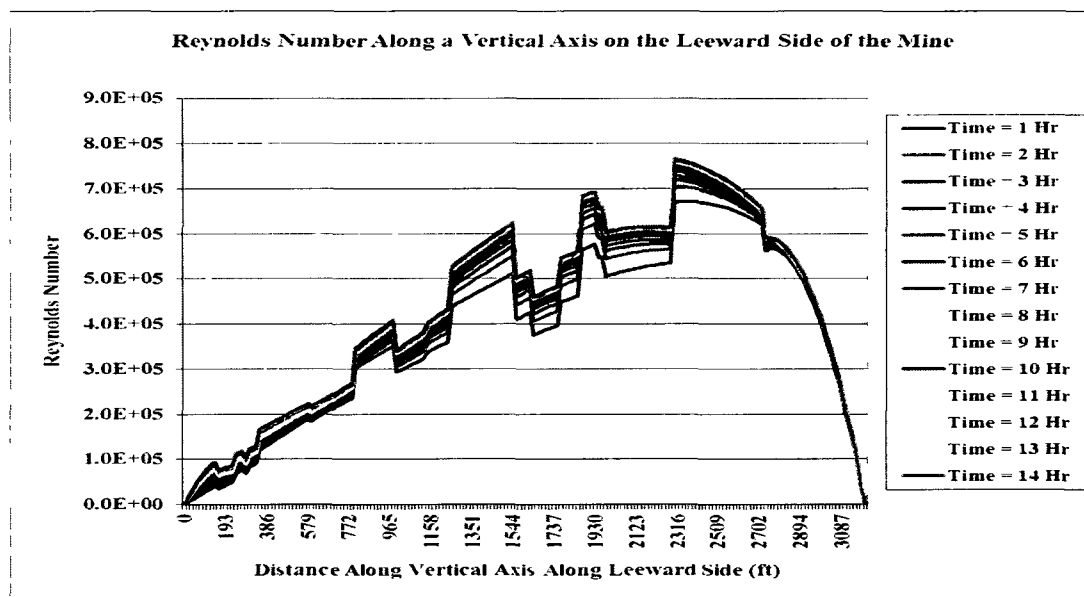**Reynolds Number Along a Vertical Axis Along the Center of the Mine**
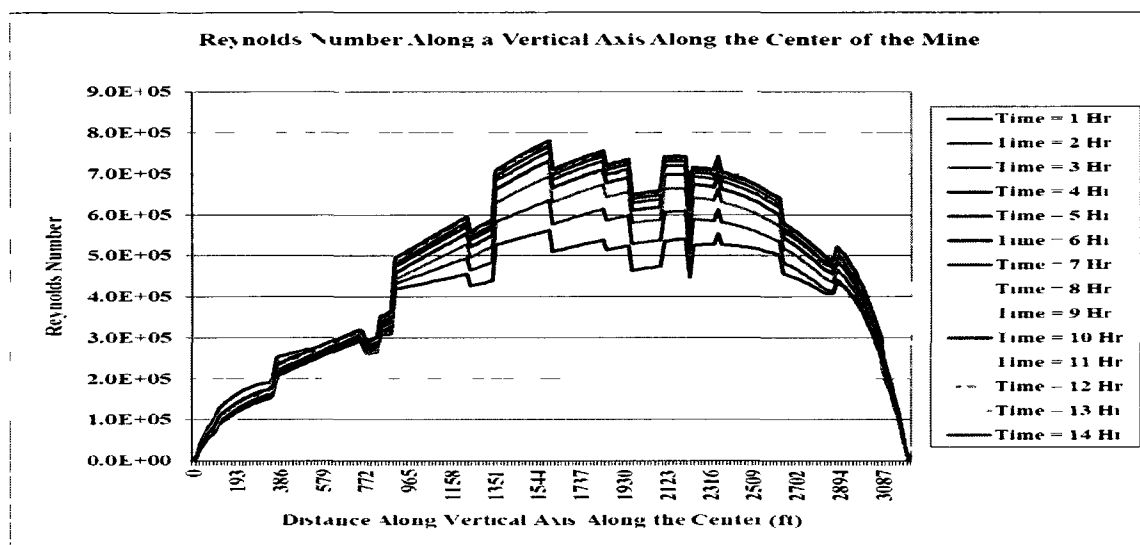

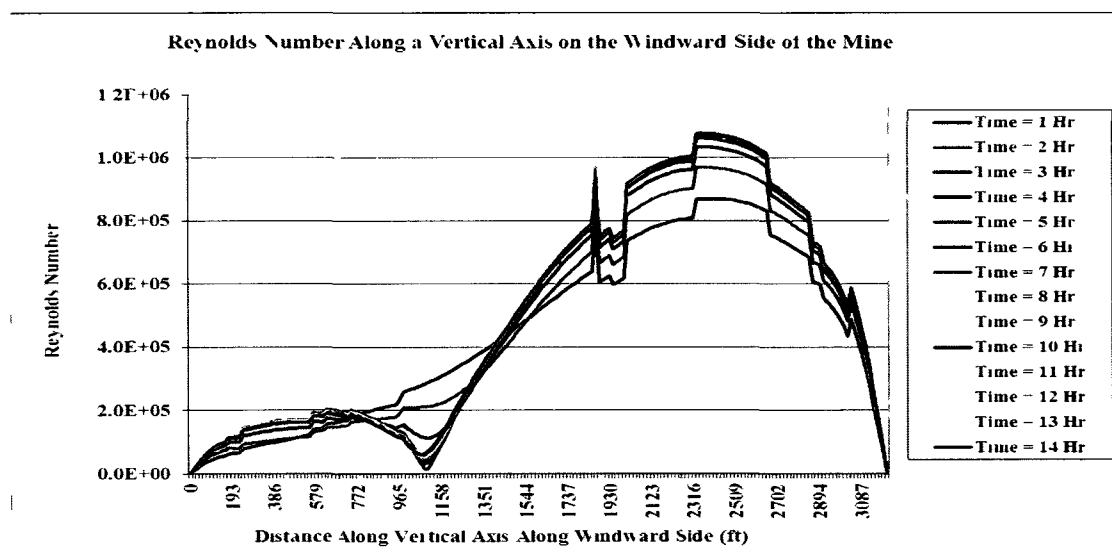Figure 5.25: Re along a Vertical Axis at the Center on December 13, 2004

Figure 5.26: Re along a Vertical Axis on the Windward Side on December 13, 2004

In figures 5.21 to 5.23, the Re was plotted along the production benches (including the floor). In these figures, it can be clearly seen that the flow regime changes between laminar, quasi-turbulent/quasi-laminar and turbulent over both time and space. It can be particularly seen that the flow transitions to a turbulent one along the length of the axis as time progresses. Moreover, as altitude increases, it can be seen that most of the

flow, throughout the model run time, is largely situated in the intermediate, quasi-turbulent zone. This reinforces the assumption that the flow in the model space is ideally neither laminar, nor turbulent, but an intermediate, quasi-turbulent flow. The turbulence that have been encountered in these graphs (where the flow transitions beyond quasi-turbulent) contribute to the turbulent mixing of the pollutants in the open-pit. Similar trends are seen in the figures 5.24 to 5.26. Also, it can be seen that an increase in altitude brings about a sharp increase in the Reynolds number. This is counterintuitive, as the flow toward the top of the model space is laminar. This dicrepancy can however be explained in terms of the large hydraulic diameter that would figure in the calculation of the Reynolds number.

5.6. Limitations of the Validation Model

Mathematical modeling is a scientific exercise with the objective of developing simplified mathematical statements that relate to one another in the same way as the processes that are being modeled. The utility of a model is dependent on the ability of the model to closely approximate real conditions.

The limitation of the model validation procedures are related to the degree of required or desired correspondence between model prediction and reality and the additional costs required to achieve incremental improvements in validation statistics.

Another point to be considered with regard to the immobility of the mine equipment is the fact that the simulation is started at a certain point in time in the life of the mine. This fact influences the difference between reality and the model simulation as done in COMSOL® in subtle but important ways and is discussed as follows.

The mine in situ is in an environment that obviously was not initiated at a point in time in the recorded past. The geology and the atmospheric conditions that the mine was subjected to at inception have existed, from the point of view of mathematical modeling, for a period of time that can reasonably be considered to be infinity. The establishment of the mine in this physical environment led to drastic changes in the

topography of the area, resulting in alterations of its microclimate. The atmosphere encountered in the mine pit at the present date is a result of the incremental changes made to the mine pit that altered the topography, at the same time changing the energy balance of the system. It may be argued that any energy transmitted into the microclimate of the mine at any stage will eventually be transported to the atmosphere outside the mine, and thus any process of energy or mass exchange would eventuate in an equilibrium with the larger atmosphere. However, this argument presupposes a continuum of mass and energy exchange between the mine microclimate and larger atmosphere. Such a continuum may not exist and, even if it does, may be intermittent. As seen before, there may be material barriers that prohibit interplay, i.e., a trough-shaped mine profile confines the atmosphere near the mine floor within its high walls, giving rise to the air quality problems encountered by the mine. The existence of inverted air layers coupled with cold temperatures often inhibit diffusion, thus preventing natural dissipation of trapped pollutants. Thus it can be seen that the microclimate of the mine, while being a subset of the larger planetary climate in terms of initial conditions, may not necessarily be in such equilibrium with it that the microclimate in a mine space can legitimately be considered a local perturbation of planetary occurrences. In other words, mine microclimates are proactive, not reactive. They might react to more global events like rain or snow, and are definitely sensitive to temperature fluctuations in the planetary climate (seasonal change), but such interactions are slow and, within a limited time frame, a mine microclimate would have distinctive features that demand a separate evaluation. One important feature of a mine microclimate is that the mass generated in it tends to remain within it. This, coupled with the fact that the mine microclimate may similarly trap and pool energy as well, means that the salient features of that climate can only be precisely understood as the integration over time of all the changes, both small and large, occurring in the physical environment. In order to gain a mathematical understanding of this microclimate, it would thus be necessary to start a simulation from the inception of the mine and incorporate all the changes made in the mine environment over the period of

time leading up to the end of the simulation (time at which results are desired). If such a simulation was to be carried out, it would be the definitive exercise for model validation. Such a simulation, however, is not feasible for obvious reasons. The alternative is to start the simulation at a point in time in the life of the mine. In order for such a simulation to generate a realistic representation of the results at the point in time in question, a plethora of data for the start time of the simulation are needed. Such data are rarely available, rendering the model simulation an approximation of reality depending on the accuracy and availability of the data. All simulations are approximations. In the absence of adequate data, the model is started at a point of time in the life of a mine from a position of neutrality. This indicates that at the model start time, the mine, theoretically, comes into existence in the final form, i.e., in the geometrical shape in which it is deemed to exist at the time of simulation. Equipment and other ancillaries are deemed to be in position and producing at the appointed time. It is as if a particular instant in the life of the mine is chosen as a starting point, and all history of activity and energy or mass transfer are not taken into account. If, starting from this point, the simulation progresses to a certain subsequent point in time for which data are available, and at that point in simulation time, the results given by the model closely match the acquired data, the model can be said to be validated. In order for the model to converge on the acquired data at the prescribed time, the model must be started at an adequate period of time before, preferably from a time at which data for the important conditions are available. If the model is started at the initial time after incorporating acquired data and the physical processes initiated in the model transform those initial conditions to a demonstrably valid output at the end of the prescribed time, the model can be said to be behaving in a manner close to reality.

One of the considerable problems of numerical modeling of open pit ventilation is discrepancy of input and output boundary conditions for meteorological profiles. An effective scheme of boundary conditions for inlet velocity, for example, is often

assumed. Since all data from the initial starting time of the model are not available, all conditions imposed on the model are not realistic..

CHAPTER VI: Sensitivity Analysis

6.1. Introduction

In chapters III, IV and V, the development of a two-dimensional (2D) model, as well as the development and validation of a three-dimensional model (3D) have been presented. This chapter analyzes the sensitivity of several variables those are believed to have significant influence on the transport and distribution of gaseous pollutants in an open-pit. The model was validated with data from three dates during the winter months of 2004-2005 (December 13, 2004, January 3, 2005 and February 24, 2005)..
The sensitivity analysis presented in this chapter is based on the specific model validated for December 13, 2004 as good validation results were obtained on this date. During model validation, several parameters that were deemed to have significant effects on the concentration distribution of the gaseous pollutants in the open pit were considered. Since model results can be strongly dependent on the boundary conditions in any CFD model, various boundary conditions set and their influence on model predicted results was analyzed.

During the CFD analysis, each parameter was then varied independently, while holding all other variables constant, and the effect of the variations is examined on the distribution profile of the gaseous pollutants in the open pit.

6.2. Choice of Variables

The following parameters were selected for sensitivity analysis.

- Influent Velocity (and Gust Airflow)
- Temperature
- Diffusivity Coefficient
- Slope Angle
- Geometry of the open pit

There are many known and unknown parameters that influence the flow of air within an open-pit. The aforementioned parameters were chosen because during the development of the model, these parameters were noted to be the most important inputs to the model. Moreover, Belousov (1995) noted that temperature difference between different areas around the pit is a significant cause of breeze circulation in mine pits. Both Baklanov (1984) and Aloyan et al. (1982) noted that the velocity of air flow in the pit, coupled with a variety of factors such as the nature and movement of sources and the existence of surface absorption of pollutants play a crucial role in the final concentration of pollutants in an open pit. This is particularly true for influent air currents in open pit mines with a complex geometry and topography. When the vertical and horizontal extent of the pit is comparable, the back flow and tear-off and leeward movements might play an important role. The importance of these parameters is explained briefly below.

Influent Velocity: The influent velocity is introduced directionally from the edge of the model pit. The air flow enters the model space and, upon interacting with the native air mass, initiates flow in the model space that carries the pollutants via advection. Some of the pollutants may be transported out of the mine space by this advective current. Thus, stronger the current, more pollutants may be transported out of the pit. The concentration of pollutants in the pit should decrease with increasing velocity.

It has been sometimes observed that the velocity of air flowing into the mine environment may increase over time, it is sustained at that higher velocity for a brief period of time and then reduces gradually to the original velocity. Such a flow pattern is known as a gust velocity, and represents a spike in the influent velocity profile. As velocity is a very important parameter in the present study, the presence of a gust velocity is deemed to have a significant effect on the concentration profile in an open pit. Thus the influence of gust velocities in examined in this study.

Temperature: As the temperature of the mine pit increases, the air in the depths of the pit should ideally gain energy and expand, thus setting up a convective current which is likely to transport some of the pollutants out of the pit. Thus the concentration of pollutants in the pit is expected to decrease with increasing temperature. Since the density of air in the model space is held constant, a natural consequence of this association is that temperature may not show any significant effect on the air flow, and thus, the transport of gaseous pollutants out of the pit.

Diffusivity Coefficient: As discussed in previous chapters, the diffusivity coefficient, is not just the molecular diffusivity rate that occurs due to mass diffusion, but also encompasses numerous other factors including the projection velocity of the mass into the model space, and the additional heat that the projected mass contains. The value for the diffusivity coefficient was assumed, and it was hypothesized that a change in the value would bring about a change in the concentration profiles. Thus the diffusivity coefficient was varied to investigate its effects on concentration distribution.

Slope Angle: A very important factor in the establishment of the inversion cap is the geometry of the mine. A flatter geometry would make it easier for the advective wind to transport the pollutants out of the open-pit, while narrower pit geometry would retain the pollutants in the pit. The pit slope was thus varied to investigate the extent of its influence on the distribution of pollutant concentration.

Geometry of the Open Pit: In most open pit mines, the geometry changes with time. Typically, the overall slope angle of the pit is a basic design parameter of mine design, and is generally maintained throughout the life of the mine. But, other geometrical dimensions, such as length, breadth and depth increase as the production in the pit progresses. A larger pit is expected to retain more pollutants in the pit, increasing the concentration in the open pit. The open pit created in the model space to examine the effects of pit geometry is referred to in this chapter as the 2010 pit. It is longer, wider

and deeper than the 2004 – 2005 pit that has been used to validate the 3D model, as well as to perform most of the sensitivity analysis.

To examine the sensitivity of these variables, these parameters were individually varied, and the concentration profiles were studied along the bench 1150, as well as a vertical axis extending from the pit bottom to the top of the inversion cap. The vertical axis is located roughly at the mid-section of the open pit. The following figures (6.1 and 6.2) show the lines along which the concentration profiles are studied and presented, both in the horizontal and the vertical axes. NO was chosen as the sample gas for the sensitivity analysis. The validation exercise described in this chapter provides sufficient evidence that the model constructed in COMSOL® provides predictions that closely match the reality observed on the ground. Although in every case, the model underpredicts observed data to a limited extent, the results of the model may be used for future mine ventilation design purposes.
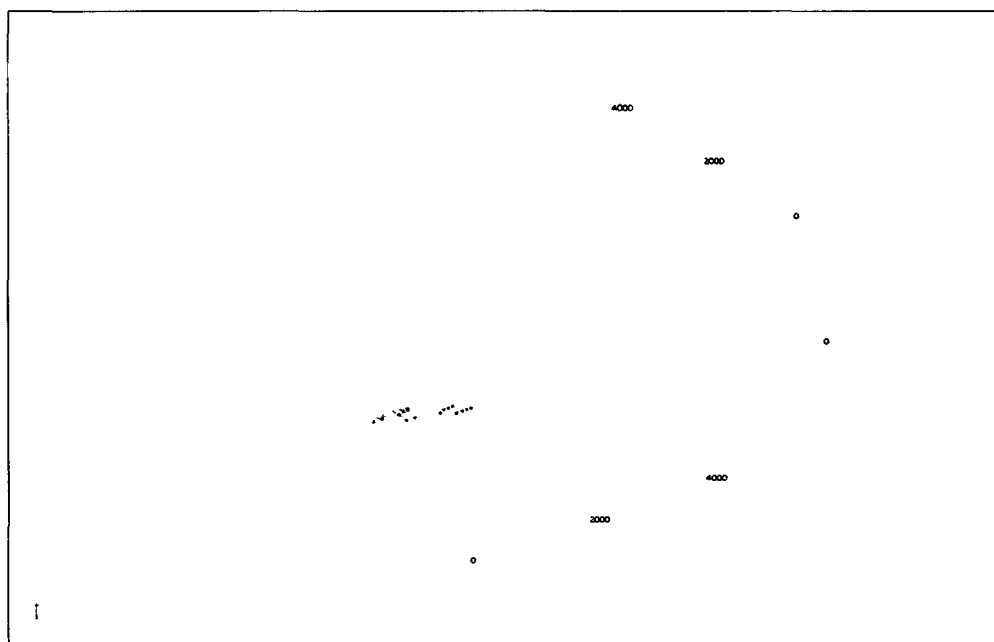
Figure 6.1: Position of the Horizontal Line (colored red) on Bench 1150 in Isometric View

In figure 6.1, the position of the horizontal line is shown in an isometric view. The line (marked in red) extends along the 1150 bench, in an east-west direction, through the length of the pit. The line is located at a height of six feet from the bench floor, which is considered to be the approximate breathing height for a person. Figure 6.2 shows the location of the same line on a plan view.
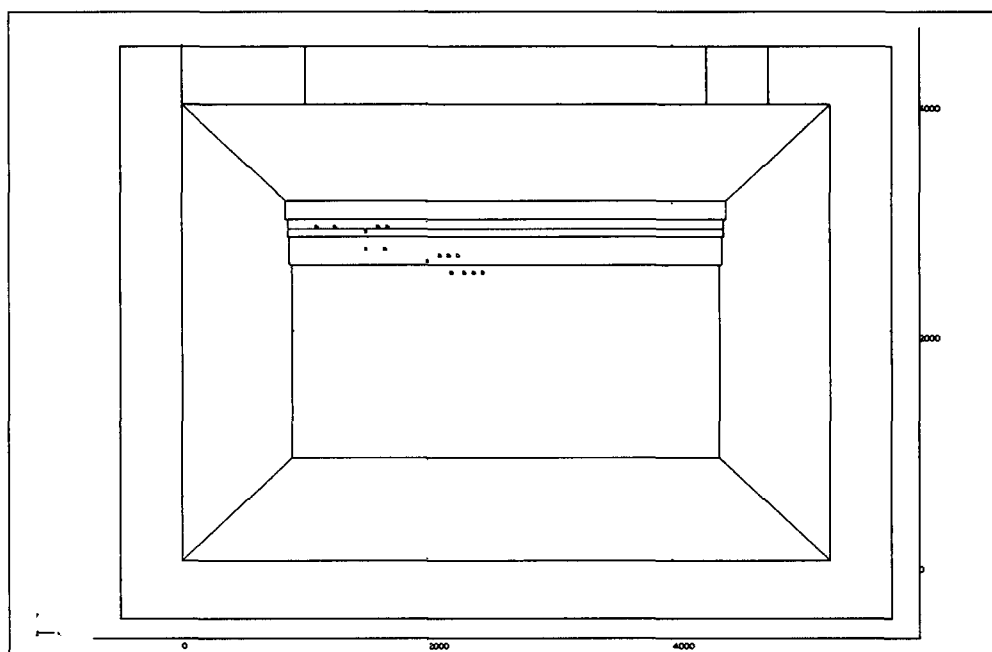
Figure 6.2: Plan View Showing the location of the Horizontal Line (colored red) on Bench 1150

Figure 6.3 shows the location of the vertical line in the open pit along which concentrations of gaseous pollutants are predicted. The line in located roughly at the mid-section of the open pit, and as shown in figure 6.3, extends from the pit bottom to the top of the inversion cap.
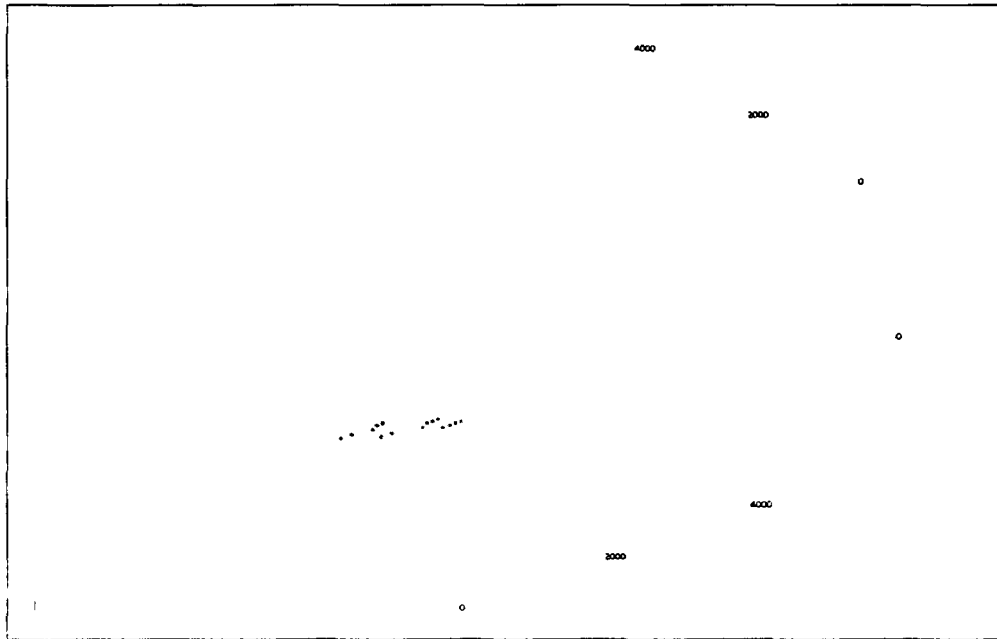
Figure 6.3: Position of the Vertical Line (Colored Red) Along the Vertical Axis in Isometric View

6.3. Influent Velocity Sensitivity

The following three influent velocities were selected to explore the effect of velocity on the concentration distribution.

- 2 ft/s
- 3 ft/s
- 5 ft/s

The following figures (6.4 – 6.9) show the concentration profiles for gaseous pollutants at the aforementioned lines in figures 6.2 and 6.3.

Concentration Profile for NO for Bench 1150 on December 13, 2004 with Velocity = 2 ft/s
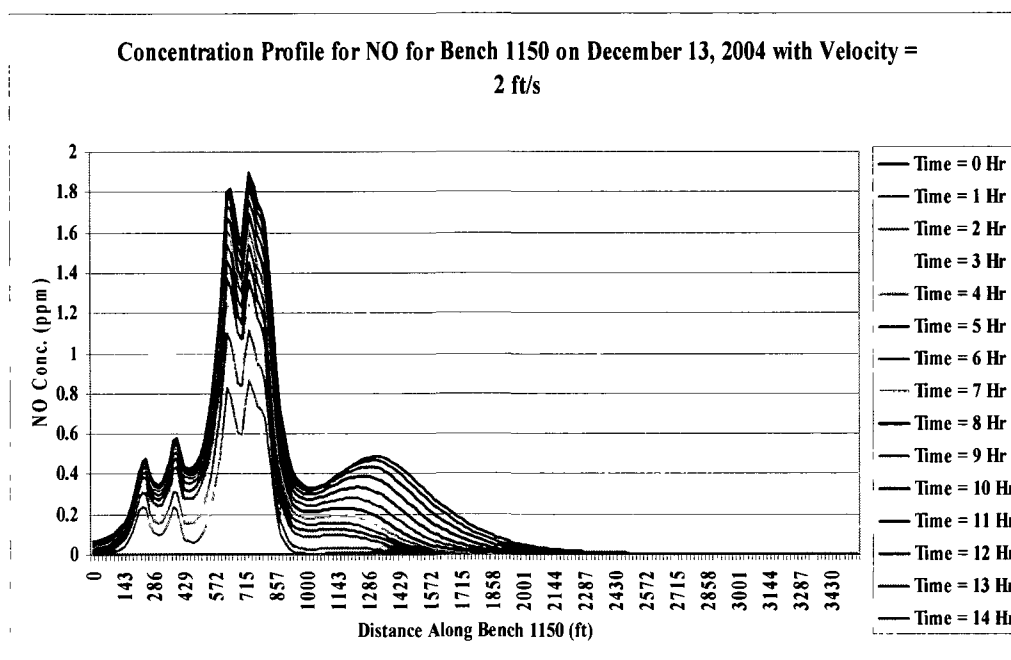
Figure 6.4: Concentration profile for NO along bench 1150 (Influent Velocity 2 ft/s)

Concentration Profile for NO on the Vertical Axis on December 13, 2004 with Velocity = 2 ft/s
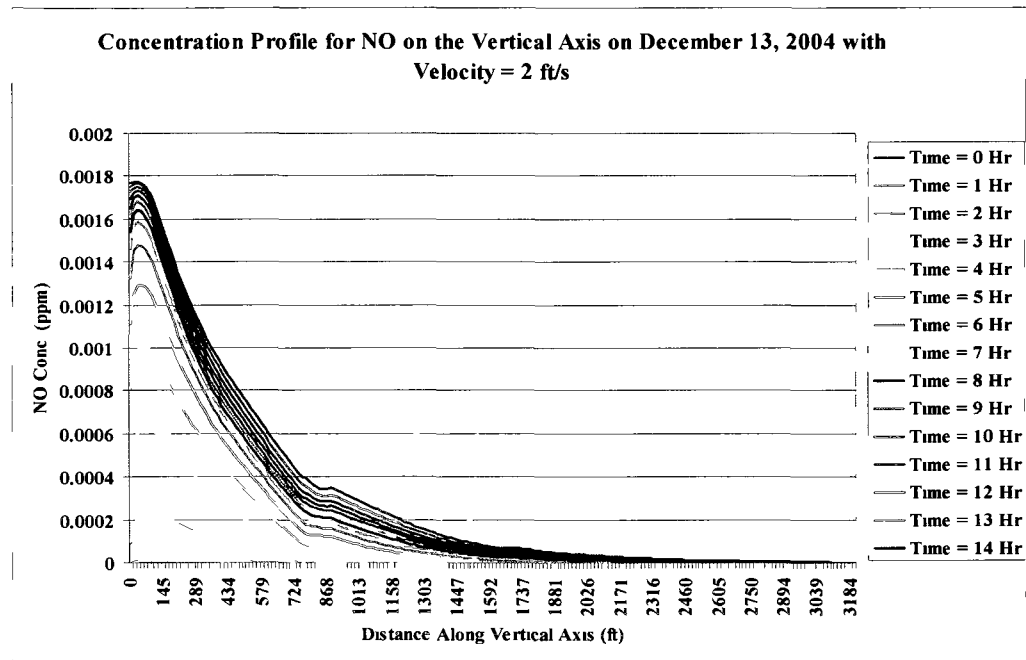
Figure 6.5: Concentration Profile for NO Along the Vertical Axis (Influent Velocity 2 ft/s)
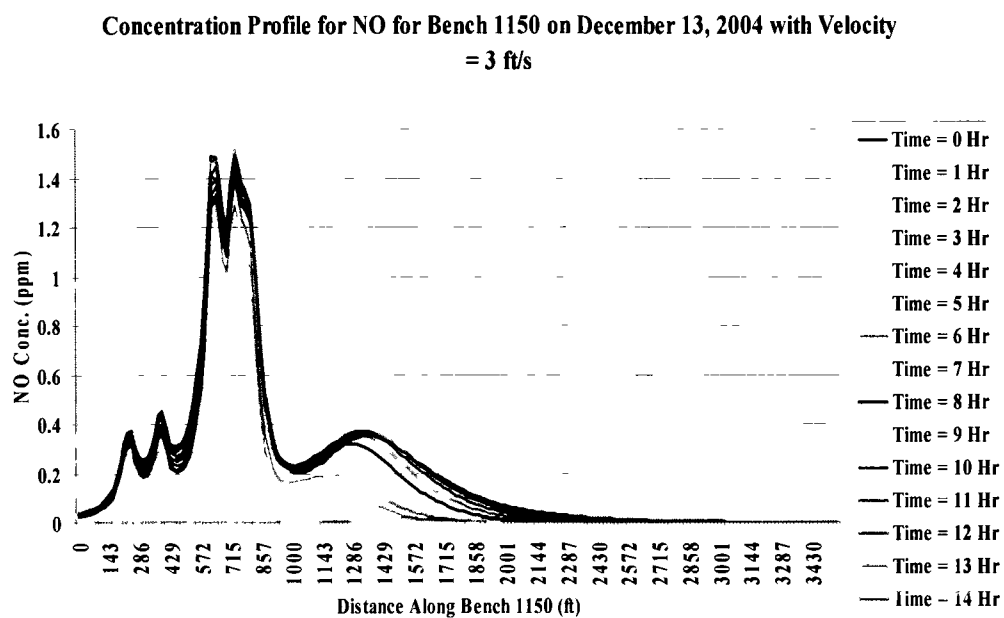
Figure 6.6: Concentration Profile for NO Along Bench 1150 (Influent Velocity 3 ft/s)
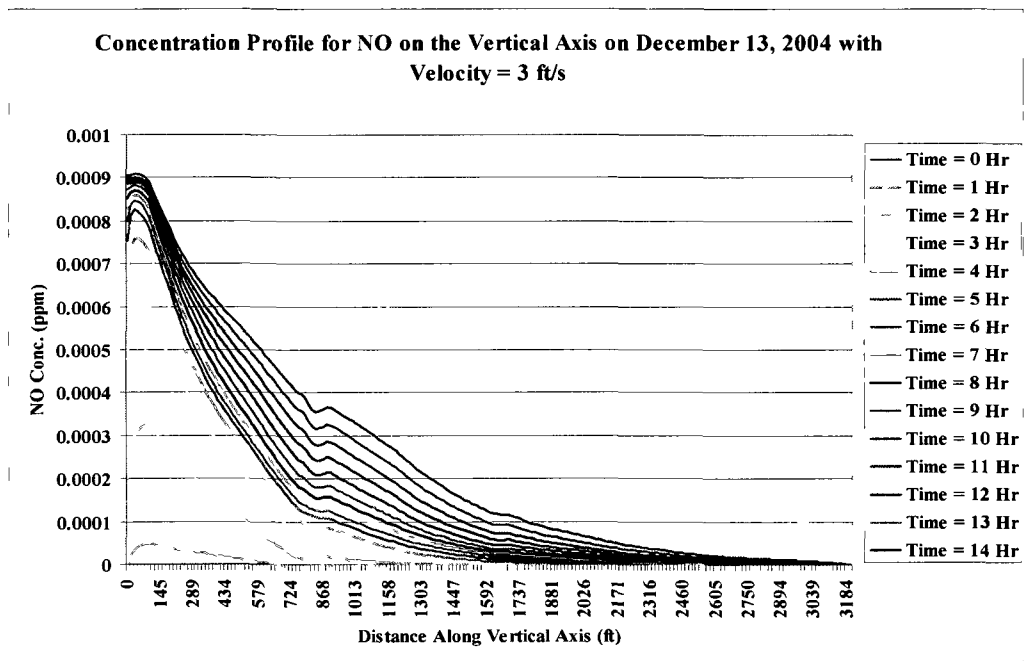
Figure 6.7: Concentration Profile for NO Along the Vertical Axis (Influent Velocity 3 ft/s)
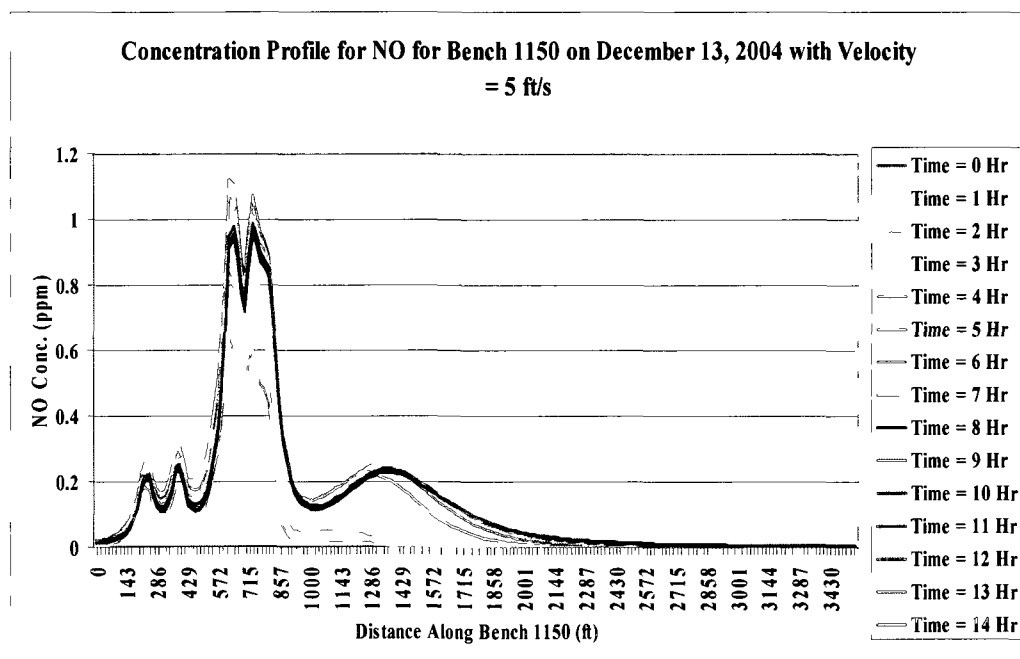
Figure 6.8: Concentration Profile for NO Along Bench 1150 (Influent Velocity 5 ft/s)
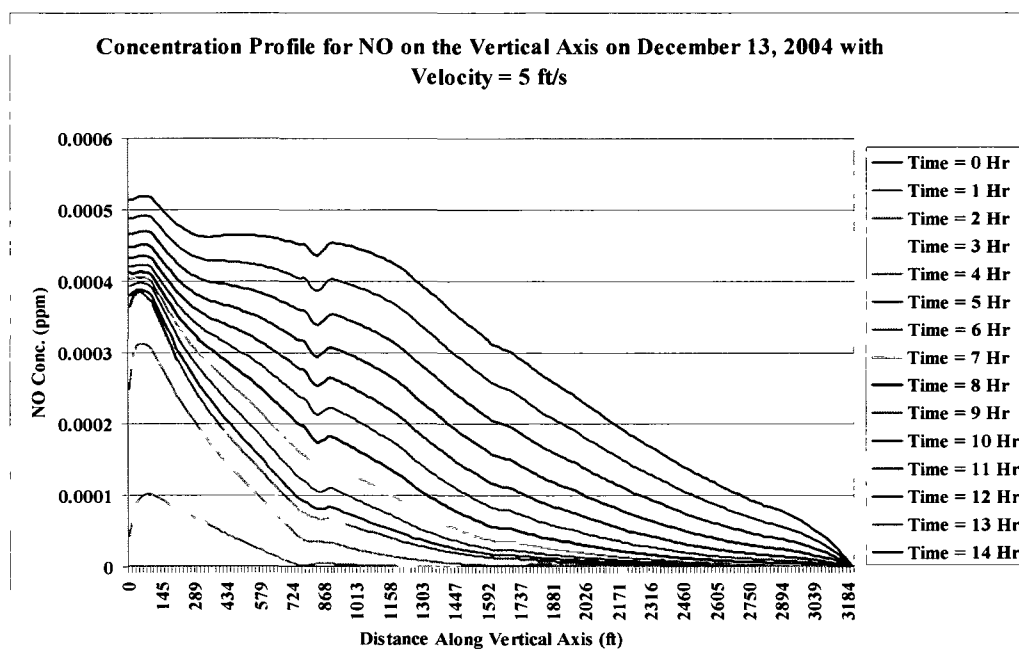
Figure 6.9: Concentration Profile for NO Along the Vertical Axis (Influent Velocity 5 ft/s)

It can be seen from figures 6.4 to 6.9 that increasing in velocity inflow partially mitigates the pollutant concentrations in the open pit. The peak values for both the locations decrease with increase in velocity, as can be seen from figures 6.10 and 6.11.
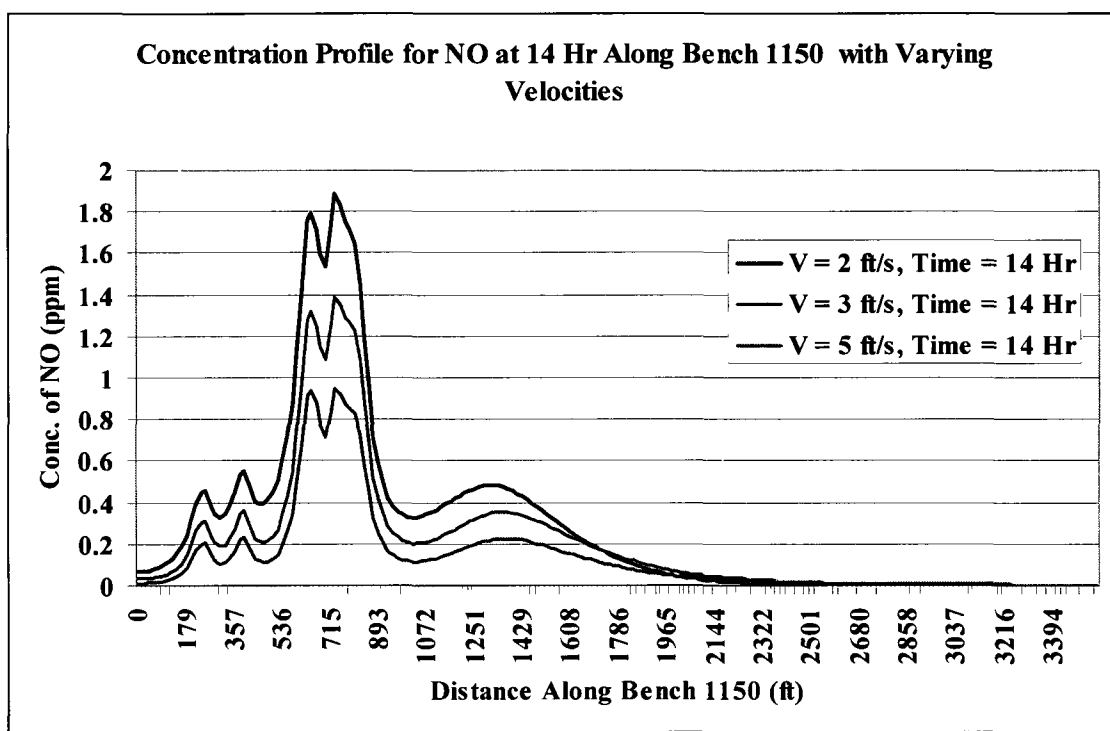
Figure 6.10: Concentration Profile for NO at 14 Hr Along Bench 1150 with Varying Velocities

Concentration Profile for NO at 14 Hr on the Vertical Axis with Varying Velocities
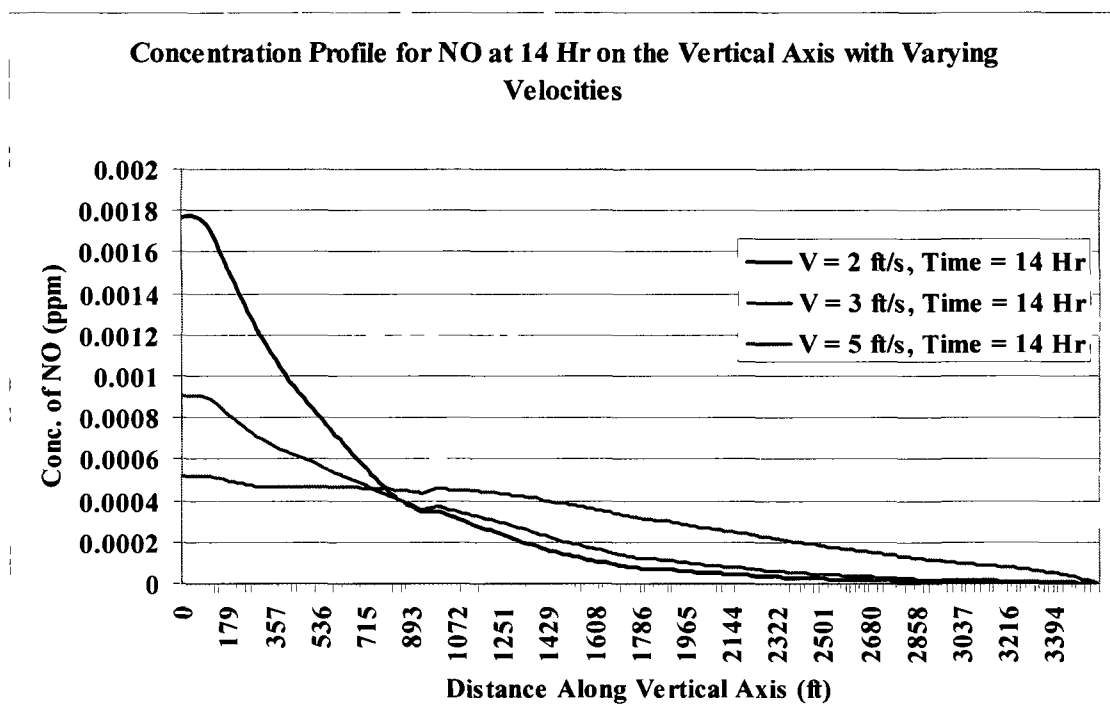
Figure 6.11: Concentration Profile for NO at 14 Hr Along the Vertical Axis with Varying Velocities

It can be further noted that while the shape of the profile along the longitudinal axis along bench 1150 did not show significant changes for the range of velocities examined here, the profile is somewhat changed for the vertical axis at the mid-section of the pit. For the lowest velocity of 2 ft/s (figure 6.5), maximum concentration can be observed at the pit bottom (approx. 0.0018 ppm, extreme left of the graph), after which the concentration steeply descends to zero near the inversion cap (extreme right of the graph). This trend continues for higher velocities (5 ft/s, figure 6.9, peak value approx. 0.0005 ppm), where a further increase in the intermediate values and a further spreading of the "tight band" is noted. It appears that recirculation zones are formed, where the pollutant is mixed, but the area of active circulation, the degree of opening and the range of the vertical current are sharply decreased, the transport of pollutants out of the open pit, however, does not happen. This effect is a result of increased mixing and advection due to increasing velocity. It can also be noted from figures 6.5,

6.7 and 6.9 that there is a temporary, localized drop in concentration around an altitude of 750 ft from the pit bottom. This small drop is due to the effect of vorticity and localized eddies that occurs there due to a backflow in the air current. Similar effects were also evident in both the 2D and the 3D models. Such airflow is capable of transporting some of the pollutant away from the sources as well as the mid-section of the pit, thus leading to a temporary although localized drop in the concentration. In the three cases studied, the flow pattern varied very little and its effect on pollution concentration was not substantial.

6.3.1. Gust Wind Sensitivity

The influent wind velocity in the pit may show substantial increase in magnitude over a short period of time, and then decrease quickly. Such a velocity profile is known as a gust wind that could remove more gaseous pollutants from the pit, or may mix the pollutants more thoroughly, thus reducing the concentrations.

Three such gust wind velocities were selected (20 ft/s, 30 ft/s and 40 ft/s) and their effect on the pollutant concentration in the pit was examined. The aforementioned velocities of gust wind were actuated in the model by increasing the influent velocity from 2 ft/s to the selected velocity for that model run (20 ft/s, 30 ft/s or 40 ft/s). The gust wind velocity was kept constant throughout the brief daylight hours, and then reduced the velocity gradually to 2 ft/s after sunset.

The following figures (6.12 through 6.17) illustrate the effect of the gust wind on the pollutant concentration in the pit.

Concentration of NO Along Bench 1150 with Gust Velocity 20 ft/s
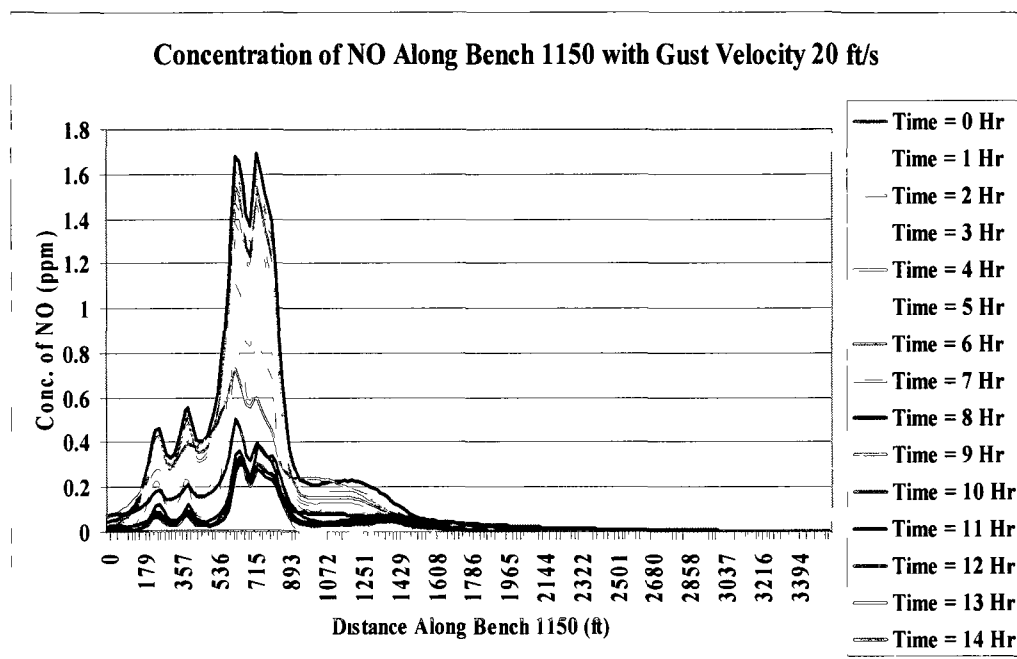
Figure 6.12: Concentration Profile for NO Along Bench 1150 (Gust Wind Velocity 20 ft/s)
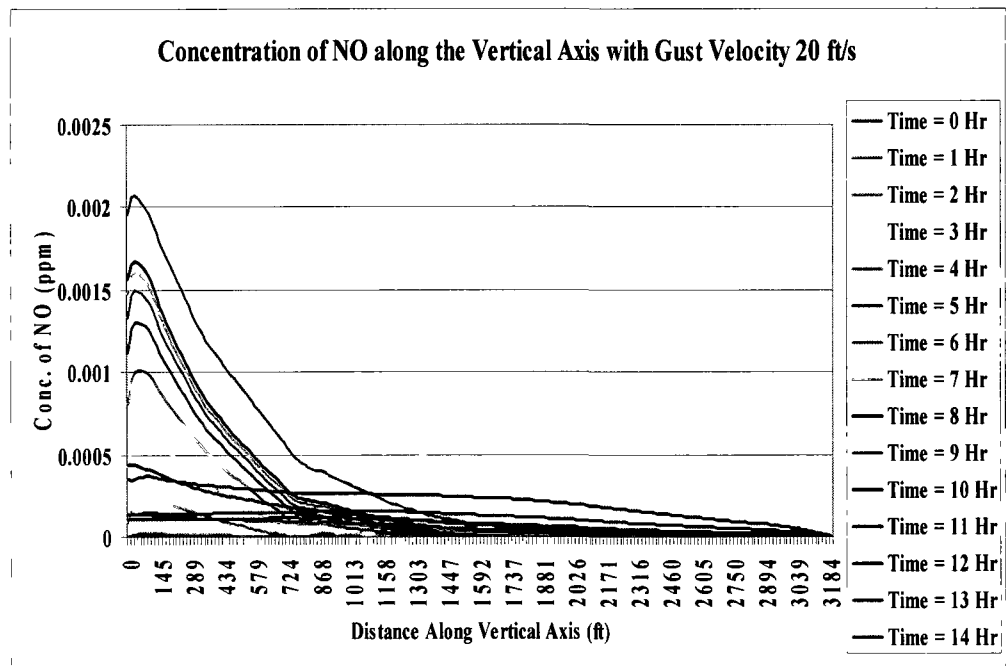
Figure 6.13: Concentration Profile for NO Along the Vertical Axis (Gust Wind Velocity 20 ft/s)
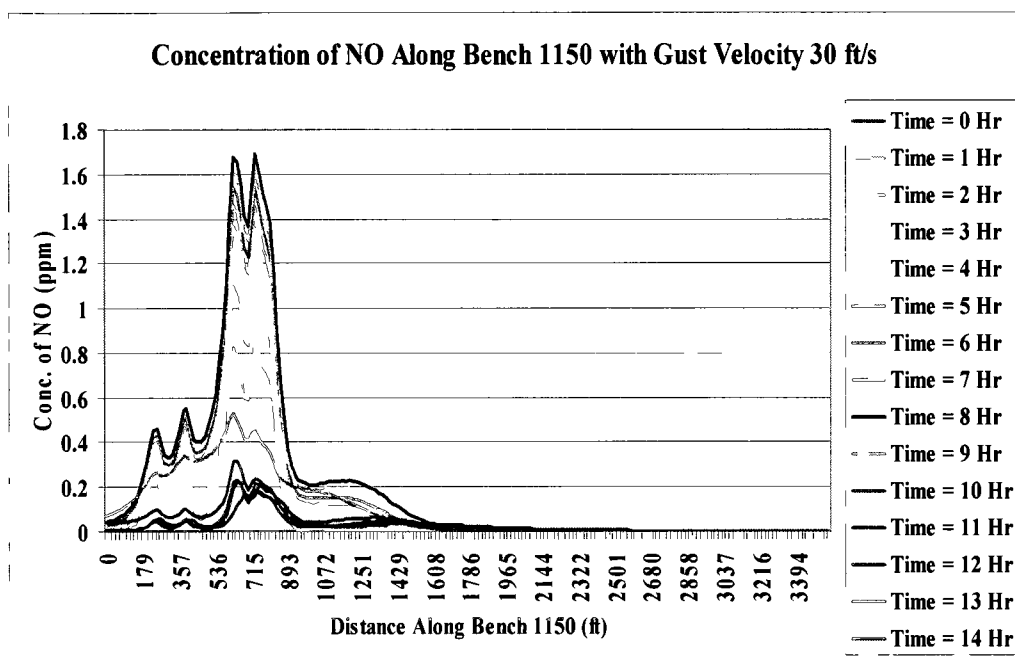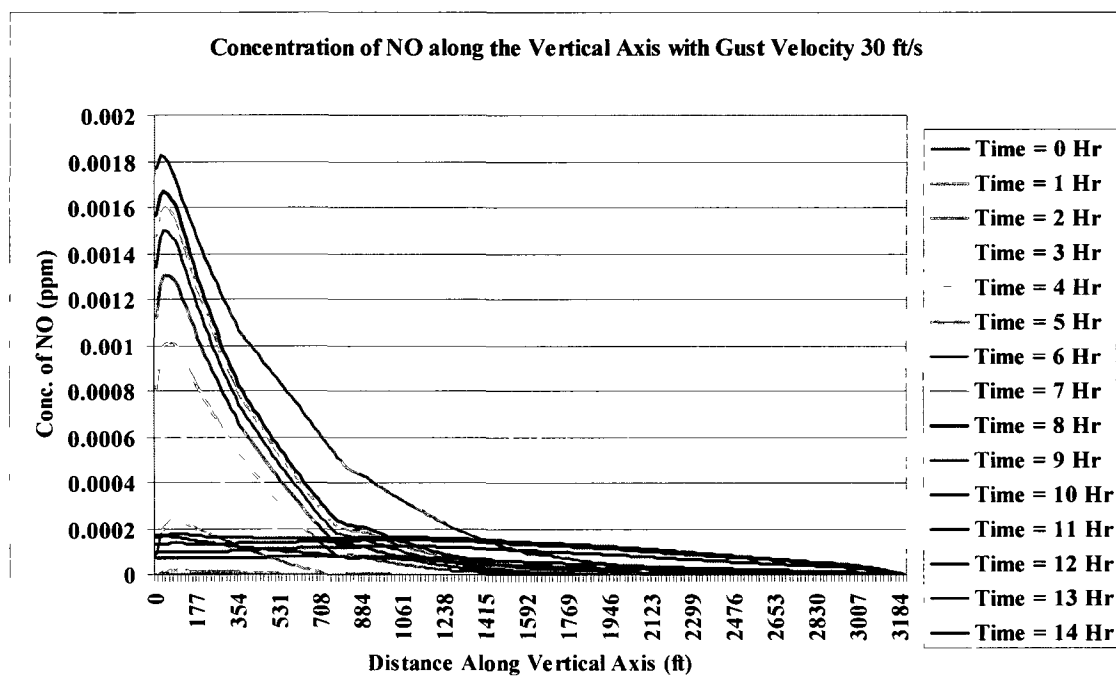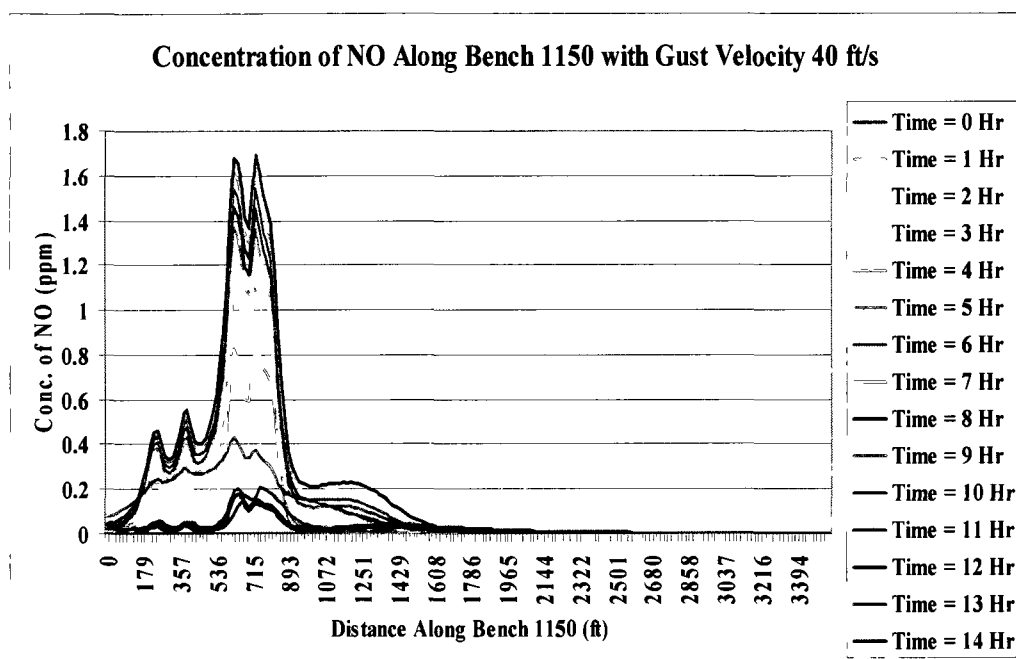
Concentration of NO Along Bench 1150 with Gust Velocity 30 ft/s

Figure 6.14: Concentration Profile for NO Along Bench 1150 (Gust Wind Velocity 30 ft/s)

Figure 6.15: Concentration Profile for NO Along the Vertical Axis (Gust Wind Velocity 30 ft/s)

Figure 6.16: Concentration Profile for NO Along Bench 1150 (Gust Wind Velocity 40 ft/s)
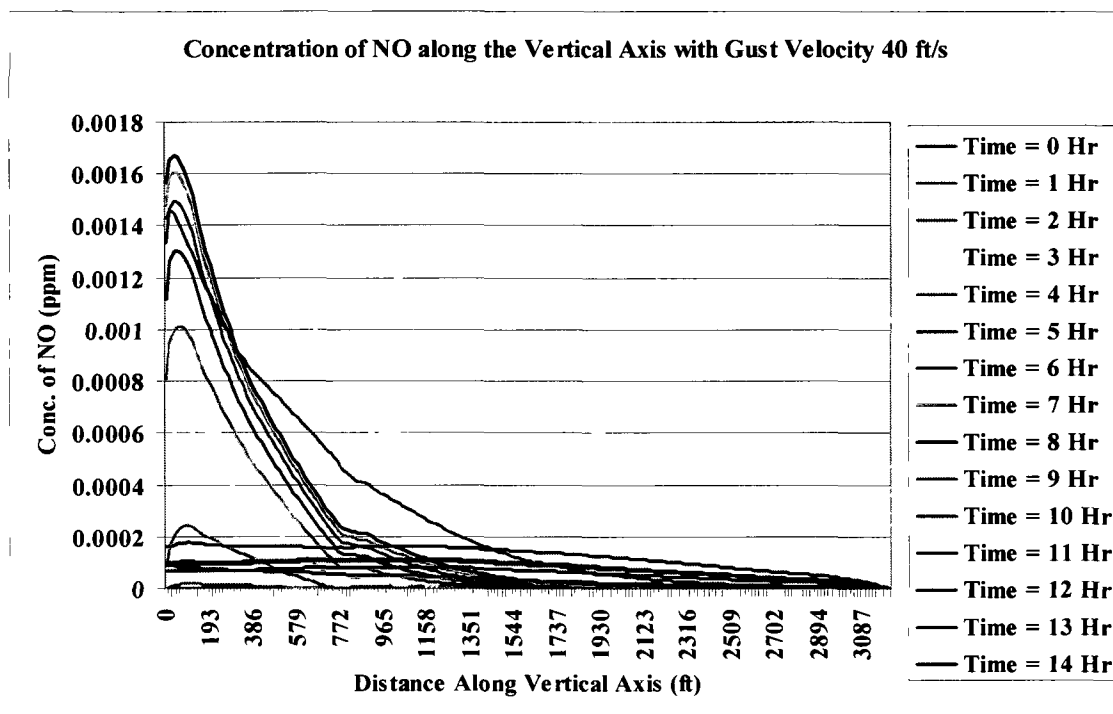
Figure 6.17: Concentration Profile for NO Along the Vertical Axis (Gust Wind Velocity 40 ft/s)

As seen in figures 6.12, 6.14 and 6.16, the concentration of the pollutants along the bench 1150 continually increase till the 8th hour of the model run (reaching a peak value of 1.7 ppm). After the 8th hour in the model run the gust wind velocity at the influent boundary is activated, which results in an immediate reduction in the pollutant concentration profile in the pit. The gust wind velocity is then turned off just before the end of the model run time. This results in the 13th hour of the model run having the lowest concentration profile, while at the end of the model run, the concentration profile is slightly higher than that registered for the 13th hour of model run.

As seen in the figures 6.13, 6.15 and 6.17 the peak concentration values along the vertical axis are close to the pit bottom (largest value approximately being 0.0021 ppm). It can be seen from figures 6.13 and 6.15 that the peak concentration values with (20 ft/s and 30 ft/s gust wind) occur at the 9th hour of the model run. Figure 6.17 (gust wind 40 ft/s), however, shows that the 8th hour has the highest concentration

profile. This may be due to the fact that a higher velocity mixes the pollutants in the pit more thoroughly, thus reducing the concentrations along the vertical axis. Also, the concentration along the vertical axis is affected sooner by the change in velocity (initiation of the gust wind velocity) than the horizontal axis along bench 1150, which is toward the bottom of the pit. It can also be seen from the figures 6.13, 6.15 and 6.17 that toward the end of the model run, the concentration is fairly evenly distributed along the vertical axis. This occurs irrespective of the gust velocity inflow, indicating that turbulent mixing forces the pollutants to distribute evenly along the vertical axis. It can be concluded that the gust wind inflow into the pit results in removal of more pollutants from the pit than a steady, low influent velocity. However, there is evidence of a highly turbulent flow in the flow regime as a result of the gust wind. Once the flow regime becomes turbulent, increase in the gust velocity does not significantly alter the concentration profile in the open pit. This is primarily because the gust wind, while mixing the pollutant mass in the pit air thoroughly, fails to lift the inversion cap. It appears that recirculation zones are formed, where the pollutant is mixed, but the area of active circulation, the degree of opening and the range of the vertical current are sharply decreased, therefore, the transport of pollutants out of the open pit does not happen.

6.4. Temperature Sensitivity

The following three temperature regimes were selected to explore the effect of temperature on transport and distribution of pollutants.

- 32 °F (0 °C)
- -4 °F (-20 °C)
- -40 °F (-40 °C)

The following figures (6.18 – 6.23) show the concentration profiles for gaseous pollutants at the selected locations.
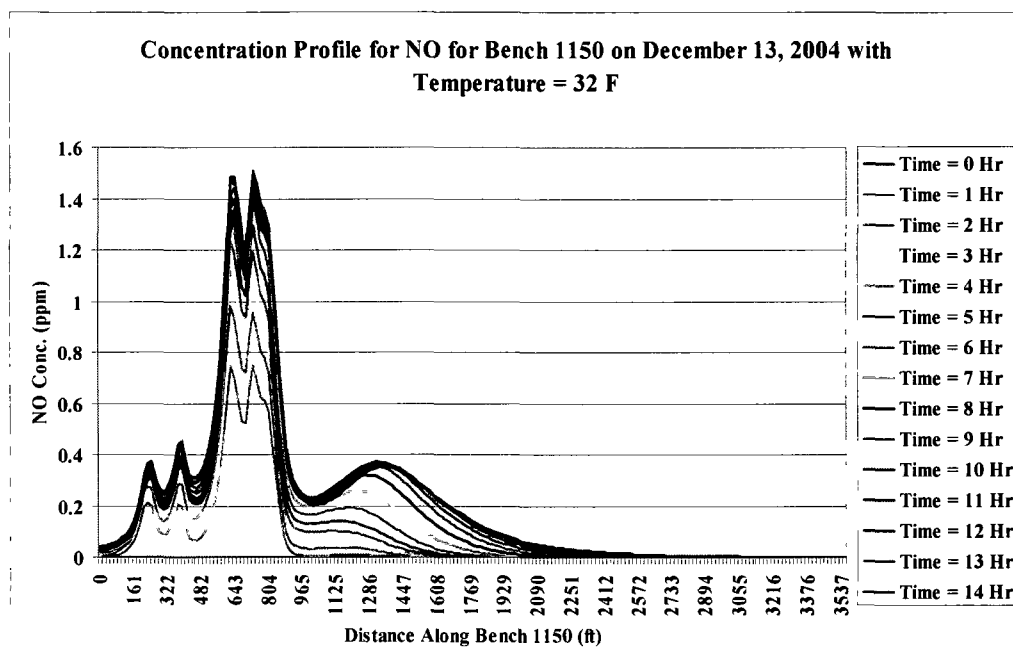
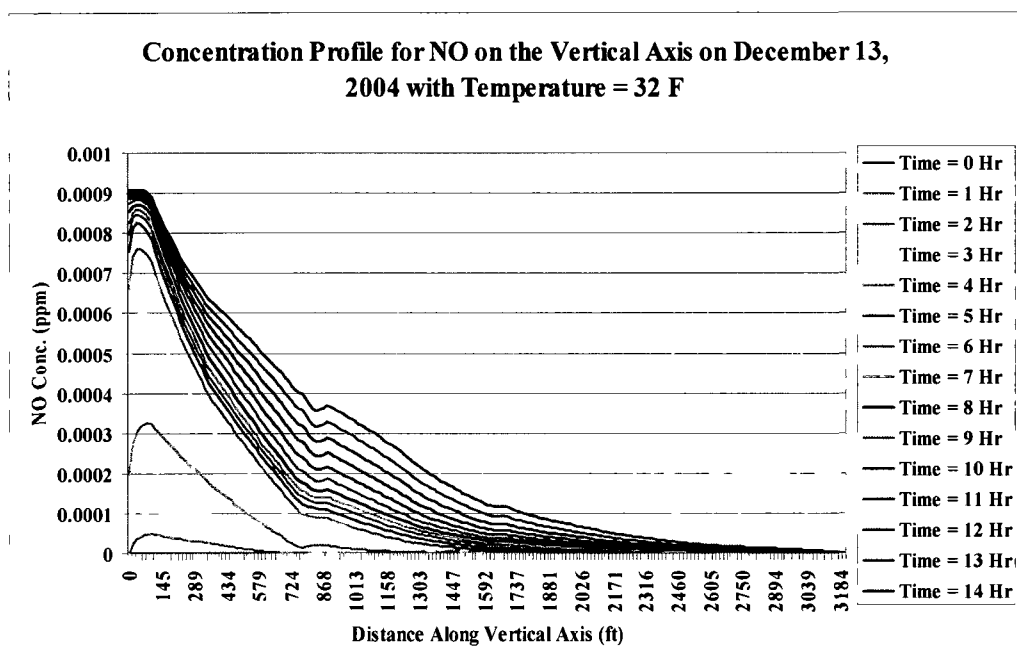Figure 6.18: Concentration Profile for NO Along Bench 1150 (Initial Temp. 32 °F)

Figure 6.19: Concentration Profile for NO Along the Vertical Axis (Initial Temp. 32 °F)
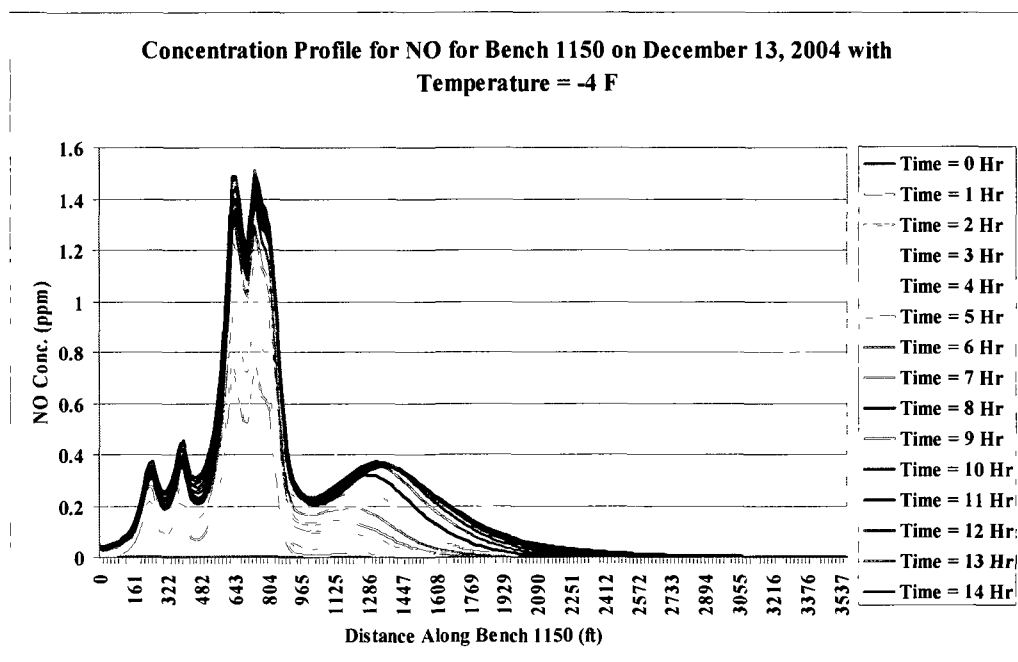
Figure 6.20: Concentration Profile for NO Along Bench 1150 (Initial Temp. -4 °F)
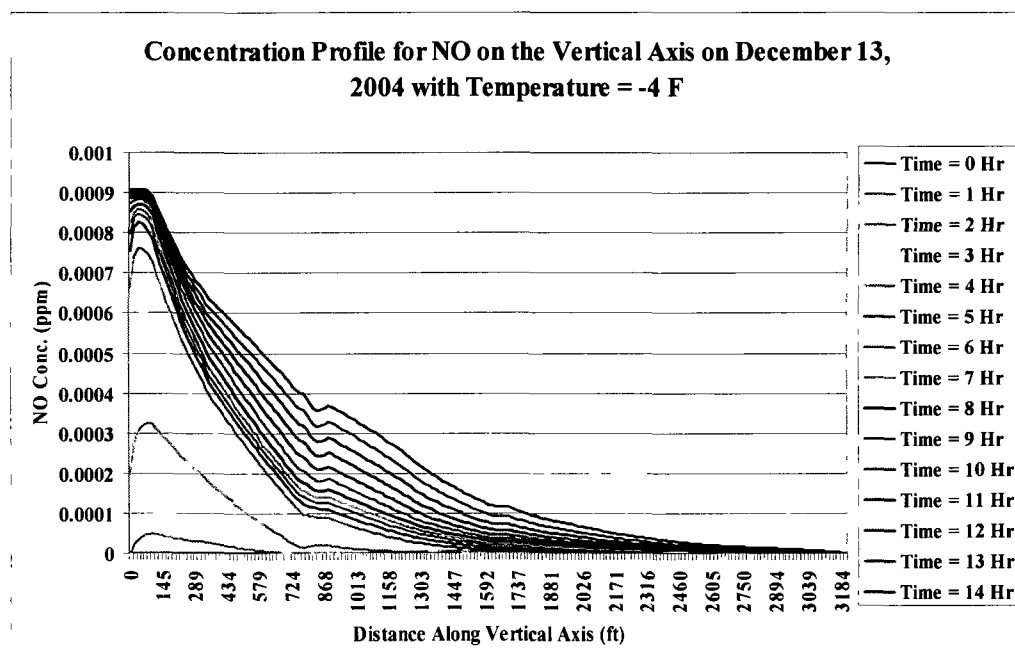
Figure 6.21: Concentration Profile for NO Along the Vertical Axis (Initial Temp. -4 °F)
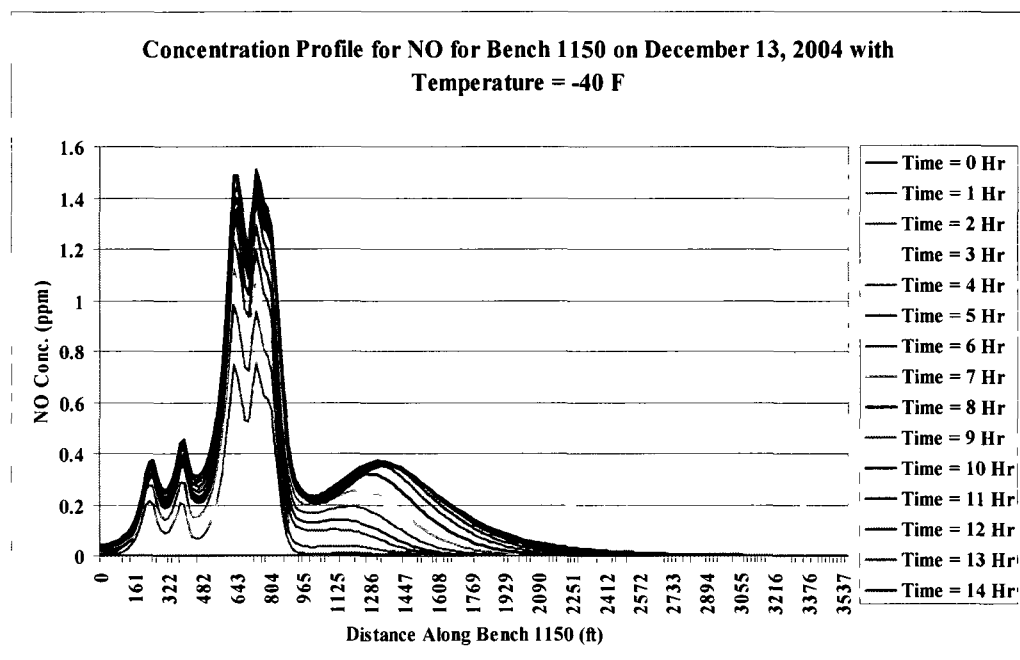
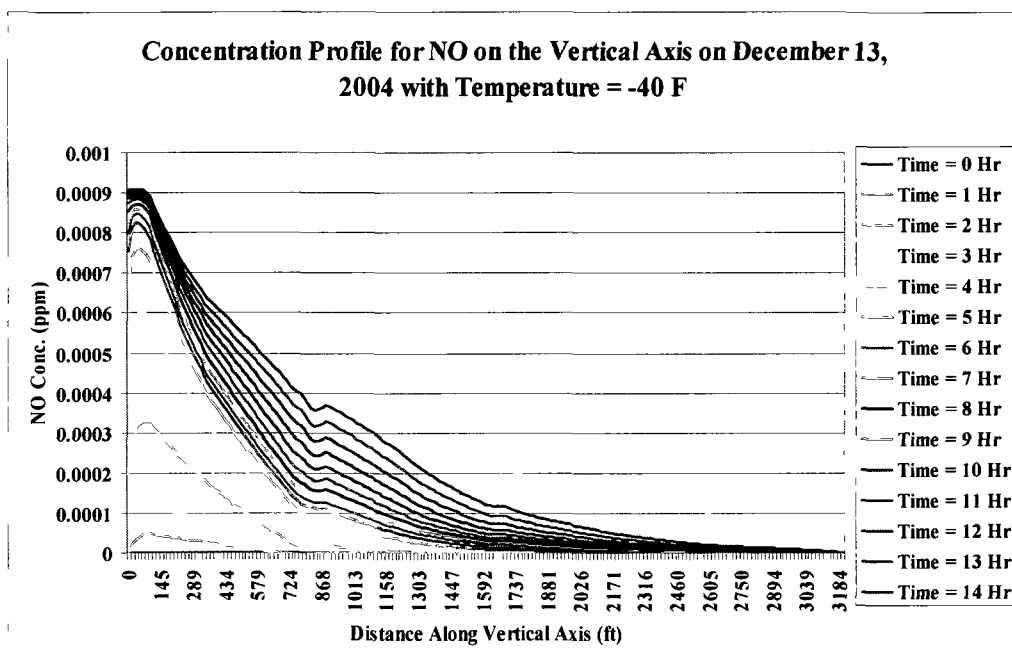Figure 6.22: Concentration Profile for NO Along Bench 1150 (Initial Temp. -40 °F)

Concentration Profile for NO on the Vertical Axis on December 13, 2004 with Temperature = -40 F

Figure 6.23: Concentration Profile for NO Along the Vertical Axis (Initial Temp. -40 °F)

Figures 6.18 to 6.23, show know changes in the concentration profiles for the three cases studied. This is a natural consequence of the assumption of incompressibility. The primary mode by which the incident heat affects the air mass is through the change of density of the air. As heat is transmitted from the surfaces of the mine to the adjacent air, air density decreases and it rises to the top. In this case, however, the density is kept constant and the primary effect of heat addition did not assist in dispersion. Although addition of heat updates the velocities, these velocities may not be strong enough to result a significant difference in the concentration profiles.

6.5. Effect of Diffusivity Coefficient on the Transport and Distribution of Gaseous Pollutants

The following three diffusion coefficients were select to explore the effect of the diffusivity coefficient on the transport and distribution of gaseous contaminants. The value of the effective diffusivity constant in the open-pit environment is not known. Thus these values are assumed and are used to highlight the sensitivity of the system to the effective diffusivity constant.

- 0.5 ft^2/s

- 1.0 ft^2/s

- 1.5 ft^2/s

These values were imposed in the entire model space. The following figures (6.24 – 6.29) show the concentration profiles at the selected locations.
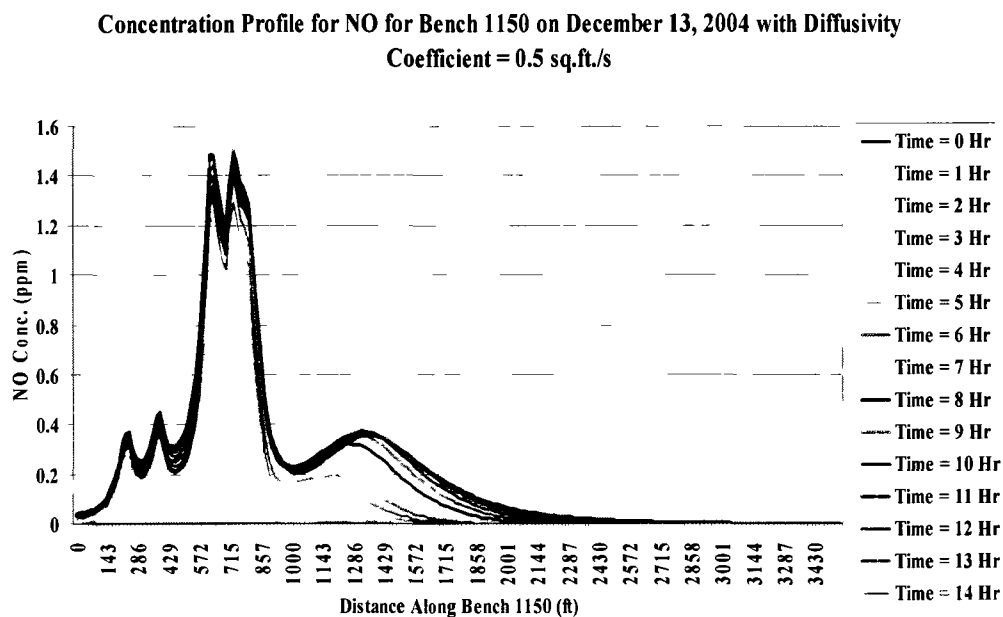
**Concentration Profile for NO for Bench 1150 on December 13, 2004 with Diffusivity
Coefficient = 0.5 sq.ft./s**

Figure 6.24: Concentration Profile for NO Along Bench 1150 (Diffusivity Coefficient
0.5 ft^2/s)

**Concentration Profile for NO on the Vertical Axis on December 13, 2004 with
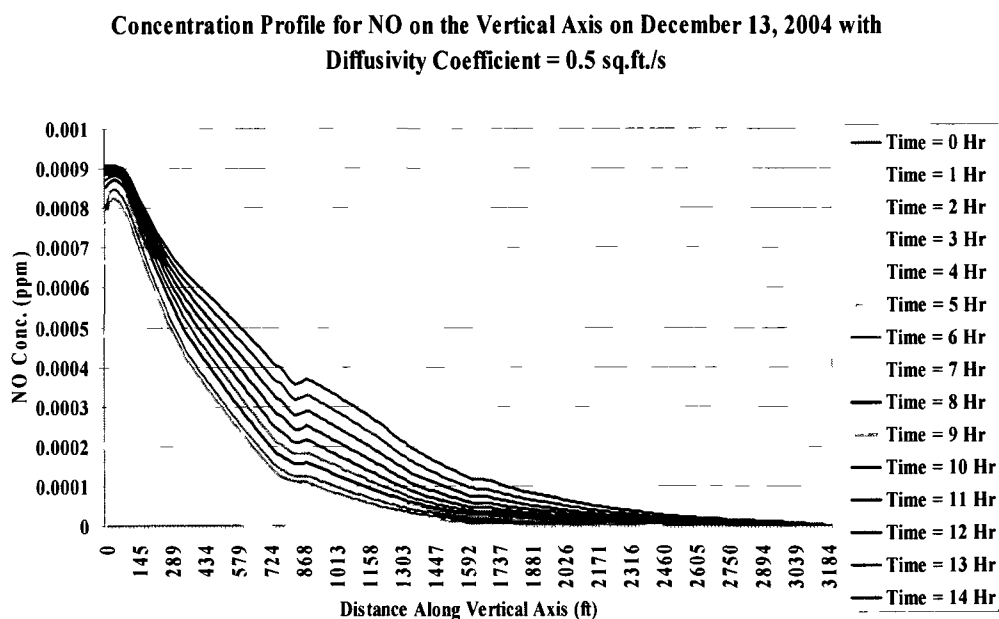Diffusivity Coefficient = 0.5 sq.ft./s**

Figure 6.25: Concentration Profile for NO Along the Vertical Axis   (Diffusivity
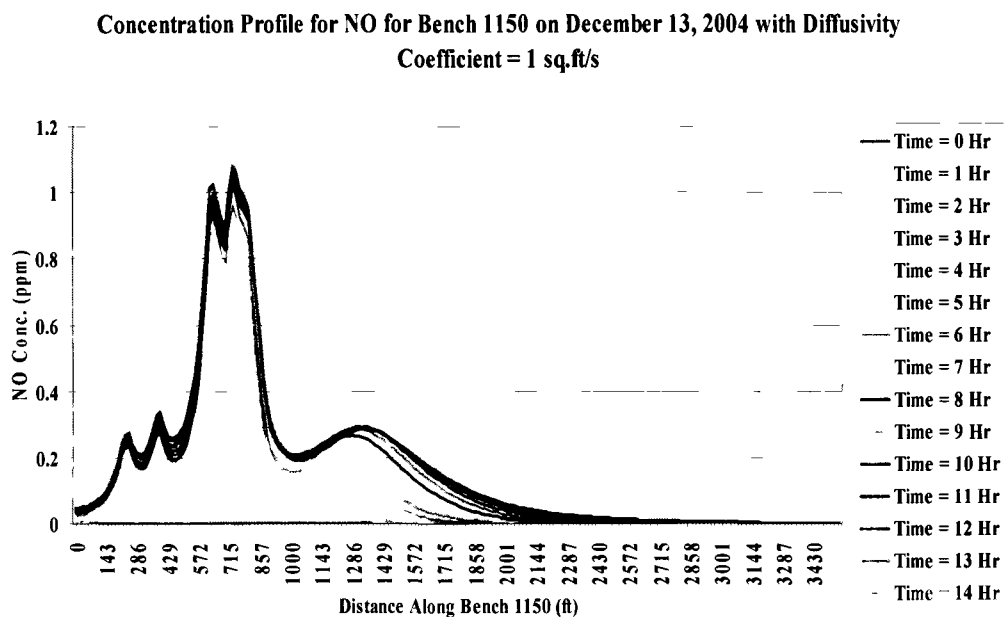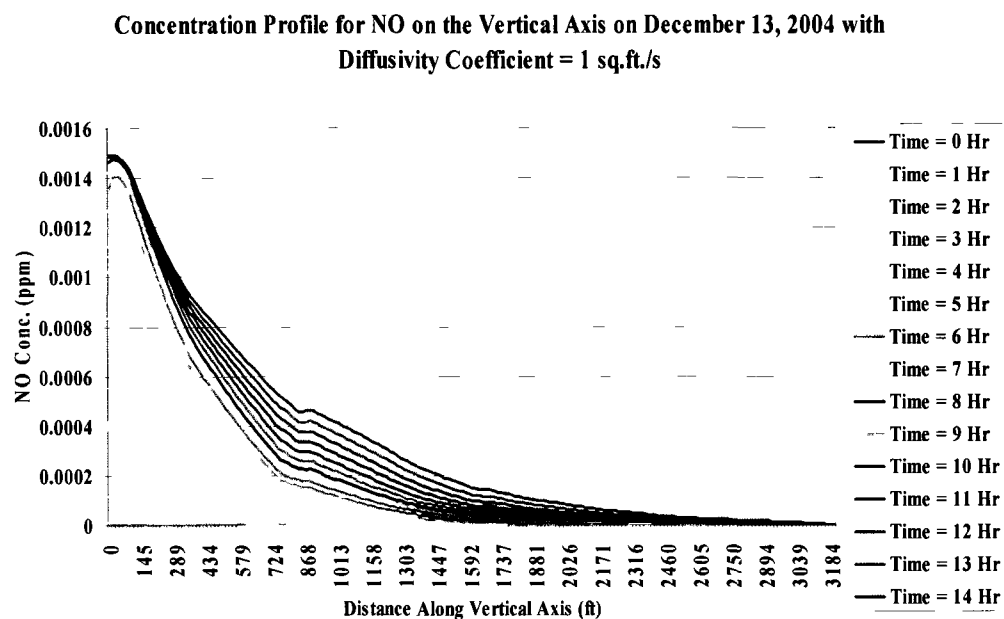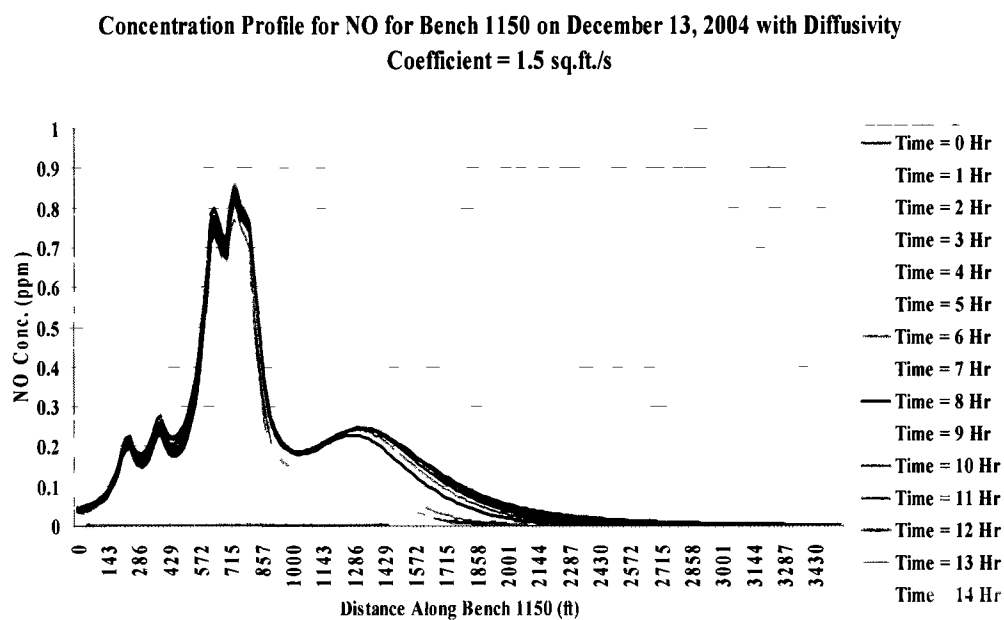Coefficient 0.5 ft^2/s

Concentration Profile for NO for Bench 1150 on December 13, 2004 with Diffusivity
Coefficient = 1 sq.ft/s

Figure 6.26: Concentration Profile for NO Along Bench 1150 (Diffusivity Coefficient
$1.0 \text{ ft}^2/\text{s}$)

Concentration Profile for NO on the Vertical Axis on December 13, 2004 with
Diffusivity Coefficient = 1 sq.ft./s

Figure 6.27: Concentration Profile for NO Along the Vertical Axis (Diffusivity
Coefficient $1.0 \text{ ft}^2/\text{s}$)

Figure 6.28: Concentration Profile for NO Along Bench 1150 (Diffusivity Coefficient 1.5 ft^2/s)

Concentration Profile for NO on the Vertical Axis on December 13, 2004 with Diffusivity Coefficient = 1.5 sq.ft./s
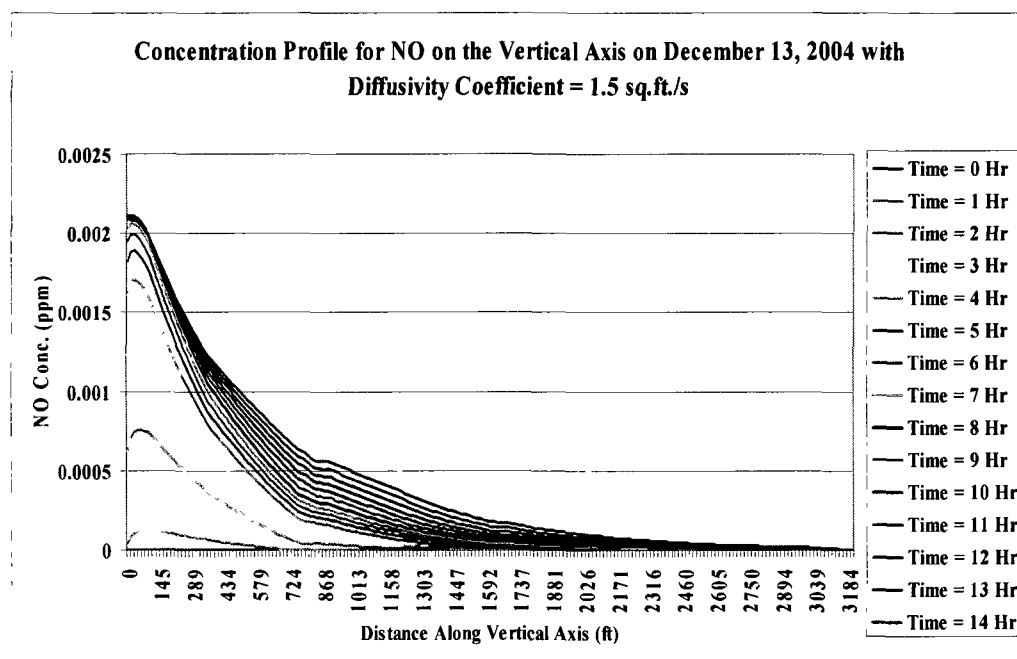
Figure 6.29: Concentration Profile for NO Along the Vertical Axis (Diffusivity Coefficient1.5 ft^2/s)

In the above figures (6.24 – 6.29), it can be observed that, in general, an increase in the diffusivity coefficient decreases the peak values registered for the horizontal (1.5 ppm in figure 6.23). The amount of pollutants in the pit is shown to decrease with increasing diffusivity This can be seen from the following figure (6.30).
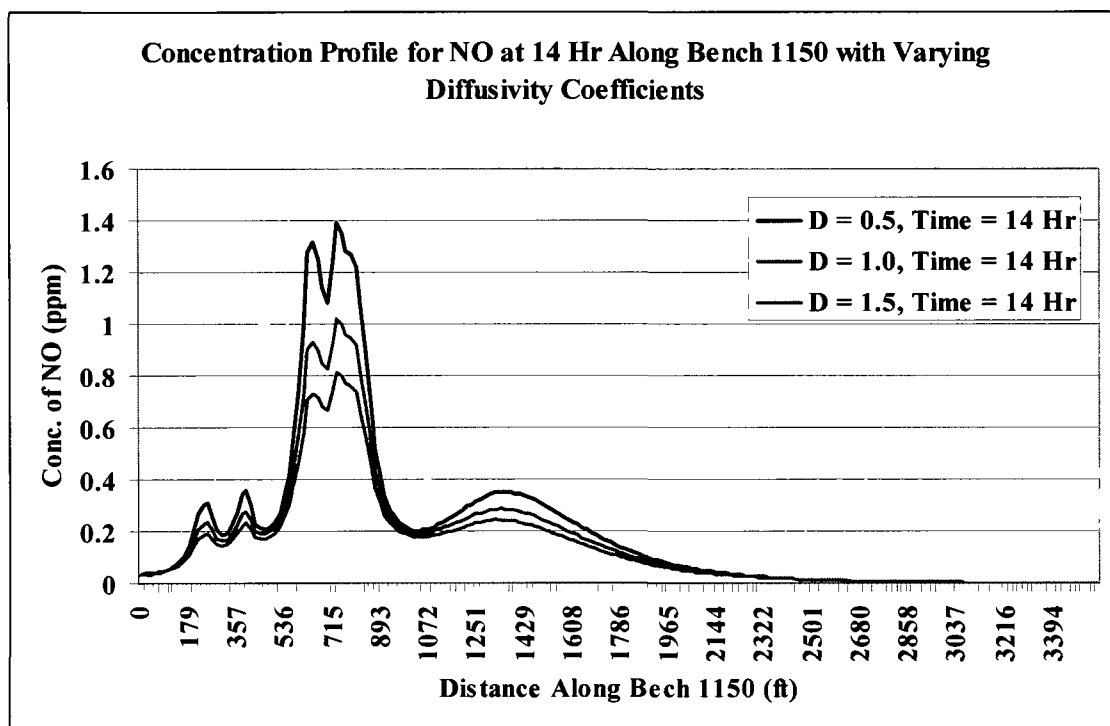
Figure 6.30: Concentration Profile for NO at 14 Hr Along Bench 1150 with Varying Diffusivity Coefficients.

The diffusivity coefficient is a measure of the rate of transmission of mass from one point in the model space to another, following the concentration gradient. A larger value of the coefficient necessitates that the pollutant mass is propelled faster, resulting in more pollutants moving outward from the sources. As these pollutants gain distance from the sources, they are picked up by the advection current, and are thoroughly mixed or are transported out of the pit. This results in less pollutants retention, thus reducing the concentration.

However, the vertical axis shows the opposite trend. For a diffusivity coefficient of 0.5 ft/s^2 (figure 6.24) the peak concentration value near the pit bottom was 0.0009 ppm, increasing to 0.0015 ppm for a diffusivity coefficient of 1 ft/s^2, and to 0.02 ppm for a diffusivity coefficient of 1.5 ft/s^2. This is because a larger diffusivity coefficient transports more pollutants from the sources to the center of the pit, where the vertical axis is located. It can also be observed that the pollutants profiles in the figures 6.25,

6.27 and 6.29 gradually coincide. This is due to the increase in the rate of mass transfer with increasing diffusivity. As more mass is projected outward by the higher diffusivity coefficient, the difference between the quantity of pollutants at a point decreases, thus causing the concentration profiles to coincide.

6.6. Effect of Changing Overall Slope Angle on Transport and Distribution of Contaminants

The following three slope angles were selected to examine the effect of the overall pit slope.

- 40°

- 43°

- 45°

The following figures (6.31 – 6.36) shown the concentration profiles at the selected locations.
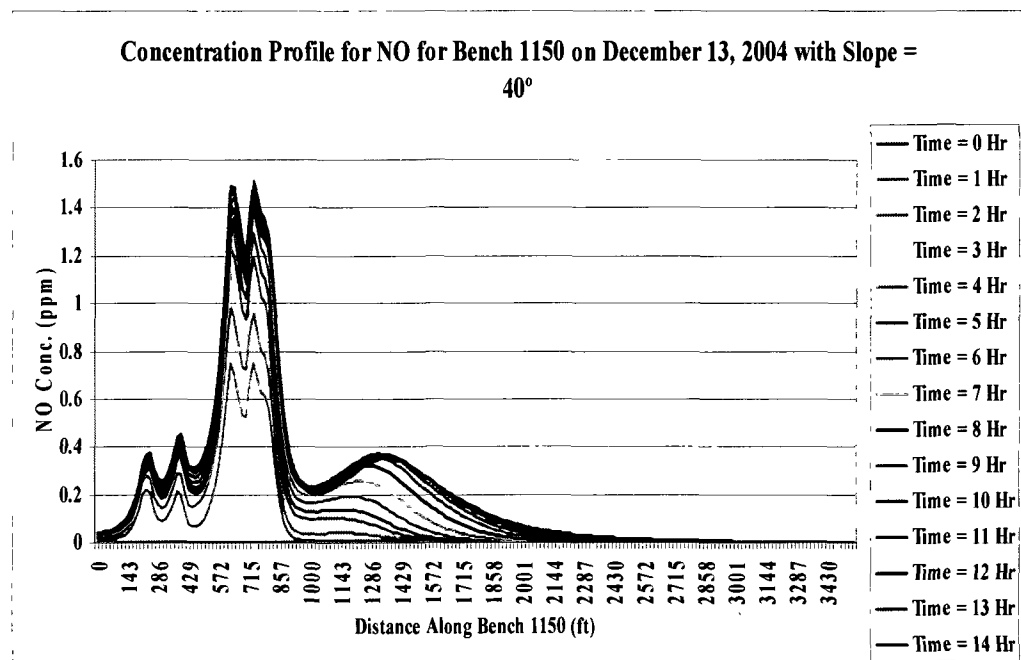

Figure 6.31: Concentration Profile for NO Along Bench 1150 with Slope Angle as 40°
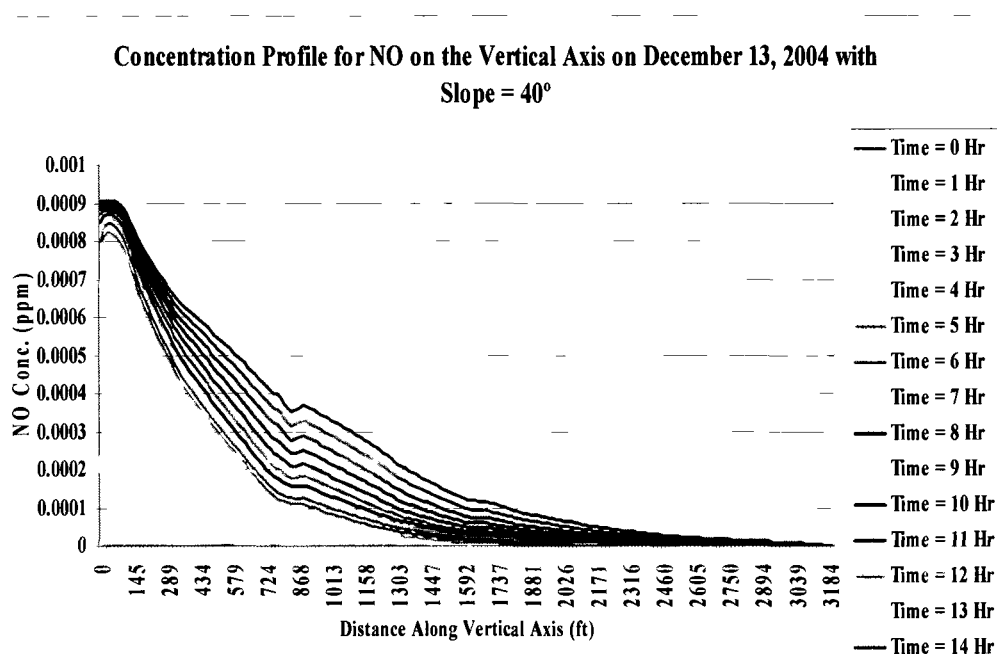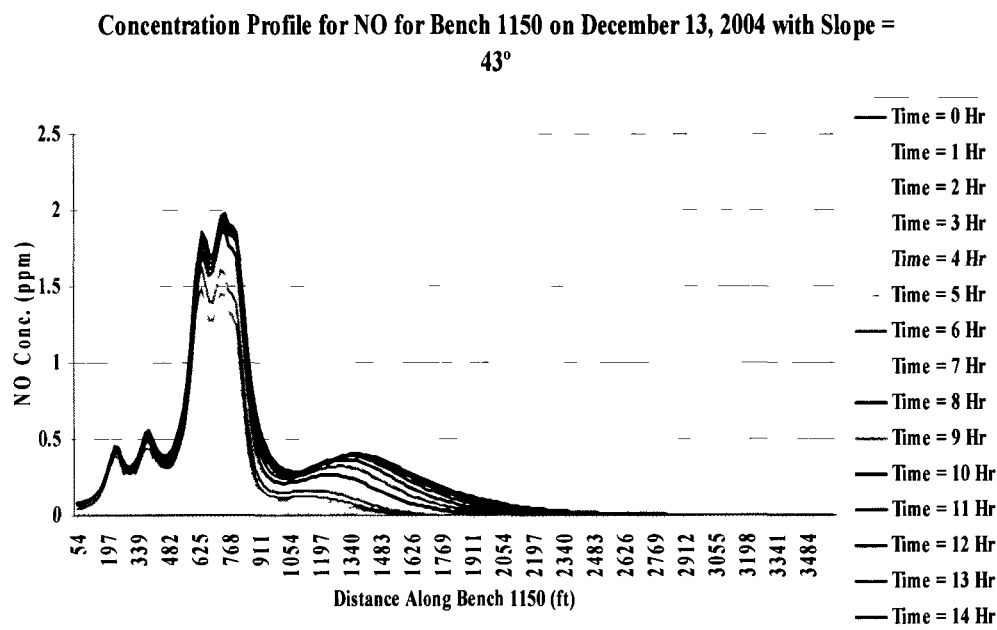
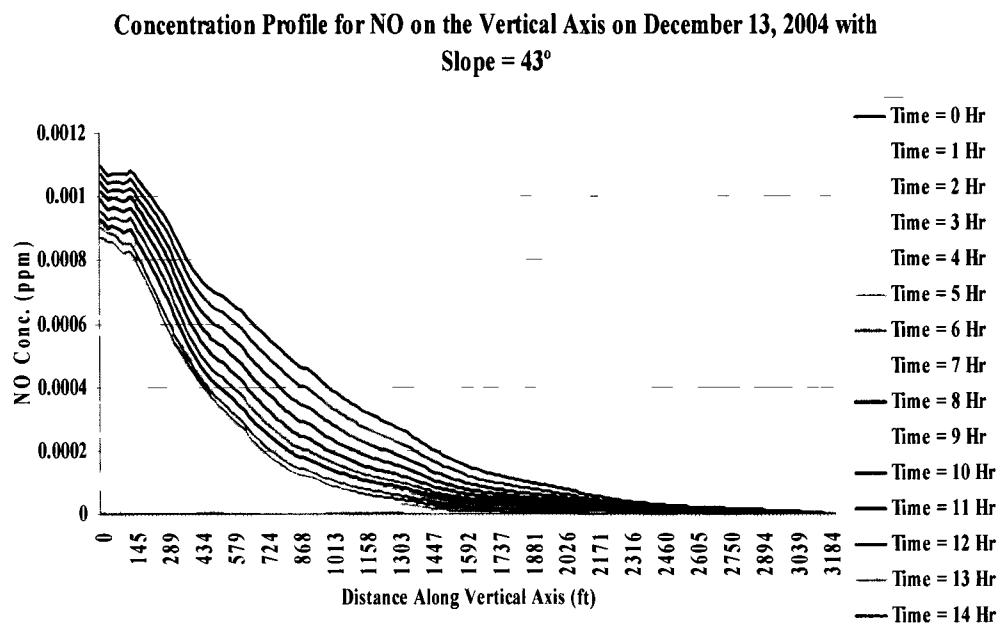**Concentration Profile for NO on the Vertical Axis on December 13, 2004 with Slope = 40°**

Figure 6.32: Concentration Profile for NO Along the Vertical Axis with Slope Angle as 40°

Concentration Profile for NO for Bench 1150 on December 13, 2004 with Slope = 43°

Figure 6.33: Concentration Profile for NO Along Bench 1150 with Slope Angle as 43°

Concentration Profile for NO on the Vertical Axis on December 13, 2004 with Slope = 43°

Figure 6.34: Concentration Profile for NO Along the Vertical Axis with Slope Angle as 43°

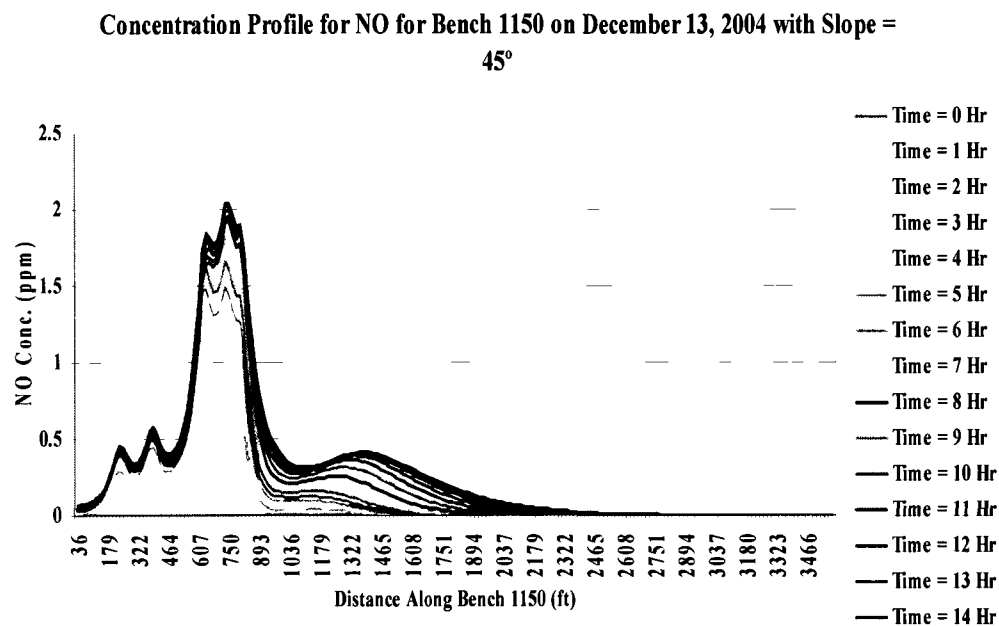**Concentration Profile for NO for Bench 1150 on December 13, 2004 with Slope = 45°**

Figure 6.35: Concentration Profile for NO Along Bench 1150 with Slope Angle as 45°
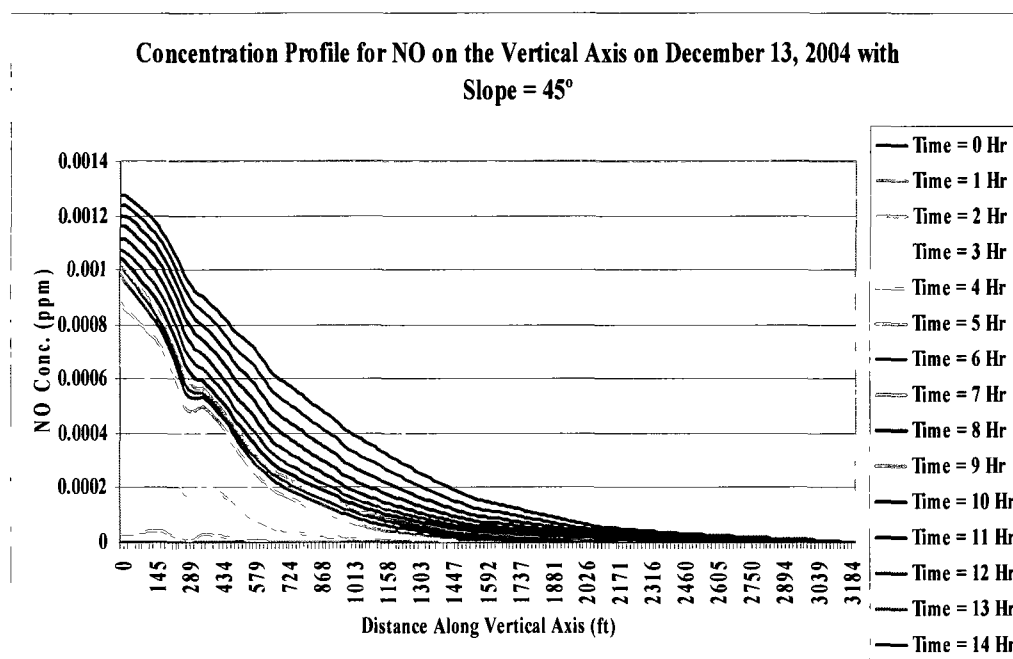
Figure 6.36: Concentration Profile for NO Along the Vertical Axis with Slope Angle as 45°

In figures 6.31 – 6.36, it can be observed that the peak pollutant concentration increases with increasing overall slope angle. This is expected, as the slope angle determines the geometry of the pit to a large extent. A narrower pit (steeper slope angles) has a tendency to impede the movement of air and retain pollutants. A comparison of figures 6.31 and 6.33 (increasing pit slope angle from 40° to 43°) shows a significant increase in the peak concentration of the pollutant along the longitudinal axis along bench 1150 (from about 1.5 ppm to 2 ppm). Any increase is, however, not noted in figure 6.35 (peak value approx. 2 ppm slope angle 45°). This may be due to increased re-circulation within the pit, which results from steeper slopes and a better mixing of pollutants.

For the vertical line at the mid-section of the pit (figures 6.33, 6.34 and 6.36), the trend continues with increasing slope angle. Furthermore, the temporary, localized drop in concentration, as explained earlier, is present for all the slope angles. It can, however, be seen that the altitude at which this mixing seems to occurs changes with the slope

angle. Figure 6.34 shows that at a slope angle of 43°, the concentration drop (indicative of turbulence and mixing) is at an approximate altitude of 150 ft from the pit bottom (its lowest altitude among all the variations). For an increased slope angle of 45°, the concentration drop occurs at an approximate altitude of 290 ft from the pit bottom (figure 6.34). For a slope angle of 40°, the height at which the drop in concentration occurs is approximately 750 ft. From this it may be concluded that the height of turbulence eddies may not decrease uniformly with the increase of slope angle, and there may be an optimum slope angle at which the least mixing of pit air occurs. Beyond that slope angle, mixing may be a result of turbulence. Although the pollutants may not escape from the pit, there is a more uniform distribution of pollutants along the vertical axis of the pit. The elevation of the turbulence zone for the steeper pit slope angle of 45° conforms to previous results.

6.7. Effect of Changing Geometry on Transport and Distribution of Contaminants

In order to investigate the effect of geometry on the transport and distribution of gaseous pollutants in the open-pit, the 2009 – 2010 geometry of the mine was selected. The pit has extended over a much larger area and depth since 2004 – 2005. The initial model was developed and validated with the 2004 – 2005 pit geometry. The geometry of the 2010 pit is shown in the figures 6.37 through 6.39.
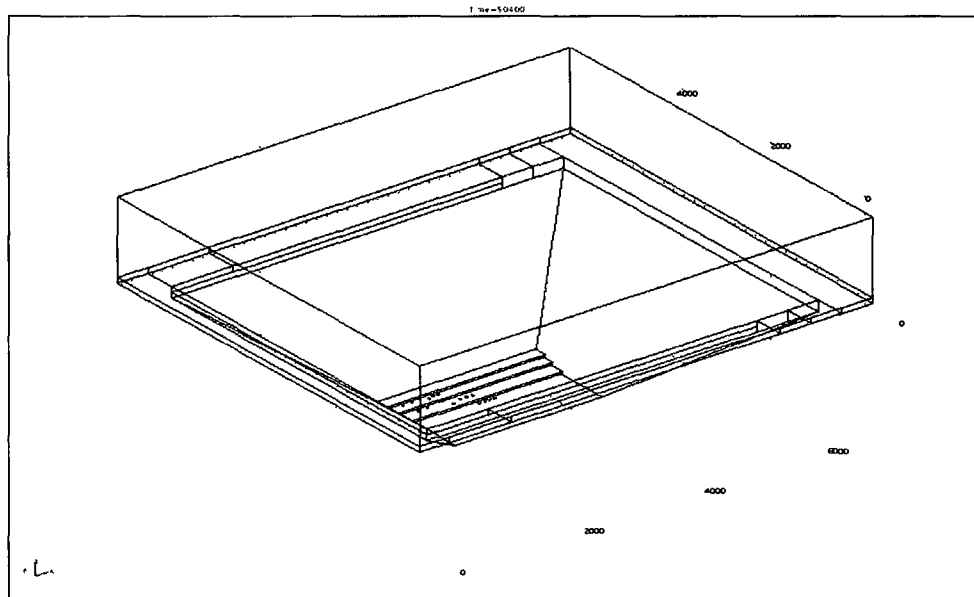
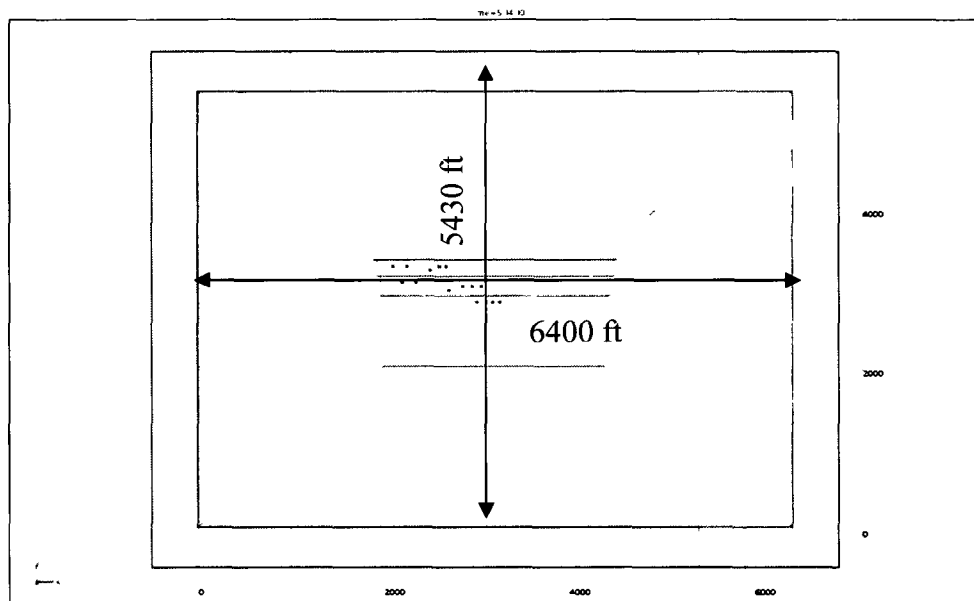Figure 6.37: Isometric View of the 2010 Pit in COMSOL®

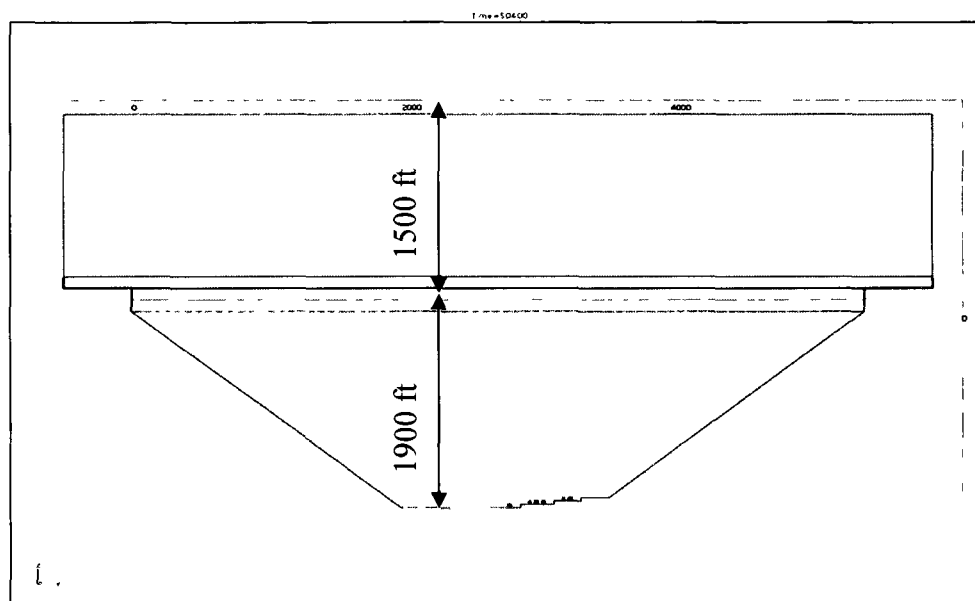Figure 6.38: Plan View of the 2010 Pit in COMSOL® with Dimensions

Figure 6.39: Profile View of the 2010 Pit in COMSOL® with Dimensions

The 2010 pit maintains the same relative proportions as that of the 2004-2005 pit described earlier. The 2010 pit is 6400 ft long at the pit-rim compared to 5280 ft for the 2004-2005 pit, is 5430 ft wide at the rim as opposed to 3960 ft for the 2004-2005 pit, and is 1900 ft deep from the pit-rim to the pit-bottom as opposed to 1500 ft for the 2005-2005 pit. The placement of the working equipment in the pit, which are also the source of the gaseous pollutants, is similar to the 2004-2005 pit. One shovel and three trucks are placed on the pit floor; one drill, one ANFO truck, one shovel and three trucks were placed on the bench above the floor; one drill, one ANFO truck, one shovel and two trucks were placed on the bench above the first bench above the floor. The following figures (6.40 and 6.45) indicate the positions of the hypothetical axes along which the concentration profiles for the pollutants have been reported. Figures 6.40 to 6.45 show the influence of geometry on the concentration profiles of gaseous pollutants in the 2010 pit.
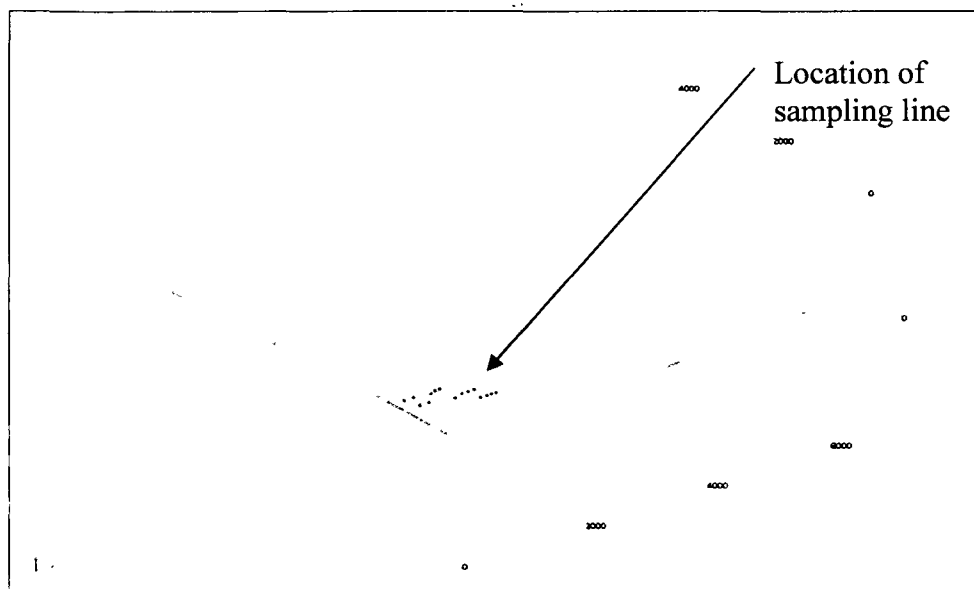
Figure 6.40: Location of the Sampling Line Along the Second Bench from Pit-Bottom
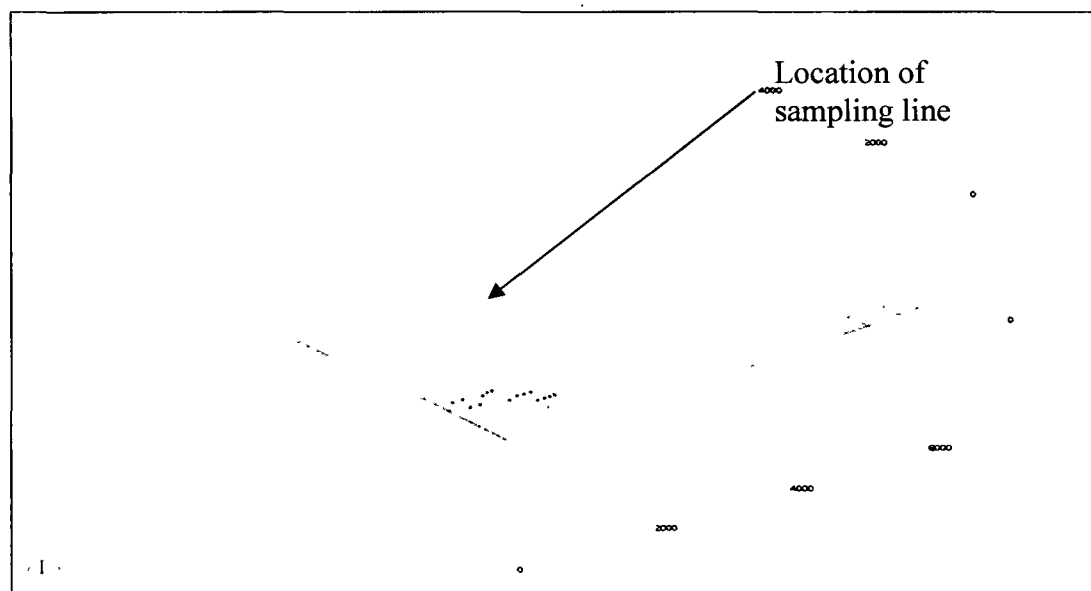

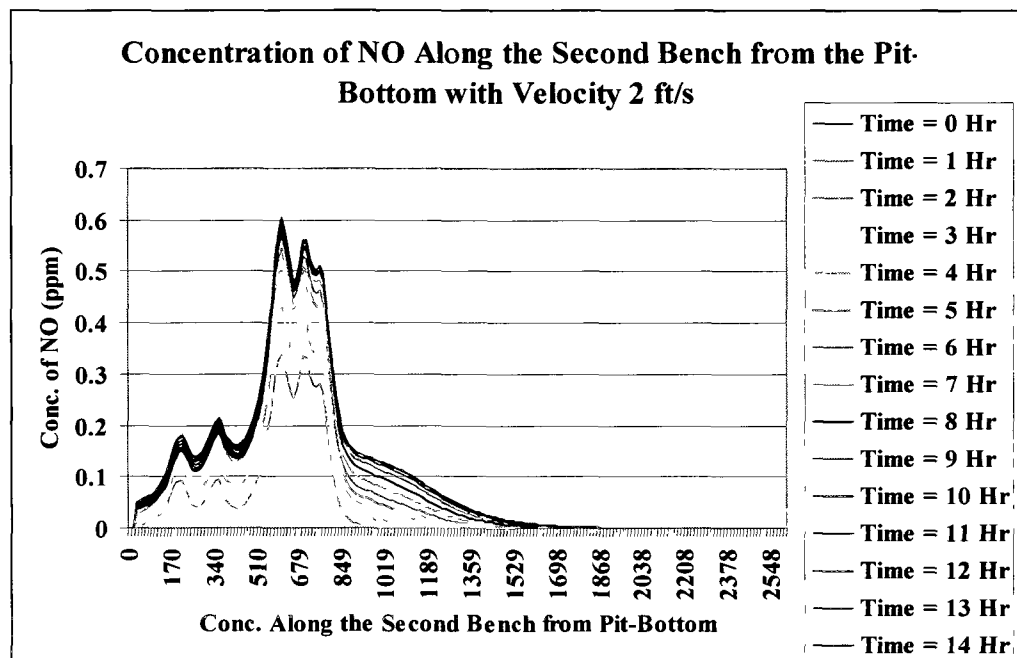Figure 6.41: Location of the Sampling Line Along the Vertical Axis

Figure 6.42: Concentration Profile for NO Along the Second Bench from the Pit-Bottom (Velocity 2 ft/s)
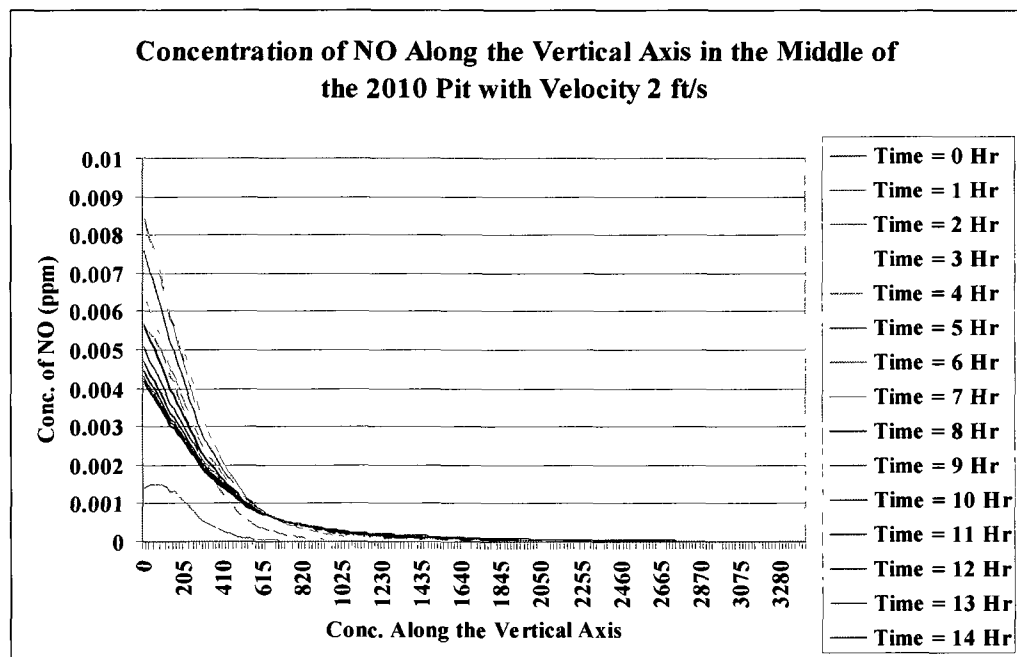

Figure 6.43: Concentration Profile for NO Along the Vertical Axis for the 2010 Pit (Velocity 2 ft/s)

Figure 6.44: Concentration Profile for NO Along the Second Bench from the Pit-Bottom (Velocity 3 ft/s)

Concentration of NO Along the Vertical Axis in the Middle of the 2010 Pit with Velocity 3 ft/s

Figure 6.45: Concentration Profile for NO Along the Vertical Axis for the 2010 Pit (Velocity 3 ft/s)
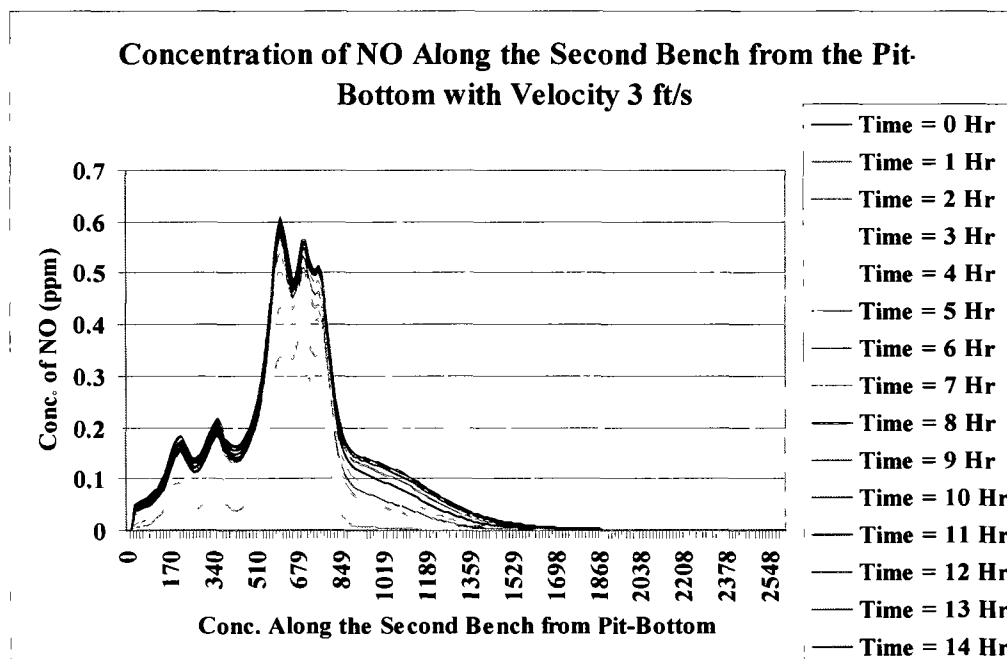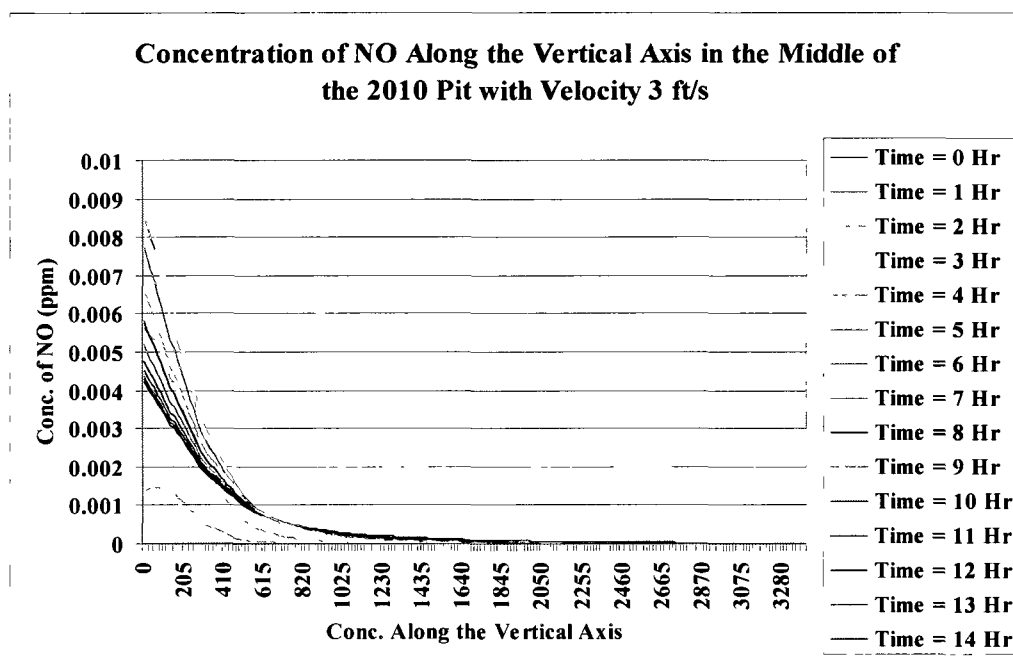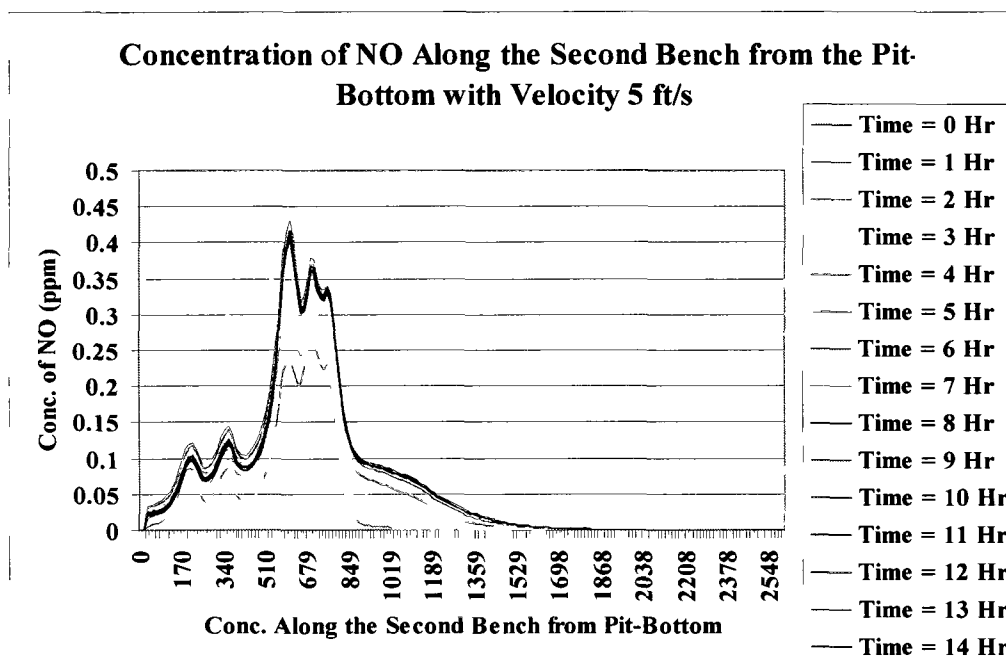
Figure 6.46: Concentration Profile for NO Along the Second Bench from the Pit-Bottom (Velocity 5 ft/s)

Concentration of NO Along the Vertical Axis in the Middle of the 2010 Pit with Velocity 5 ft/s
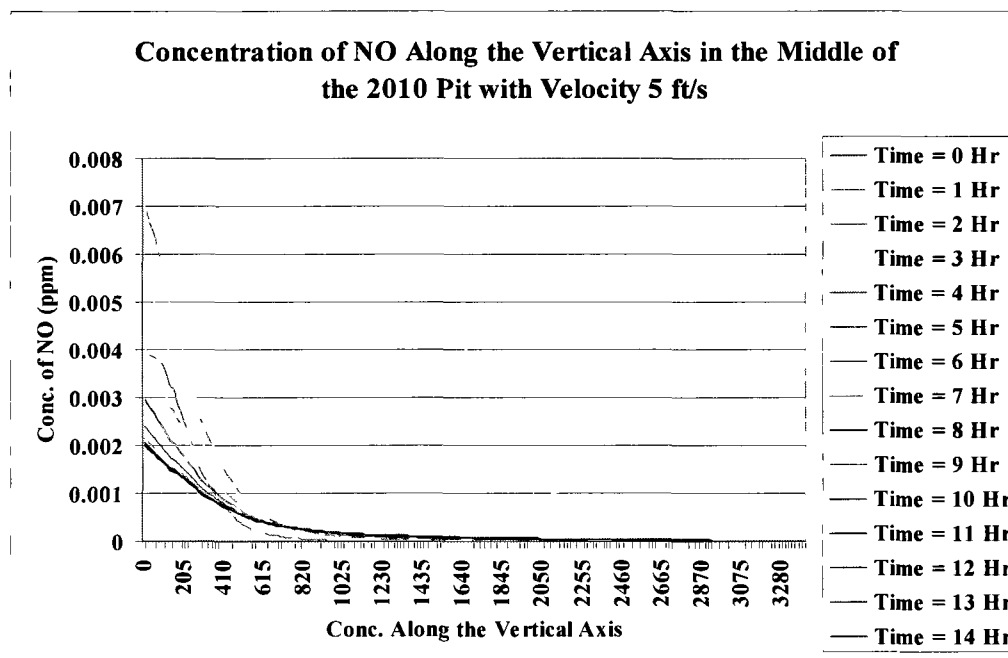

Figure 6.47: Concentration Profile for NO Along the Vertical Axis for the 2010 Pit (Velocity 5 ft/s)

Figures 6.40 to 6.45 show that the open pit geometry has significant influence on the concentration of pollutants. In these figures, it can be seen that the peak values for the concentrations profiles along the second bench from the floor are lower (0.6 ppm) than those for the pit designed according to the 2004-2005 pit geometry (1.9 ppm). This seems counterintuitive, but can be explained as follows.

The 2010 pit is significantly larger than the pit designed according to the 2004-2005 geometry, which means that the 2010 pit has a much larger volume of air in the model space. The models are run for the same length of time, and the pollutant sources emit the noxious gases at the same rate in both models. This releases the same quantity of pollutants into both models spaces, but the gases released into the 2010 model space have a much larger volume of air to be diluted in, thus reducing the effective concentration. Due to this initial bias, the peak concentrations in the 2010 pit are lower than in the earlier case. However, with careful examination it is found that the 2010

pit, due to its larger and deeper geometry, retains much more of the pollutants than the 2004-2005 pit.

The effect of velocity on the 2004-2005 pit is presented in figures 6.4 to 6.9. As seen from these figures, the peak concentration along the horizontal axis for the velocity of 2 ft/s is approximately 1.9 ppm, that for the velocity of 3 ft/s is approximately 1.5 ppm and that for the velocity of 5 ft/s is approximately 1.1 ppm. This shows a considerable removal of pollutants with increasing velocity. The same influent velocities were selected for the larger 2010 pit, and have produced markedly different results. It can be noted from the figures 6.41 and 6.43 that the increase of the influent velocity from 2 ft/s to 3 ft/s did not show significant changes in the peak concentrations or the concentration profiles along the horizontal axis, keeping it at around 0.6 ppm. An increase of influent velocity to 5 ft/s reduces the peak concentration marginally to 0.42 ppm. This indicates some improvement but is by no means a significant drop. Thus it can be seen that the same variation in influent velocity, which produces a significant effect on concentration profiles in the 2004-2005 pit, has virtually no effect on the pollutant concentrations in the 2010 pit. From this fact it can be concluded that the 2010 pit clearly retains a much higher amount of the pollutants.

Figures 6.42, 6.44 and 6.46 present the effects of velocity on the pollutant concentration profiles along the vertical axis for the 2010 pit. As expected, it can be clearly seen that the concentration drops with increasing velocity, but again, the drop is miniscule for a change of velocity from 2 ft/s to 3 ft/s, and only slightly more for a velocity of 5 ft/s. This confirms that the deeper and larger geometry is an impediment to removal of pollutants in the field. But the effect of increasing velocity can be seen to be clearly reflected in the time at which the peak concentration along the vertical axis is reached. For the velocities of 2 ft/s and 3 ft/s, the peak concentration is reached four hours of model time, while for the velocity of 5 ft/s, the peak concentration is reached after two hours of model time. This is because the faster influent velocity

removes more pollutants from the model space sooner, thus reducing the peak concentration and the length of time after which such a peak is attained.

6.8. Summary

- It can be seen from the results presented in this chapter that influent velocity has a significant influence on the pollutant concentration in the pit. In general, higher influent velocities remove more pollutants from the pit, thus reducing its concentration. Presence of a gust reduces the peak concentration of the pollutants in the pit. A gust wind also increases the turbulent mixing of the pollutants. As turbulence in the pit air occurs mainly along the vertical axis, the gust wind velocity also tends to spread the concentration of pollutants more evenly along the vertical axis. For pollutant removal, this means that the leeward updraft will bring more pollutants to the rim of the pit but the windward downdraft will take more pollutant back to the pit bottom.

- The effect of temperature on the removal of pollutants in the pit is negligible This is a natural consequence of the assumption of incompressibility in the Navier-Stokes subroutine. Field observations support the fact that temperature aids in removing the inversion cap, thus helping remove pollutants. These models, however, did not show significant changes.

- An increase in the diffusivity coefficient has a positive effect on the removal of pollutants from the pit. Since the diffusivity coefficient is a measure of the transfer of mass along the concentration gradient, a higher diffusivity coefficient transfers more mass throughout the model space, thus carrying it from the source to an altitude where convection removes the mass from the model space.

- The effect of pit slope on the removal of pollutants is more complicated. The results indicate that while, in general, a lower pit slope facilitates the removal of pollutants from the pit, an increasing pit slope may not increase the

concentration of pollutants in the pit monotonically. An increasing pit slope also restricts the geometry of the flow regime, thus increasing turbulence in the pit air. Such turbulence often results in better mixing of pollutants in the pit, thus reducing the concentration toward the pit bottom.

- A substantial change in pit geometry shows a significant effect on the concentration of pollutants in the pit. In general, a larger and a deeper pit has a tendency to retain much of the pollutants generated inside the pit, thus increasing the concentration. A larger and deeper pit may also restrict the movement of air, reducing the effective depth up to which the pollutants may be removed purely by advection, thus increasing the pollutant level in the pit.

CHAPTER VII: Summary, Conclusions and Future Work

7.1. Summary and Conclusions

Ventilation of open pit mines under air inversion is a complex physical process. A number of natural phenomena contribute to the flow of air and transport of pollutants in an open pit. A comprehensive study of open pit ventilation encompasses many fields such as meteorology, pit geometry, solar radiation, exhaust gas potential of the working equipment, air temperature profile in the mine and close atmospheric monitoring in the mine pit.

The research, presented in this dissertation, demonstrates the possibilities of CFD techniques in solving ventilation problems in open pit mines. This research examined the transport and distribution of gaseous pollutants in open-pit mines in the arctic and sub-arctic regions under air inversion. Idealized models of two-dimensional (2D) and three-dimensional (3D) models were developed to study the velocity regimes and the pollutant concentration profiles in an open pit mines. Eulerian dispersion techniques were used in the model to simulate the transport of contaminants in an open pit under air inversion.

Most of the prior research in open pit ventilation assumed the flow regime in an open pit mine to be turbulent. This research departs from that assumption. No prior assumption is made regarding the flow characteristics of the model. Consequently the flow can be turbulent, quasi-turbulent or laminar, depending on the physics of the flow conditions.

The 2D model was used primarily to understand the complexities of the system and to characterize the important variables and parameters in the model. The simpler geometry of the 2D model allowed the model to converge quickly. The model results indicated that velocity, temperature, diffusivity coefficient and slope angle are important parameters for the problem. While the importance of temperature was not evident in the model as a natural consequence of the incompressibility assumption in the Navier-Stokes governing equations, velocity was found to be a key factor that

influenced the movement of the pollutants in the pit. Increasing velocity removed more pollutants from the mine pit. It was observed that some of the air entering the model space flowed back towards the origin of the flow. This phenomenon is termed as backflow, and is regarded as an important characteristic of the flow regime. Presence of backflow suggested that not only the air, but the gaseous pollutants transported by the air by advection also would flow back toward the origin of the flow. It was observed that influent velocity had a significant effect on the concentration distribution or transport of pollutants in the pit. Higher velocities transported more pollutants out of the open pit.

Though the variation of temperature did not indicate any significant effect on the pollutants, the lack of variation might be explained by the fact that the heat supplied here might not be enough to lift the inversion cap. The constant air density assumed for the model space might also neutralize temperature effects.

The backflow in the model resulted from the fact that air flow was not restricted to only turbulent flow. Presence of backflow might appear to be a logical mode of flow in deep open-pit mines in arctic regions.

The flow regime was laminar at the origin, but as the flow progressed toward the center of the pit, the influent air, in its attempt to displace the in-situ colder, heavier air, took the path of least resistance and lost its laminar character. This did not, however, mean that the flow automatically became turbulent. The flow became quasi-turbulent, and generated local eddies towards the pit bottom. The total energy of the quasi-laminar flow as well as the small local eddies was not sufficient to lift the inversion cap that settled on the mine profile, but both the quasi-turbulent flow and the local eddies did remove some pollutant mass from the pit bottom, either due to turbulent mixing, or due to advection.

An idealized 3D model was developed based on an existing open pit mine. Although the geometry of the model did not conform exactly to the actual pit profile, the scale of the model and the dimensions closely resembled the existing pit.

The 3D model was validated using data collected from the selected open-pit mine. The validation exercise proved that the model, simulated the exchanges of mass and energy in an in-situ arctic open-pit mine with reasonable accuracy. Influent air velocity, as before, emerged as an important parameter. Increasing velocity decreased the pollutant concentration in the open-pit. A large diffusivity coefficient was also found to be important in transporting pollutants out of the open-pit. Larger pit geometry retained more pollutants in the pit, while an increasing pit slope angle increased the pollutant concentration in the pit up to a point, and dispersed the pollutants due to turbulent mixing at very high slope angles. The most important conclusion that was drawn from this research was that natural ventilation alone could not remove the pollutants from an open pit or lift the inversion cap.

7.2. Future Work

While the 3D model is closely representative of reality, there is scope for further improvement in the model. Due to the fact that the actual pit geometry could not be imported into COMSOL®, the model was not closely representative of the selected open-pit mine geometrically. Thus flow characteristics and peculiarities of the actual mine could not be captured with this model. In the absence of the actual geometry, the model was developed using simple geometric objects like rectangular parallelepipeds and trapezoids. The pollutant sources in the model were represented by cubes. It is thus possible that the model could not be properly scaled to the flow regime.

Weather data collected for the model was from a NOAA station located close to the mine. While the data is accurate and reliable, the topographic difference and the distance between the NOAA station and the actual mine may add some bias to the data. If possible, more reliable weather data has to be collected from the mine site and incorporated into the model.

The assumption of incompressibility for the Navier-Stokes governing equations renders the model unable to detect the variation of pollutant concentrations due to variation in temperature. Air is compressible, and though the depth of the pit and the

temperature variations between the top and the bottom of the pit may not be large enough to effect a significant variations in air density within the pit, lack of compressibility may hurt model sensitivity.

Many of the chemicals in the air in an open pit may react in the presence of sunlight to form compounds entirely different from the original ones. This may be beneficial to pollutant concentration in the pit by reducing pollutant mass, or may add more toxins to the pit air, thus lowering air quality. While most of the air inside the pit may not be exposed to sunlight during the winter months, and even then, cold temperatures may retard the photochemical reactions, Chemical interaction within the pit may have significant effect on pollutant concentration.

The following points may be considered while extending the present work in future.

- Since the 3D model is closely representative of reality, remediation techniques can be modeled using it. There may be several conceivable remediation techniques, including an exhaust fan and duct system, a push-pull ventilation system (in which a forcing and an exhaust fan could be used in tandem), or addition of extra heat near the pit bottom. Some of these techniques may be modeled using the existing or similar 3D models.

- In order to capture the effect of temperature on the pollutant concentration, a compressible flow model should be studied.

- Importing the actual geometry of a selected mine would provide more accurate results, and thus modeling an in-situ pit may be attempted using other Fluid Dynamics software such as Fluent.

References

Allwine, K. J., Bian, X., Whiteman, C. D., Thistle, H. W., 1997, " Valdrift – A Valley Atmospheric Dispersion Model", Journal of Applied Meteorology, 36, 1076-1087.

Aloyan, A.E., Baklanov, A.A., Penenko, V.V., 1982, "Fictitious Regions of Numerical Simulation of Quarry Ventilation", Meteorologiya i Gidrologiya, 7, 42 – 49.

Baklanov, A. A. & Rigina, O. Yu., 1993, "Effectiveness of Cascade Ventilation Systems for Open pit Mines", Soviet Mining Science, 152-157 (In Russian).

Baklanov, A. A., 1984, " Determining the Propagation of Impurity in the atmosphere of a Pit on the Basis of Mathematical Modeling", Soviet Mining Science, 20(5), 402-407.

Bandopadhyay, S & Izaxon, V. Yu., 2005, " Health and Safety Problems in Mining in the Arctic", Proceedings of the 8th. International Symposium on Mining in the Arctic, Melinikov & Reshetnyak (Editors), Mining Institute of the Kola Science Center, Russian Academy of Sciences, 139-156.

Bandopadhyay, S., & Ramani, R.V., 1988(July), "Mass Transfer Problems in Mine Ventilation: Some Solution Strategies", Proceedings of the 4th International Mine Ventilation Congress, A.D.S. Gillies (Ed), The Australian Institute of Mining and Metallurgy, 73-83.

Bandopadhyay, S. & Ramani, R.V., 1984, "Convection-Diffusion Equations in Mine Ventilation Planning", Proceedings of the 3rd International Mine Ventilation Congress, The Institution of Mining and Metallurgy, The Institution of Mining Engineers, England, M.J. Howes and M.J. Jones (Editors), 397- 404.

Bandopadhyay, S. & Ramani, R.V., 1983(October), "Computer-aided Analysis of Exhaust Dispersions in Underground Air- ways", The Canadian Institute of Mining and Metallurgical Bulletin, 76(858), 69-74.

Bandopadhyay, S. & Ramani, R.V., 1985, "Mine Planning with Diesel-Powered Equipment - Ventilation Considerations", Proceedings of the 2nd U.S. Mine Ventilation Symposium, P. Mousset-Jones (Editor), A. A. Balkema Publication, 627-636.

Belousov, V. I., 1985, "Natural Dynamic Ventilation of Open pit Mines", Soviet Mining Science, 21 (3), 264-267.

Belousov, V. I., 1990 (March), " Ventilation of Open pit Mines by Controlling the Boundary Layer of the Wind Stream", Soviet Mining Science, 25(3), 267-270.

Belousov, V. I., 1995(May), "Breeze Circulation in Open Pit Mines", Journal of Mining Science, 31(3), 216-220.

Bowling, S.A., 1986, "Climatology of High-Latitude Air Pollution as Illustrated by Fairbanks and Anchorage, Alaska", Journal of Climate and Applied Meteorology, 25, 22-34.

COMSOL® Multiphysics User Manual, 2007, "COMSOL® 3.4 MODELING"; October,

Dmitriev, M.T. & Shadrin, A.S., 1973(March-April), "Formation of Photochemical Smog in Open Pits", Translated from Fiziko-Technicheskie Problemy Razrabotki Poleznykh Iskopaemykh, 2, 97-100.

Fomin, A.A., 1996, "Modeling of Natural Convection in an Open Pit", Fluid Dynamics, 31(4), 490 – 496.

Hartman, B. & Wendler, G., 2005, "Climatology of the Winter Surface Temperature Inversion in Fairbanks, Alaska", Geophysical Institute, University of Alaska, Fairbanks, AK 99775.

Holty, J.G., 1973(December), "Air Quality in a Sub-arctic Community Fairbanks Alaska", Arctic, 26(4), 292 – 302.

Huai, T., Shah, S.D., Miller, J.W., Younglove, T., Chernich, D.J., Ayala, A., 2006, "Analysis of Heavy-duty Diesel Truck Activity and Emissions Data", Atmospheric Environment, 40, 2333 – 2344.

Ierardi, J. A., 2009, Worcester Polytechnic Institute Internet Archives, (http://users.wpi.edu/~ierardi/PDF/)

Jacob, D.J., 1999, "Introduction to Atmospheric Chemistry", Princeton University Press, 14 – 15.

Meroney, R.N. & Grainger, C., 1992, "Nighttime Flow and Dispersion Over Large Basins or Mining Pits", Measurement and Modeling of Environmental Flows, The American Society of Mechanical Engineers, HTD-232.

National Renewable Energy Laboratories, Golden, Colorado – The Solar Radiation Data Manual for Buildings.

Peng, X. & Lu, G.R., 2005, "Physical Modeling of Natural Wind and its Guide in Large Open Pit Mines", Journal of Wind Engineering and Industrial Aerodynamics, 54-55; 473 – 481.

Reichardt, P.B. & Reidy, S.K., 1980(June), "Atmospheric Polycyclic Aromatic Hydrocarbons: an Aspect of Air Pollution in Fairbanks, Alaska", Arctic, 33(2), 316-325.

Shah, S.D., Cocker, D.R. III, Johnson, K.C., Lee, J.M., Soriano, B.L., Miller, W., 2006, "Emissions of Regulated Pollutants from in-use Diesel Back-up Generator", Atmospheric Environment, 40, 4199 – 4209.

Sharan, M. & Modani, M., 2006, "A Two-dimensional Analytical Model for the Dispersion of Air-pollutants in the Atmosphere with a Capping Inversion", Journal of Atmospheric Environment, 40(3), 3479-3489.

Yong, S., Feng, X. S., Wei, F. S., 2000, "Three-Dimensional Non-hydrostatic Numerical Simulation for the PBL of an Open Pit Mine", Boundary Layer Meteorology, 94, 197-224.

Skobunov, V. V., 1962, "Dissipation of Admixtures from Point Sources", On Air Pollution in Mines—Theory, Hazards, and Control, Academy of Sciences of the USSR Mining Institute.

Tandon, N. & Bhaskar, R., 1998, " Numerical Fluid Modeling for Idealized and Actual Geometry of a Large Open pit Mine", Proceedings of the 91st Annual Meeting and Exhibition of Air and Waste Management Association, San Diego, CA,(98-MA3A-04 (A71)).

TRC Environmental Consultants Inc., 1985, Dispersion of airborne particulates in surface coal mines data analysis; EPA-450/4-85-001; USEPA, NC.

Reed, W.R., 2005, "Significant Dust Dispersion Models for Mining Operations", NIOSH IC 9478, Pittsburgh, P.A..

Winges, K.D., 1990, "Fugitive Dust Model (FDM) User's Guide (Revised)", Vol.1, User's Instructions, US EPA/910/988/202/R,.

www.timeanddate.com – Last accessed June 2010.

APPENDIX
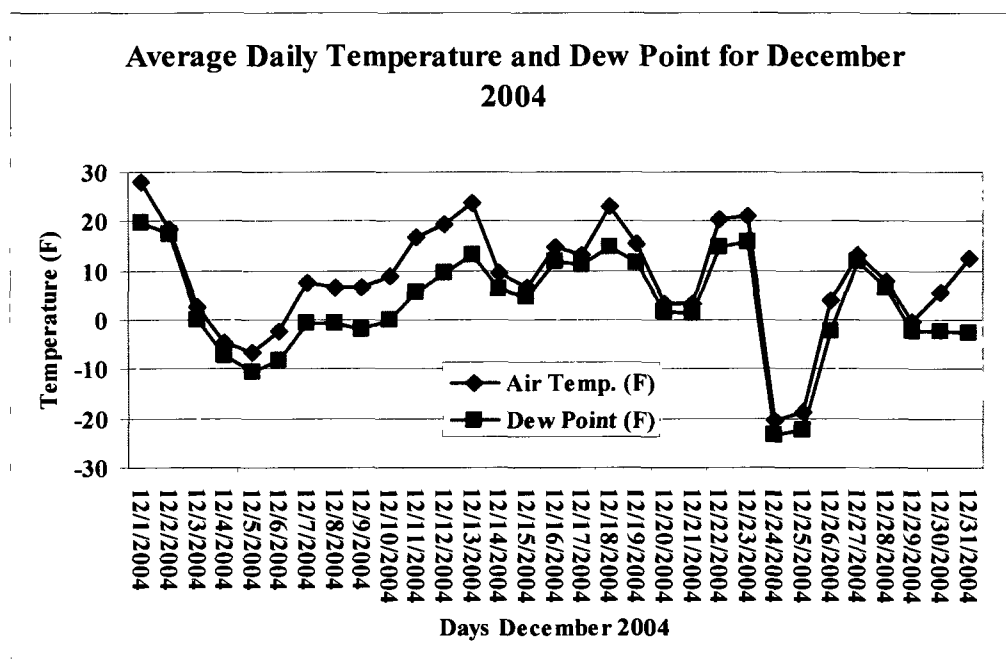
Figure A-1: Average Daily Temperature and Dew Point for December 2004

Average Daily Wind Speed and Gust Wind Speed for December 2004
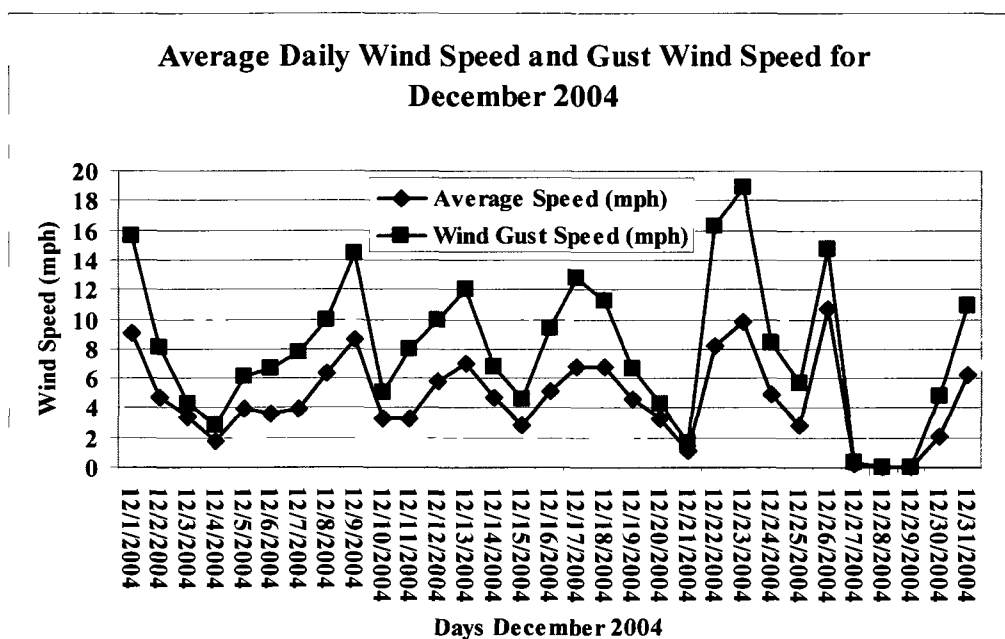
Figure A-2: Average Daily Wind Speed and Gust Wind Speed for December 2004

Average Daily Relative Humidity Percentage for December 2004
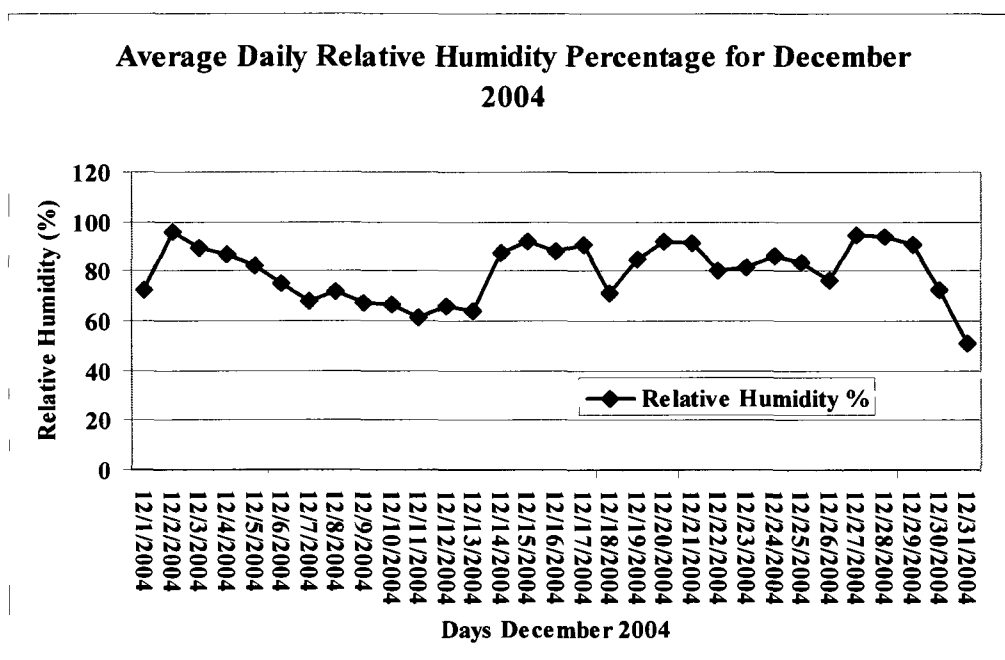
Figure A-3: Average Daily Relative Humidity Percentage for December 2004

Average Daily Pressure for December 2004
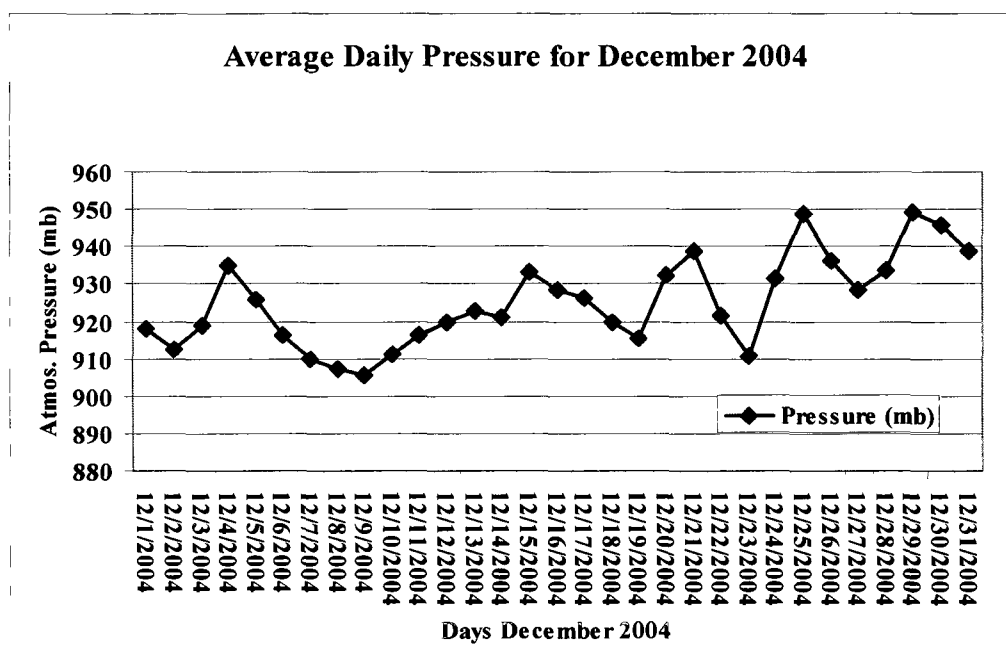
Figure A-4: Average Daily Pressure for December 2004

Histogram for Wind Direction for December 2004
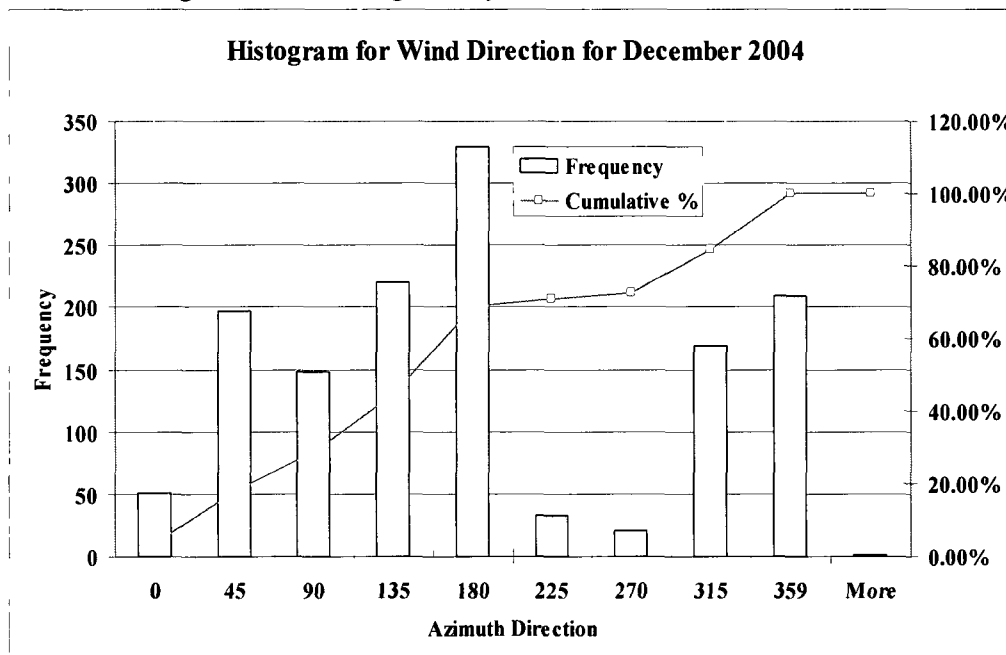
Figure A-5: Histogram of Wind Direction for December 2004

Histogram for Gust Direction for December 2004
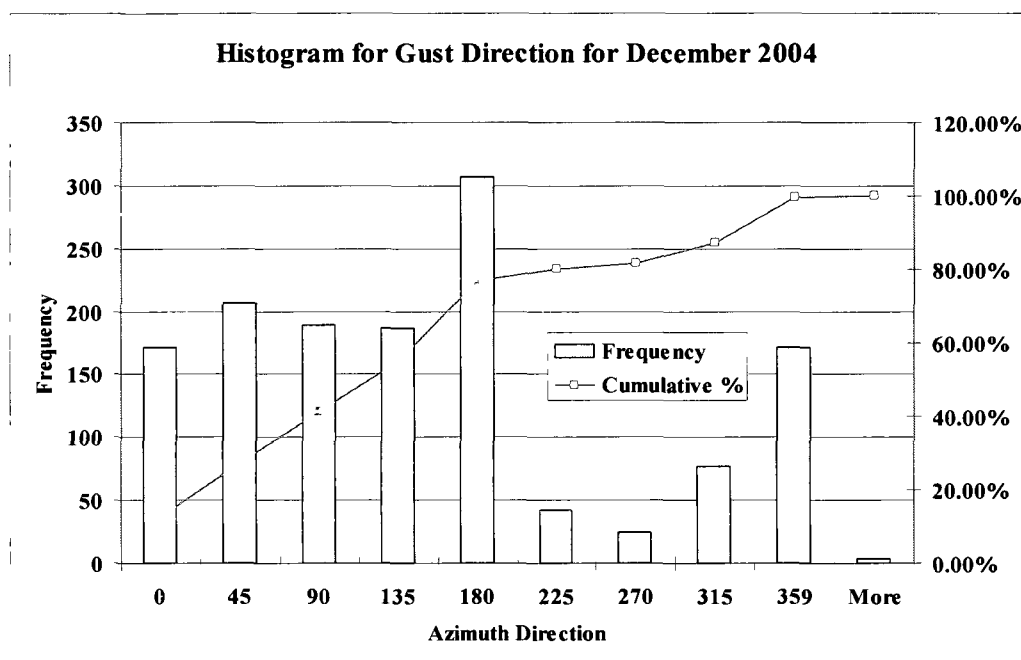
Figure A-6: Histogram of Gust Wind Direction for December 2004

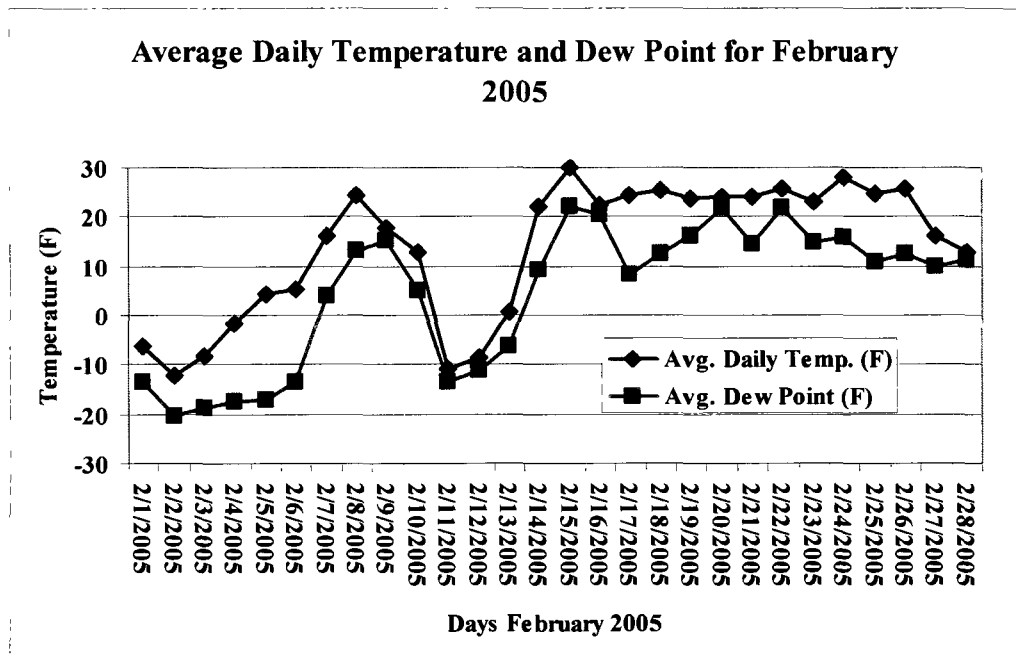**Average Daily Temperature and Dew Point for January 2005**
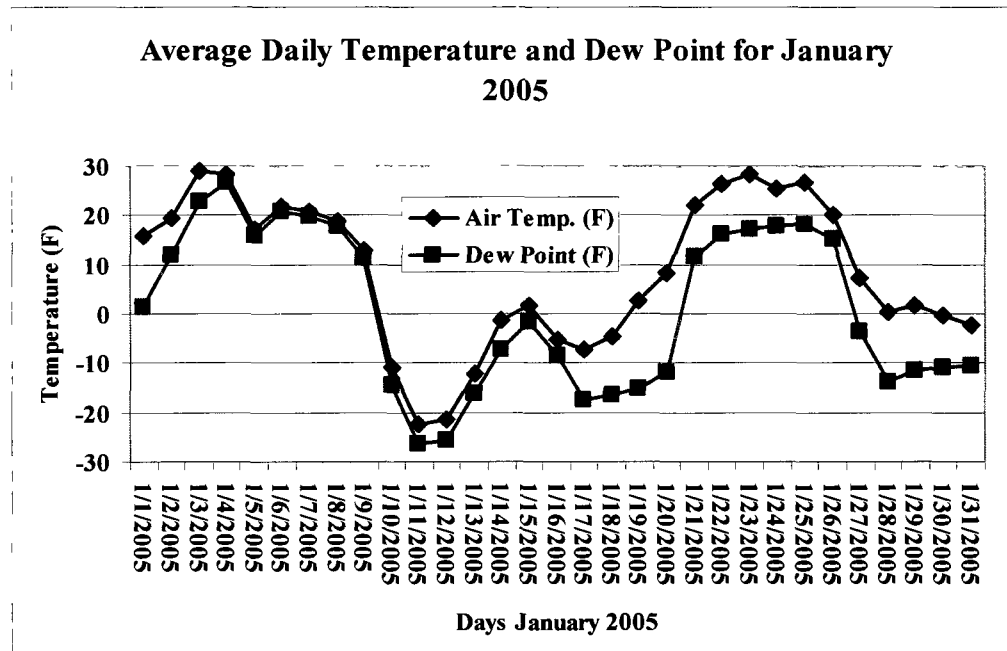
Figure A-7: Average Daily Temperature and Dew Point for January 2005
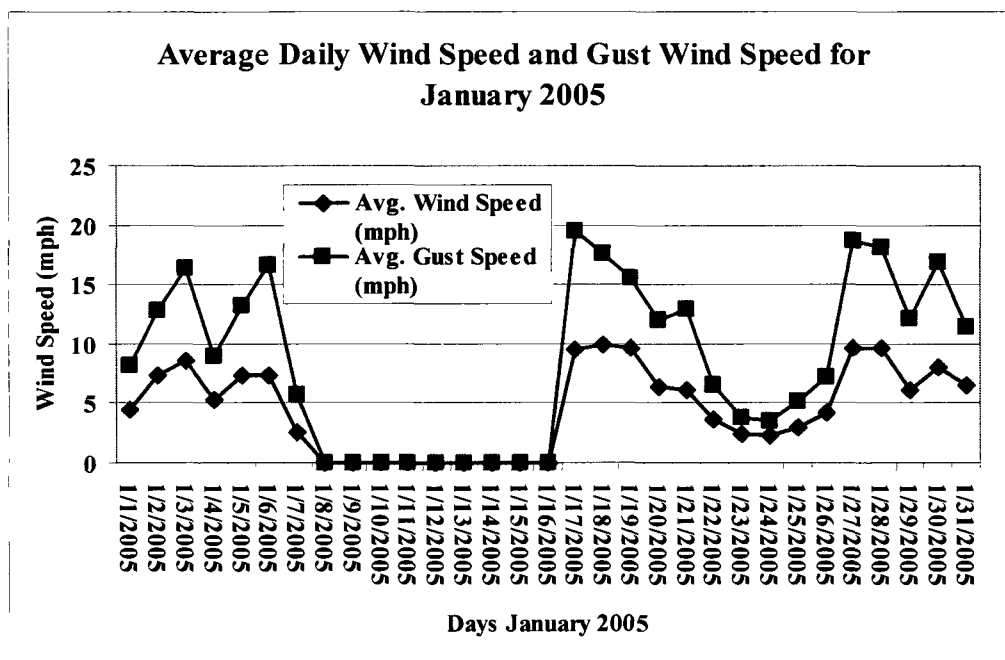
Figure A-8: Average Daily Wind Speed and Gust Wind Speed for January 2005
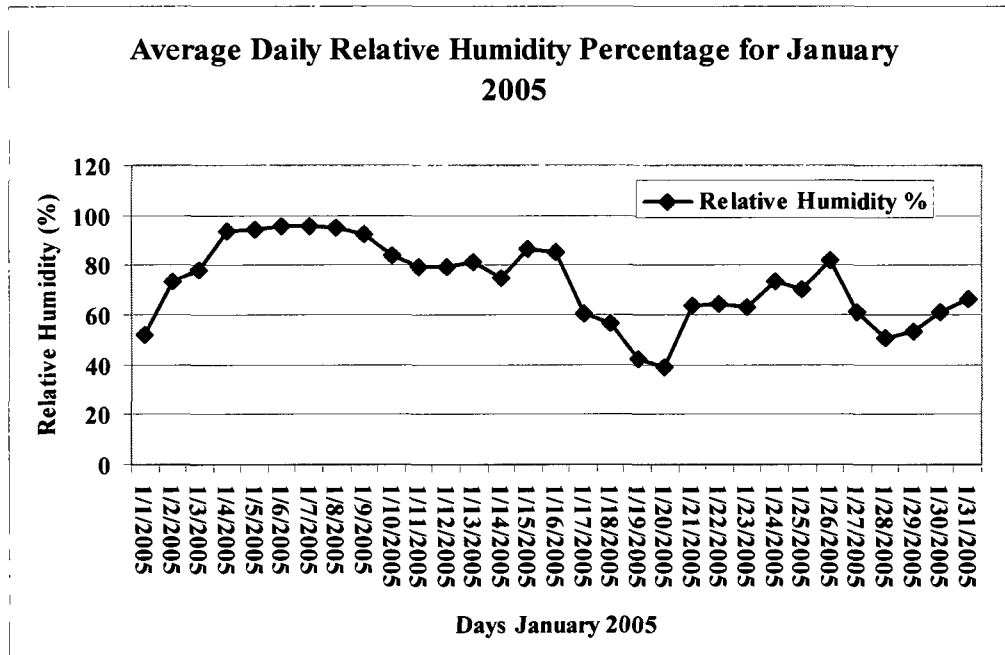
Figure A-9: Average Daily Relative Humidity Percentage for January 2005
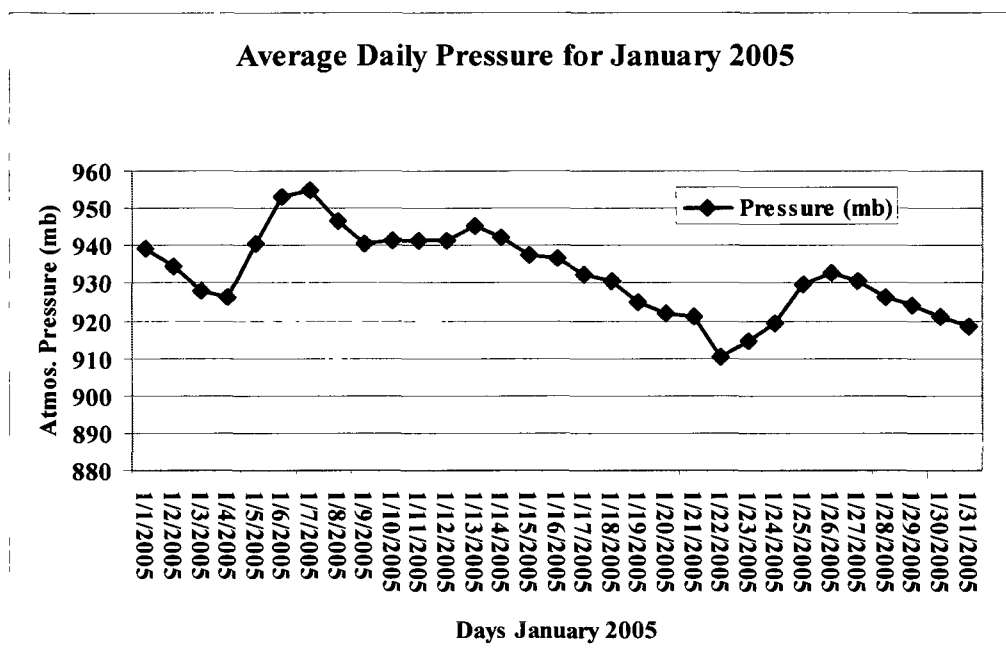
Figure A-10: Average Daily Pressure for January 2005
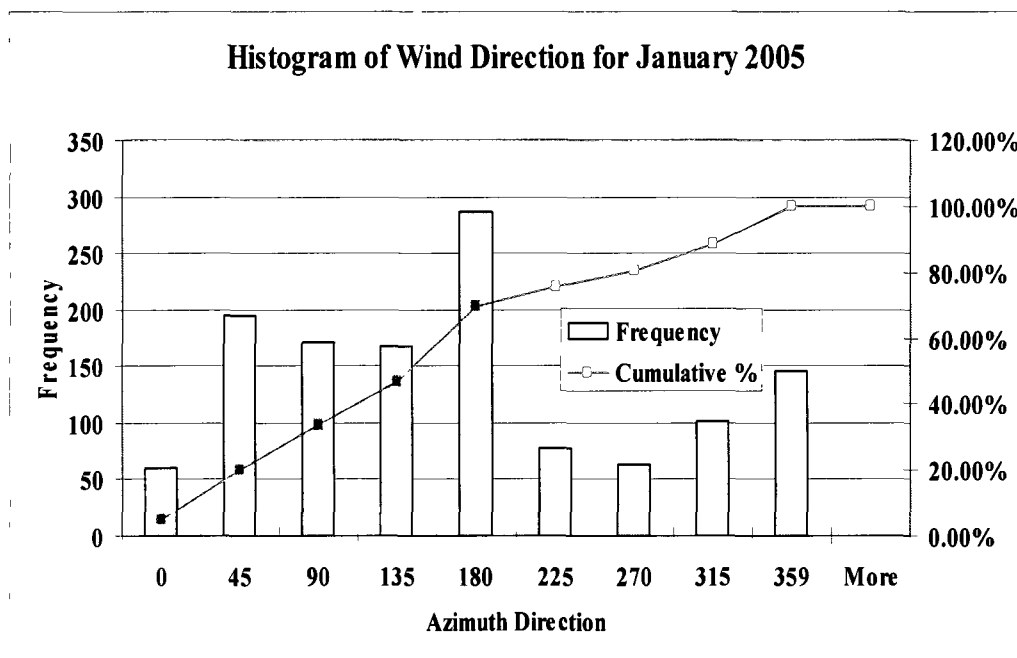
Figure A-11: Histogram of Wind Direction for January 2005
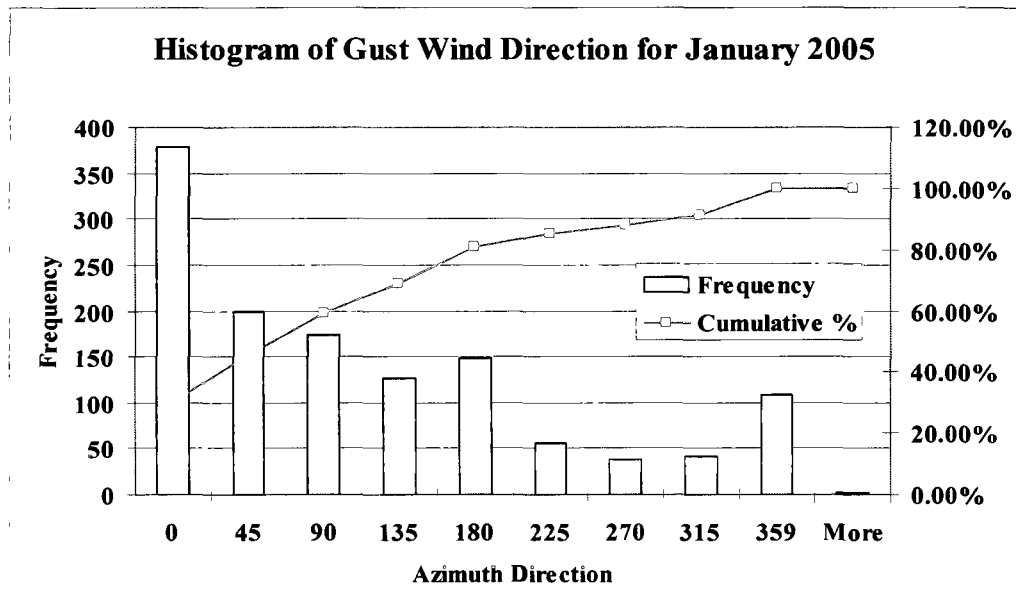
Figure A-12: Histogram of Gust Wind Direction for January 2005

Figure A-13: Average Daily Temperature and Dew Point for February 2005
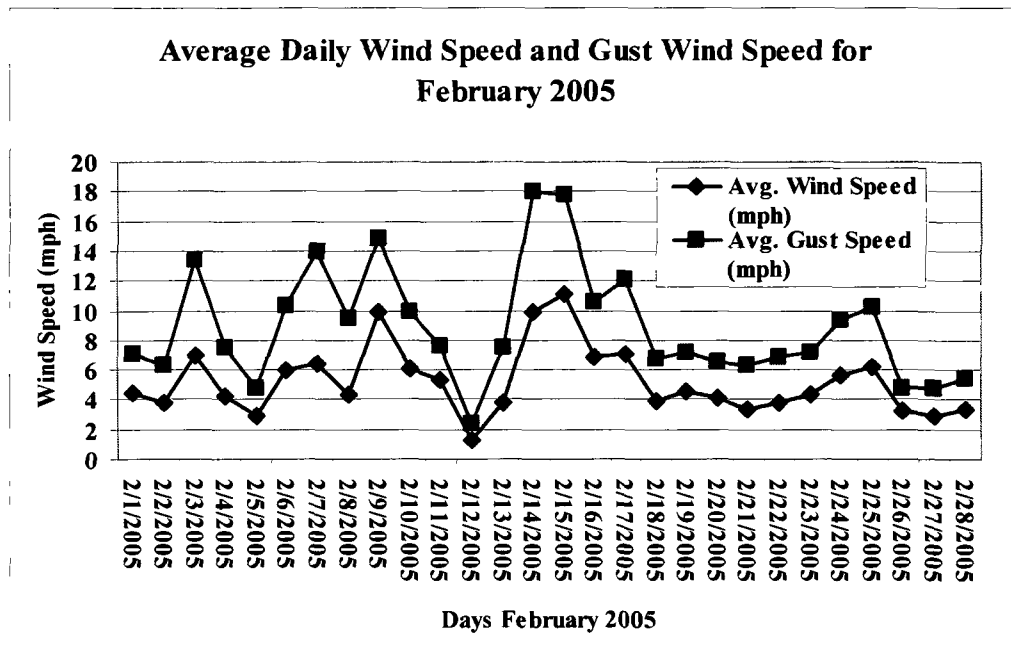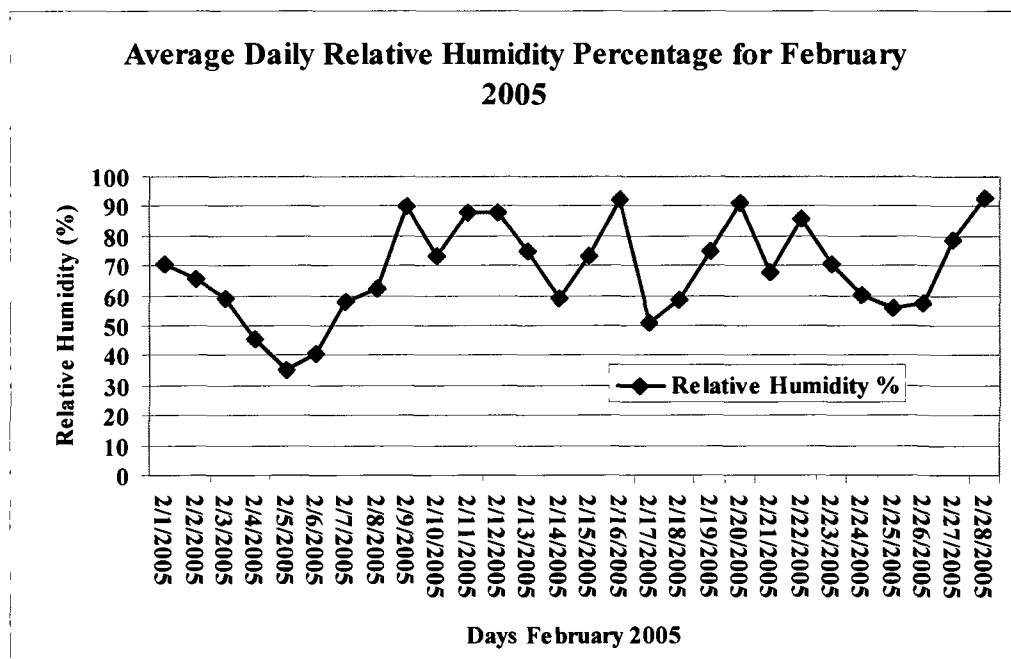
Figure A-14: Average Daily Wind Speed and Gust Wind Speed for February 2005

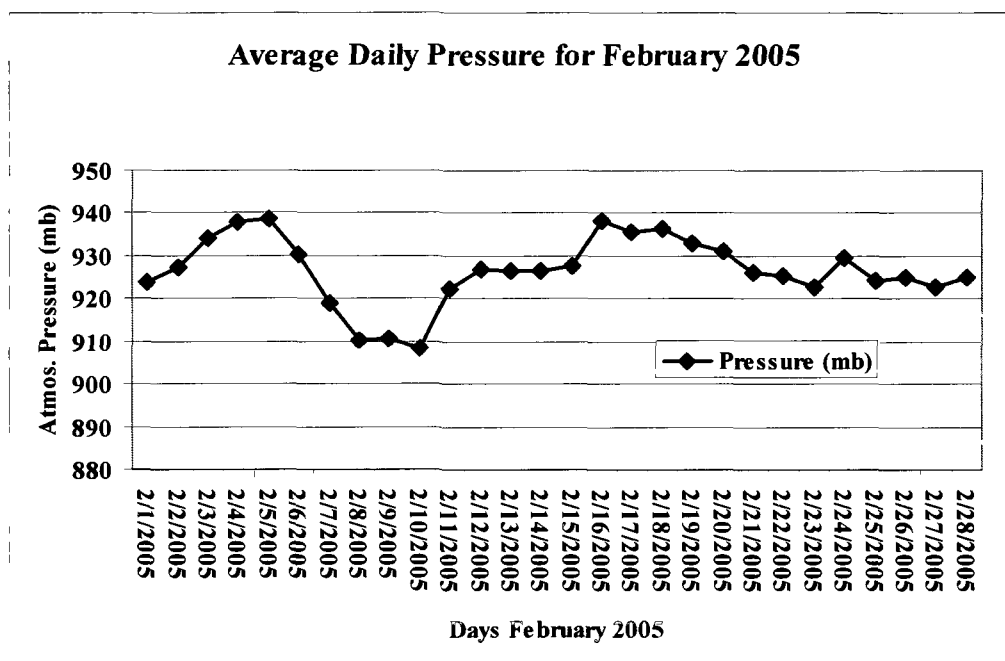Figure A-15: Average Daily Relative Humidity Percentage for February 2005
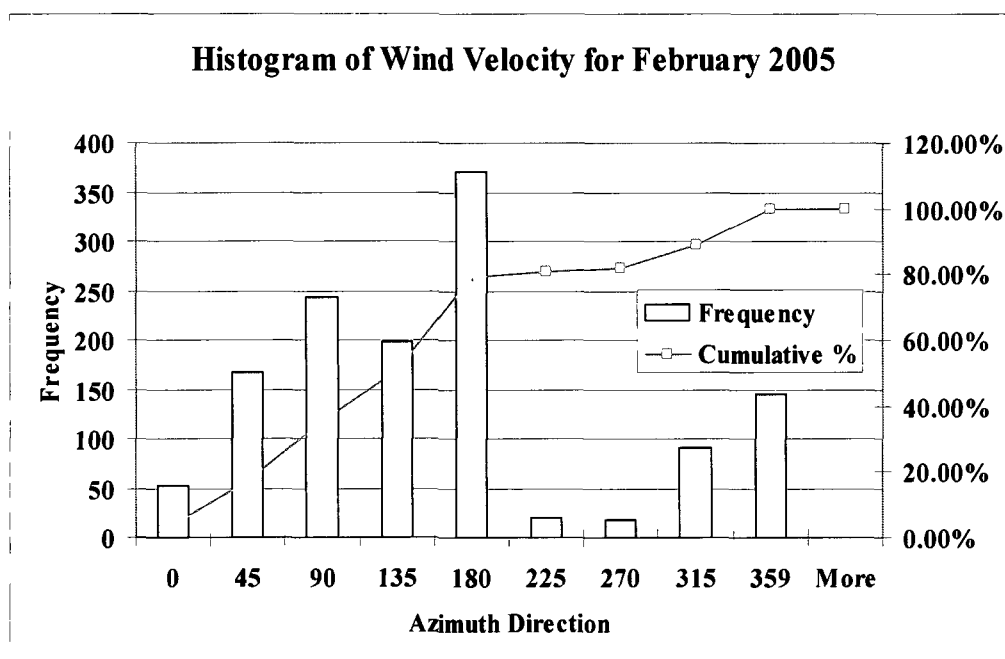
Figure A-16: Average Daily Pressure for February 2005

Figure A-17: Histogram of Wind Direction for February 2005
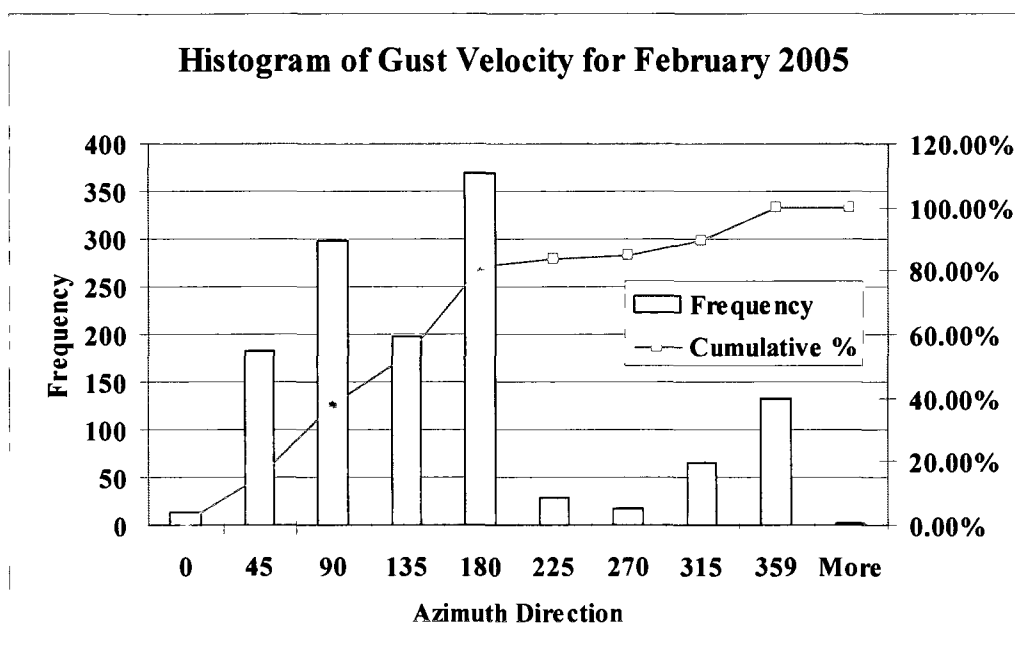
Histogram of Gust Velocity for February 2005

Figure A-18: Histogram of Gust Wind Direction for February 2005